6. SITE 673[1]

Shipboard Scientific Party[2]

HOLE 673A

Date occupied: 1800, 22 July 1986

Date departed: 2300, 23 July 1986

Time on hole: 29 hr

Position: 15°31.90′N, 58°48.60′W

Water depth (sea level, corrected m, echo-sounding): 4660.8

Water depth (rig floor, corrected m, echo-sounding): 4671.3

Bottom felt (rig floor, m, drill-pipe measurement): 4677.9

Distance between rig floor and sea level (m): 10.5

Total depth (rig floor, m): 4714.3

Penetration (m): 36.4

Number of cores (including cores with no recovery): 4

Total length of cored section (m): 36.4

Total core recovered (m): 33.3

Core recovery (%): 91.4

Oldest sediment cored:
Depth sub-bottom (m): 36.4
Nature: mud/calcareous mud
Age: Miocene
Measured velocity (km/s):–

HOLE 673B

Date occupied: 2300, 23 July 1986

Date departed: 1230, 28 July 1986

Time on hole: 4 days, 13 hr, 30 min

Position: 15°31.92′N, 58°48.49′W

Water depth (sea level, corrected m, echo-sounding): 4679.8

Water depth (rig floor, corrected m, echo-sounding): 4690.3

Bottom felt (rig floor, m, drill-pipe measurement): 4689.2

Distance between rig floor and sea level (m): 10.5

Total depth (rig floor, m): 5019.8

Penetration (m): 330.6

Number of cores (including cores with no recovery): 35

Total length of cored section (m): 330.6

Total core recovered (m): 247.5

Core recovery (%): 74

Oldest sediment cored:
Depth sub-bottom (m): 330.6
Nature: siliceous mudstone
Age: early Miocene
Measured velocity (km/s): 1.8

Principal results: Located 13 km from the deformation front, Site 673 penetrated a total of 331 m, crossed two lithologic units, and provided insights on the structural development of an evolving accretionary prism. Extending from the seafloor to 74 mbsf, lithologic Unit 1 consists of Pleistocene and Pliocene calcareous muds and marls, probable reworked claystone blocks of Miocene age, and matrix-supported conglomerates and breccias; Unit 1 is interpreted as a slope deposit. Unit 2 includes massive middle and lower Miocene claystones and siliceous claystones. This facies is lithologically similar to, but significantly less condensed than, that recovered at Site 672 on the Tiburon Rise; Unit 2 is composed of hemipelagic sediments apparently accumulated below the calcite compensation depth.

An overturned section more than 50 m thick indicates relatively large-scale folding and distinguishes Site 673 from sites closer to the deformation front. Associated biostratigraphically documented thrust faulting occurs at at least three intervals in the lower and middle Miocene section. The downhole extent of the Miocene section indicates substantial structural thickening due to steepening of bedding dips, associated folding, and thrusting. Calcite veins found along scaly fabric zones associated with a major fault zone, in otherwise carbonate-free rocks, suggests fluid flow occurs along these scaly zones through fracture permeability.

Seismic line CRV 128 through Site 673 shows arcward dipping reflectors which are also expressed, although at a shallower dip, on seismic line A-3 which intersects CRV 128 near Site 673. Single reflectors recorded on both seismic lines define a common plane dipping west at about 12°, suggesting that the reflections are not artifacts of seismic processing. Bedding dips are variable in magnitude and orientation at Site 673 indicating they cannot generate the reflections. Slight acoustic impedance contrasts occur, however, across biostratigraphically defined faults, suggesting that these features may be the source of the reflections. If the faults are represented by the largely planar reflections that define imbricate packages, then the faults are highly discordant to the internal structure of the packages. In Hole 673B a chloride minimum between 120 and 215 mbsf lies be-

[1] Mascle, A., Moore, J. C., et. al., 1988. *Proc., Init. Repts. (Pt. A), ODP*, 110: College Station, TX (Ocean Drilling Program).

[2] J. Casey Moore (Co-Chief Scientist), Dept. of Earth Sciences, University of California at Santa Cruz, Santa Cruz, CA 95064; Alain Mascle (Co-Chief Scientist), Institut Français du Pétrole, 1-4 Ave Bois-Preau, B.P. 311, 92506 Rueil Malmaison Cedex, France; Elliott Taylor (Staff Scientist), Ocean Drilling Program, Texas A&M University, College Station, TX 77840; Francis Alvarez, Borehole Research Group, Lamont-Doherty Geological Observatory, Columbia University, Palisades, NY 10964; Patrick Andreieff, BRGM, BP 6009, 45060 Orleans Cedex-2, France; Ross Barnes, Rosario Geoscience Associates, 104 Harbor Lane, Anacortes, WA 98221; Christian Beck, Département des Sciences de la Terre, Université de Lille, 59655 Villeneuve d'Ascq Cedex, France; Jan Behrmann. Institut für Geowissenschaften und Lithosphärenforschung, Universität Giessen, Senckenbergstr. 3, D6300 Giessen, FRG; Gerard Blanc, Laboratoire de Géochimie et Métallogénie U. A. CNRS 196 U.P.M.C., 4 Place Jussieu, 75252 Paris Cedex 05, France; Kevin Brown, Dept. of Geological Sciences, Durham University, South Road, Durham, DH1 3LE, U.K. (current address: Dept. of Earth Sciences, University of California at Santa Cruz, Santa Cruz, CA 95064); Murlene' Clark, Dept. of Geology, LSCB 341, University of South Alabama, Mobile, AL 36688; James Dolan, Earth Sciences Board, University of California at Santa Cruz, Santa Cruz, CA 95064; Andrew Fisher, Division of Marine Geology and Geophysics, University of Miami, 4600 Rickenbacker Causeway, Miami, FL 33149; Joris Gieskes, Ocean Research Division A-015, Scripps Institution of Oceanography, La Jolla, CA 92093; Mark Hounslow, Dept. of Geology, Sheffield University, Brook Hill, Sheffield, England S3 7HF; Patrick McLellan, Petro-Canada Resources, PO Box 2844, Calgary, Alberta Canada (current address: Applied Geotechnology Associates, 1-817 3rd Ave. NW, Calgary, Alberta T2N OJ5 Canada); Kate Moran, Atlantic Geoscience Centre, Bedford Institute of Oceanography, Box 1006, Dartmouth, Nova Scotia B2Y 4A2 Canada; Yujiro Ogawa, Dept. of Geology, Faculty of Science, Kyushu University 33, Hakozaki, Fukuoka 812, Japan; Toyosaburo Sakai, Dept. of Geology, Faculty of General Education, Utsunomiya University, 350 Mine-machi, Utsunomiya 321, Japan; Jane Schoonmaker, Hawaii Institute of Geophysics, 2525 Correa Road, Honolulu, HI 96822; Peter J. Vrolijk, Earth Science Board, University of California at Santa Cruz, Santa Cruz, CA 95064; Roy Wilkens, Earth Resources Laboratory, E34-404 Massachusetts Institute of Technology, Cambridge, MA 02139; Colin Williams, Borehole Research Group, Lamont-Doherty Geological Observatory, Columbia University, Palisades, NY 10964.

tween two biostratigraphically defined thrust faults and is centered on a prominent section of overturned beds. Similarly, a chloride low correlates with a fault at about 292 mbsf in Hole 673B. Both chloride minima are probably associated with active fluid flow along these deformed zones. The absence of methane anywhere in the section, and especially associated with the chloride minima, suggests that the fluids did not originate at depths as great as those sampled below the décollement at Site 671.

BACKGROUND AND OBJECTIVES

The Barbados Ridge comprises a broad accretionary prism that has been developing at least since the Paleogene (e.g., Westbrook, 1982; Biju-Duval et al., 1982). Initial convergence beneath the Lesser Antilles forearc dates from the middle Eocene as indicated by the age of arc magmatic activity (Mascle et al., 1987); the beginning of substantial accretionary activity in the Paleogene also is consistent with probable offscraped deposits having this age, from the Island of Barbados (Fig. 1) (e.g., Speed and Larue, 1982). Lacking other insular exposures of the accretionary complex, it is worthwhile to drill series of systematically spaced holes to evaluate overall structural and hydrogeologic evolution of the prism. Site 673 is located 13 km arcward of the deformation front, on an accretionary prism that is almost 130 km wide at this latitude (See cross-section B-B', Speed et al., 1984). Therefore, if the accretionary prism has grown progressively seaward, rocks to be cored at Site 673 may have been accreted in the Miocene or Pliocene. Site 673 provides the opportunity to investigate these somewhat earlier accretionary processes in contrast to the focus on modern accretionary and hydrogeologic activity at DSDP Sites 541, 542, and ODP Site 671 near the deformation front.

The rate of convergence of Atlantic Ocean crust beneath the Caribbean plate is variously estimated at between 2 and 4 cm/year (Minster and Jordan, 1978; Sykes et al., 1983). A balanced cross-section constructed from the drilling and seismic data near the deformation front indicates a convergence rate of less than 1 cm/yr (see Summary Chapter, this volume). Either the plate-tectonic geologically derived estimates of convergence rate may be in error, or the unaccounted convergence could be distributed across the accretionary prism (e.g, Biju-Duval et al., 1982; Moore and Biju-Duval, 1984). One goal of Site 673 is to document and determine the magnitude of this distributed deformation.

Site 673 occurs at about the mid-point of the two-degree seaward facing slope of the front of the accretionary prism (Figs. 2 and 3). This frontal slope is succeeded in an arcward direction by an undulating high with significantly more sediment cover above the accretionary material. Apparently this plateau is a region of relatively less active deformation, whereas the seaward facing slope is one of more rapid uplift of the accreted materials.

The seismic décollement, or principal boundary between the accretionary prism and the underthrusting sedimentary sequence, is located about 1.2 seconds below Site 673 (Fig. 3). Clearly, the accretionary prism has undergone a systematic thickening process in an arcward or westward direction. Specifically, the accreted sediment above the décollement is about twice as thick at Site 673 as that cored at Site 671. Mechanical arguments indicate that accretionary prisms must thicken to retain their critical taper and continue forward growth (Davis et al., 1983). The ex-

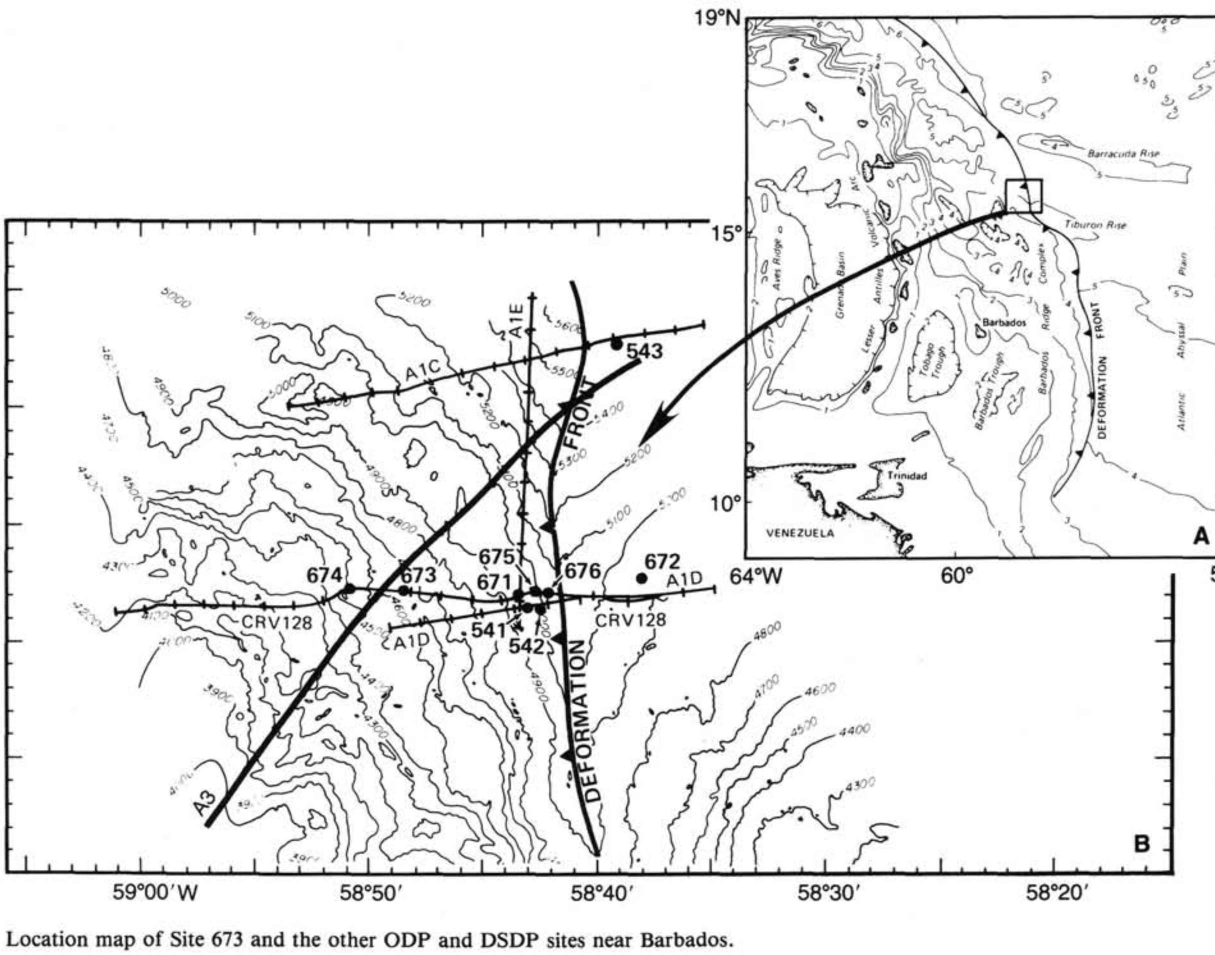

Figure 1. Location map of Site 673 and the other ODP and DSDP sites near Barbados.

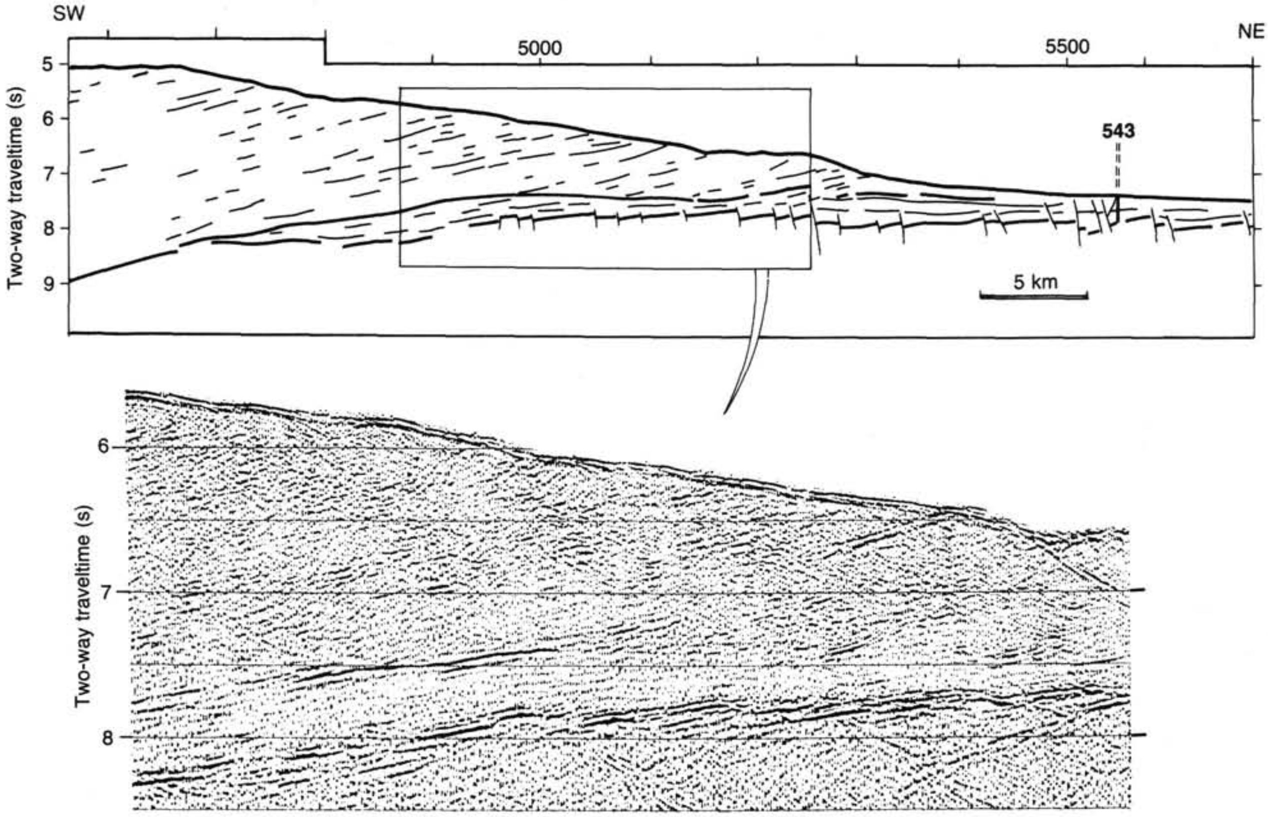

Figure 2. Line drawing of seismic line A-3 with inset of actual data. Note well-developed landward-dipping reflectors. Line A-3 intersects line CRV 128 at an angle of about 45 degrees near Site 673 (Fig. 1). Vertical exaggeration of A-3 is 3.3 to 1 at seafloor.

act mechanism of thickening however it not well understood. At least five possibilities exist:

1. Thickening could occur in response to internal shortening of the offscraped thrust packages; a process evident in the offscraped thrust sheets at Site 671 (see Conclusions Site 671).

2. Alternatively, thickening could be occurring by mass addition or underplating at the base of the accretionary prism (Figs. 2 and 4; Watkins et al., 1981). Underplating requires transfer of material from the underthrusting to overthrusting masses through the décollement zone. Thrust sheets or duplexes can be transferred due to the down-stepping of the décollement in discrete jumps (Westbrook and Smith, 1983); alternatively, the décollement zone may gradually migrate down-section with the incremental transfer of material to the overlying plate. On seismic line CRV-128 the seismic décollement locally cuts both up and down section. However, these changes of the décollement position appear to be related to highs and lows in the oceanic crust over which the sediment has been depositionally draped; the seismic décollement, being very planar tends to cut sedimentary layers off the highs leaving somewhat thicker sections in the intervening lows (Fig. 3).

3. Secondary imbrication or stacking of the accreted material along discrete faults that cut and partially duplicate the prism is also a viable means of thickening.

4. A seaward taper to the accretionary prism could be generated by the accretion of thicker sediment packages during its earlier history.

5. Accretionary prisms might also increase in thickness arcward owing to the progressive deformation and incorporation of slope deposits.

The seaward-facing slope of the accretionary prism is punctuated by low-amplitude highs one to several kilometers wide that trend approximately north–south. These highs are especially prominent on the lowermost slope, where they represent tectonic packages separated by thrust faults (Fig. 3). The thrust faults are correlated with landward-dipping reflectors that intersect the bottom in the intervening lows (see Seismic Stratigraphy section, Site 671 chapter). Site 673 is located on the seaward slope of one of these small highs; as placed on seismic line CRV-128, several landward-dipping reflectors underlie Site 673. Additionally, seismic line A-3, which crosses CRV 128 near Site 673, shows many landward-dipping reflectors (Fig. 2). Although we believe some of these landward-dipping reflectors represent faults, others could be bedding surfaces, or even dewatering conduits (Cloos, 1984).

The principal objectives at Site 673 are as follows:

1. To define the age of local offscraping and therefore approximate the rate of accretion.

2. To investigate the development of structural fabrics across the accretionary prism and especially to make comparisons to fabrics developed at the toe of the prism at Sites 541, 542, and 671.

3. To provide lithologic data on former deposits of the Atlantic abyssal floor which now probably make up the offscraped material at Site 673.

4. To determine the vertical motions of the site and, in combination with results from structural geology and seismic data, infer whether the accretionary prism thickens by shortening and imbrication of thrust packages or by underplating.

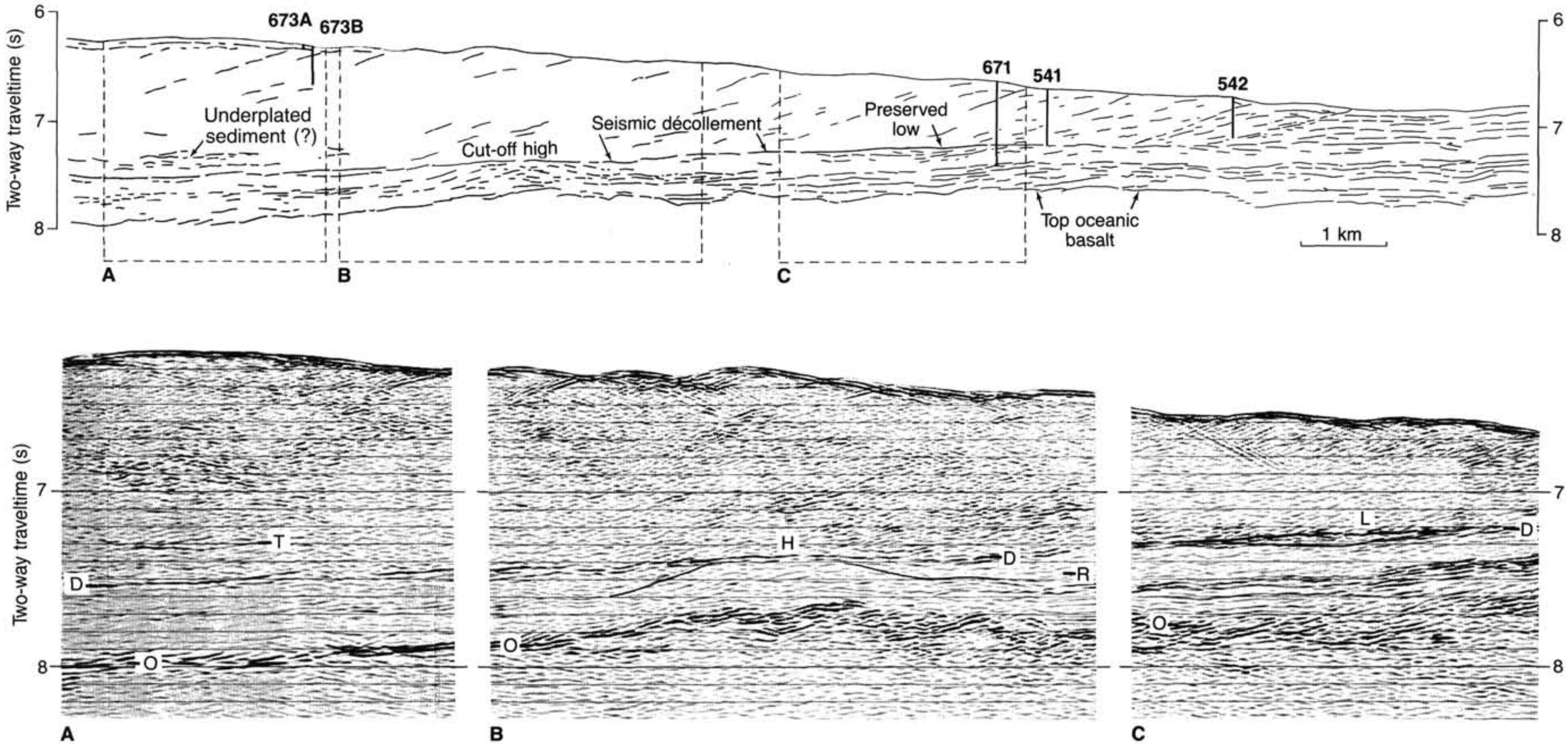

Figure 3. Line drawing of part of seismic line CRV-128 with insets of seismic data. Note prominence of seismic décollement on line drawing and all inset data sections (D on latter). Top of oceanic basalt (O in insets) is also a well-defined reflector. Conspicuous low-dipping reflector (T) about 200 ms above seismic décollement in inset A may represent top of underplated package. Reflector R on inset B shows how sediment is draped over highs in oceanic basaltic basement and in turn cut off just below H by the planar décollement surface (D). Conversely, lows in the oceanic basement allow the development of local sediment ponds (immediately below L in inset C) that are preserved beneath the décollement. Vertical exaggeration is about 1.7 to 1 at seafloor.

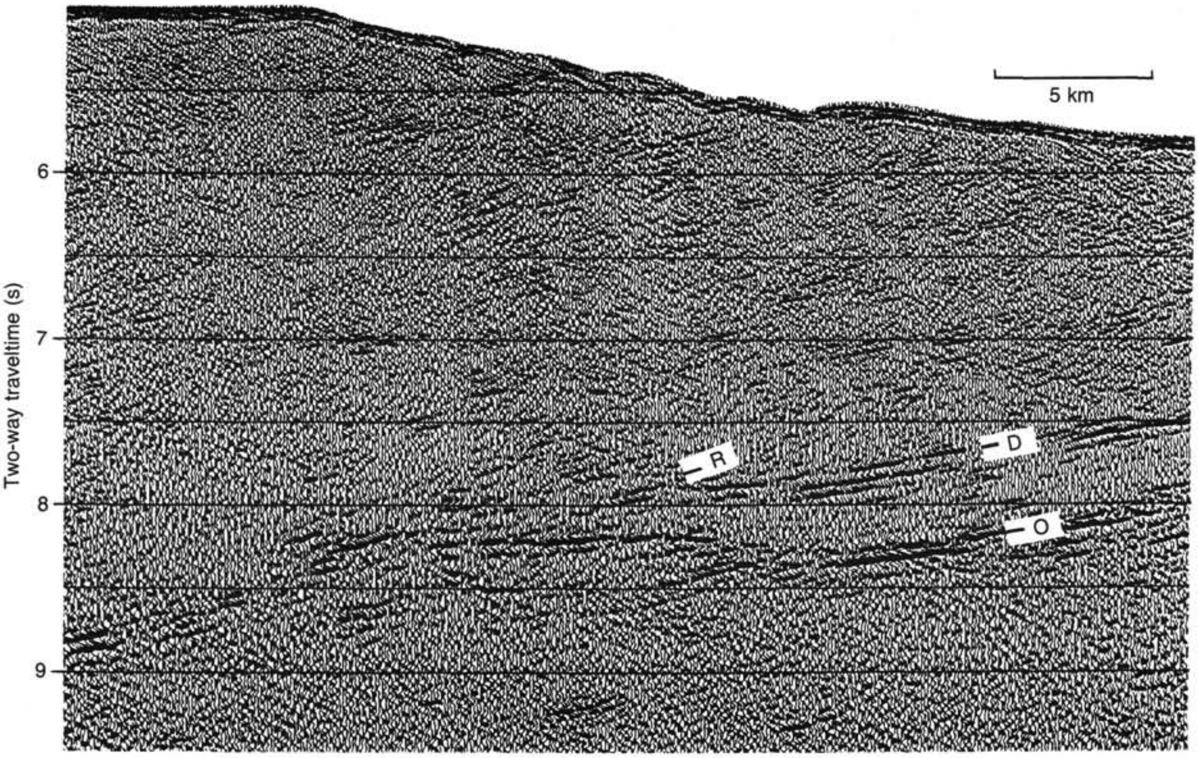

Figure 4. Portion of seismic line A-3 showing reflector (R) that we interpret as a ramp along which seismic décollement (D) cuts down to top of oceanic basalt surface (O). Vertical exaggeration at seafloor is 3.33 to 1.

5. To determine if fluids are flowing upward through the accretionary prism, especially through the examination of pore-water chemistry and heat-flow data.

6. To establish whether landward-dipping reflectors represent bedding surfaces, thrust faults, fluid dewatering conduits, or artifacts of the seismic processing.

OPERATIONS

Site 673

Site 673 is located approximately 8 km upslope of Site 671 on the Lesser Antilles forearc. The purpose of drilling at this site was to sample sediments within the thickened accretionary wedge. We hoped these cores would provide insights into the mechanisms and styles of deformation that occur in the transition from initial offscraping to uplift and subaerial exposure. The site was approached from the seaward side and chosen by the co-chief scientists based on dead-reckoning navigation from Site 672 and the seismic records from underway geophysics, since the GPS navigation system was not operative. A beacon and a spar buoy were dropped at 1800 hr on 22 July 1986. The geophysical gear was retrieved and the ship turned around to return to the spar buoy and beacon position. Comparison of the actual beacon drop position relative to the desired site location resulted in a needed 1.5-km offset to the east of the original beacon position. While we steamed to the new site, the spar buoy was sited and the original beacon was seen floating beside it. The ship proceeded to the new requested location, still under dead reckoning navigation, and dropped a second beacon. The onset of darkness precluded launching an inflatable boat to search for the first beacon until the following morning. Alas, the derelict beacon was never located.

Hole 673A

Hole 673A is located at 15°31.90'N, 58°48.60'W. The BHA consisted of a long-toothed APC-XCB 11-7/16"-diameter core bit with a six-drill-collar bottom hole assembly. The flapper valve was removed from the float valve to allow for logging without dropping the bit.

The mudline was established at 4677 m of drill pipe. The hole was cored using the APC to 4714 m (36.4 mbsf), where two cores with 65,000-lb pullout precluded further APC work. Recovery was excellent in this interval, and Cores 110-673A-3H and -4H were oriented using the Eastman multishot equipment.

The XCB core barrel was dropped to continue coring, and a normal XCB core was recovered; however, the drilling record indicated that the bit had not been advanced after the last APC core and thus the XCB was full of cuttings and fill. The sediment in this barrel was therefore not considered a core. The next core barrel would not pressure up when landed and when the overshot was dropped to recover the core barrel, a 15,000-lb overpull was required to free the sandline. Upon retrieving the sandline, we discovered the link jar had parted at the lower end of the sinker bar, and the jars and overshot were lost. Brown clay was found on the end of the sinker bar, indicating a failure of the BHA.

The pipe was tripped out of the hole, leaving the bottom drill collar, core bit, head sub, top sub, landing-saver sub and jar-overshot in the hole. Careful examination of the positioning and drilling recorder records do not indicate excessive weight, torque, or the vessel moving off location. It is surmised from examination of the broken thread on the end of the Gammaloy collar that improper makeup between the head sub and the drill collar may have occurred and that the bottom collar wobbled off while drilling.

We cored 36.4 mbsf and recovered 33.3 m of sediment (91.4%) at Hole 673A, moving off-hole at 2300 hr on 23 July 1986.

Hole 673B

Hole 673B is offset 600 m east of Hole 673A in a slightly thicker slope sediment sequence. The objectives here were the same as at Hole 673A, namely to drill to a maximum of 600 mbsf and log the formation if possible. A six-drill-collar bottom-hole assembly was used. The bit consisted of 11-7/16"-diameter APC deep throat, long tooth with sealed journal bearings. The flapper was not installed in the float valve. If the hole proved to be stable the formation could be logged without dropping the bit.

The first APC core established the mudline at 4689.2 m of drill pipe. Six cores were taken to 45.6 mbsf where pullout forces of 55,000 lb required the XCB system be deployed. A downhole temperature measurement was taken using the APC pocket shoe with Von Herzen heat flow recorder on Cores 110-673B-3H. Recovery in the APC-sampled section was 100%.

The hole was cored by XCB methods from 45.6 to 330.6 mbsf. The formation was composed of sticky clay that softened with depth, and sediments which decreased in age as the well deepened. These formation characteristics, and the fact that many of the stratal beds were tilted at 45°, made drilling conditions difficult. Below 200 mbsf, 1700 to 2500 lb of pump pressure were required to brake circulation. After circulation was obtained the pressure dropped back to a pressure consistent to the strokes on the pump. Numerous flushes of salt water-polymer based mud were used in an attempt to improve hole conditions with little effect. Torque and drag on the drill string continued to increase with depth and frequently the well exhibited backflow when making a connection or retrieving a core.

After cutting Core 110-673B-35X, the fishing neck on the XCB latch was engaged with the sandline overshot and the core barrel pulled up through the bottom-hole assembly into the 5-1/2" drill pipe. The winch operator stopped the winch to check the hanging weight of the sandline, which indicated that the core barrel was not attached. The operator returned the overshot to bottom in an attempt to re-engage the core-barrel fishing neck and gain back the correct weight. When the winch was reversed, the line pulled tight and the cable depthometer indicated that the inner barrel had hung-up 52 m above the bit.

The sandline could not be freed from the core barrel by pulling or jarring action, so a sandline cable cutter was fabricated and deployed as a go-devil down the pipe. The cable cutter did not work and the pulling cycles on the sandline were resumed until the line parted 2200 m below the ship.

The drill string was recovered and the junk sandline in the pipe was cut into 30-m pieces for disposal. Once recovered, the BHA was found completely balled up with sticky mud. It appears that the soft formation had packed off around the drill string below 200 mbsf and circulation had been lost into the formation. When the core-barrel latch was released after Core 110-673B-35X, formation pressure created from pumping while cutting the core pushed the core barrel up the BHA. Thus, when the winch operator stopped to check the tool weight after clearing the drill collars, the inner barrel attempted to by-pass the sandline. We think the sandline snagged in the gap between its swivel shaft and body thus wedging the barrel in the drill pipe. A spacer was subsequently installed to narrow the gap in the swivel and prevent the line from becoming so impaired in the future.

The total cored interval in Hole 673B was 330.6 m with a recovery of 247.5 m (74%). HPC recovery at Site 673 was 100% and XCB operations resulted in 69% recovery. The coring summary for Site 673 operations is listed in Table 1. The *Resolution* departed Site 673 at 1230 hr on 28 July 1986 after 5.8 days of operations.

STRUCTURAL GEOLOGY

Site 673 lies 13 km arcward of ODP Site 671 and west of DSDP Sites 541 and 542 (Leg 78A). Despite only moderate core recovery and quality below 80 m sub-bottom depth, Site 673 documented a number of major structural elements that are associated with the continuing development and thickening of the earlier accreted portions of the Barbados Ridge accretionary complex (Fig. 5). The sequence recovered at Site 673 makes up two main structural units: an upper slope cover sequence, and a lower unit of accreted sediments.

Slope Sediments

The upper 74 m of section (to the base of Core 110-673B-8X) consists of interbedded hemipelagic sediments of Pleistocene to Pliocene age, debris flow deposits, and slumped masses of Miocene material, interpreted as a slope cover sequence (see Lithostratigraphy section, this chapter).

Structurally, this upper sequence is characterized by extremely variable bedding dips, apparently indicating either extensive folding on a scale of a few meters or blocks in random orientations (Fig. 5). The section between 5 and 50 mbsf is also extensively faulted. The faults are discrete structures, commonly only millimeters thick and having predominantly steep dips (between 50° and 70°). Three faults have small reverse offsets; the sense of offset on the rest of the faults is indeterminate. Low angle and horizontal faults are common between 10 and 25 mbsf (Core 110-673B-3H). These faults crosscut, and thus postdate, the high-angle faults (Fig. 6).

The majority of the deformation in the slope sequence may be the product of gravity sliding and slumping, accounting for its structural complexity. The reverse faults in this section could have resulted from later compressional deformation of the sequence; alternatively, the faults may have formed as a result of slumping during deacceleration of the sliding mass. Although no normal faults were identified in the slope sequence, the nature of the deposits suggests that many of the high-angle faults could be extensional features associated with slumping. The slope cover sequence lies with an angular unconformity on an accreted sequence of lower Miocene sediments, with a basal, matrix-supported breccia composed of reworked Miocene material (see Lithostratigraphy section for discussion).

Accreted Sediments

The homogeneity of the lower Miocene section (lithologic Unit 2, see Lithostratigraphy section) and downhole decrease in core recovery and quality resulted in a scarcity of recorded bedding dips in the accreted sediments. However, detailed biostratigraphic control enabled good delineation of four tectono-stratigraphic packets (Fig. 5). These packets are separated by both biostratigraphic (see Biostratigraphy section, this chapter) and structural discontinuities (thrusts 1–3). Thrust 1 is in a section of poor recovery; however, the positions of thrusts 2 and 3 are marked by zones of scaly clay fabrics.

Packet 1

Packet 1 is bounded by the angular unconformity with slope deposits above and thrust 1 below. The sediments within the packet consist of relatively homogeneous lower Miocene sediments. Bedding dips range between 0° and 60°, indicating that the section is folded. A few minor discrete faults, including a normal fault at 80 mbsf, were recorded within the packet. Thrust 1 was not directly observed and is inferred only from biostratigraphic results (radiolarian Zone R10 over radiolarian Zone R8).

Packet 2

Packet 2 is bounded by thrust 1 above and thrust 2 below. The packet consists of a lower Miocene sequence underlain by an indeterminate sequence of possible middle Miocene age. The

Table 1. Coring summary, Site 673.

Core no.	Date July 1986	Time	Sub-bottom top (m)	Sub-bottom bottom (m)	Meters cored (m)	Meters recovered (m)	Percent recovery
110-673A-1H	23	0445	0.0	7.9	7.9	7.91	100.0
110-673A-2H	23	0615	7.9	17.4	9.5	9.77	103.0
110-673A-3H	23	0900	17.4	26.9	9.5	8.91	93.8
110-673A-4H	23	1100	26.9	36.4	9.5	6.74	70.9
					36.4	33.33	
110-673B-1H	24	1015	0.0	7.6	7.6	7.65	100.0
110-673B-2H	24	1145	7.6	17.1	9.5	9.75	102.0
110-673B-3H	24	1315	17.1	26.6	9.5	10.05	105.8
110-673B-4H	24	1415	26.6	36.1	9.5	9.75	102.0
110-673B-5H	24	1610	36.1	45.6	9.5	9.74	102.0
110-673B-6H	24	1700	45.6	55.1	9.5	9.67	102.0
110-673B-7X	24	1922	55.1	64.6	9.5	6.67	70.2
110-673B-8X	24	2115	64.6	74.1	9.5	6.85	72.1
110-673B-9X	25	0215	74.1	83.6	9.5	6.70	70.5
110-673B-10X	25	0445	83.6	93.1	9.5	4.01	42.2
110-673B-11X	25	0730	93.1	102.6	9.5	2.83	29.8
110-673B-12X	25	1010	102.6	112.1	9.5	4.85	51.0
110-673B-13X	25	1215	112.1	121.6	9.5	4.04	42.5
110-673B-14X	25	1405	121.6	131.1	9.5	6.91	72.7
110-673B-15X	25	1610	131.1	140.6	9.5	9.68	102.0
110-673B-16X	25	1759	140.6	150.1	9.5	8.56	90.1
110-673B-17X	25	1953	150.1	159.6	9.5	6.10	64.2
110-673B-18X	25	2217	159.6	169.1	9.5	5.15	54.2
110-673B-19X	26	0019	169.1	178.6	9.5	9.12	96.0
110-673B-20X	26	0215	178.6	188.1	9.5	1.68	17.7
110-673B-21X	26	0400	188.1	197.6	9.5	2.22	23.3
110-673B-22X	26	0615	197.6	207.1	9.5	4.06	42.7
110-673B-23X	26	0815	207.1	216.6	9.5	8.24	86.7
110-673B-24X	26	1000	216.6	226.1	9.5	9.79	103.0
110-673B-25X	26	1200	226.1	235.6	9.5	6.47	68.1
110-673B-26X	26	1415	235.6	245.1	9.5	3.89	40.9
110-673B-27X	26	1620	245.1	254.6	9.5	2.20	23.1
110-673B-28X	26	1806	254.6	264.1	9.5	9.73	102.0
110-673B-29X	26	2018	264.1	273.6	9.5	9.78	103.0
110-673B-30X	26	2205	273.6	283.1	9.5	9.57	101.0
110-673B-31X	27	0025	283.1	292.6	9.5	9.77	103.0
110-673B-32X	27	0218	292.6	302.1	9.5	9.40	98.9
110-673B-33X	27	0408	302.1	311.6	9.5	4.03	42.4
110-673B-34X	27	0550	311.6	321.1	9.5	9.72	102.0
					321.1	238.63	

most striking structural feature of Site 673 was the identification, using detailed biostratigraphy, of a major overturned anticline (Fig. 5; see Biostratigraphy section for further details). The upper limb is upright and has a downhole thickness of 40 m (Cores 110-673B-11X to -15X). The axial plane of the fold runs through Core 110-673B-15X or -16X, at approximately 145 mbsf. The inverted lower limb of the fold dips at 60° to 80° and has a downhole thickness of approximately 60 m (Cores 110-673B-15X to -21X). Equivalent biostratigraphic subzones are approximately the same width on both limbs of the fold, implying that they have broadly similar dips.

Thrust 2 lies within a section of indeterminate age that extends from Core 110-673B-21X to -26X (195–240 mbsf, Fig. 5). Its position may correspond to any, or all, of a series of scaly clay zones developed in Cores 110-673B-22X and -24X (Fig. 5). However, a reversal in physical properties trends occurs near 200 mbsf (see Physical Properties section, this chapter). In addition, the region between 200 and 220 mbsf is characterized by the common occurrence of calcite veins in areas of scaly clay and mud-filled vein structures (see below). These data suggest that this zone experienced high fluid pressures. It is therefore likely that the main zone of displacement occurs between 200 and 210 mbsf (Core 110-673B-22X) in a zone where scaly clays are particularly intense (see Fig. 7).

There are three possible interpretations of the folded zone between 100 and 200 mbsf (Fig. 8). The main differences concern the geometry of the fold itself (compare Figs. 8a and 8b), and whether the age of thrust 1 is prefolding (Fig. 8c) or postfolding (Figs. 8a and 8b).

Packet 3

Packet 3 is bounded by thrust 2 above and thrust 3 below. The lower Miocene sequence is upright, according to the biostratigraphy. Bedding dips in the sequence vary between 0° and 35°. A number of scaly clay zones occur within the packet without biostratigraphic inversions across them, implying that imbrication may be occurring with throws below the limit of biostratigraphic resolution (between 10 and 20 m). The distinctive, brown radiolarian claystone sequence found within the décollement zone at Site 671, occurs in this packet at 260 mbsf (Core 110-673B-28X). However, it does not appear to be the locus of any major faulting or stratigraphic inversion at Site 673. At the time this packet was accreted, the décollement must have been localized deeper in the stratigraphic sequence. Thrust 4 corresponds to a 5-m-thick zone of scaly clays at 310 mbsf (Core 110-673B-33X). The scaly clay fabric here has variable dips ranging from subhorizontal to 80° and has probably suffered minor folding.

Packet 4

Packet 4 is bounded by thrust 4 above and corresponds to the bottom two cores of Hole 673B. No bedding dips or other structural features were observed within this packet, but biostratigraphic evidence indicates that this part of the section is inverted.

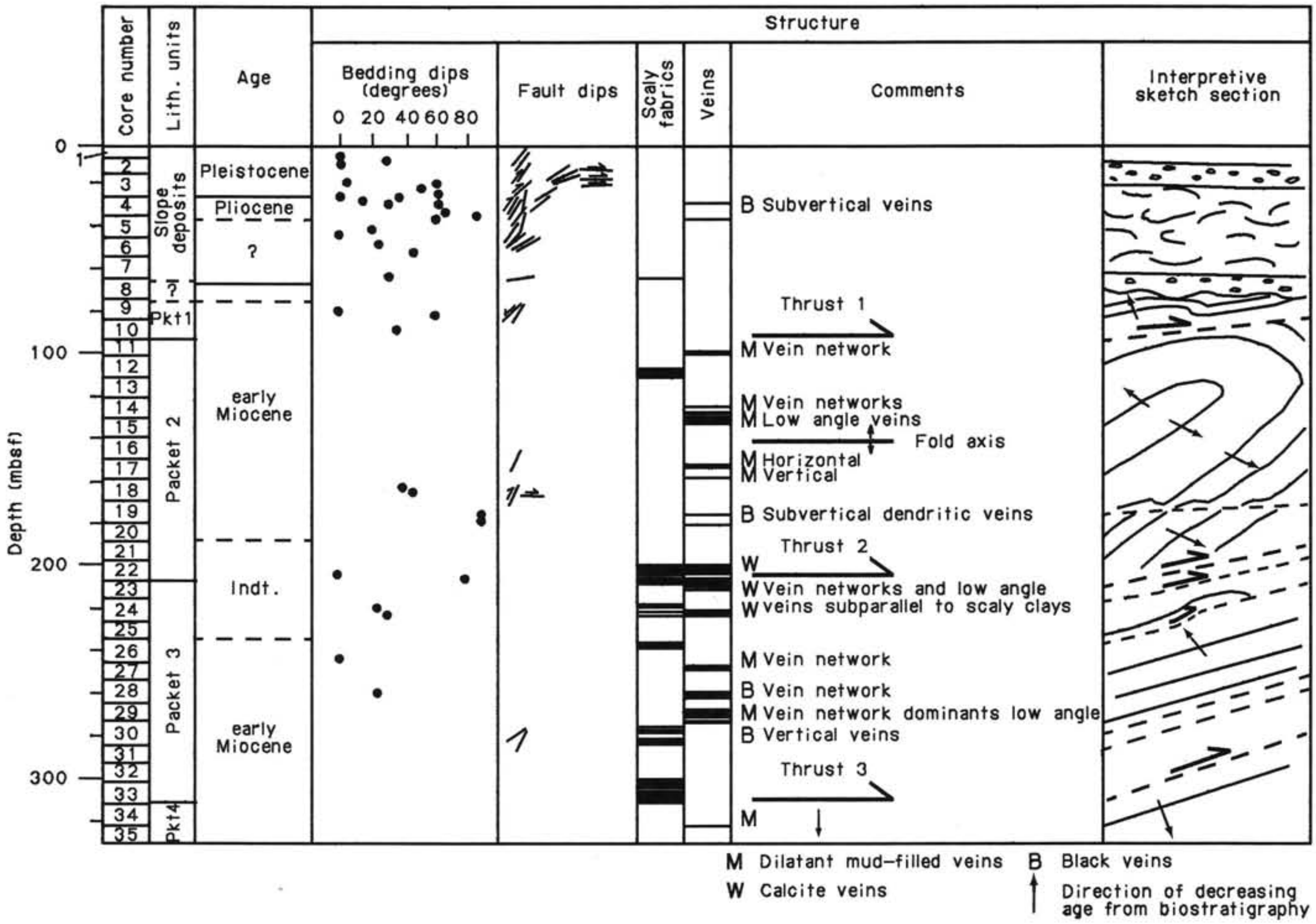

Figure 5. Structural log of data derived from Hole 673B, depicting true dips of bedding and small discrete fault surfaces, the downhole distribution of zones of scaly fabric development, and the nature and occurrence of mineralized and mud-filled veins. An interpretive sketch section illustrates the main structural features present in the hole. The cores are unoriented, thus dip azimuths are unknown.

Veins and Mineralization

Structures that can be broadly defined as veins have been observed in Site 673 cores. A summary of their distribution and form is given in Fig. 5. They can be classified into two groups:

1. Mineralized faults and fractures. These can be subdivided into calcite veins and fractures filled with a black fine-grained material that may be an amorphous manganese phase.

The calcite veins are principally associated with the scaly clays in fault zones that occur around thrust 2, between 200 and 220 mbsf (Fig. 5). They both cut, and are disrupted by, the scaly fabric in the fault zones. The calcite veins tend to be oriented subparallel to the scaly clay fabric in fault zones (Fig. 9), indicating that the latter may function as dewatering conduits through fracture permeability. In contrast, mildly deformed interfault areas in the same region contain calcite veins having a variety of dips, locally forming a network or anastomosing pattern (Fig. 10).

The fractures filled with the black amorphous mineralogical phase are developed throughout the sequence, first appearing in the slope sequence at 30 mbsf (Fig. 5). These fractures occur in a variety of orientations, sometimes forming networks. They are most prominently developed in the lithostratigraphic horizon that corresponds to the décollement zone at Site 671 (Fig. 11). Dendritic veins occur in Core 110-673B-19X (Fig. 12).

2. Clay-filled dilatant vein structures are a common feature throughout the cored section (Fig. 5). They occur in a variety of orientations, commonly as networks. These veins are most abundant in Core 110-673B-14X in the upper limb of the anticline in packet 2. There, both predominantly subhorizontal and vertical dilatant veins occur within a few meters of each other.

Summary

The important structural features of Site 673 are:

1. A deformed slope sediment sequence in which the deformation may result from a combination of large-scale slumping and possible effects of compressional tectonics.
2. The identification of four packets of accreted lower Miocene sediment separated by three thrusts.
3. The identification of a large anticlinal fold (half-wavelength of corresponding fold pair may exceed 100 m) with an overturned lower limb.
4. The observation of three different vein types, including mud-filled dilatant veins and calcite veining. The calcite veining, in particular, appeared to be closely related to the presence of a major fault zone (thrust 2).
5. The décollement may have been located deeper within the stratigraphic sequence at the time of accretion.

LITHOSTRATIGRAPHY

Sediment Lithology: Description

The sediments recovered at Site 673 are divided into two distinct lithostratigraphic units on the basis of visual core descrip-

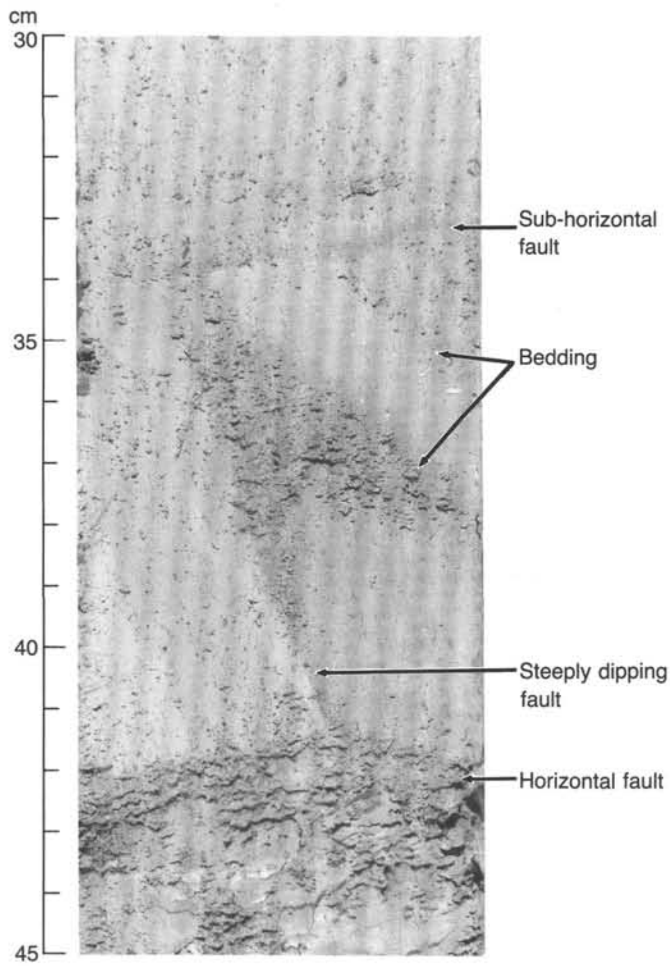

Figure 6. Photograph of Section 110-673B-3H-2 showing cross-cutting relationships of high-angle and low-angle faults at 19 mbsf. The use of a piston corer through this section means that the cross-cutting horizontal faults are tectonic features and not a facet of drilling disturbance.

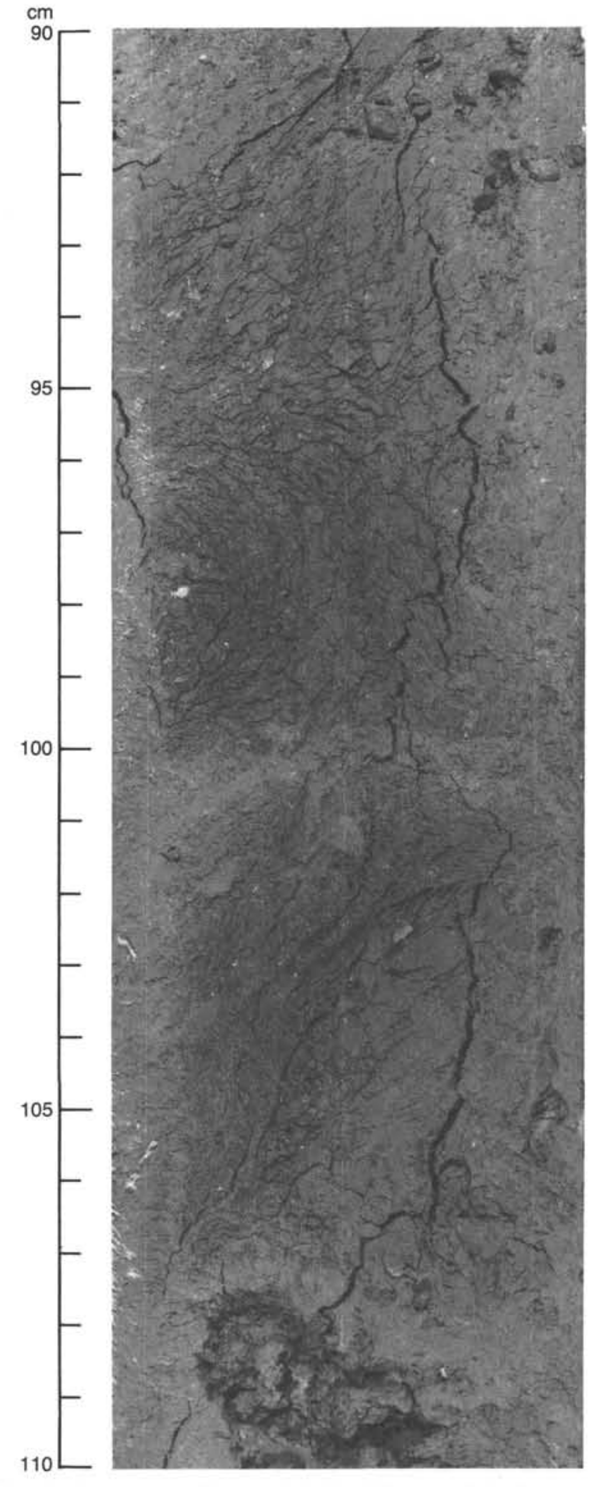

Figure 7. Photograph of Core 110-673B-22X. Part of the intense scaly clay fabrics developed in a wide zone of deformation that occurs between 200 and 220 mbsf (located near thrust 2). In this section the scaly clay fabrics are relatively steeply dipping and appear to be folded.

tions and smear-slide analyses (Table 2). Lithologic Unit 1 includes both reworked slope and hemipelagic deposits, and Unit 2 consists of an uplifted, deformed Miocene hemipelagic sequence.

Lithologic Unit 1 (0–74.1 mbsf in Hole 673B, 0-36.4 mbsf in Hole 673A)

The unit consists of three sublithologies: yellow brown foraminifer/nannofossil calcareous muds and marls, matrix-supported conglomerates and breccias, and blocks of greenish gray Miocene claystone (Fig. 13). Clasts in the matrix-supported conglomerates and breccias consist mostly of greenish gray compacted claystone; clay grains are plastered around detrital quartz and feldspar grains. Based on fossil age determinations in Cores 110-673A-3H, -4H, and -8X, and based on lithologic similarities, we interpret all clasts of compacted claystone to be Miocene in age. Brownish claystone clasts also occur locally and may be weathered greenish gray claystone fragments. In addition, minor calcareous mud and marl clasts occur in these units. Clasts range in size from 0.5 to 20 cm and are angular to rounded (Fig. 14). Furthermore, conglomerates and breccias may be associated with gradual color changes of the deposit. For example, in a 120-cm-thick breccia horizon in Core 110-673B-1H, Section 4, 116–150 cm to Section 5, 0–86 cm, there is a gradual color change from greenish gray to pale olive to light yellowish brown. This breccia interval is carbonate-free, and smear-slide observations suggest that all clasts were originally compacted Miocene claystone. The matrix of all conglomerates and breccias generally consists of noncalcareous clay and may be reworked Miocene clay. The large Miocene claystone blocks observed in Unit 1 commonly have brecciated margins and contain deformational features (e.g., vein structure, scaly fabrics) similar to those recognized in the Miocene section of Site 671

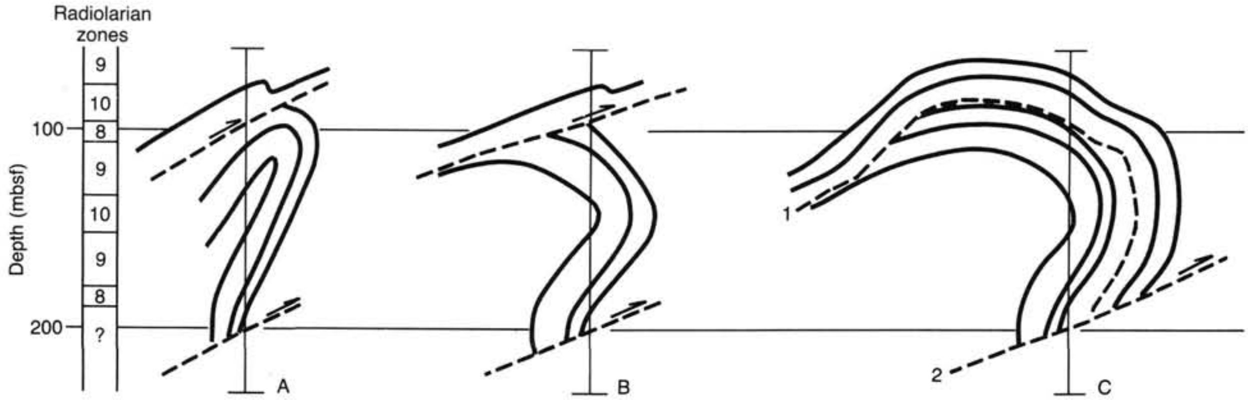

Figure 8. Three possible fold and thrust geometries that fit the information gathered on the fold in packet 2. The dip of the upper limb of the fold is not known; however, the radiolarian zones (see Biostratigraphy Section) are approximately the same thickness on either limb and therefore may be dipping at roughly the same angle (60°–80°). Geometries A and B depict thrust 1 as postfolding structure cutting across the fold. Geometry C has thrust 1 predating the fold, which may be a ramp anticline to thrust 2 modified by continued ductile folding.

and deeper in Hole 673B (see Structural Geology section). Individual blocks may be as large as 15 to 25 m thick (Hole 673A, Fig. 13), estimated from measuring the thickest greenish gray claystone interval in Unit 1. Ash occurs both as discrete beds in the calcareous muds and marls and as disseminated ash particles in the calcareous muds/marls and conglomerates/breccias; the latter occurrence suggests intense bioturbation.

Lithologic Unit 2 (74.1–330.6 mbsf)

The unit was cored only in Hole 673B and consists of a homogeneous sequence of massive, middle(?) and lower Miocene, greenish gray claystones and siliceous claystones with common radiolaria, sponge spicules, and diatoms. A detailed stratigraphic succession is difficult at Site 673 because the Miocene sequence has been repeated at least four times by intense folding and faulting (see Biostratigraphy and Structural Geology sections, this chapter). This sequence is lithologically similar to, but less condensed than, the middle to lower Miocene section recovered in the reference Site 672. For example, at Site 672 a 38-m-thick brown claystone interval includes radiolarian zones 9–13 whereas at Site 673 a 9.5-m-thick brown claystone encompasses only part of radiolarian Zone R11, suggesting more rapid deposition at Site 673. On the other hand, structural thickening may also play a role. Finally, a single silty siliceous marlstone interval occurs in Core 110-673B-18X, Section 3, 15–40 cm; its genesis in this sequence is unknown.

Depositional Processes

Four processes are recognized in Unit 1:

1. Hemipelagic deposition of foraminifera, nannofossils, and clay, forming the background sedimentation. This process accounts for the yellowish brown foraminifer/nannofossil calcareous muds and marls.
2. Submarine sliding and slumping of Miocene claystone blocks; this process is partly based on the interpretation of the inferred fault contact at 7.9 mbsf in Hole 673A as a landslide fault surface and not a thrust fault.
3. Debris flow transport and deposition of clay and claystone clasts, leading to many of the common matrix-supported conglomerates and breccias.
4. *In-situ* submarine weathering of exposed Miocene claystone causing brecciation and alteration of the rock. However, the overall importance of weathering in generating the breccias of Unit 1 remains unclear.

Unit 1 may have been deposited at two different sites, either somewhere on the accretionary complex slope or along the trench before offscraping. Determining the site of deposition will help constrain the age of accretion of this sequence. Two pieces of evidence suggest that the contact between Unit 1 and Unit 2 is an angular unconformity. An angular unconformity can only form after sediments are offscraped and tilted (i.e., not in the trench). First, bedding at the base of conglomerates in Sections 110-673B-8X-2 and -8X-3 dips 30°; beds just below the contact in Unit 2 (Section 110-673B-9X-4) dip 50°. Second, the claystones of Unit 2 just below the contact are relatively strongly deformed and compacted and thus probably did not arrive at the trench on the surface of the subducting plate. Because the overlying hemipelagic muds and marls are relatively uncompacted (determined by visual analysis), Unit 1 and Unit 2 could not have formed together at the trench and been subsequently subducted or offscraped. Therefore we interpret Unit 1 to have been deposited entirely on the slope.

One unresolved problem with our interpretation is that no ages are currently available from the matrices of conglomerates and breccias in the lower half of Unit 1 (from 38.7 to 74.1 mbsf). This is especially troublesome because conglomerate and breccia matrices are mostly carbonate-free, and where carbonate is found (e.g., silty mudstone at 67–68 mbsf), nannofossils yield Miocene ages. If the conglomerates, breccias, and slide blocks from the lower half of Unit 1 were deposited during the Pliocene and/or Pleistocene, could they have been transported without mixing in the carbonate-rich hemipelagic muds and marls? Alternatively, does the lower half of Unit 1 represent earlier deposition and should therefore be considered a separate lithologic unit?

Unit 2 is a greenish gray hemipelagic claystone. It is significantly more siliceous than the middle to lower Miocene sections recovered at either Site 671 or 672, leading to greater radiolarian biostratigraphic resolution.

Additionally, radiolarian zones are as much as ten times thicker, but the structural complexities preclude accurate comparisons of depositional rates (Fig. 15). However three general structural features can be observed in the age versus depth plot in Figure 15. First, the unconformity between 35 and 74.1 mbsf forms a clear biostratigraphic discontinuity. Repetition of sequences by thrusting is evident at 93, 200–210, and 310 mbsf. Finally, an overturned sequence appears between 131.1 and 188.1 mbsf, and a second overturned section is found below 311.6 mbsf. In addition to large-scale fold and thrust fault

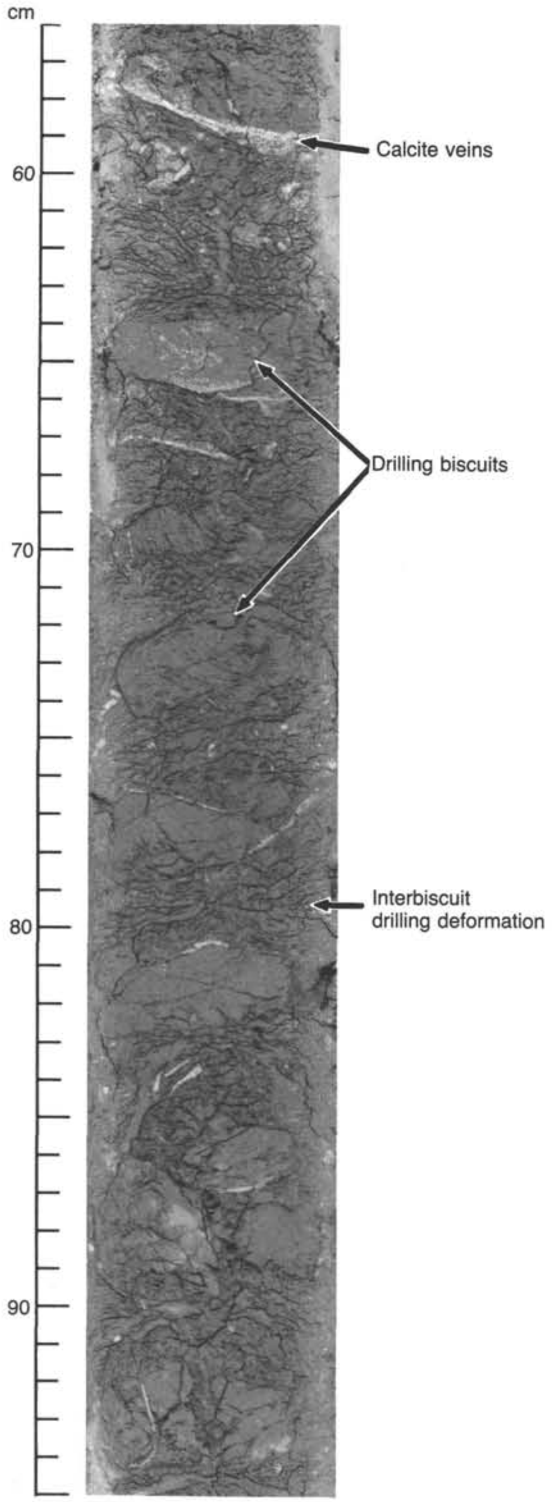

Figure 9. Photograph of Section 110-673B-24X-3, showing white calcite veins that are developed subparallel to a mild, low-angle scaly clay fabric in the drilling biscuits.

structures, this unit is locally highly deformed internally, and significantly contains syntectonic carbonate veins which may shed light on diagenesis of this unit.

Ash Occurrence

Ash intervals were recorded at Site 673 as at Sites 671 and 672 (Fig. 16). However, because of the limited stratigraphic section recovered, the usefulness of Figure 16 is restricted. Comparison of ash beds in calcareous muds and marls between Holes 673A and 673B shows poor correlation below the first bed at 0.5 mbsf, even though the holes are only 400 m apart. This observation appears to support our interpretation of highly mobile slope deposition for Unit 1.

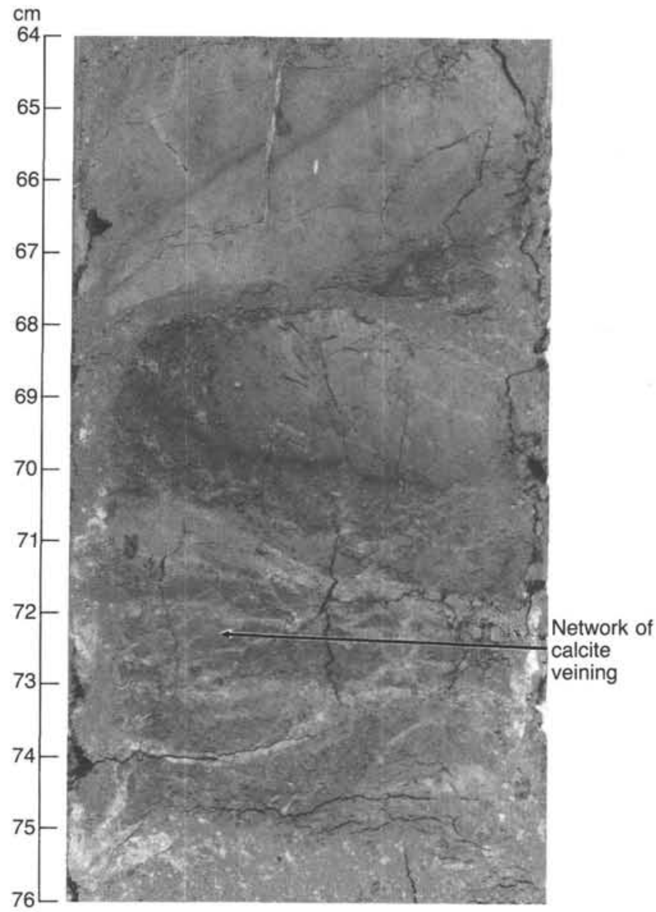

Figure 10. Photograph of Section 110-673B-23X-1, showing a network of calcite veins developed in a relatively undeformed region at 207 mbsf. Note the calcite veining along the high-angle reverse fault near the top of the picture.

Bulk Mineralogy

Sixty-eight samples from Hole 673B were analyzed for bulk mineralogy according to the X-ray diffraction methods outlined in Chapter 1, this volume. The results are presented in terms of cumulative percent of total clay minerals, quartz, plagioclase, and calcite in Figure 17.

Two major sediment types are apparent from this diagram. The first type contains roughly 20% to 40% total clay minerals, 5% to 15% quartz, 5% to 20% plagioclase, and 30% to 55% calcite. This mineralogy is characteristic of the shallowest sample analyzed (Sample 110-673B-1H-4, 71 cm, from 5.2 mbsf) and of the samples analyzed between 15 and 34 mbsf. The second major sediment type (present in samples from 5.9 to 9.6 mbsf and from 41.2 mbsf to the base of the hole) has quartz and plagioclase contents similar to those of the first sediment type, but is essentially calcite-free and has clay mineral contents ranging from 70% to 90%. Three samples analyzed from ash-rich horizons in Cores 110-673B-18X and -19X (160–172 mbsf) have unusually high plagioclase contents (30%–60%). In addition, percentage plagioclase is slightly lower (0%–12%) at depths greater than 222 mbsf.

Figure 11. Photograph of Section 110-673B-28X-6, showing networks of large fractures infilled by black, fine-grained material that is thought to be an amorphous manganese phase. The occurrence of this black phase is also a feature of the stratigraphic horizon that is located within the décollement zone in Hole 671B (263 mbsf).

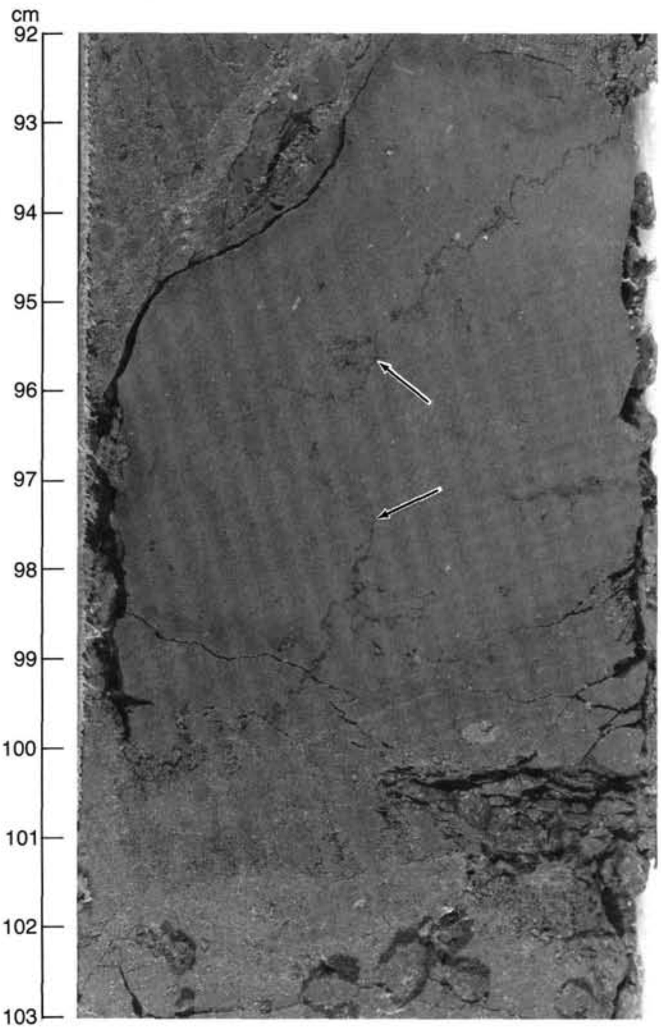

Figure 12. Photograph of Section 110-673B-19X-3, showing dendritic veins (arrows) containing the black, possibly manganese, amorphous phase (173 mbsf). Thin sections reveal that the veins are not styolitic features and contain an amorphous phase not yet identified.

The calcite-rich sediment type is representative of the marls in the hemipelagic slope sediments of the upper portion of lithologic Unit 1. All of the marls analyzed for mineralogy are of late Pliocene or early Pleistocene age. In addition to these calcareous sediments, the lower half of Unit 1 contains Miocene claystone, both as large blocks and in conglomerates and breccias. These probably reworked claystones are of the second sediment type identified by X-ray mineralogy. The Miocene claystones of lithologic Unit 2 are of the second sediment type. These claystones are mineralogically homogeneous despite intense faulting of the section and are very similar in bulk mineralogy to lower and middle Miocene claystones sampled at Sites 671 and 672 (see the respective site summary chapters, this volume).

BIOSTRATIGRAPHY

Biostratigraphic Summary

The biostratigraphy at Site 673 is influenced by tectonic deformation within the Barbados accretionary wedge. Recovered sediments range in age from early Miocene to early Pleistocene. Thrust faulting and folding have caused the repetition and consequent thickening of the lower Miocene section. This interval is composed of siliceous clay that is overlain by a thin package of carbonate sediments of Pliocene/Pleistocene age. Middle and upper Miocene sediments are not observed at this site.

The lower Miocene siliceous clays were deposited below the paleo-CCD and therefore contain few carbonate microfossils. Radiolarian faunas are abundant and well preserved and provide excellent age resolution throughout this interval. The carbonate sediments at the top of the section yield both planktonic foraminifers and calcareous nannofossils of moderate to good preservation.

The lower Miocene section is greatly expanded between Samples 110-673B-8X-1, 142–144 cm through -35X, CC. Evidence that this interval has been tectonically thickened is given by multiple reversals of the biostratigraphic sequence. Radiolarian zones were frequently repeated (see Fig. 18) and identify the location of thrust faults and folds within the sequence.

Carbonate-rich sediments occur between Samples 110-673B-1H, CC and -5H-2, 79–81 cm. They range in age from early Pleistocene to late Pliocene. A missing sedimentary section was indicated near the Pliocene/Pleistocene boundary between Samples 110-673B-5H-1, 79–82 cm and -5H-2, 79–81 cm by the absence of nannofossil zones. Missing foraminifer zones are detected between Samples 110-673B-3H, CC and -4H, CC. Intervals barren of siliceous and carbonate microfossils occur in Sections 110-673B-5H, CC through -7X, CC and between Sections 110-673B-21X, CC and -25X, CC.

Calcareous Nannofossils

Carbonate sediments at Site 673 are confined almost entirely to the interval between Samples 110-673B-1H-1, 80–82 cm and -5X-2, 79–81 cm. This interval is carbonate rich and contains well-preserved nannofossil floras which range in age from early Pleistocene to late Pliocene. Nannofossiliferous sediments at the top of the hole overlie nearly 300 m of siliceous clay which is virtually barren of carbonate microfossils.

Samples 110-673B-1H, 80–82 cm through -3H-4, 80–82 cm are early Pleistocene in age based on specimens of *Pseudoemiliania lacunosa* without *Helicosphaera sellii* and are assigned to the *Pseudoemiliania lacunosa*/small gephyrocapsa Zone of Gartner (1977). Zonal resolution was difficult for this interval owing to intervals of low fossil abundance and poor preservation. In contrast, Samples 110-673B-3H-5, 80–82 cm and -4H-2, 80–82 cm contain an abundant and well-preserved assemblage of nannofossils and are assigned to the early Pleistocene *Helicosphaera sellii* Zone of Gartner (1977). *H. sellii, Pseudoemiliania lacu-*

Table 2. Lithologic units at Site 673.

Unit	Lithology	Core Range (core-section)	Depth (mbsf)	Age
1	Interbedded calcareous mud and marl with matrix-supported conglomerates and breccias and claystone blocks. Locally altered by submarine weathering.	673A: 1H-1 to 4H, CC 673B: 1H-1 to 8X, CC	0–36.4 0–74.1	early Pleistocene to late Pliocene plus indeterminate
2	Greenish gray claystone and mudstone, often siliceous; massive and structureless.	673B: 9X-1 to 35X, CC	74.1–330.6	early Miocene

nosa, Gephyrocapsa carribeanica, and *G. oceanica* are common assemblage components. Oligocene taxa are reworked in Cores 110-673B-2H and -3H. Samples 110-673B-4H-3, 80–82 cm through -4H-5, 80–82 cm are placed within the *Calcidiscus macintyrei* Zone of Gartner (1977) owing to the presence of *C. macintyrei*.

Samples 110-673B-4H-6, 80–81 cm through 5H-1, 79–82 cm are Pliocene in age and are assigned to the *Discoaster brouweri* Zone CN12 of Okada and Bukry (1980). *D. brouweri* is present in Samples 110-673B-4H-6, 80–82 cm through 5H-1, 79–81 cm without *D. pentaradiatus*, which suggests the subzonal designation of CN12d. Missing sedimentary section is indicated by a biostratigraphic gap between Samples 110-673B-5H-1, 79–82 cm and -5H-2, 79–81 cm. The *D. pentaradiatus* and *D. surculus* subzones of Okada and Bukry (1980) were not identified. Sample 110-673B-5H-2, 79–81 cm is placed within the *D. tamalis* subzone (12a) of Okada and Bukry (1980) owing to the presence of *D. tamalis* without *Reticulofenestra pseudoumbilica*.

Below Sample 110-673B-5H-2, 79–81 cm the sediments are nearly barren of carbonate microfossils. Rare intervals of early Miocene carbonate occur in Samples 110-673B-8X-2, 142–144 cm, 8X-3, 29–31 cm, -17X-4, 127–130 cm, and -18X-3, 30–32 cm. These intervals are assigned to Zone CN3 of Okada and Bukry (1980) based on the presence of *Helicosphaera ampliaperta* and *Sphenolithus heteromorphus* without *S. belemnos*.

Planktonic Foraminifers

The great majority of sediments drilled at Site 673 were deposited below the CCD. As a result, only four cores yielded planktonic foraminifers.

Cores 110-673A-1H through -4H are barren of foraminifers, except very rare fragments of *Globorotalia* cf. *tumida* (Pleistocene–late Pliocene) observed in Section 110-673A-1H, CC.

Sections 110-673B-1H, CC through -3H, CC are early Pleistocene in age. Sample 673B-1H, CC contains sparse and poorly-preserved foraminifers including *Globorotalia truncatulinoides, G. crassaformis, Globigerinoides trilobus, Pulleniatina obliqueloculata* and *Neogloboquadrina dutertrei*. No zonal assignment is possible from this assemblage.

In contrast, the rich and well-preserved microfaunas identified in Sections 110-673B-2H, CC and -3H, CC can be placed within the early Pleistocene, *Globorotalia hessi* subzone of the *G. truncatulinoides* Zone, owing to the occurrence of frequent and typical specimens of the subzonal marker. The *Globorotalia menardii–G. tumida* complex (including abundant *G. tumida flexuosa*) is well represented in Sample 110-673B-2H-CC, while *G. truncatulinoides* is lacking. This "mutual incompatibility" between the two taxa, previously noted by Hemleben and Auras (1984) within the same biostratigraphic interval in Holes 541 and 543, is also confirmed in Section 110-673B-3H, CC; there, *G. truncatulinoides* is frequent and the *G. menardii-G. tumida* complex is absent.

The earliest Pleistocene, *Globorotalia viola* subzone of the *G. truncatulinoides* Zone, has not been identified.

The Pleistocene/Pliocene boundary, as defined by the last downhole occurrence of *G. truncatulinoides*, is between Sections 110-673B-3H, CC and -4H, CC.

Section 110-4H, CC is assigned to the late Pliocene, *Globorotalia tosaensis* Zone, on the basis of the presence of the zonal marker and the absence of either *G. miocenica* or *G. exilis. Globigerinoides ruber, G. conglobatus, G. trilobus, G. sacculifer, Globorotalia menardii, G. scitula, Neogloboquadrina dutertrei, Pulleniatina obliqueloculata*, and *Sphaeroidinella dehiscens* are among the dominant forms found in this sample.

Cores 110-673B-5H through -35X are barren of foraminifers.

Radiolaria

Hole 673A

Samples 110-673A-1H-3, 56–57 cm through -3H-3, 70–72 cm are barren of radiolarians. In Sample 110-673A-3H-5, 70–72 cm, radiolarians are moderately preserved but are rare and lack age indicaters.

In Samples 110-673A-3H-6, 70–72 cm through -4H, CC, radiolarians are frequent and occur with moderate quality of preservation. The radiolarian assemblages are almost the same except that Samples 110-673A-4H-05, 46–47 cm and -4H, CC contain rather common *Calocycletta costata* and *Calocycletta virginis*. They are assigned to the *Dorcadospyris alata* Zone of Reidel and Sanfilippo (1978), which is late early Miocene or early middle Miocene in age.

Hole 673B

Samples 110-673B-1H-4, 68–70 cm through -8X-2, 74–75 cm are barren of radiolarians except for the trace occurrence of reworked specimens from the Eocene and Oligocene in Cores 110-673B-2H and -3H. Sample 110-673B-8X-3, 74–75 cm could not be assigned because of few occurrences of radiolarians.

In Samples 110-673B-8X-4, 74–75 cm through -21X-1, 66–67 cm and Sections 110-673B-26X, CC through -35X, CC, radiolarians are common to abundant and occur in highly diverse assemblages of moderate to good preservation. Samples 110-673B-21X, CC through -26X-3, 12–15 cm are barren.

Sample 110-673B-8X-4, 74–75 cm and Section -8X, CC are assigned to the *Calocycletta costata* Zone. *C. costata, Liriospyris stauropora, Liriospyris parkerae, Dorcadospyris dentata*, and *Dorcadospyris alata* are present. *D. dentata* is consistently more abundant than its descendent, *D. alata*.

Samples 110-673B-9X-1, 67–68 cm through -10X, CC are assigned to the *Stichocorys wolffii* Zone because of the presence of *S. wolffii* and the absence of *C. costata*.

Samples 110-673B-11X-1, 62–63 cm and -13X-3, 7–10 cm are placed in the lowest part of the *Dorcadospyris alata* Zone owing to the presence of *C. costata, D. alata*, and *Cannartus laticonus*, and the absence of *D. dentata*.

Sections 110-673B-13, CC through -14X, CC are assigned to the *Calocycletta costata* Zone because of the presence of *C. co-*

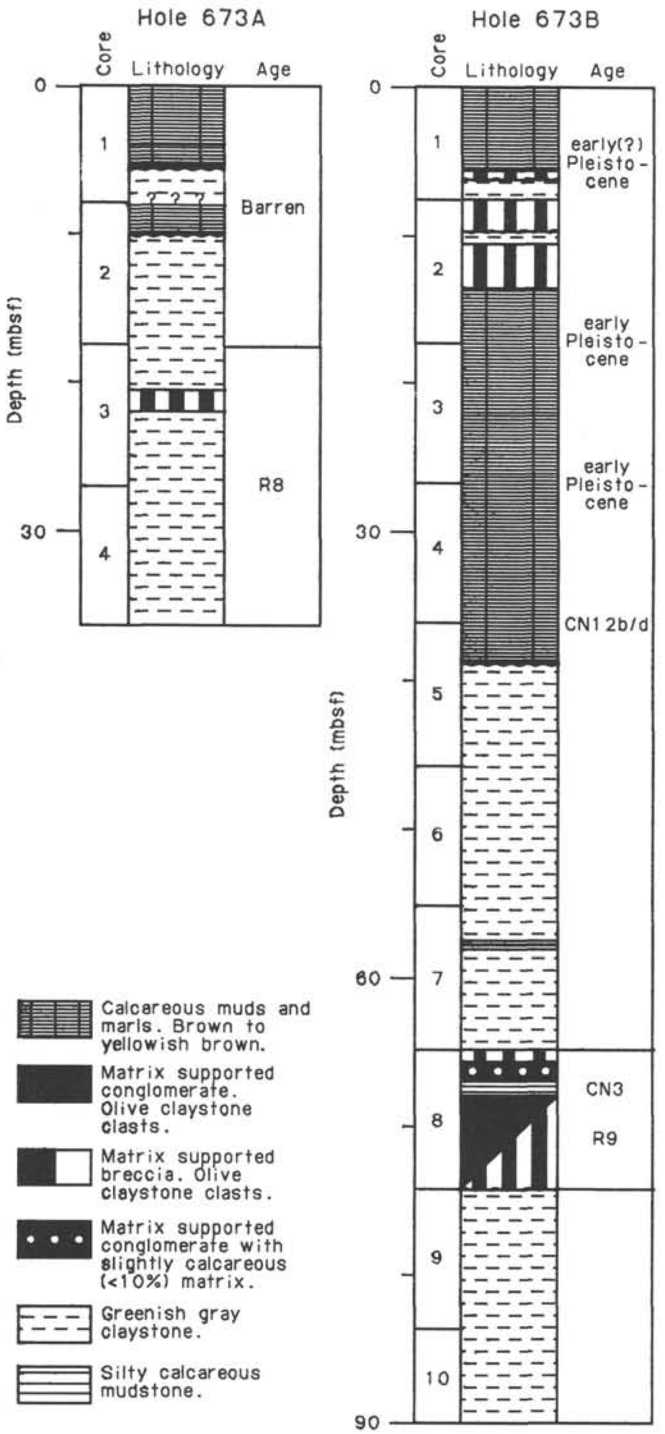

Figure 13. Schematic diagram of slope facies recovered in Holes 673A and 673B. The positions of fossil age determinations are indicated, to emphasize the ambiguity of determining the age of the slope deposits.

stata and *D. dentata* and the absence of *D. alata*. The first appearance of *L. parkerae*, which subdivides the upper part of the *Calocycletta costata* Zone, is found in Section 110-673B-13X, CC.

Samples 110-673B-15X-4, 72–74 cm through -16X, CC are assigned to the upper part of the *Stichocorys wolffii* Zone owing to the presence of *S. wolffii* and *D. dentata* and the absence of *C. costata*.

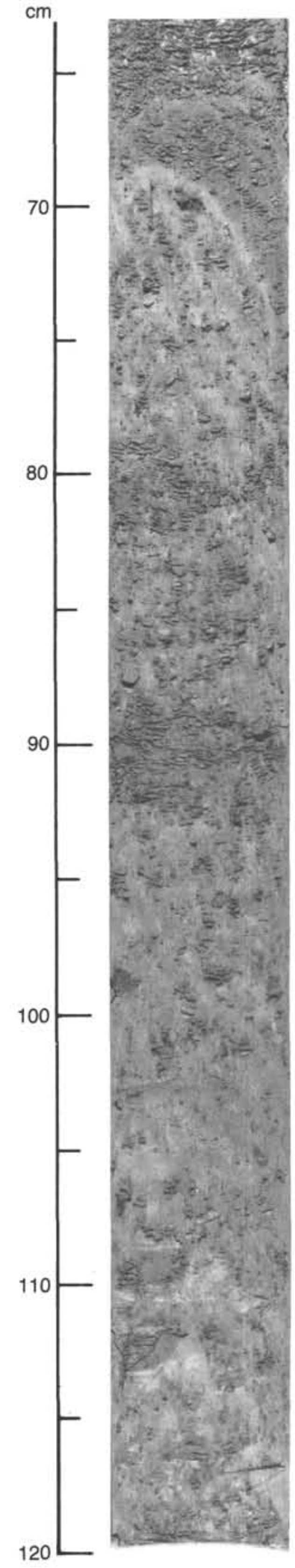

Figure 14. Photograph of claystone-clast breccia from Sample 110-673B-2H-4, 63–120 cm. Gravel-sized clasts are clearly harder than the surrounding matrix, although the lithologies appear similar.

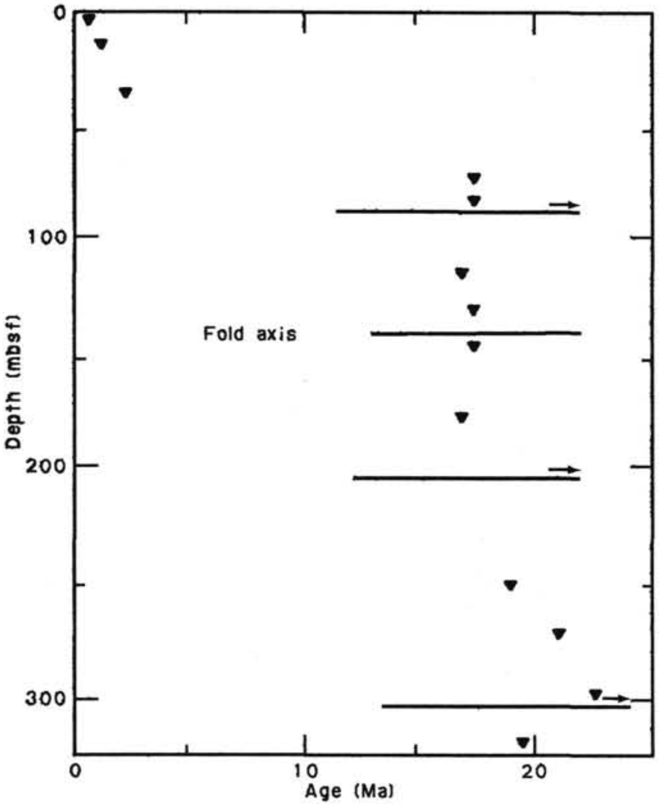

Figure 15. Age vs. depth plot from biostratigraphic age determinations.

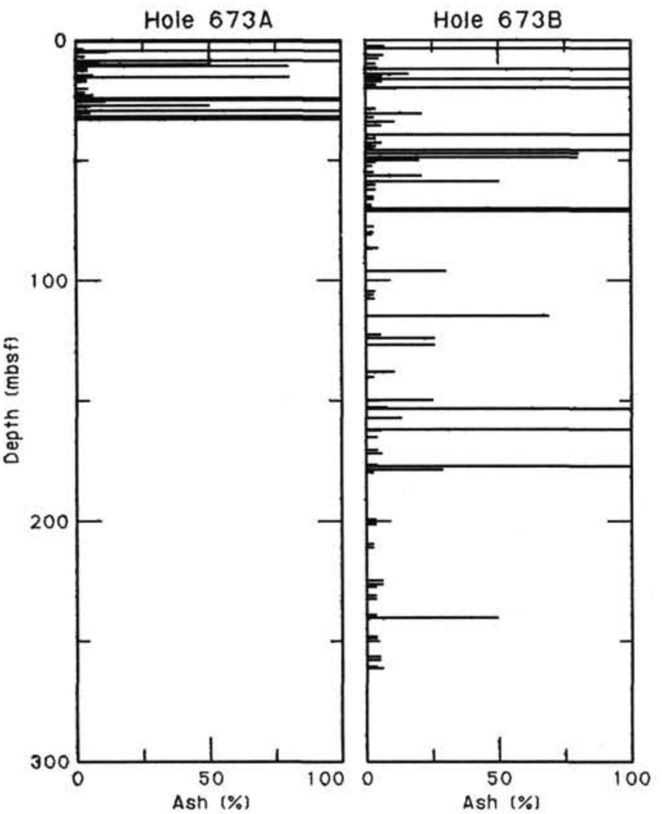

Figure 16. Concentration of ash vs. depth for Holes 673A and 673B.

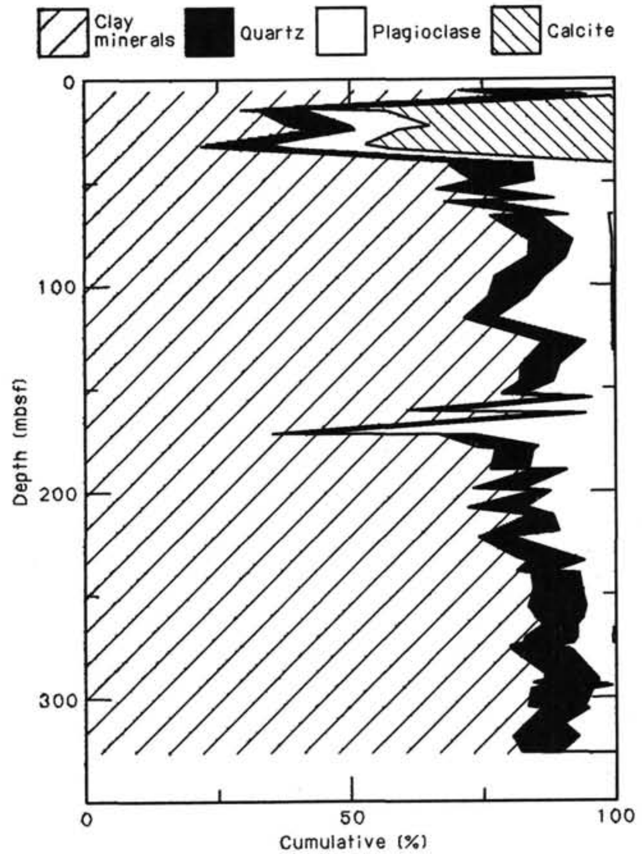

Figure 17. Bulk mineralogy of Site 673 samples expressed as cumulative percentages of total clay minerals, quartz, plagioclase, and calcite.

Samples 110-673B-17X-1, 61–64 cm through -19X-6, 62–63 cm are assigned to the *Calocycletta costata* Zone. In Samples 110-673B-17X-1, 61–64 cm and -18X, CC, *Carpocanopsis cingulata, L. stauropora* and *D. dentata* occur as well as *C. costata* and *L. parkerae*, without notable quantities of *D. alata*. In Samples 110-673B-19X-1, 62–63 cm and -19X-2, 62–63 cm, *C. cingulata* is absent. In Samples 110-673B-19X-3, 62–63 cm through -19X-6, 62–63 cm, *C. cingulata* is also absent and *L. parkerae* is more abundant than its ancestor, *L. stauropora*.

In Section 110-673B-19X, CC, *D. alata* occurs in equal numbers as its ancestor, *D. dentata*, with the co-occurrence of *C. costata* and *L. parkerae*. Samples 110-673B-19X, CC through -21X-1, 45-46 cm are therefore assigned to the basal part of the *Dorcadospyris alata* Zone.

After the barren interval (Samples 110-673B-21X, CC through -26X-3, 12–15 cm), radiolarians occur again below Section 110-673B-26X-CC.

Sections 110-673B-26X, CC through -27X, CC are assigned to the lower part of *Stichocorys wolffii* Zone because of the presence of *S. wolffii* and the absence of *C. costata. L. stauropora*, and *D. dentata* co-occurred in Section 110-673B-26X, CC, but both are not there.

Cores 110-673B-28X-1, 27–29 cm through -29X are assigned to the *Stichocorys delmontensis* Zone. *S. delmontensis* and *Carpocanopsis bramlettei* are present and *S. wolffii* is absent. The top of *Dorcadospyris ateuchus* Zone is found in Sample 110-673B-28-7, 25–27 cm.

Samples 110-673B-30X-1, 88–89 cm through -33X, CC are assigned to the *Cyrtocapsella tetrapera* Zone owing to the presence of *C. tetrapera, C. cornuta, C. cingulata, Lychnocanoma elongata*, and *D. ateuchus* and the absence of *S. delmontensis,*

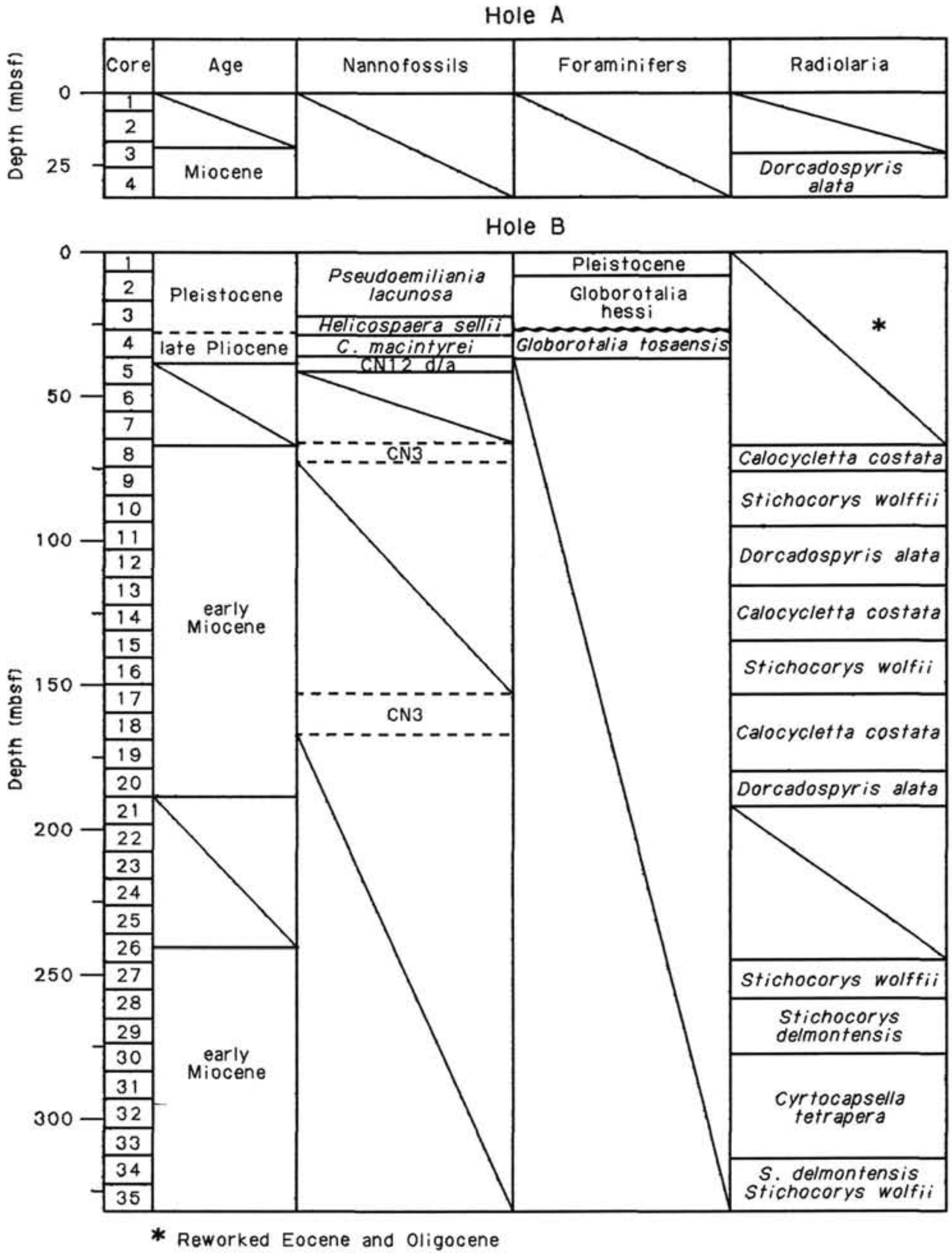

Figure 18. Biostratigraphic summary, Site 673.

C. bramlettei, and *S. wolffii*. In Samples 110-673B-31X-4, 86–88 cm through -33X, CC, *Calocycletta serrata* is found.

Samples 110-673B-34X-1, 23–25 cm through -34X-7, 25–27 cm are assigned to the upper part of *S. delmontensis* Zone. *S. delmontensis* and *C. bramlettei* are present and *S. wolffii* and *D. ateuchus* are absent.

Sections 110-673B-34X, CC through -35X, CC are assigned to the lower part of *Stichocorys wolffii* Zone, because of the presence of *S. wolffii, S. delmontensis*, and *C. cingulata* and the absence of *C. costata, D. dentata*, and *L. stauropora*.

The repetitions and reversal arrangement of the zones (Fig. 18) may subdivide the section below Core 110-673B-8X into the following four packages.

1. Samples 110-673B-8X-4, 74–75 cm through -10X, CC: normal sequence, *C. costata* Zone to *S. wolffii* Zone.
2. Samples 110-673B-11X-1, 62–63 cm through -26X-3, 12–15 cm: a) above Core 110-673B-16X: normal sequence, lower part of *D. alata* Zone to *S. wolffii* Zone; b) below Core 110-673B-16X: reversed sequence, *S. wolffii* Zone to the middle Miocene radiolarian barren zone (see Note below).
3. Sections 110-673B-26X, CC through -33X, CC: normal sequence, *S. wolffii* Zone to *C. tetrapera* Zone.
4. Samples 110-673B-34X-1, 86–88 cm through -35X, CC: reversed sequence, upper part of *S. delmontensis* Zone to *S. wolffii* Zone.

Note: Sections 110-673B-21X, CC through -26X-2 are not assigned to any age owing to the nonfossiliferous character of the sediments. This interval may be middle Miocene, however, by virtue of the fact that it is barren. In previous sites—Sites 671 and 672 of this Leg and Sites 541 and 543 of DSDP Leg 78 — the middle Miocene interval is nonfossiliferous and defined at its base by radiolarian-rich lower Miocene sediments which are placed around the top of the *C. costata* Zone or the lower part of *D. alata* Zone. The same relation, although inverted, is shown in Cores 110-673B-20X to -21X. Oligocene and Eocene sediments are more or less fossiliferous.

PALEOMAGNETICS

Samples were taken for paleomagnetic analysis from both Holes 673A and 673B. The objectives of the paleomagnetic measurements are outlined in the Paleomagnetics Section of the Site 671 chapter, this volume. Whole-core susceptibility measurements were performed on some of the initial cores from each hole, although these measurements were discontinued when it became apparent that the hole penetrated a structurally complex sequence (Fig. 19).

Remanence Measurements

The methods and instrumentation used in the remanence measurements are outlined in Chapter 1. All of the samples from this site were demagnetized on board ship. The NRM intensity and inclinations for Holes 673A and 673B are shown in Figures 20, 21, and 22. The samples dominantly have steep NRM inclinations largely reflecting the drilling-induced remanence which, in the majority of the samples, forms a major component of the remanence. The types of sample behavior during demagnetization are essentially similar to those described for Site 671, although a larger proportion of samples do not show a well-defined stable end point as in Figure 23, but rather progressive planar movement even at the highest demagnetization fields (Figs. 24, 25, 26, and 27). Those samples with weaker NRM intensities do not tend to show the rapid decrease of intensity during demagnetization that occurs in the samples with stronger NRM intensities (Figs. 23 and 28). A small proportion of samples have shallow NRM intensities and shallow high coercivity components (i.e., the component present at high demagnetization fields, which the demagnetization process is attempting to isolate), and some have directions which may move little during demagnetization (Figs. 28 and 29). In common with Site 671, the Pleistocene and Pliocene calcareous muds and marls and Miocene greenish gray claystones tend to have NRM intensities above 10 mA/m. The Miocene siliceous claystones generally have much lower NRM intensities, reflecting the lesser detrital input (Fig. 22A).

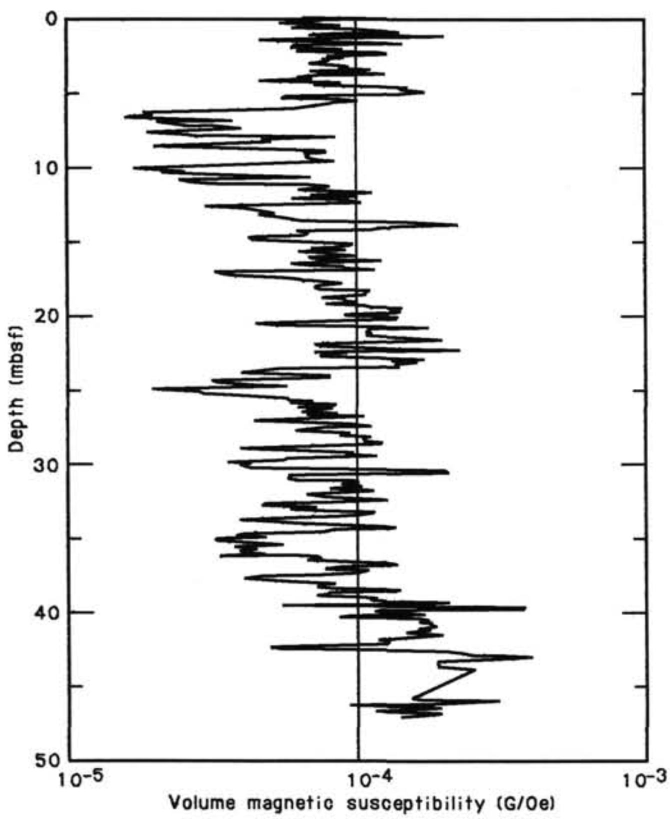

Figure 19. Whole-core susceptibility data for Hole 673B.

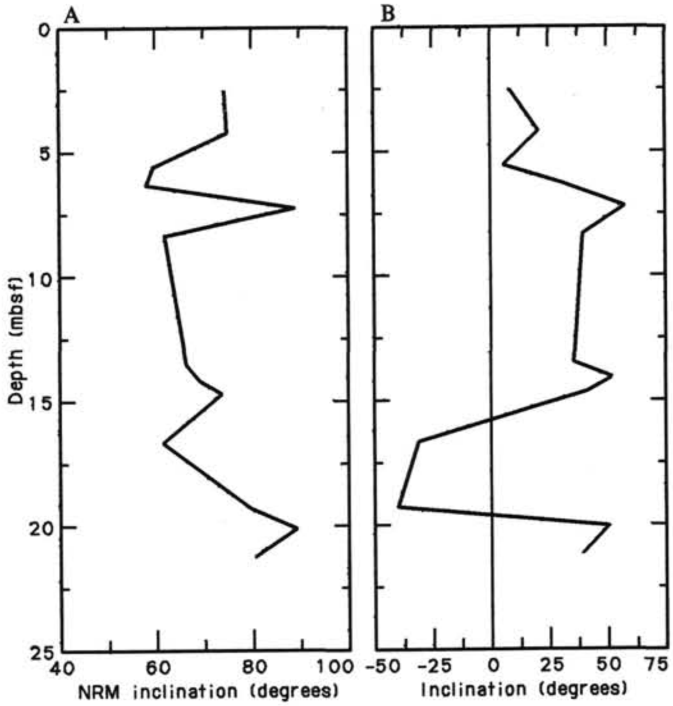

Figure 20. A. NRM inclination and B. high-coercivity component inclination for samples from Hole 673A.

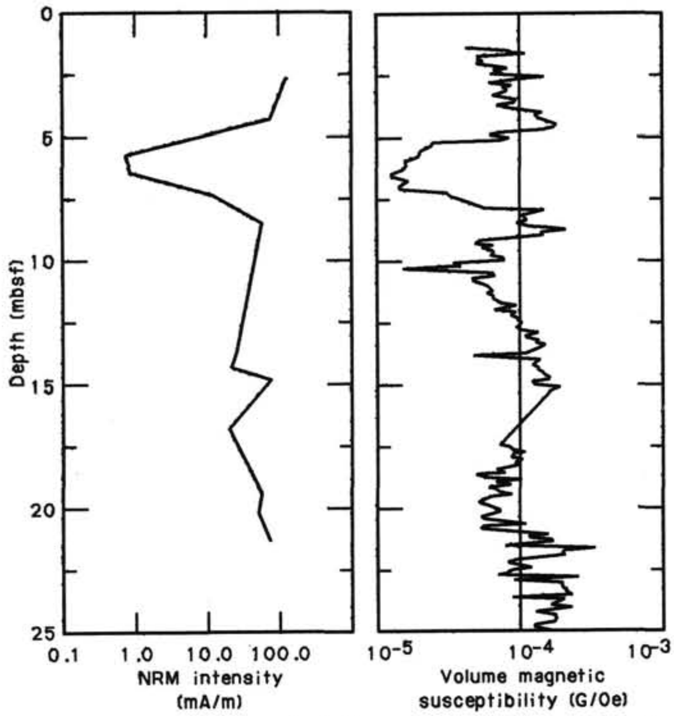

Figure 21. NRM intensity and whole-core magnetic susceptibility for Hole 673A.

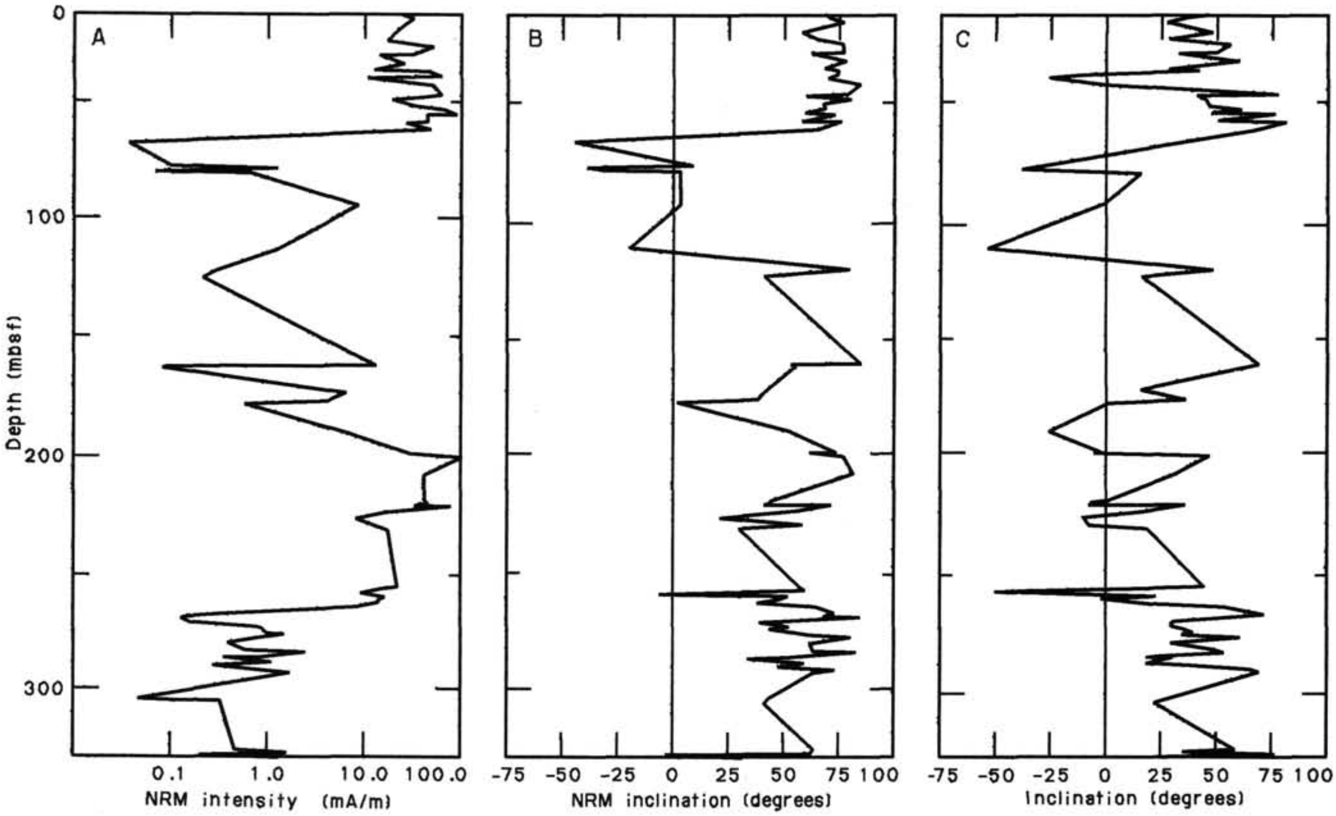

Figure 22. A. NRM intensity. B. NRM inclination. C. High-coercivity component inclination for samples from Hole 673B. Those samples not showing a stable high-coercivity component or not demagnetized are not represented in C.

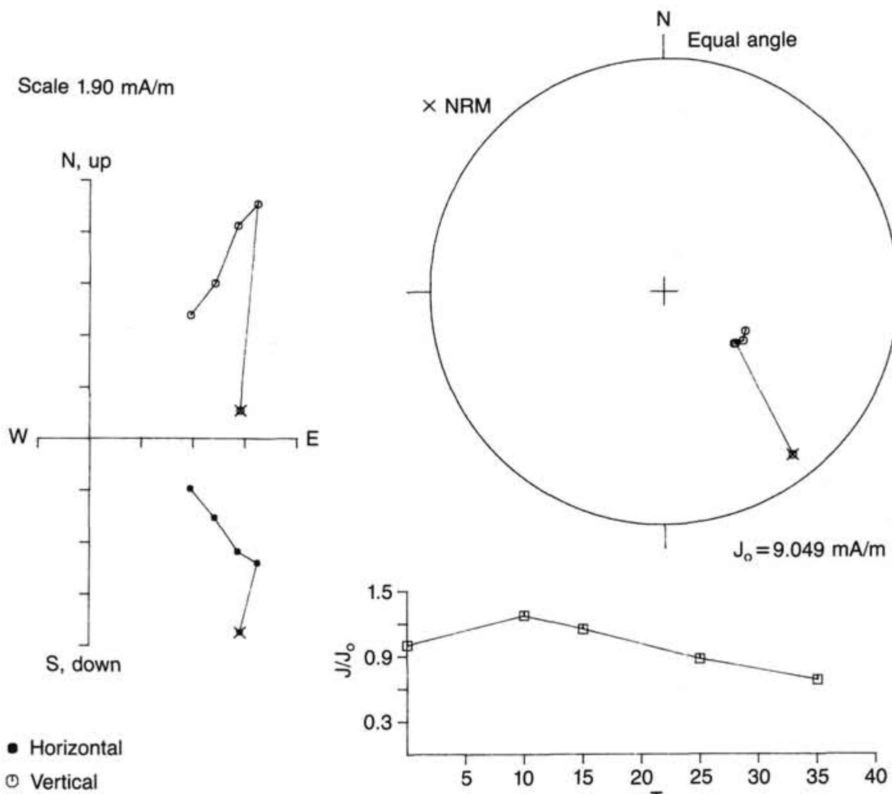

Figure 23. Demagnetization data for Sample 110-673B-28X-3, 2 cm, which indicates that this sample has a well defined, negative inclination, stable end point.

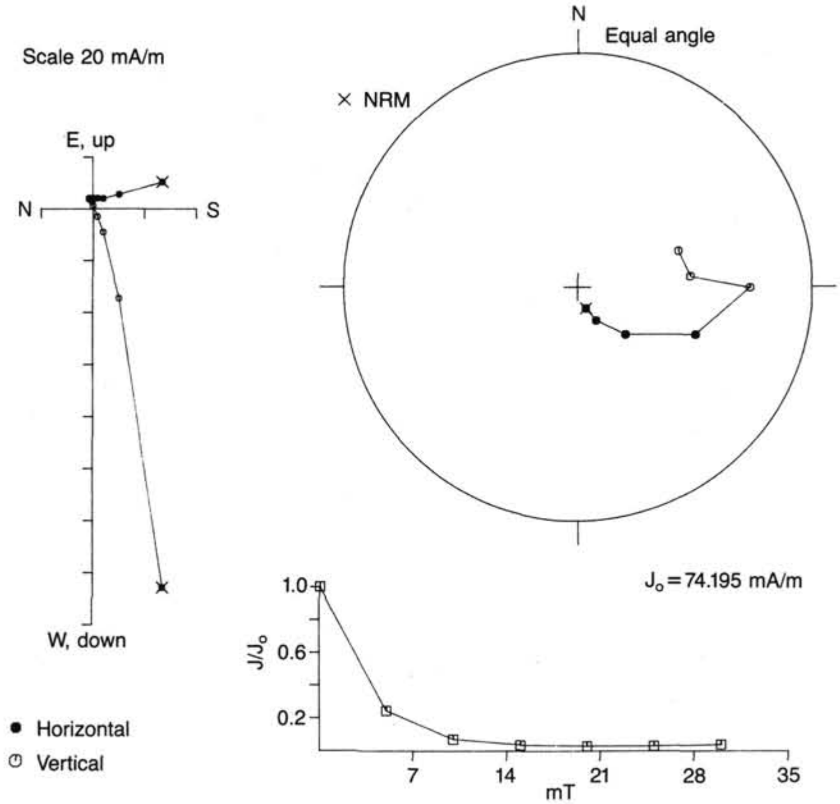

Figure 24. Demagnetization data for Sample 110-673A-3H-4, 25 cm (see Site 671 chapter, Paleomagnetics section, Figure 24, for the explanation of diagrams). This sample displays a very rapid reduction of the intensity with demagnetization, and a negative high-coercivity component.

The high-coercivity components of magnetization extracted from the sample demagnetization data (using criteria outlined in Paleomagnetics Section, Site 671 chapter) have generally positive inclinations greater than 25°, which for the section below 250 mbsf in Hole 674B (Fig. 22C) are little different from the NRM inclinations.

GEOCHEMISTRY

Introduction

Site 673 was drilled near the proposed Site LAF 3, i.e., upslope from Site 671. In this report we present a brief summary of the geochemical data obtained in Holes 673A and 673B.

Inorganic Geochemistry

The data are presented in Tables 3 and 4 as well as in Figure 30.

Discussion

Chloride

The concentration gradient of dissolved chloride shows a great deal of complexity (Fig. 30). In Hole 673A a small subsurface minimum was observed, but this site was soon abandoned.

Below 50 mbsf in Hole 673B, chloride concentrations decrease with an especially steep gradient between 105 and 136 mbsf. Below 200 mbsf a maximum occurs, followed by a sharp minimum at 290 mbsf. We are convinced that these data are essentially correct, as special precautions were taken to avoid contaminating the samples, and initial squeezing pressures were always relatively low. Therefore, we suggest that in these sediments, which show signs of tectonic activity, conduits for the advection of lower salinity waters may develop, tapping essentially the same low-salinity source as Sites 671 and 672. Indeed, faults have been postulated to occur at about 90 mbsf, 200 mbsf, and 290 mbsf (see Structural Geology, this chapter). The low-chloride concentrations are especially noticeable at the thrust faults T_2 and T_3. Relatively constant chloride concentrations occur between 140 and 200 mbsf in a vertically folded section probably caused by thrusting. The injections of low-salinity waters must have occurred during the last 200,000 years or so, recently enough that diffusion has not erased the changes ($(2Dt)^{1/2}$ = 50 m, with the diffusion coefficient D = 2.0E-6 cm^2/s). Similar arguments apply to the low-chloride concentrations at 290 mbsf.

Calcium and Magnesium

The calcium and magnesium concentration gradients (Fig. 30) are characterized by respectively sharp increases or decreases with depth in the upper 80 m of the sediment column. Slight upward curvature indicates uptake of Mg and release of Ca in the upper Pleistocene section, but to a large extent the gradients are created by the relatively high Ca and the relatively low Mg concentrations below 80 mbsf. Compared to Site 671, the overall depletion of Mg is significantly greater in the deeper sediment column, and remains remarkably constant. Similarly, calcium concentrations below 80 m are almost constant and co-vary with chloride, i.e., show dilution effects. Any effects of transport across the much deeper seated décollement, located almost 1000 m below the cored sections, cannot be identified.

Sodium and Potassium

The concentration profile of (Na + K) is given in Fig. 30 and is to some extent affected by the expected decrease in K (no more than 10 mmol/L), but mostly by the dilution process leading to low chlorides. Typically the ratio of (Na + K)/Cl (Fig. 30)

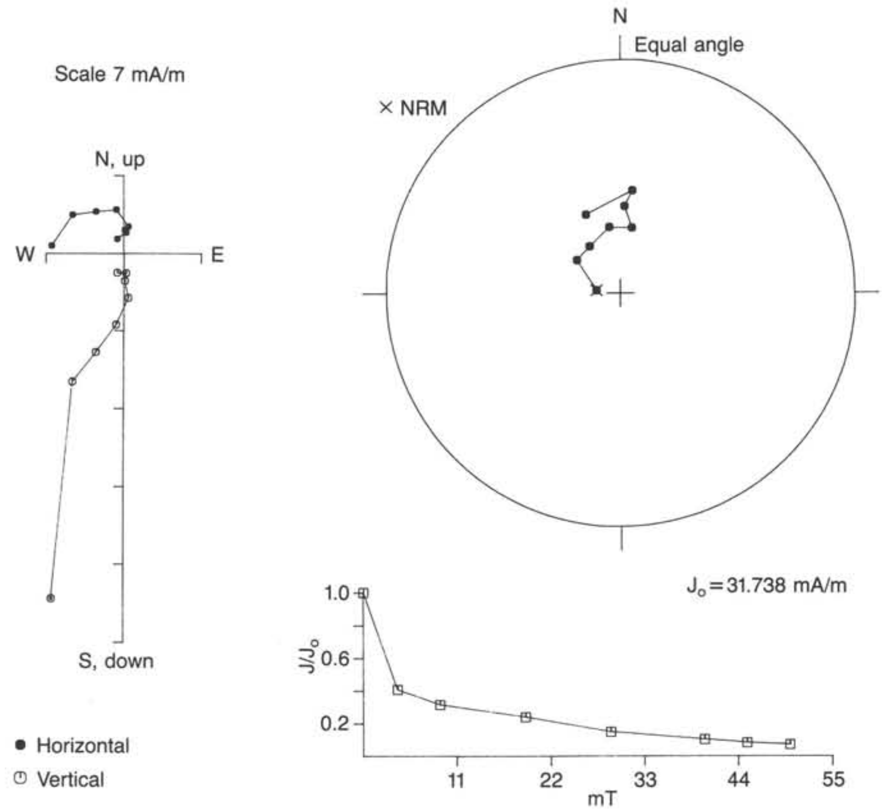

Figure 25. Demagnetization data for Sample 110-673B-4H-2, 123 cm. This sample possesses a steep, high-coercivity component.

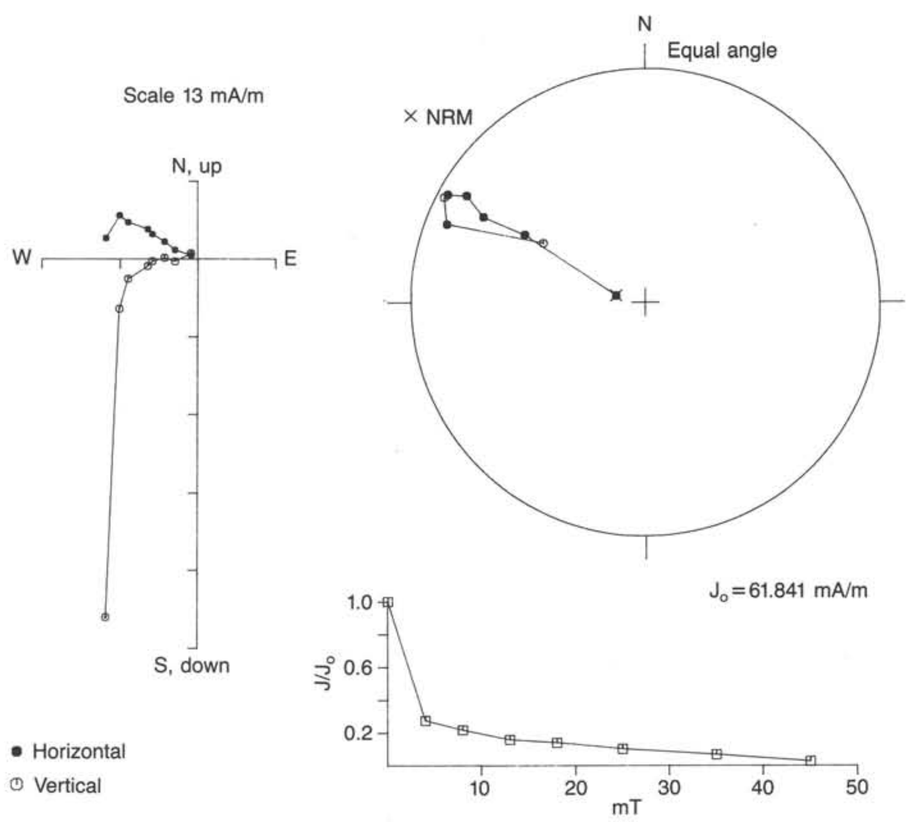

Figure 26. Demagnetization data for Sample 110-673B-5H-2, 90 cm, which indicates a probable shallow, negative high-coercivity component. This strongly overlaps a positive component, as seen by the strongly curved demagnetization path on the vertical projection of the Zijderveld plot.

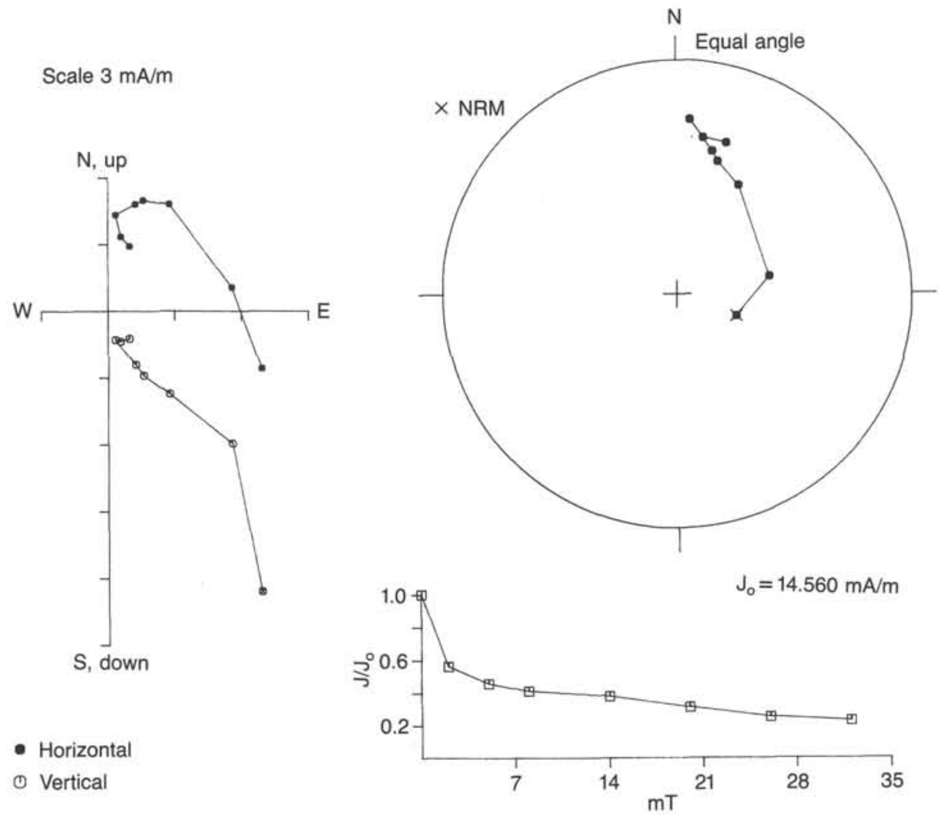

Figure 27. Demagnetization data for Sample 110-673B-28X-2, 37 cm.

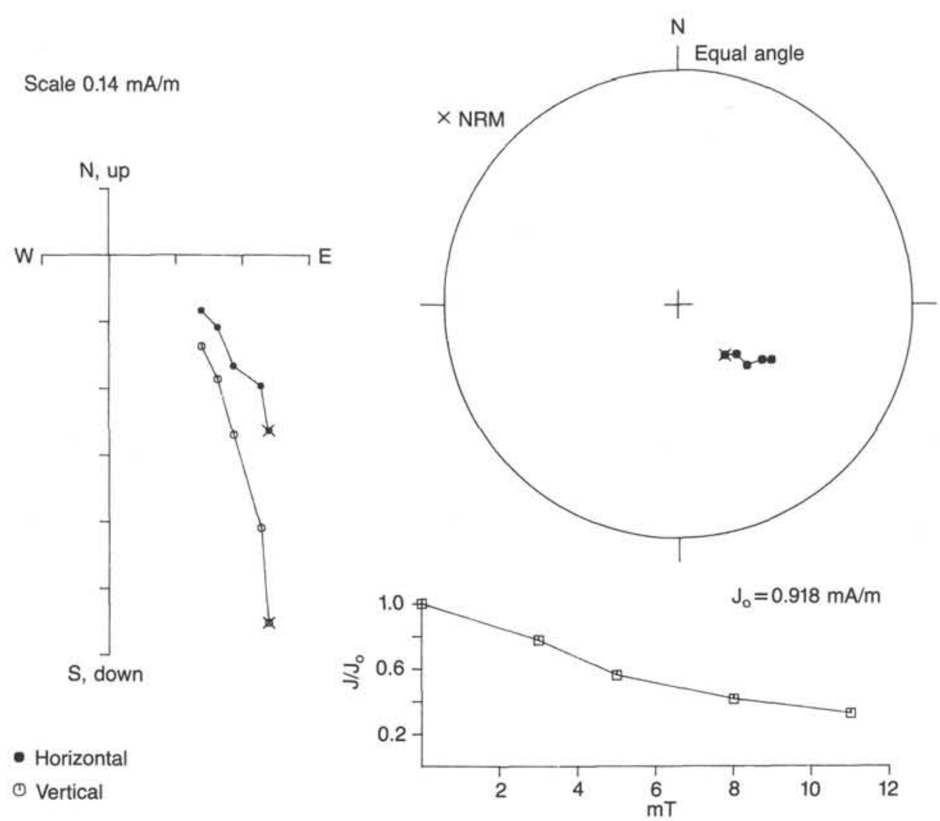

Figure 28. Demagnetization data for Sample 110-673B-30X-2, 18 cm, which shows a small amount of planar movement on the stereonet, and curved demagnetization paths on the Zijderveld diagram, perhaps indicating that it has not reached a stable end point.

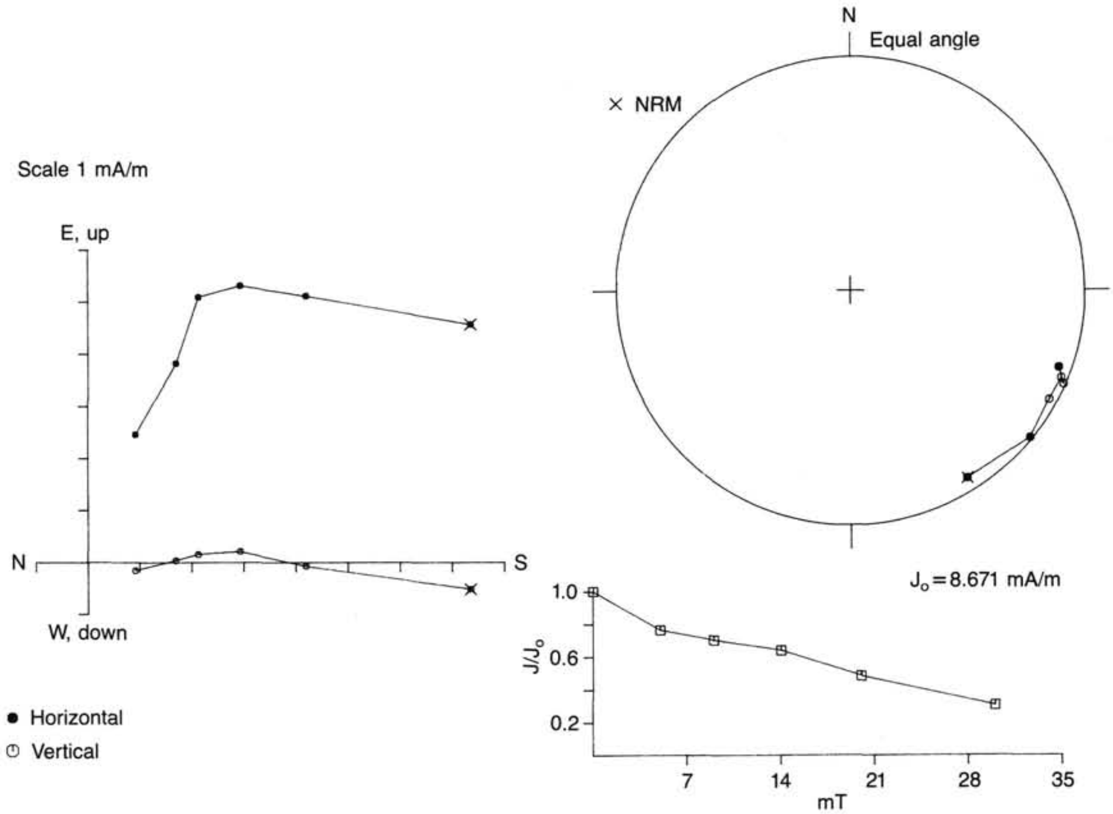

Figure 29. Demagnetization data for Sample 110-673B-11X-1, 97 cm, which has a shallow NRM inclination and a shallow high-coercivity component.

Table 3. Interstitial water pH, alkalinity, salinity, and chlorinity data, Site 673.

Core 110-	Section	Interval (cm)	Depth (mbsf)	pH	Alkalinity (mmol/L)	Salinity (‰)	Chlorinity (mmol/L)
Hole 673A							
1	4	145-150	6	7.24	2.79	34.5	552
2	5	145-150	16	8.18	2.76	33.5	535
3	6	145-150	28	8.25	2.41	33.8	547
4	2	145-150	35	8.33	2.93	33.8	556
Hole 673B							
1	4	145-150	6	7.79	2.88	34.7	549
2	5	145-150	15	8.08	2.65	34.5	559
3	5	145-150	24	n.d.	2.46	n.d.	569
4	5	145-150	34	7.79	1.37	34.0	563
5	4	145-150	42	8.20	2.18	33.5	559
7	1	145-150	57	n.d.	1.49	33.0	555
9	3	145-150	79	7.96	1.74	32.2	551
12	2	140-150	105	8.10	3.01	32.0	549
15	5	140-150	136	7.96	3.62	30.0	512
18	2	140-150	164	n.d.	n.d.	29.5	513
22	2	140-150	200	n.d.	n.d.	28.2	505
25	4	140-150	230	n.d.	n.d.	31.0	541
28	5	140-150	260	7.73	2.97	32.2	543
31	6	140-150	290	n.d.	n.d.	28.2	491
34	5	140-150	318	7.66	3.17	32.5	548

n.d. = not determined.

shows minor changes with depth, again confirming that any effects of the deeply buried basement on the overlying sediment column are not noticeable at these relatively shallow depths.

Sulfate and Ammonia

Sulfate depletions in Hole 673B are considerably larger than at Site 671 (Fig. 30), as are the increases in ammonia (Fig. 30). This is mostly because a longer period of effective isolation owing to folding and thrusting has caused a diminished resupply of sulfate from the overlying ocean. This in turn will enable bacterial reduction of sulfate to be more efficient in removing sulfate from the interstitial waters. Below 200 mbsf SO_4 reduction is complete.

Silica

The dissolved silica profile (Fig. 30) again reflects the lithology. Higher values below 75 mbsf are mainly owing to the higher content of amorphous silica (radiolaria) in these sediments. The barren zones are typically characterized by low silica concentrations.

Conclusions

1. The sediments exhibit effects of diagenetic processes leading to Mg uptake, sulfate reduction, and ammonia production; these diagenetic effects are more pronounced than those observed at Site 671, mostly because of a diminished communication with the overlying ocean as a result of folding and thrusting processes.
2. Localized low chloride concentrations occur, as at Sites 671 and 672, suggesting migration of low salinity waters along thrust faults. Aside from dilution of various components, the advective process seems to have little geochemical effect in sediment pore water.

Dissolved Methane and Organic Carbon

Methane

Methane was below the limit of detection in interstitial waters at Site 673. This lack of methane suggests that methane produced in the underthrusted sediment is essentially carried

Table 4. Interstitial water calcium, magnesium, ammonia, silicon, sulfate, sodium and potassium, and ratio of sodium and potassium to chlorine data, Site 673.

Core 110-	Depth (mbsf)	Ca (mmol/L)	Mg (mmol/L)	NH_4 (μmol/L)	Si (μmol/L)	SO_4 (mmol/L)	Na + K (mmol/L)	(Na + K)/Cl
Hole 673A								
1	6	12.6	50.6	95	405	25.1	479	0.87
2	16	16.3	45.2	135	222	22.1	459	0.86
3	28	21.3	34.4	165	606	18.3	475	0.87
4	35	22.3	33.6	200	655	16.8	481	0.865
Hole 673B								
1	6	13.0	50.1	60	529	25.3	476	0.87
2	15	16.5	43.1	130	346	23.1	490	0.88
3	24	20.4	36.9	205	458	19.6	496	0.87
4	34	23.2	31.7	235	317	17.0	488	0.87
5	42	26.7	28.6	250	148	14.8	480	0.86
7	57	30.0	21.6	360	120	11.2	475	0.86
9	79	34.0	14.5	470	730	5.1	465	0.84
12	105	32.0	15.9	530	n.d.	5.2	466	0.85
15	136	30.1	14.6	510	650	4.2	434	0.85
18	164	29.0	14.3	525	670	1.5	432	0.84
22	200	29.2	13.5	525	185	0.0	422	0.835
25	230	31.1	15.8	600	177	3.6	457	0.844
28	260	31.3	14.8	515	1103	0.0	453	0.835
31	290	27.1	13.8	560	672	0.0	412	0.84
34	318	31.4	15.7	n.d.	n.d.	0.5	457	0.835

n.d. = not determined.

along the décollement toward the deformation front at the toe of the accretionary prism. This result agrees with the lack of a diffusive methane gradient that was noticed in the offscraped sedimentary series above the décollement in Hole 671B. Despite zero sulfate concentrations at greater depths, no microbial production of methane appears to occur.

Organic Carbon (Rock-Eval Results)

Rock-eval data are given in Table 5. The plot of total organic carbon (TOC) vs. depth in Hole 673B (Fig. 31) shows very low and quite constant organic carbon (<0.2%). These organic matter values are too low to allow an exploitation of Rock-Eval parameters. Similar to Site 671, we notice that the offscraped sediments, Pleistocene to lower Miocene, contain residual organic matter.

Conclusion

At Site 673, the low chlorinity anomalies are not correlated with methane anomalies. This result supports the hypothesis that thermogenic methane production occurs only in underscraped sediment.

PHYSICAL PROPERTIES

Introduction

In addition to providing basic mechanical, thermal, electrical, and acoustic information about sediments of the region, the physical properties measurements on Leg 110 may provide considerable insight into the processes which have created the Lesser Antilles accretionary wedge. Several measurement programs were conducted in the course of drilling at Site 673. The specific properties measured were as follows: 1. Index Properties—bulk density, grain density, porosity, and wet and dry water content; 2. Undrained vane shear strength; 3. Compressional wave velocity; 4. Thermal conductivity; and 5. Formation factor, an electrical resistivity measurement.

Wherever possible, measurements in a single section were made in close proximity to each other so that comparisons could be made between various properties. Occasionally, this was not possible, such as when there was limited solid "biscuit" material for accurate measurements of thermal conductivity, velocity, and resistivity. Lack of sufficient solid material became a more severe problem with greater depth in Hole 673B. As a consequence there were fewer values of these properties as compared to the other index properties.

Results are reported in this section for physical-property measurements made in Holes 673A and 673B; however, owing to the short length (four cores) of Hole 673A only data from Hole 673B have been plotted on figures for this summary.

Index Properties

Methods

The methods employed to measure index properties at Site 673 have been previously described in Chapter 1. Further details on specific measurement techniques and their limitations may be found in Boyce (1976).

Results

Index properties measured on cores from Holes 673A and 673B are listed in Tables 6 and 7, respectively. The following data are tabulated according to core, section, interval, and depth below the seabed: water content (calculated as percentage dry weight), water content (calculated as percentage total weight), porosity, bulk density, and grain density.

Profiles of water content, porosity, bulk density, and grain density against depth for Hole 673B are displayed in Figure 32. Also shown are radiolarian zones, ages, and lithology as well as tectonic packages. As expected, the porosity and water content decrease with depth while bulk density increases with depth through the Pleistocene sediments to about 45 mbsf. No obvious trends are visible in these three properties through the upper Pliocene (and barren section) to a depth of about 65 mbsf. Some of the scatter in these data over this interval is explained by the chaotic nature of much of the sediment, which is comprised of hemipelagic debris flow and slump deposits. Within Cores 110-673B-8X and -9X (lower Miocene, radiolarian Zones R9 and R10) there is a discernible trend of decreasing water con-

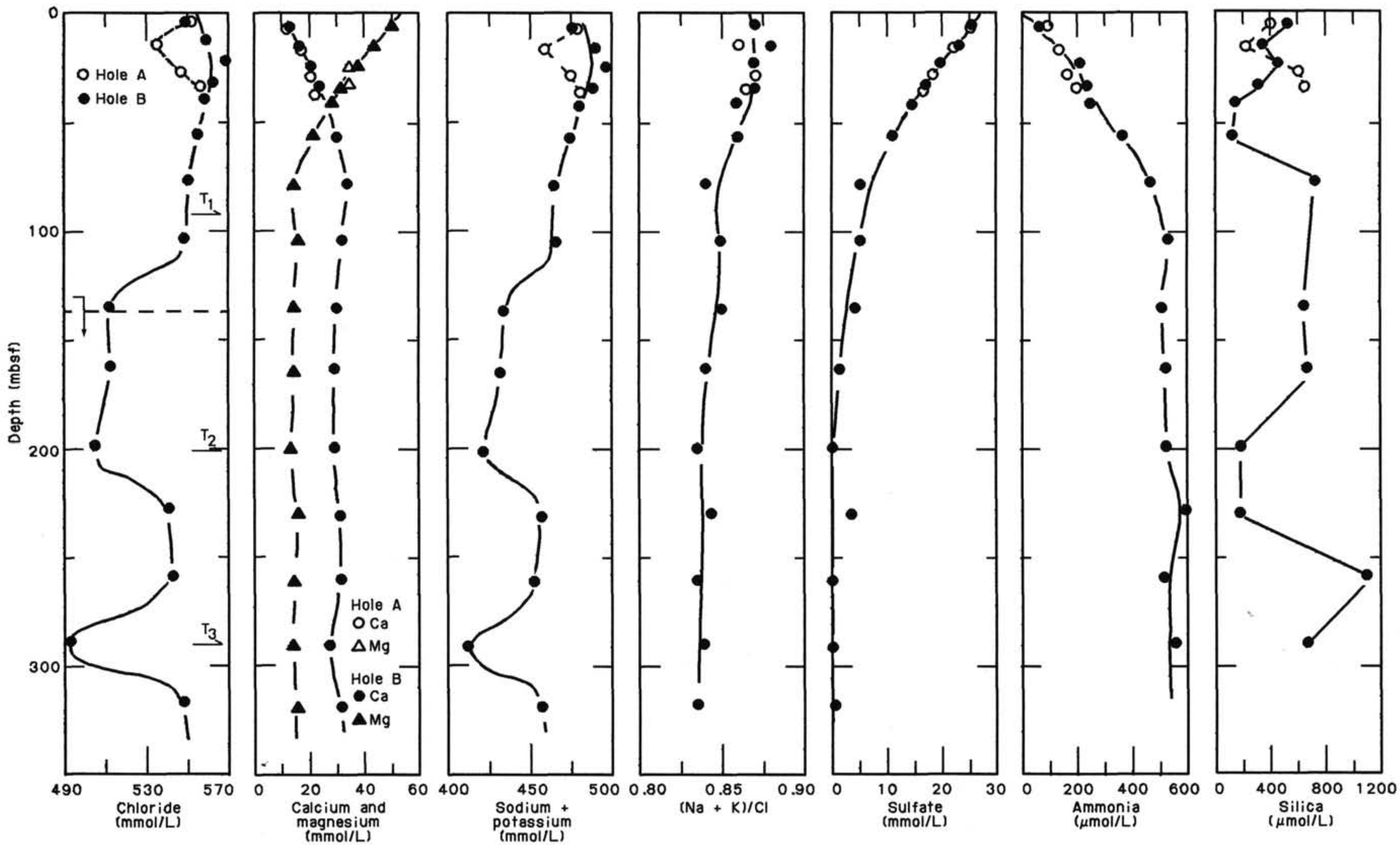

Figure 30. Profiles of chloride, calcium, magnesium, sodium plus potassium, (Na+ K)/Cl, sulfate, ammonia, and silica, vs. depth at Site 673.

Table 5. Rock-Eval geochemistry data, Hole 673B.

Core 110-673B-	Section	Interval (cm)	Depth (mbsf)	Temp. (°C)	S_1	S_2	S_3	PI	S_2/S_3	PC	TOC	HI	OI
1	4	145-150	6	477	0.16	1.47	0.09	0.10	16.33	0.13	0.13	1130	69
3	5	145-150	24	486	0.04	0.13	2.39	0.25	0.05	0.01	0.01	1300	23900
4	5	145-150	34	529	0.05	0.15	2.35	0.25	0.06	0.01	0.01	1500	23500
5	4	145-150	42	536	0.05	1.16	0.26	0.04	4.46	0.10	0.09	1288	288
7	1	145-150	57	491	0.07	1.06	0.31	0.06	3.41	0.09	0.09	1177	344
9	3	145-150	79	509	0.06	1.18	0.27	0.05	4.37	0.10	0.10	1180	270
12	2	140-150	105	567	0.05	1.12	0.51	0.04	2.19	0.09	0.09	1244	566
15	5	140-150	136	524	0.05	1.55	0.62	0.03	2.50	0.13	0.13	1192	476
18	2	140-150	164	552	0.03	1.36	0.73	0.02	1.86	0.11	0.11	1236	663
25	4	140-150	230	566	0.04	1.00	0.40	0.04	2.50	0.08	0.08	1250	500
28	5	140-150	260	500	0.02	1.16	0.04	0.02	29.00	0.09	0.09	1288	44
31	6	140-150	290	540	0.02	0.75	0.26	0.03	2.88	0.06	0.06	1250	433
35	5	140-150	348	498	0.03	1.05	0.02	0.03	52.50	0.09	0.08	1312	25

S_1 (mg HC/g rock) = volatile hydrocarbons; S_2 (mg HC/g rock) = kerogen-derived hydrocarbons; S_3 (mg CO_2/g rock) = organic CO_2 from kerogen; PI (S_1 + S_2) = productivity index; S_2/S_3 = kerogen-type index; PC = petroleum potential; TOC = total organic carbon; HI (100 S_2/C_{org}) = hydrogen index; OI (100 S_3/C_{org}) = oxygen index.

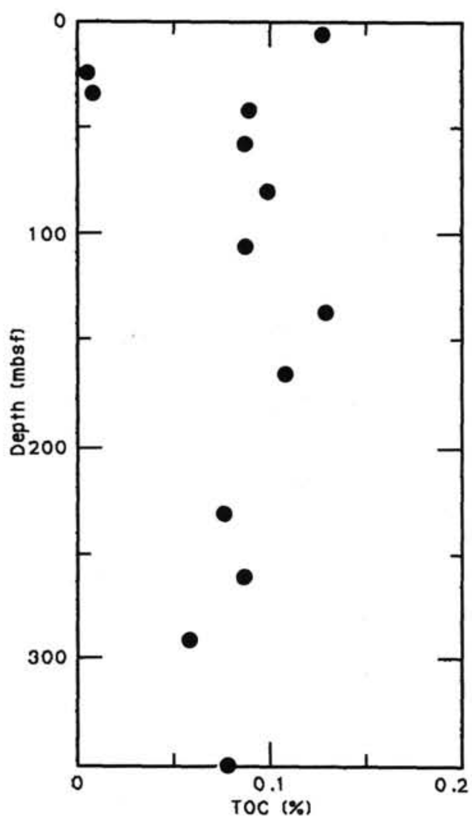

Figure 31. Plot of total organic carbon vs. depth, Site 673.

tent and porosity with depth. With the exception of one value in Core 110-673B-10X, this trend appears to cross the boundary between slumped and accreted sediment (between Cores 110-673B-8X and -9X).

Below the first biostratigraphic inversion (between Cores 110-673B-10X and -11X, 93 to 103 mbsf) in the second tectonostratigraphic package, a trend of decreasing water content and porosity and increasing bulk density is apparent to about the bottom of Core 110-673B-16X at 150 mbsf. This repetition of the same trend as observed in the lower Miocene above the thrust would be expected for two stratigraphically similar sedimentary packages. Through Cores 110-673B-17X to -20X (approximately 160 to 190 mbsf) which comprise the underlimb of a folded lower Miocene section there is a slight trend towards increasing water content and porosity and decreasing bulk density with depth to the bottom of Core 110-673B-19X (179 mbsf).

Below this sequence of decreasing age, in the upper portion of this barren section, a sharp trend of decreasing water content and porosity and increasing bulk density is noted. Although only three points define this decline, its appearance is correlative with a more intense scaly fabric and vein structure in this interval. A second major thrust may be located at this depth. Within the section between Cores 110-673B-24X (226 mbsf) to about half way through -26X (245 mbsf) there are no discernible trends in water content or porosity, although the bulk density does decrease somewhat. This decrease may be attributable to the concomitant decrease in the grain density seen over the same interval.

Between Cores 110-673B-26X and -33X (245 to 310 mbsf) is a stratigraphic sequence with age decreasing upward defined by radiolarian Zones R10, R11, and R12. A slight trend towards deceasing water content and porosity is seen through this interval. As noted previously the increase in bulk density may be a consequence of increasing grain densities.

The few measurements below the third major thrust at a depth of about 312 mbsf do not show a consistent trend with depth, although several low bulk densities are coincident with a cluster of low grain densities within Core 110-673B-35X.

Compressional Wave Velocity

Methods

Methods employed to measure compressional wave velocity at Site 673 are detailed in Chapter 1. Data were read from the P-Wave Logger over the upper 60 mbsf and the Hamilton Frame apparatus was used to determine velocities in the more indurated sediments.

Results

Compressional wave velocity is plotted vs. depth below seabed in Figure 32 and the results are listed in Tables 8 and 9. Velocity shows a reasonably smooth trend of slow increase over the upper 110 m of core. The velocity increase at around 110 mbsf suggests this level as the source of an observed reflector on the seismic profile at this site. Below 125 mbsf, velocities continue to increase until approximately 170 mbsf, where two measurements suggest a decrease in velocity with depth. The poor condition of the recovered core between 175 and 210 mbsf precluded measurements within that depth interval, however the re-

Table 6. Index properties summary, Hole 673A.

Core 110-673A-	Section	Interval (cm)	Depth (mbsf)	% Water (wet)	% Water (dry)	Porosity (%)	Bulk density (g/cm³)	Grain density (g/cm³)
1	2	70	2.20	51.4693	106.0550	74.7804	1.4885	2.7182
1	4	70	5.20	50.4654	101.8790	75.7394	1.5376	2.7962
2	1	105	8.95	52.5220	110.6240	76.6028	1.4942	2.6955
2	3	139	12.29	45.6148	83.8735	72.1753	1.6211	2.6498
2	4	78	13.18	39.0933	64.1856	65.9868	1.7293	2.6749
2	6	70	16.10	44.9498	81.6522	70.9409	1.6169	2.5663
3	2	40	18.41	40.3872	67.7492	66.4348	1.6853	2.6078
3	5	66	22.14	41.6619	71.4146	68.2783	1.6790	2.6231
4	2	86	28.70	49.4024	97.6378	73.2814	1.5197	2.6796
4	3	80	30.14	47.9798	92.2331	72.1863	1.5414	2.6252
4	4	99	31.83	47.2005	89.3958	71.2675	1.5469	2.5348

sults of index property measurements suggest another reflector within the disturbed zone.

Below 210 mbsf there is first a decrease in velocity (to 240 mbsf) and then scatter about higher velocity values. The increase in velocity at about 245 mbsf might well be the location of another reflector in the seismic record. The scatter seen in the data below 250 mbsf is partially the result of lithology. The faster velocities seen at these depths are representative of the major lithology of the core: a hard green mudstone or claystone. Lower velocities come from determinations made for lithologies that were somewhat atypical, such as the brown clay layers.

It is useful to look at the relationship between velocity and water content (calculated as percentage of total weight) for samples from Hole 673B (Fig. 33). The data have been arbitrarily divided into three depth ranges to better understand how relationships change within the units as depth increases. Also plotted on the figure is a theoretical relationship used to model unconsolidated sediment velocities (Kuster and Toksoz, 1974). This line is meant as a reference; those data falling on or near the line have probably not undergone any measurable degree of cementation. Those points falling above the line suggest that some processes other than simple compaction (water loss or primary consolidation in the soil mechanics sense) have been active in their history.

The velocities of the shallowest sediment samples are slightly below those that would be predicted by theory, not an unreasonable result considering that the grain moduli used for the prediction were those of calcite, and that the clays which compose most of the Site 673 sediments are probably somewhat less stiff than lime. These upper sediments at Site 673 appear to be unlithified.

Samples from lower in the column (100–200 mbsf) seem to show some small amount of stiffening. For the same range of water content as samples from the upper 100 m, they have higher velocities.

The third set of data, from below 200 mbsf, seem to exhibit a change from relatively unlithified to a more lithified regime. The deepest samples, with the higher velocities (Fig. 32), have much the same water contents as those samples which fall close to the theoretical curve. All of the samples below 200 mbsf appear to have lost water relative to those from above that depth.

Formation Factor

Methods

Formation factor is the ratio of the electrical resistivity of an interval of core to the electrical resistivity of the sediment pore fluid, which, in these data, is assumed to be that of normal sea water. The use of formation factor in marine sediments and a description of the basic methodology employed during Leg 110 is described in Manheim and Waterman (1974) and in Chapter 1.

Results

Values of the calculated formation factors from Holes 673A and 673B are listed in Tables 10 and 11, respectively. For comparative purposes a plot showing formation factor and porosity variation with depth below the seabed for the first 100 mbsf is given in Figure 34. Drilling disturbance and severe biscuiting precluded making accurate measurements below about 80 mbsf.

Both horizontal and vertical formation factors are seen to increase with depth to nearly 50 mbsf. However, an unexplained anomaly exists in the upper 15 m of the core. A sharp increase in the formation factor to a value of 2.6 and a very sharp decrease back to about 1.7 is not matched by porosity, water content, or bulk density trends. Below about 50 m there are too few measurements to see any trends. In contrast to conditions seen at Site 671 the grain densities at this depth vary considerably and may offer some clue as to the reason for this oddity in conductive behavior.

The slightly higher resistivity seen in the vertical direction may be related to the presence of opened microcracks in the horizontal direction.

Undrained Shear Strength

Methods

Undrained shear strength was obtained on selected core sections with a motorized miniature vane shear device. The procedures followed are outlined in Chapter 1. Measurements were taken to a maximum angle of rotation of between 92 and 100 degrees. All APC-collected cores were tested for undrained shear strength. However, only the least disturbed (upper cores) sampled with the XCB were tested owing to sample disturbance and biscuit formation.

Results

Peak and postpeak (residual) undrained shear strength data obtained by the minivane device in Holes 673A and 673B are listed in Tables 12 and 13, respectively. Postpeak strength is defined as the undrained shear stength at an axial rotation of between 90 and 100 degrees, irrespective of whether a constant shearing resistance or strength has been reached.

Figure 35 is a plot of minivane undrained shear strength vs. depth for Hole 673B where the advanced piston corer was used. A linear trend of increasing strength with depth as observed at Sites 672 and 671 is not apparent on this plot. Undoubtedly the presence of a slumped sequence through this depth introduces the notable scatter in the peak undrained shear strengths. As de-

Table 7. Index properties summary, Hole 673B.

Core 110-673B-	Section	Interval (cm)	Depth (mbsf)	% Water (wet)	% Water (dry)	Porosity (%)	Bulk density (g/cm^3)	Grain density (g/cm^3)
1	2	70	2.20	51.8835	107.8290	75.4492	1.4898	2.6038
1	4	70	5.20	48.3772	93.7129	73.1309	1.5487	2.7516
1	5	27	6.27	45.1321	82.2559	69.6553	1.5812	2.6753
2	2	52	9.62	48.4867	94.1247	73.4406	1.5518	2.6640
2	4	12	12.22	42.4216	73.6763	67.7833	1.6370	2.6576
2	6	74	15.84	45.5146	83.5353	70.4154	1.5850	2.6848
3	2	30	18.90	43.0237	75.5116	68.3130	1.6267	2.7740
3	4	90	22.50	45.1953	82.4662	69.4851	1.5751	2.7266
3	6	67	25.27	39.1353	64.2989	62.3251	1.6316	2.5273
4	2	70	28.80	41.9659	72.3124	66.7975	1.6307	2.7566
4	4	67	31.77	41.3362	70.4628	67.0211	1.6611	2.7003
4	4	70	31.80	40.8485	69.0573	67.4751	1.6923	2.8709
4	6	65	34.75	36.0981	56.4898	60.0200	1.7034	2.7413
5	2	70	38.30	38.2901	62.0486	63.1793	1.6904	2.7260
5	4	65	41.25	40.7986	68.9149	66.8546	1.6788	2.6982
5	6	10	43.70	37.5158	60.0404	59.5460	1.6261	2.6493
6	2	72	47.82	39.3826	64.9692	64.4711	1.6772	2.6611
6	4	77	50.87	39.7817	66.0626	65.3303	1.6825	2.6259
6	6	64	53.74	41.3246	70.4292	66.8204	1.6566	2.6424
7	3	82	58.92	39.0855	64.1644	64.9096	1.7014	2.6943
8	2	81	66.91	39.8623	66.2850	65.4239	1.6815	2.6492
8	2	138	67.48	40.7132	68.6716	65.3795	1.6452	2.5779
8	10	23	71.31	39.6947	65.8229	65.8960	1.7007	2.6878
9	2	73	76.33	39.0457	64.0573	63.8906	1.6764	2.5999
9	4	60	79.20	37.2705	59.4147	61.5426	1.6917	2.5508
10	3	31	86.91	42.3287	73.3965	68.6991	1.6628	2.2984
12	2	11	104.21	40.6106	68.3801	68.6039	1.7307	2.6827
12	3	45	106.05	36.1357	56.5821	62.3202	1.7669	2.7163
13	2	100	114.60	40.8550	69.0759	66.3384	1.6635	2.6265
13	3	72	115.82	46.1135	85.5752	71.1624	1.5810	2.5893
14	2	70	123.80	38.7129	63.1665	63.8630	1.6901	2.7166
14	4	54	126.64	37.2838	59.4483	62.2830	1.7114	2.6047
15	4	40	136.00	40.0134	66.7039	65.0130	1.6646	2.5979
15	6	67	139.27	36.2497	56.8621	60.8430	1.7196	2.5689
16	4	133	146.43	36.6725	57.9092	61.3354	1.7135	2.6218
16	6	20	148.30	35.7760	55.7050	61.0413	1.7480	2.5912
17	2	91	152.51	36.2980	56.9809	61.6478	1.7400	2.6720
17	3	73	153.83	33.7187	50.8722	58.7397	1.7847	2.5716
17	4	94	155.54	30.8536	44.6206	55.4619	1.8416	2.6494
18	1	103	160.63	33.5554	50.5013	58.1020	1.7739	2.5798
18	3	24	162.84	28.9268	40.7000	51.6604	1.8297	2.5788
19	3	40	172.50	35.7970	55.7560	60.5463	1.7328	2.6086
19	5	133	176.43	38.3935	62.3206	63.2354	1.6874	2.5926
20	1	35	178.95	37.1674	59.1531	62.4017	1.7201	2.7002
21	2	18	189.78	34.7326	53.2159	60.3356	1.7797	2.5656
22	2	25	199.35	31.3783	45.7266	56.3581	1.8401	2.7265
23	1	25	207.35	22.7722	29.4870	45.2543	2.0359	2.7296
24	2	58	218.68	32.4734	48.0897	58.2084	1.8364	2.7057
24	4	0	221.10	34.3499	52.3226	61.0164	1.8198	2.7856
24	6	118	225.28	31.9358	46.9200	56.9292	1.8263	2.6655
25	2	106	228.66	31.9004	46.8437	57.7143	1.8535	2.7567
25	4	62	231.22	33.1657	49.6238	58.4934	1.8069	2.7301
26	3	40	239.00	33.2683	49.8539	57.2738	1.7637	2.5827
26	3	44	239.04	31.5402	46.0711	55.8715	1.8148	2.6161
27	1	24	245.34	39.2214	64.5315	64.2924	1.6794	2.7081
27	2	22	246.82	33.4354	50.2299	58.3328	1.7874	2.6488
28	2	73	256.83	31.5585	46.1103	56.2020	1.8245	2.6207
28	4	115	260.25	33.2388	49.7877	57.6482	1.7768	2.6027
28	5	55	261.15	33.0691	49.4077	56.5975	1.7534	2.5540
29	3	70	267.80	32.1050	47.2863	56.3331	1.7976	2.6018
29	5	87	270.97	29.3284	41.4995	52.7602	1.8430	2.5614
29	7	2	273.12	31.0881	45.1128	54.4886	1.7957	2.6500
30	3	21	276.81	29.7595	42.3681	54.8786	1.8893	2.7145
30	4	36	278.46	30.3188	43.5107	55.0005	1.8585	2.6982
30	10	3	282.93	31.0076	44.9436	55.8950	1.8468	2.6389
31	4	61	288.21	29.7551	42.3590	55.0919	1.8969	2.7024
31	6	45	291.05	26.4866	36.0296	50.9776	1.9718	2.7172
32	2	11	294.21	26.2824	35.6529	49.3537	1.9238	2.6236
33	3	13	305.23	29.1666	41.1764	53.9266	1.8942	2.7078
34	5	117	318.77	32.3515	47.8229	56.1656	1.7786	2.6251
35	2	70	323.30	32.8485	48.9170	57.6265	1.7973	2.5428
35	4	133	326.93	35.4655	54.9558	60.3088	1.7422	2.5509
35	10	63	329.55	31.3050	45.5709	55.6076	1.8198	2.5371

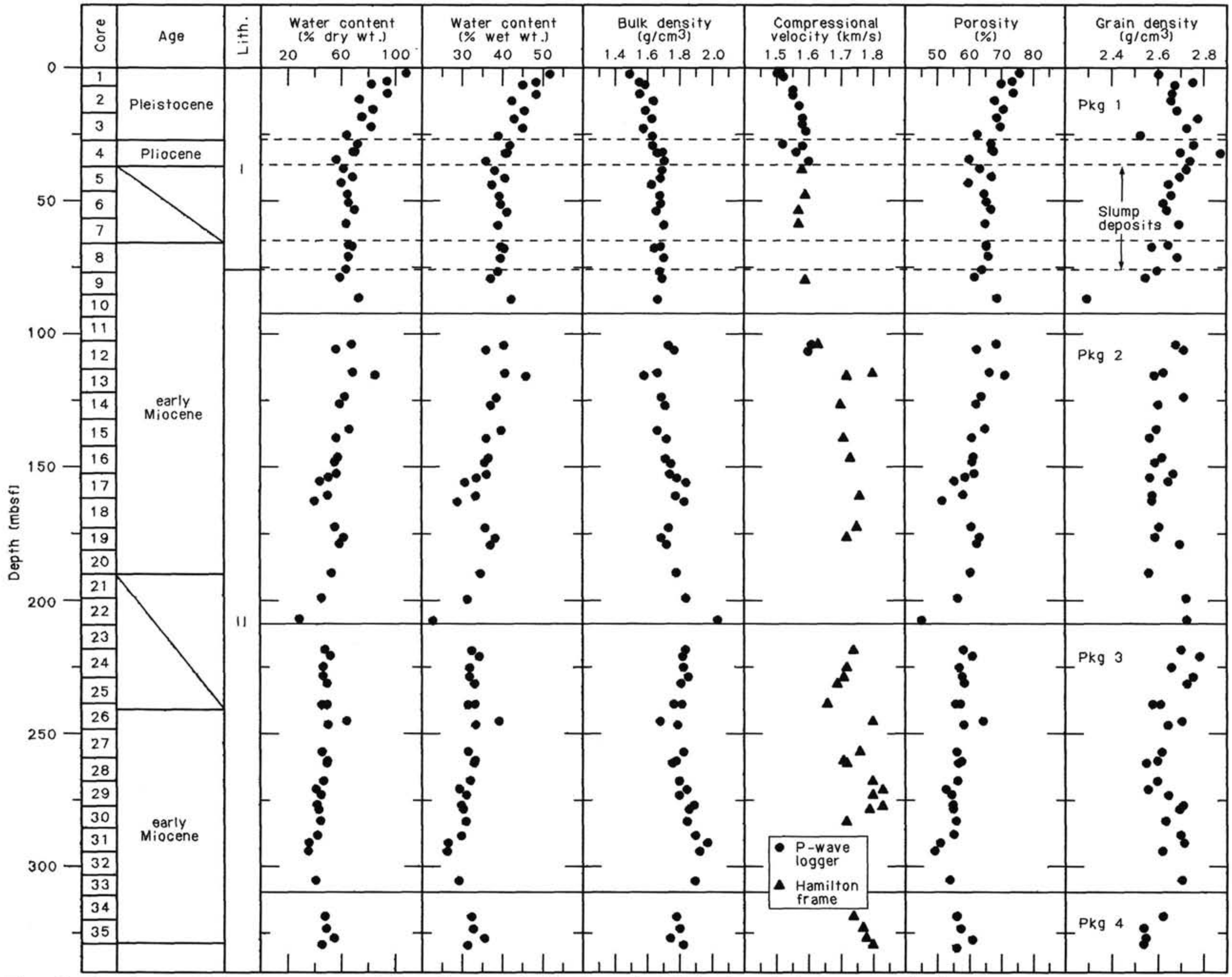

Figure 32. Biostratigraphy, lithology, water content (relative to dry and total weights), porosity, bulk density, grain density, compressional velocity measured by the Hamilton Frame apparatus and the P-wave logger vs. depth, Hole 673B.

Table 8. Compressional wave velocity, Hole 673A.

Core 110-673A-	Section	Interval (cm)	Depth (mbsf)	Vel(A)* (km/s)	Vel(B)* (km/s)
1	2	70	2.20		1.5600
1	4	70	5.20		1.5000

*Velocity measured parallel (Vel A) and perperdicular (Vel B) to cored direction.

Table 9. Compressional wave velocity, Hole 673B.

Core 110-673B-	Section	Interval (cm)	Depth (mbsf)	Vel(A)* (km/s)	Vel(B)* (km/s)
5	2	70	38.30	1.5900	1.5800
6	2	72	47.82		1.5900
6	6	64	53.74	1.5700	1.5700
7	3	82	58.92		1.5700
9	4	140	80.00		1.5900
12	2	11	104.21		1.6300
13	2	100	114.60	1.7600	1.8000
13	3	72	115.82		1.7200
14	4	54	126.64	1.6900	1.7000
15	6	67	139.27		1.7100
16	5	15	146.75		1.7300
18	1	130	160.90		1.7600
18	1	130	160.90		1.7600
18	3	24	162.84		1.6800
19	3	40	172.50		1.7500
19	5	133	176.43		1.7200
24	2	58	218.68		1.7400
24	4	0	221.10		2.9000
24	6	118	225.28		1.7200
25	2	106	228.66	1.7000	1.7100
25	4	62	231.22		1.6900
26	3	40	239.00		1.7900
26	3	44	239.04	1.6700	1.6600
27	1	24	245.34	1.7900	1.8000
28	2	73	256.83	1.7500	1.7600
28	4	115	260.25		1.7100
28	5	55	261.15		1.7200
29	3	70	267.80	1.7600	1.8000
29	5	87	270.97	1.8000	1.8300
29	7	2	273.12	1.7800	1.8000
30	3	22	276.82		1.8300
30	4	47	278.57		1.7900
30	10	5	282.95	1.7400	1.7200
34	5	117	318.77		1.7400
35	2	70	323.30	1.7700	1.7700
35	4	133	326.93	1.7900	1.7800
35	10	63	329.55	1.8200	1.8000

*Velocity measured parallel (Vel A) and perpendicular (Vel B) to cored direction.

scribed above, coring disturbance and artifacts of the test procedure (e.g., cracking) provide additional nonsystematic scatter in the data.

Figure 36 is the stress distribution plot for Hole 673B. The total (lithostatic) shows a nearly linear increase with depth.

Thermal Conductivity

Methods

The thermal conductivities of sediment cores at Site 673 were measured using the needle probe technique (Von Herzen and Maxwell, 1959). Details of the test procedure and the steps taken to reduce unexplained variability due to core disturbance and transient thermal effects are described in Chapter 1.

Results

Thermal conductivity measurements for Holes 673A and 673B are listed in Tables 14 and 15, respectively. Figure 37 shows

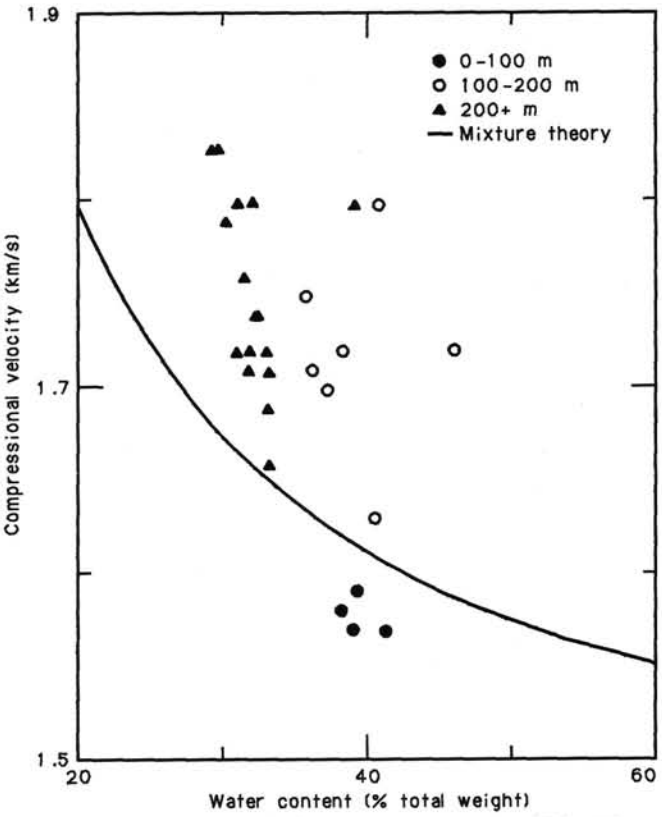

Figure 33. Compressional velocity vs. wet water content, Hole 673B.

Table 10. Sediment formation factor, Hole 673A.

Core 110-673A-	Section	Interval (cm)	Depth (mbsf)	F-horiz.	F-vert.
1	2	70	2.20	1.6100	1.6700
1	4	70	5.20	1.5900	1.6500
2	4	88	13.28	2.3900	2.3900
2	6	66	16.06	2.5000	2.6700
3	2	60	18.61	2.4500	2.5800
3	5	76	22.24	2.4200	2.5600

Table 11. Sediment formation factor, Hole 673B.

Core 110-673B-	Section	Interval (cm)	Depth (mbsf)	F-horiz.	F-vert.
1	2	73	2.23	1.4700	1.6600
1	4	73	5.23	1.8300	1.9500
1	5	33	6.33	1.9700	2.2400
2	2	47	9.57	2.5300	2.6000
2	4	20	12.30	2.3000	2.2300
2	6	66	15.76	1.8600	1.9800
3	2	35	18.95	1.6700	1.7900
3	4	77	22.37	1.7600	1.8200
3	6	50	25.10	1.9800	2.0700
4	2	60	28.70	1.8900	2.2500
4	4	65	31.75	2.2500	2.3700
4	6	60	34.74	2.5600	2.7500
5	2	65	38.25	1.9400	1.8200
5	4	65	41.25	2.7300	3.0700
5	4	10	40.70	2.9400	3.3100
6	2	70	47.80	3.4000	3.6000
6	4	70	50.80	3.6400	3.7900
6	6	73	53.83	3.4000	3.4000
7	3	47	58.57	2.9200	3.2800
9	4	48	79.08	3.4000	3.8000

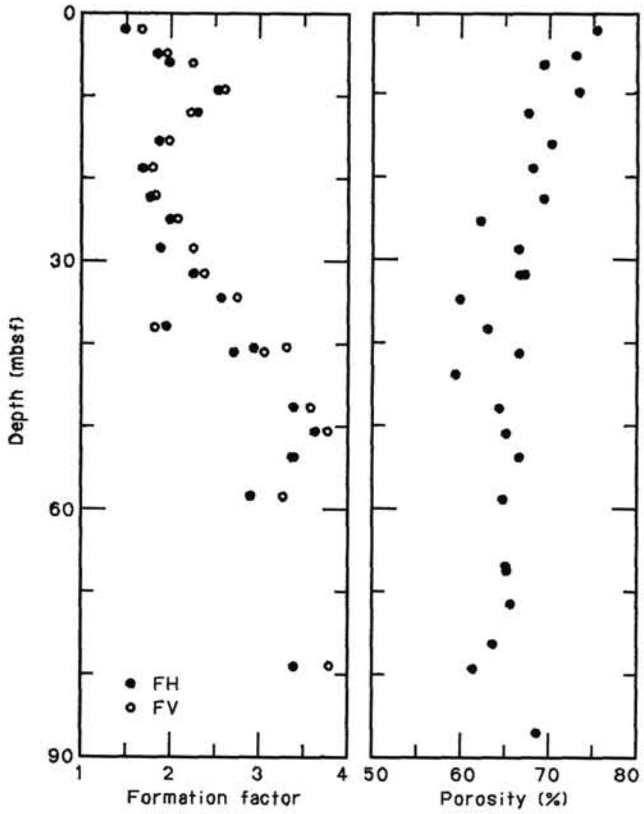

Figure 34. Vertical (FV) and horizontal (FH) formation factor and porosity vs. depth, Hole 673B.

Table 12. Vane shear strength, Hole 673A

Core 110-673A-	Section	Interval (cm)	Depth (mbsf)	Peak (kPa)	Post-peak (kPa)
1	3	0	3.00	12.9121	6.9212
1	2	75	2.25	9.6897	5.5370
1	4	75	5.25	15.4537	0
2	1	105	8.95	20.7501	10.1436
2	4	75	13.15	49.5606	23.0557
2	6	70	16.10	64.5604	41.5047
3	2	40	18.41	76.0882	0
3	5	67	22.15	94.5373	0

the 673B thermal conductivity and water content data (calculated as percentage of total) plotted against depth below the seabed. Within the upper 40 m (Pleistocene and upper Pliocene) there is an obvious trend of increasing thermal conductivity with depth from near 1.05 W/m°C to about 1.3 W/m°C. This trend is very well matched by a concomitant decrease in wet water content with depth below the seabed.

From 40 mbsf to the bottom of Hole 673B there are insufficient data to define any obvious trends. There is considerable unexplained scatter in the thermal conductivity data through the underthrust portion of the second tectonic package, despite the relatively well-defined decline in wet water content through this section. Although suspect measurements were removed from the dataset, several anomalous data points remain.

Summary

1. Repetitive trends in a selection of index properties provide a reasonable match to the decreasing age upward and downward components of the tectono-stratigraphic packages identified in Hole 673B. In general, however, an overall trend of decreasing porosity and water content with depth is observed.

2. Compressional velocity shows an increasing trend with depth and a correspondence of occasional high values with reflectors on the seismic record (110 and 245 mbsf).

3. Within the upper 50 mbsf the calculated formation factor shows a well-defined increase with depth matched by a concomitant decrease in porosity, except for an anomalous peak at about 10 mbsf.

Table 13. Vane shear strength, Hole 673B.

Core 110-673B-	Section	Interval (cm)	Depth (mbsf)	Peak (kPa)	Post-peak (kPa)
1	2	70	2.20	8.9908	
1	3	2	3.02	9.2223	4.6066
1	4	70	5.20	14.5255	9.4628
1	5	28	6.28	27.4353	16.6110
2	2	54	9.64	46.1113	41.5002
2	3	2	10.62	41.5002	27.6668
2	4	14	12.24		25.3703
2	6	75	15.85	34.5835	20.7410
3	2	0	18.60	71.4816	
3	2	30	18.90	36.8981	20.7410
3	4	90	22.50	50.6952	23.0557
3	6	67	25.27	43.7967	27.6623
4	2	0	28.10	64.5604	
4	2	70	28.80	46.1113	25.3703
4	4	70	31.80	83.0095	41.5047
4	6	65	34.75	96.8293	55.3245
5	2	70	38.30	78.3802	34.5835
5	4	70	41.30	202.8940	43.7967
5	6	15	43.75	165.9960	43.7967
6	2	80	47.90	83.0095	27.6623
6	4	75	50.85	126.8060	34.5835
6	6	75	53.85	152.1760	39.1901

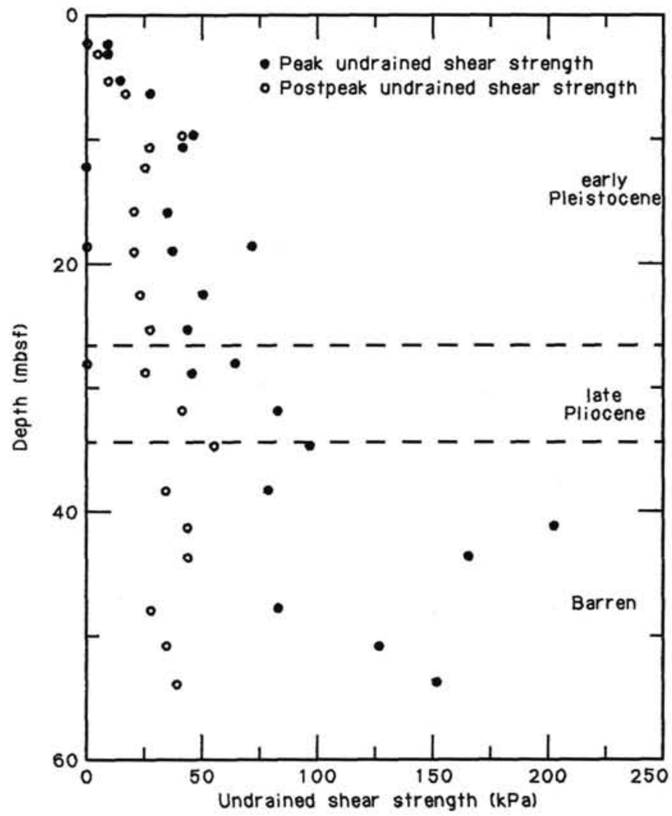

Figure 35. Peak and postpeak shear strength vs. depth, Hole 673B.

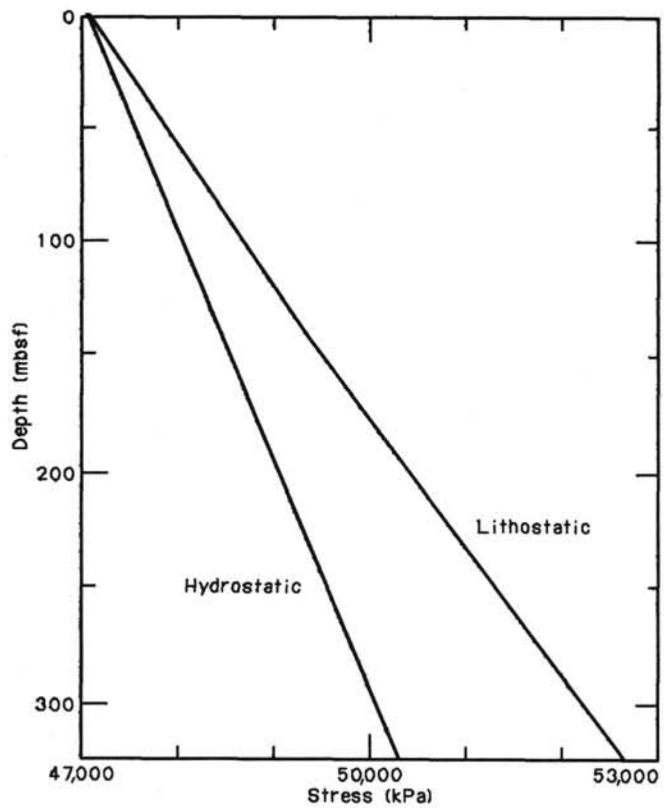

Figure 36. Lithostatic and hydrostatic stress distribution for Hole 673B calculated from measured bulk density and assumed pore-water density of 1.025 g/cc.

Table 14. Thermal conductivity, Hole 673A.

Core 110-673A-	Section	Interval (cm)	Depth (mbsf)	Cal/cm·°C·s ($\times 10^{-3}$)	W/m °C
1	2	75	2.25	2.5000	1.0500
1	4	75	5.25	2.3400	0.9800
3	2	70	18.71	2.8500	1.1900
3	4	30	21.31	2.4700	1.0300
3	6	70	23.68	2.6300	1.1000
4	2	80	28.64	2.6700	1.1200
4	3	80	30.14	2.8400	1.1900

4. There is a notable increase in variability in the undrained shear strength profile with depth as compared to Sites 671 and 672.

5. Thermal conductivity measurements over the upper 45 mbsf tend to increase with the decreasing water content, however considerable scatter is noted below this depth.

6. In general the index data for the Miocene sediments at Site 673 show notably less variation than was observed for Miocene sediments seaward of the accretionary prism at the reference hole, Site 672.

SEISMIC STRATIGRAPHY

Site 673 is located on the lower slope of the accretionary complex which has an average seaward slope of about 2° with local intervals as steep as 5° to 8°. Seismic reflection profiles over the lower slope usually show only major reflectors such as the décollement, underthrust sediments, and the top of the oceanic crust; they generally fail to resolve the internal structure of accreted series. Three conditions have to be fulfilled to get clearly defined reflectors: (a) Acoustic impedance constrasts

Table 15. Thermal conductivity, Hole 673B

Core 110-673B-	Section	Interval (cm)	Depth (mbsf)	Cal/cm·°C·s ($\times 10^{-3}$)	W/m °C
1	2	70	2.20	2.5700	1.0740
2	2	70	9.80	2.6400	1.1040
2	4	70	12.80	2.7400	1.1490
2	6	70	15.80	2.8300	1.1860
3	2	70	19.30	2.8200	1.1810
3	4	70	22.30	2.6400	1.1040
3	6	70	25.30	2.9800	1.2490
4	2	70	28.80	3.0000	1.2540
4	4	70	31.80	2.8800	1.2050
4	6	70	34.80	3.1600	1.3240
5	2	70	38.30	3.1600	1.3240
5	4	70	41.30	2.7900	1.1680
5	6	17	43.77	2.8900	1.2100
6	2	75	47.85	3.0100	1.2160
6	4	75	50.85	2.9000	1.2160
6	6	75	53.85	2.8400	1.1880
9	2	75	76.35	2.7900	1.1670
9	4	75	79.35	2.6500	1.1090
10	2	65	85.75	2.5200	1.0560
11	2	86	95.46	2.9100	1.2180
12	2	55	104.65	3.7500	1.5710
13	2	70	114.30	2.9200	1.2210
13	3	40	115.50	3.0400	1.2720
14	2	70	123.80	2.8700	1.2030
14	4	70	126.80	2.8100	1.1770
15	4	70	136.30	3.1400	1.3160
15	6	70	139.30	3.6600	1.5340
16	4	60	145.70	2.8300	1.1830
17	2	80	152.40	2.6200	1.0950
17	4	70	155.30	3.1000	1.2980
18	2	25	161.35	2.9200	1.2240
25	4	80	231.40	2.9000	1.2150
28	4	60	259.70	3.3800	1.4170
28	6	70	262.80	3.4000	1.4210
29	4	70	269.30	2.4100	1.0080
29	6	43	272.03	2.2700	0.9480

(acoustic impedance = velocity × density) must be present in the sediments; (b) Such constrasts must be followed over a distance of at least 10 shotpoints (500 m on conventional seismic lines such as A3, 250 m on a high-resolution profile such as CRV-128) to give a resolvable reflector; (c) Dips along reflective surfaces have to be shallower than 30–35° to return reflected energy. The almost complete absence of reflectors in the accreted series means that at least one, and possibly all of these conditions are missing. Site 673 penetrated monotonous lower Miocene claystones and mudstones having few lithologic contrasts, and bedding dips are often in excess of 40°. Nevertheless, recent reprocessing of lines A3 and CRV-128 have shown the presence of weak and discontinuous arcward-dipping reflectors (Figs. 38 and 39). Such reflectors are common features within accretionary prisms. Site 673 and the associated seismic lines provide a test of whether these reflectors are related to geologic structures or are seismic artifacts. If the projection of Site 673 on line CRV-128 is correct, the correlations shown on Figure 38 suggest that the arcward-dipping reflectors are the seismic expression of thrust faults that bound internally deformed packets of accreted sediments. Moreover, the bedding dips observed in the cores are clearly discordant to the seismic reflectors (see Structural Geology). At the intersection point of CRV-128 and A3 the seismic reflectors dip 12° trending N83° W, and 5° trending S43° W, respectively. A great circle fit though these two surfaces indicates a true dip of the reflectors of 12° trending N74° W. The structural coherence of the two dipping surfaces suggest that they are not seismic artifacts. The true dip of the reflectors is nearly parallel to the plate convergence vector (Minster and Jordan, 1978), and, within the error of determination, indicates that CRV-128 is essentially normal to the strike of the thrusts that generate the reflectors.

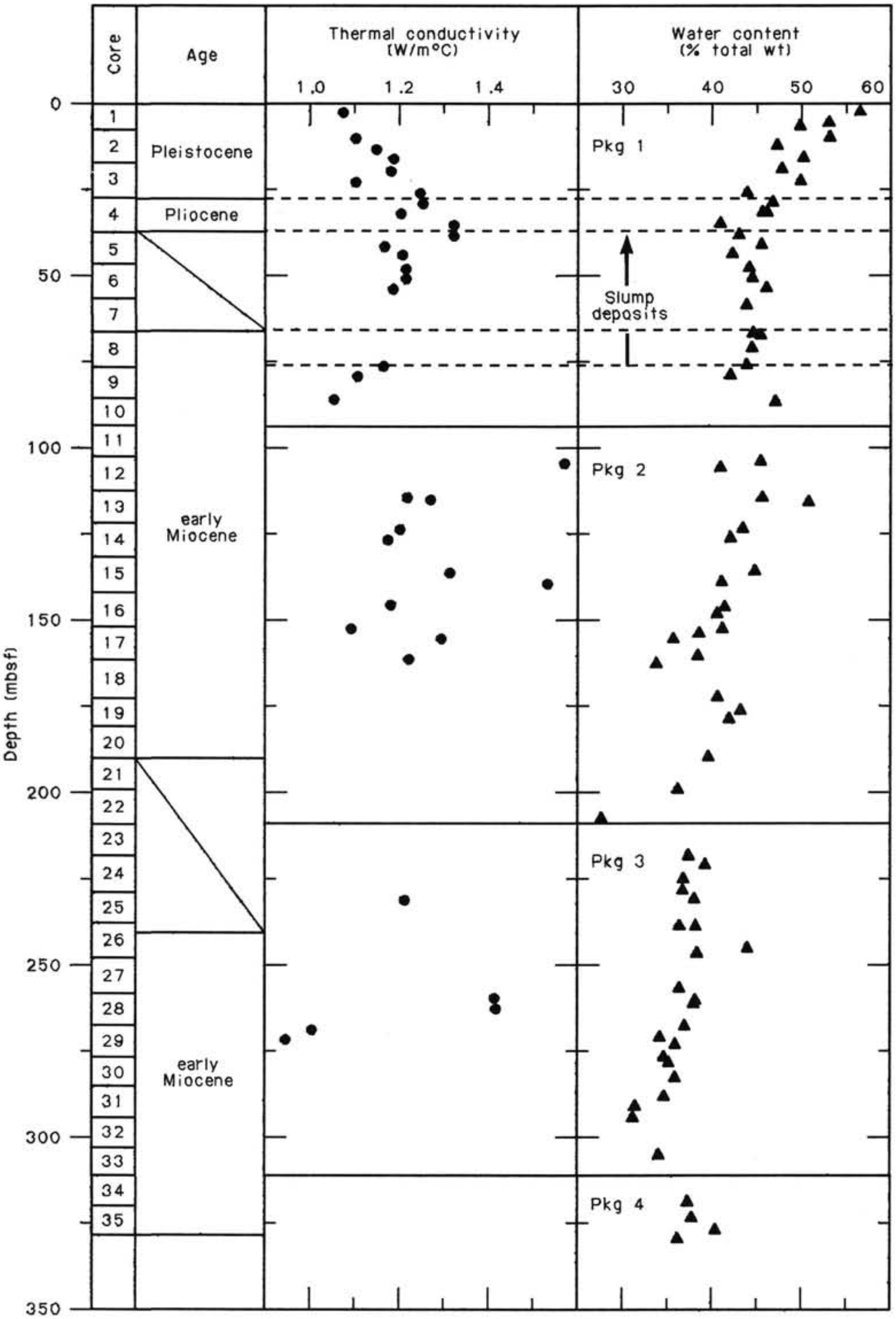

Figure 37. Thermal conductivity and wet water content versus depth, Hole 673B.

HEAT FLOW

Introduction

Site 673 is located 13 km west of the deformation front of the Lesser Antilles accretionary complex and 8 km west of Site 671. If thermal models of convergent margins (e.g., Hsü and Toksoz, 1979) are applicable we should expect to measure a lower thermal gradient at Site 673 than at Site 672. The heat-flow values summarized by Speed et al. (1984) support these models. Similarly, the sediments at Site 673 should be more compacted (Biju-Duval, Moore et al., 1984) and thus less likely to sustain interpore fluid flow (Westbrook and Smith, 1983; Von Huene and Lee, 1983), although flow through fractures may still be possible.

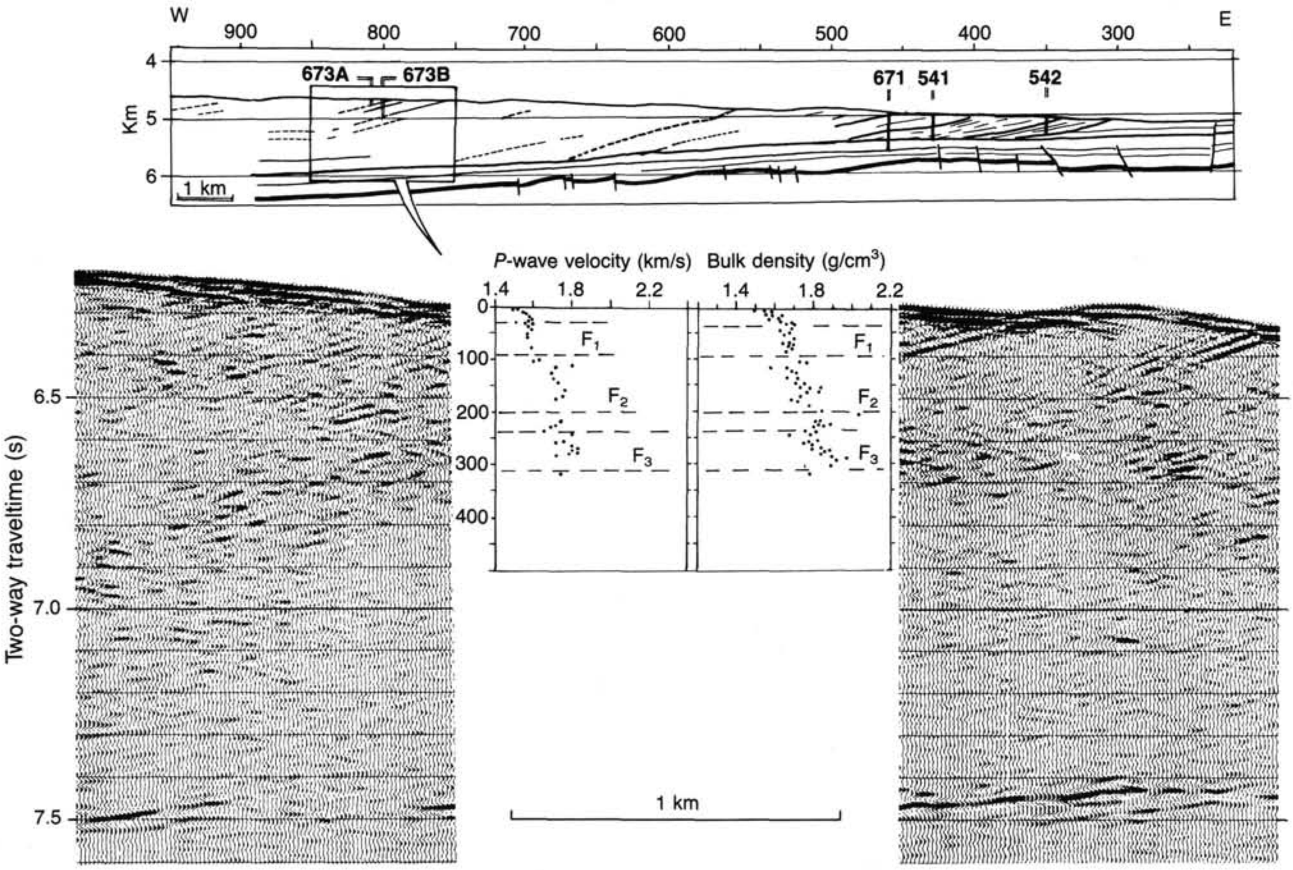

Figure 38. Top: Depth section of line CRV 128. No vertical exaggeration. Bottom: Projection of densities and P-wave velocities from Hole 673B on line CRV-128. The lower reflector at 7.5 s is the décollement separating accreted series (above) from underthrust ones (below). F_1, F_2 and F_3 are biostratigraphically defined thrust faults (see Structural Geology section).

Methods and Results

See Chapter 1 of this volume for a discussion of experimental methods, intertool calibration and data reduction. Vital tool properties are summarized in Table 16, and temperature measurements at Site 673 are tabulated in Table 17.

Hole 673A

The APC tool was deployed once in Hole 673A while we took Core 110-673A-4H, at a depth of 36.4 mbsf. Before firing the APC mechanism, the cutting shoe was held in the bit at 25 mbsf to measure the bottom water. Because the APC barrel was pumped down the drill pipe, the water in the hole during this measurement should have been close to bottom-water temperature. A temperature of 2.20°C (±0.05°C) was measured and substantiated by later runs with the APC tool and the T-probe in Hole 673B. This temperature is close to bottom-water temperatures measured at Sites 671 and 672. After making this measurement, the tool was fired into the sediment. This deployment produced a reliable temperature record (Figs. 40 and 41) and an extrapolated sediment temperature of 5.68°C (±0.05°C).

Hole 673B

Hole 673B was offset 600 m east of Hole 673A. The APC tool was deployed twice, while taking Cores 110-673B-3H and -5H. Run 110-673B-3H recorded sediment temperatures at 26.6 mbsf (Figs. 42 and 43) with an equilibrium value of 4.22°C (± 0.05°C). A poor battery connection on run 110-673B-5H resulted in data loss.

The WSTP tool was deployed after taking Core 110-673B-8X to a depth of 74.7 mbsf. The drillers' record indicates that there was at least 2 m of sediment fill at the bottom of the hole during this deployment and suggests that the tool lodged about 1 m above the true hole bottom. This interpretation is supported by the temperature record from this run (Fig. 44). After the WSTP tool landed and was latched into the bit, but before it was purposely pushed into the sediment, the temperature of the thermistor rose sporadically to nearly 12°C. The sediment pressure record from this run displays oscillations of 300 to 400 psi before the tool was pushed in, suggesting that during this time the probe was slipping in and out of the sediment fill. Finally, when the bit and tool were rested on bottom and held down, the pressure record stabilized and the probe temperature began to drop towards equilibrium. Because the fill originated at some unknown distance above the bottom of the hole, and probably cooled significantly while falling, the equilibrium sediment temperature calculated for this run (7.24°C, ±0.05°C) is considered a lower bound.

Interpretations

From the two measurements in Hole 673A (bottom water and sediment at 36.4 mbsf), the calculated thermal gradient is 96°C/km (Fig. 45). From the two APC tool measurements in Hole 673B (bottom water and sediment at 26.6 mbsf) the calculated thermal gradient is 76°C/km. If all four temperature measurements from the two holes are included in the calculation, the linear-least-squares best-fitting thermal gradient forced through

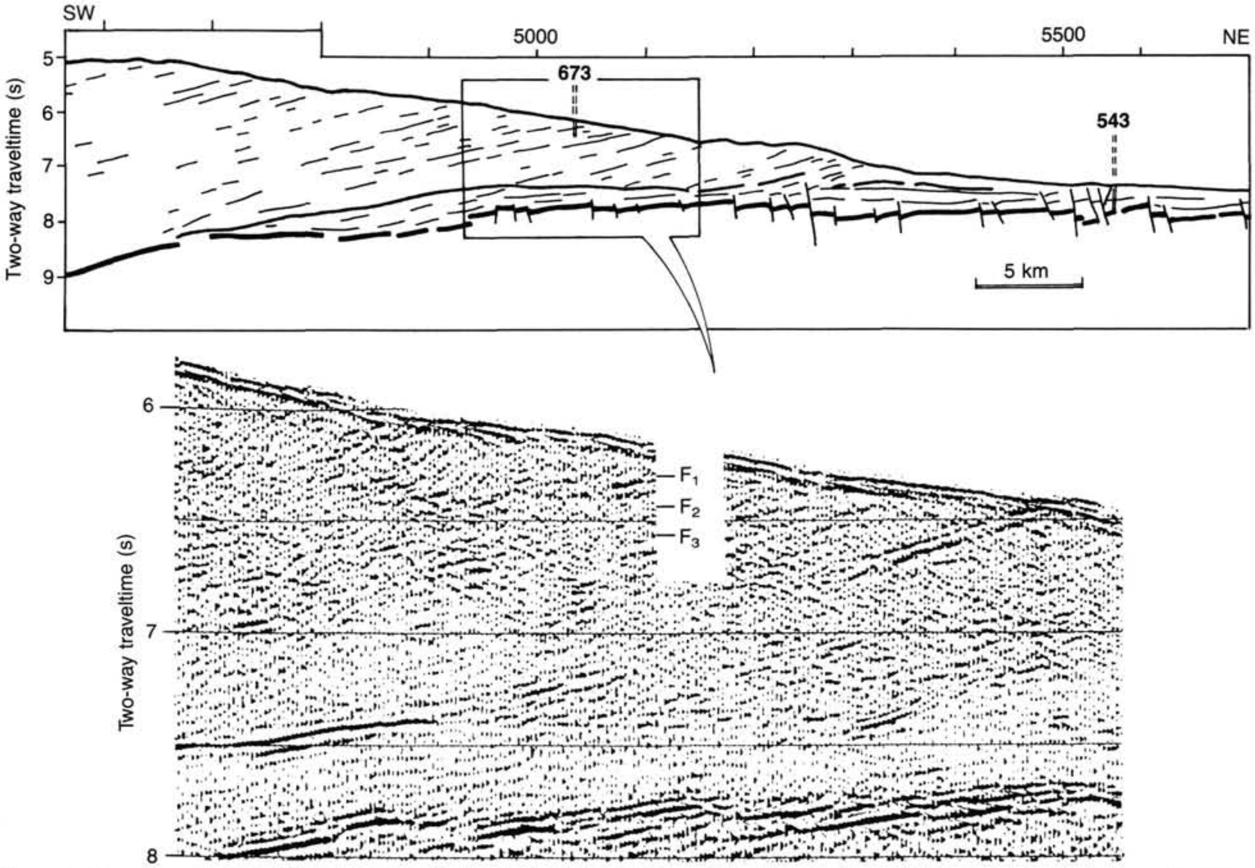

Figure 39. Top: Time section of line A3. Vertical exaggeration is about 3.7 at the seafloor. Bottom: Projection of some of the main structural features of Site 673 (see Fig. 44) on line A3. Site 673 is 1 km northwest of the profile. The reflector on the left at 7.5 s is the décollement and the reflector at 8 s is the top of the oceanic crust.

Table 16. Temperature measurement instruments used at Site 673.

Tool	Thermistor housing	Thermistor resolution	Recorder program
APC Tool	Steel annular cylinder ID: 0.0617 m OD: 0.0786 m	0.02°C	15-second recording interval
T-probe	Steel cylindrical probe 0.0125 m dia	0.05°C	5.12-second recording interval

Table 17. Temperature measurement summary at Site 673.

Hole/depth (mbsf)	Tool	Equilibrium T (est error)°C	Sediment/water temperature
673A, 673B B 0.0	APC-tool No. 6	2.20 (0.05)	water
673B/26.6	APC-tool No. 6	4.22 (0.05)	sediment
673A/36.4	APC-tool No. 6	5.68 (0.05)	sediment
673B/74.7	T-probe No. 14	7.24 (0.05)	sediment

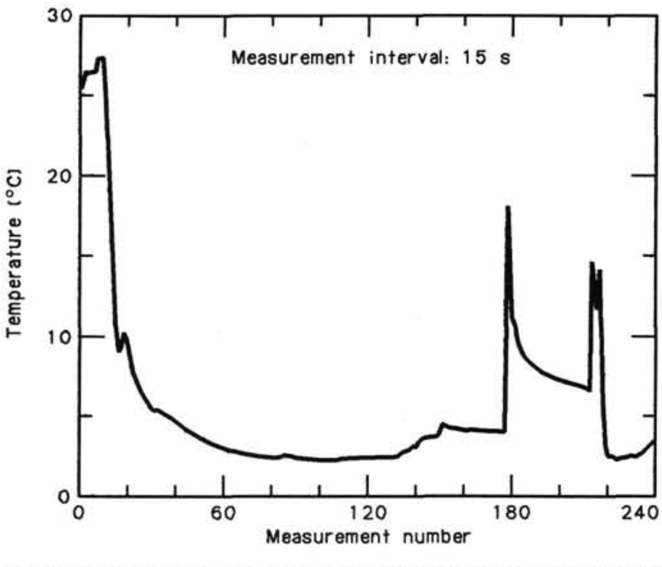

Figure 40. Temperature vs. time record for first deployment of APC tool, Core 110-673A-4H, 36.4 mbsf.

bottom water is 73°C/km. The recent slump noted in the cores from Hole 673B (Structural Geology and Biostratigraphy sections, this chapter) may be responsible for lowering the surface thermal gradient since mass movements will often cool sediment to near bottom-water temperatures (Langseth, 1965). The thermal gradient at Site 673 is calculated to be between 76 and 96°C/km. Considering that the two sediment-temperature measurements from Hole 673B are suspect, the gradient is probably closer to 96 than to 76°C/km.

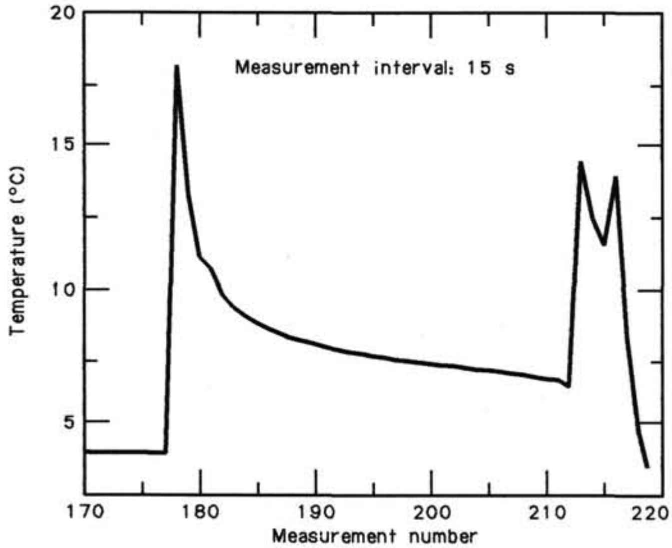

Figure 41. Detail of record of first APC tool deployment, Core 110-673A-4H, 36.4 mbsf, showing sediment temperature.

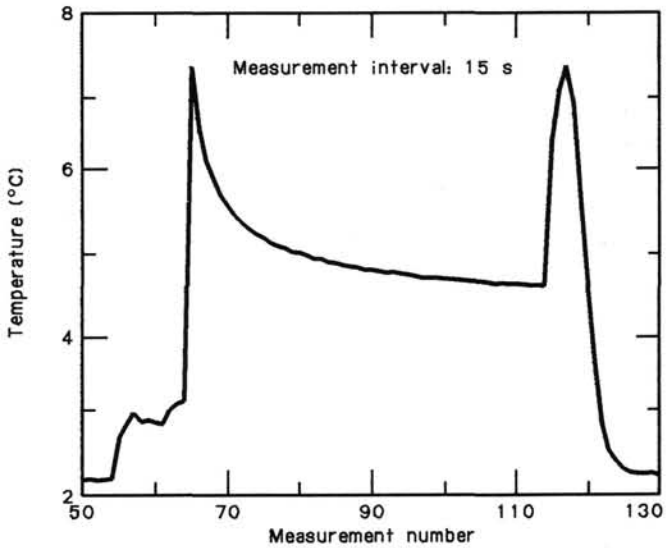

Figure 43. Detail of record of second deployment of APC tool, Core 110-673B-3H, 26.6 mbsf, showing sediment temperature.

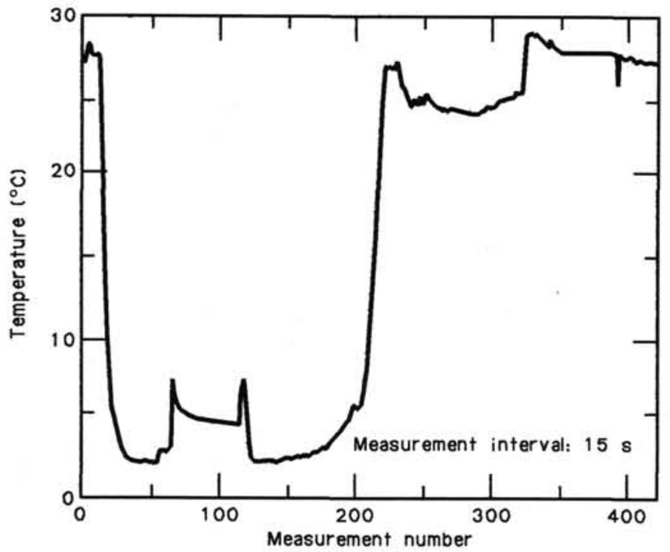

Figure 42. Temperature vs. time record for second deployment of APC tool, Core 110-673B-3H, 26.6 mbsf.

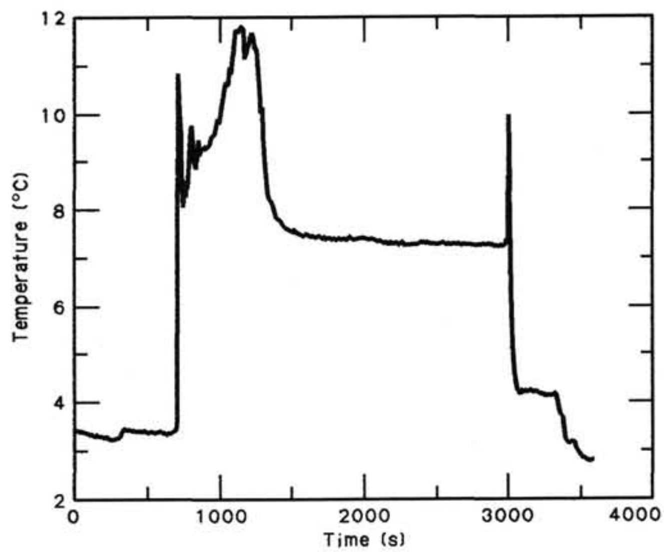

Figure 44. Temperature vs. time record for deployment of T-probe, after Core 110-673B-8X. Depth is 74.7 mbsf.

Changes in thermal conductivity (Fig. 46) were taken into account by numerically integrating the thermal resistance of the sediment column above each temperature-measurement depth (see Heat Flow section, Site 672 chapter). There is considerable nonlinearity in the resistance-temperature relationship (Fig. 47) but the thermal regime is assumed to be conductive. If only the three APC tool measurements are included, the conductive heat flow is 100 mW/m^2; if all four data are incorporated, the calculated heat flow is 80 mW/m^2. Because the T-probe measurement from Hole 673B is a lower bound only, the true conductive heat flow at Site 673 is probably closer to 100 mW/m^2 than it is to 80 mW/m^2.

This heat-flow value is significantly higher than that theoretically expected for 90-Ma crust (Anderson and Skilbeck, 1982; Lister, 1977), predicted by thermal models of accretionary complexes (e.g., Hsü and Toksoz, 1979), or measured over the Lesser Antilles accretionary complex prior to Speed et al. (1984). However, the heat flow measured at Site 673 is in general agreement with values measured at Site 541 (Davis and Hussong, 1984) and along a transect at 15°30'N during the Leg 110 site survey (Langseth et al., 1986). The latter paper noted that surface heat-flow values increased westward at this latitude and suggested that penetrating thrusts act as conduits for warm fluid raising surface heat-flow values. Site 673 is located west of the westernmost measurement made by Langseth, et al. (1986) at 15°30'N so that a direct comparison of results is impossible.

Apparently, the processes which resulted in high surface thermal gradients at Sites 671 (>100°C/km) and 672 (79°C/km) are active 13 km west of the deformation front. Two major thrusts cored in Hole 673B (Structural Geology and Biostratigraphy sections, this chapter) coincide with pore-water chloride anomalies (Geochemistry section, this chapter) suggesting that they could be loci of periodic, interstitial (subhorizontal), fluid migration. The temperature data at Site 673 are consistent with the migration of warm fluid along these faults, but are too sparse to instill more confidence in this interpretation.

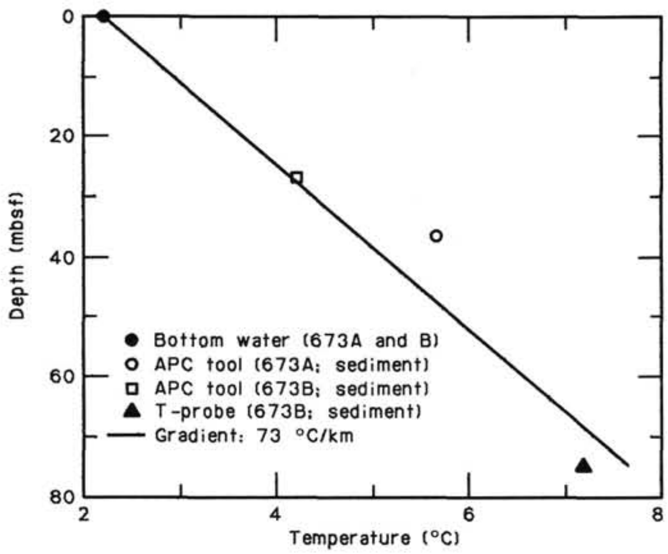

Figure 45. Plot of downhole temperatures vs. depth at Site 673.

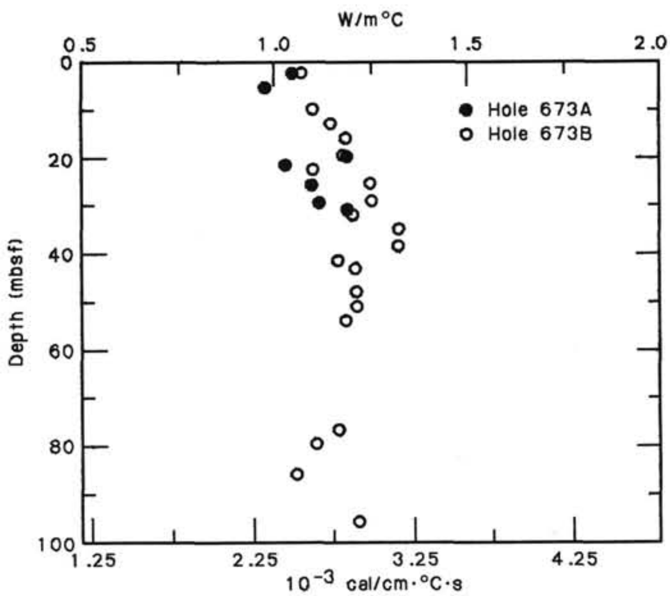

Figure 46. Plot of thermal conductivity vs. depth at Site 673.

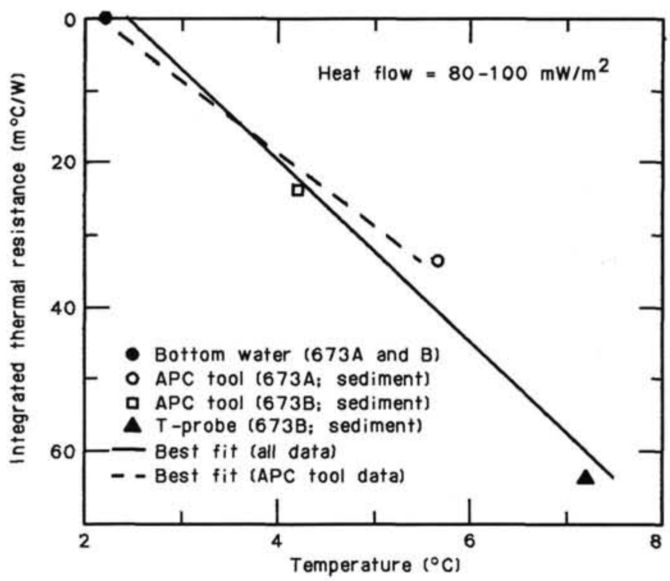

Figure 47. Plot of downhole temperatures vs. integrated thermal resistance at Site 673. Linear-least-squares best-fitted curves generated with APC data alone and with all data are shown.

CONCLUSIONS

Site 673 involved a 36-m penetration at Hole 673A, a 600-m eastward offset to Hole 673B, followed by a penetration 331 m deep. Both holes were terminated because of technical problems. Nevertheless, important data were gathered on slope sedimentary processes and the structural and hydrogeologic evolution of the offscraped sedimentary deposits.

The cored section at Site 673 is subdivided into two lithologic units (Fig. 48). Unit 1 consists of Pleistocene and Pliocene calcareous muds and marls, reworked claystone blocks of probable Miocene age, and matrix-supported conglomerates and breccias. The latter lithology shows signs of submarine weathering and was probably derived from nearby outcrops of Miocene sediment. Facies of Unit 1 clearly document active slope erosion and resedimentation.

In Hole 673B the unequivocal Pliocene (2.2 Ma) sediments extend to 39 mbsf but matrix-supported conglomerates and breccias including lower Miocene fossils occur as deep as 74 mbsf. Thus, the slope sediments could be either 39 or 74 m deep. The lack of similar matrix-supported conglomerates and breccias in Unit 2, plus an apparent angular unconformity between the conglomeratic deposits and Unit 2, suggest that the former are slope deposits and that the lower Miocene fossils in the conglomerates are reworked. Alternatively, the Miocene conglomeratic deposits could be considered as the true age of the beginning of slope sedimentation at about 17 Ma. However, if slope deposition began this long ago, a much thicker and seismically resolvable sedimentary blanket should have accumulated. In summary, slope sedimentation must have been initiated by 2.2 Ma but probably did not begin as long ago as 17 Ma.

Lithologic Unit 2 consists of massive middle and lower Miocene claystones and siliceous claystones. This facies is lithologically similar to, but significantly less condensed than, that recovered at Site 672 on the Tiburon Rise. Owing to the complex folding and faulting, original thicknesses are not apparent at Site 673. Unit 2 apparently accumulated hemipelagic sediment below the calcite compensation depth.

Site 673 provides a structural perspective on the continuing deformation of offscraped deposits as they are uplifted and dewatered. Documentation of a thick overturned section with the necessity of relatively large-scale folding distinguishes Site 673 structurally from other sites downslope to the east. Associated biostratigraphically-documented thrust faulting occurs at at least three intervals in the lower and middle Miocene section. The downhole extent of the lower and middle Miocene section indicates substantial structural thickening because of steeping of bedding dips and small-scale thrusting. Apparently thrust packages, similar to those defined at Sites 541, 542, and 671, undergo significant internal deformation by folding and faulting to create sequences like that cored at Site 673 (Fig. 49). The lower Miocene brown clay(stone) interval in Core 110-673B-28X appears to correlated to the stratigraphic interval along which the décollement is now developing (see Site chapters 671 and 672). The absence of major faulting in this interval at Site 673 suggests that the décollement surface was positioned at a deeper stratigraphic interval during the offscraping of the Site 673 sequence. The occurrence of calcite veins along zones of scaly fabric, associated with a major fault zone in otherwise carbonate-free rocks, suggests fluid flow takes place through fracture permeability of the scaly zones. Thus, even though scaly fabrics in the décollement zone at Site 671 are not conspicuously mineralized, they could serve as fluid conduits.

At Site 673, water content and porosity decrease systematically in the extensive lower and middle Miocene section after a rapid decrease through the upper 74 m of probable slope deposits. Comparisons to age- and depth-equivalent sections from the oceanic reference sites DSDP Site 543 and ODP Site 672 indicate a porosity decrease from about 70% to 60%, reflecting a 25% decrease in total volume. Because porosity is the ratio of voids to voids plus solids, a percentage decrease in porosity is always exceeded by the total volume decrease in the rock. This porosity reduction estimate makes no allowance for erosion and accordingly it is a maximum. The accreted rocks from Barbados, which have only been slightly buried, have a dry bulk density of about 2.25 gm/cm^3 and a porosity of 17% (Larue et al., 1985). Porosities for sedimentary rocks uplifted in accretionary complexes elsewhere are typically less than 10% (Bray and Karig, 1985). The mudstones at Site 671 have moved only modestly along their ultimate dewatering path despite being substantially deformed.

Seismic reflection line CRV 128 through Site 673 shows a number of arcward-dipping reflectors which are also expressed, although at a shallower dip, on seismic line A-3. Reflectors of the two seismic lines define a common plane dipping west about 12°, suggesting that the reflections are not artifacts of seismic processing. Bedding dips are variable in magnitude and orientation at Site 673, indicating that they cannot generate the reflections. Slight acoustic impedance contrasts are observed, however, across biostratigraphically defined faults, suggesting that these features may be the source of the reflections. If the faults are represented by the largely planar reflectors that define imbricate packages, then these faults are highly discordant to internal structure of the packages; this discordance between within-package structures and their bounding surfaces appears to increase arcward from Site 541 to Site 671 and to Site 673.

The pore water at Site 673 provides critical insights on fluid transport in the accretionary prism. In Hole 673B a chloride minimum between 120 and 215 mbsf lies between two biostratigraphically defined thrust faults and is centered on a prominent section of overturned beds. Apparently this fault-bounded, overturned section makes up a significant conduit for lateral advection of low-chlorinity fluids from depth. Similarly, a chloride low correlating with a fault at about 292 mbsf in Hole 673B suggests that this is also an active conduit for fluid transport. The absence of any methane correlated with the low-chloride intervals suggests that the fluids are not as deeply derived as those sampled below the décollement at Site 671. Probably the fluids come from relatively shallowly buried, Neogene sediments of low organic content (Fig. 50). In contrast, the methane sampled at Site 671 and 672 is probably of thermogenic origin reflecting burial temperatures in excess of 70°C (see Geochemistry section). The apparent thermal gradient of 76- to 96°/km at Site 673 would permit thermogenic methane generation above the décollement, but it is likely that these are spurious temperature gradient values owing to flow of warm fluids (see Heat Flow section, Site 674).

REFERENCES

Anderson, R. N. and Skilbeck, J. N., 1982. Oceanic heat flow. *In* Emiliani, C. (Ed.), *The Sea* (Vol. 7), *The Oceanic Lithosphere*: New York (Wiley and Sons): 489-524.

Biju-Duval, B., Le Quellec, P., Mascle, A., Renard, V., and Valery, P., 1982. Multibeam bathymetric survey and high resolution seismic investigations of the Barbados Ridge complex (Eastern Caribbean): A key to the knowledge and interpretation of an accretionary wedge. *In* Le Pichon, X., Augustithis, S. S., and Mascle, J. (Eds.), Geodynamics of the Hellenic Arc and Trench: *Tectonophys.*, 86: 275-304.

Biju-Duval, B., Moore, J. C., et al., 1984. *Init. Repts. DSDP*, 78A: Washington (U.S. Govt. Printing Office).

Boyce, R. E. 1976. Definitions and laboratory techniques of compressional sound velocity parameters and wet-water content, wet bulk density, and porosity parameters by gravimetric and gamma ray attenuation techniques. *In* Schlanger, S. O., Jackson, E. D., et al., *Init. Repts. DSDP*, 33: Washington (U.S Govt. Printing Office), 931-958.

Bray, C. J., and Karig, D. E., 1985. Porosity of sediments in accretionary prisms and some implications for dewatering processes. *J. Geophys. Res.*, 90: 768-778.

Cloos, M., 1984. Landward dipping reflectors in accretionary wedges: Active dewatering conduits? *Geology*, 12:519-522.

Davis, D., and Hussong, D., 1984. Geothermal observations during Deep Sea Drilling Project Leg 78A. *In* Biju-Duval, B., Moore, J. C., et al., *Init. Repts. DSDP*, 78A: Washington (U.S. Govt. Printing Office), 593-598.

Davis, D., Suppe, J., and Dahlen, F. A., 1983. The mechanics of fold-and-thrust belts. *J. Geophys. Res.*, 88: 1153-1172.

Gartner, S., 1977. Calcareous nannofossil biostratigraphy and revised zonation of the Pleistocene. *Mar. Micropaleontology*, 2: 1-25.

Hemleben, C., and Auras, A., 1984. Variations in the calcite dissolution pattern on the Barbados Ridge complex at Sites 541 and 543, Deep Sea Drilling Project Leg 78A. *In*: Biju-Duval, B., Moore, J. C., et al., *Init. Repts. DSDP*, 78A: Washington (U.S. Govt. Printing Office), 471-508.

Hsü, A. T., and Toksoz, M. N., 1979. The evolution of thermal structures beneath a subduction zone. *Tectonophysics*, 60: 43-60.

Kuster, G. T., and Toksoz, M. N., 1974. Velocity and attenuation of seismic waves in two phase media. Part 1. Theoretical formulation. *Geophysics*, 39:587-606.

Langseth, M., 1965. Techniques of measuring heat flow through the ocean floor. *In*, Lee. W., Terrestrial Heat Flow, *Geophys. Monogr.* 8: Washington (AGU), 58-77.

Langseth, M., Westbrook, G., and Hobart, M., 1986. Geothermal transects of the lower trench slope of the Barbados accretionary prism [paper presented at the 11th Annual Caribbean Geological Conference, Bridgetown, Barbados].

Larue, D. K., Schoonmaker, J., Torrini, R., Lucas-Clark, J., Clark, M. and Schneider, R., 1985. Barbados: maturation, source rock potential and burial history within a Cenozoic accretionary complex. *Mar. Petrol. Geol.*, 2: 96-110.

Lister, C.R.B., 1977. Estimates for heat flow and deep rock properties based on boundary layer theory. *Tectonophysics*, 41: 157-171.

Manheim, F. T., and Waterman, L. S., 1974. Diffusimetry (diffusion constant estimation) on sediment cores by resistivity probe. *In* Von der Borch, C. C., Sclater, J. G., et al., *Init. Repts. DSDP*, 22:Washington (U.S. Govt. Printing Office), 663-670.

Mascle, A., Biju-Duval, B., deClarens, Ph., Munsch, H., 1987. Growth of accretionary prisms, tectonic processes from Caribbean examples. *In* Wezel, D. (Ed.), *The Origin of Arcs*: New York (Elsevier Scientific Publ. Co.), 375-400.

Minster, J. B., and Jordan, T. H., 1978. Present-day plate motions. *J. Geophys. Res.*, 83: 5331-5354.

Moore, J. C., and Biju-Duval, B., 1984. Tectonic synthesis Deep Sea Drilling Project Leg 78A: Structural evolution of offscraped and underthrust sediment, northern Barbados Ridge complex. *In* Biju-Duval, B., and Moore, J. C., et al., *Init. Repts. DSDP*, 78A: Washington (U.S. Govt. Printing Office), 601-621.

Okada, H., and Bukry, D., 1980. Supplementary modification and introduction of code numbers to the low latitude coccolith biostratigraphic zonation (Bukry 1973, 1975). *Mar. Micropaleontology*, 5: 321-325.

Riedel, W. R., and Sanfilippo, A., 1978. Stratigraphy and evolution of tropical Cenozoic radiolarians. *Micropaleontology.*, 24: 61-96.

Speed, R. C., and Larue, D. K., 1982. Barbados: Architecture and implications for accretion. *J. Geophys. Res.*, 87: 3633-3643.

Speed, R. C., Westbrook, G. K., Mascle, A., Biju-Duval, B., Ladd, J., Saunders, J., Stein, S., Schoonmaker, J., and Moore, J. C., 1984. Lesser Antilles Arc and adjacent terranes. *In* Ocean Margin Drilling Program, Regional Atlas Series, *Atlas 10*. Woods Hole: (Marine Science International).

Sykes, L. R., McCann, W. R., and Kafka, A. L., 1983. Motion of Caribbean Plate during last 7 million years and implications for earlier Cenozoic movements. *J. Geophys. Res.*, 87: 10656-10676.

Von Herzen, R. P., and Maxwell, A. E., 1959. The measurement of thermal conductivity of deep-sea sediments by a needle probe method. *J. Geophys. Res.*, 65: 1535–1541.

Von Huene, R., and Lee, H., 1982. The possible significance of pore fluid pressures in subduction zones. *In* J. S. Watkins, and C. L. Drake (Eds.), Studies in Continental Margin Geology, *Am. Assoc. Pet. Geol. Mem.*, 34: 781–791.

Watkins, J. S., et al., 1981. Accretion, underplating, and tectonic evolution, Middle America Trench, southern mexico: Results from Leg 66 DSDP. *In* Blanchet, R., and Montadert, L., (Eds.), Geology of Continental Margins, Colloque 3, 26th Internat. Geol. Cong., Paris, *Oceanology Acta*, 213–224.

Westbrook, G. K., 1982. The Barbados Ridge complex: tectonics of a mature forearc system. *In* Leggett, J. K., (Ed.), *Trench-Forearc Geology*, Sp. Publ. Geol. Soc. London, No. 10: London (Blackwells), 275–290.

Westbrook, G. K., and Smith, M. J., 1983. Long décollements and mud volcanoes: Evidence from the Barbados Ridge Complex for the role of high pore-fluid pressure in the development of an accretionary complex. *Geology*, 11: 279–283.

Ms 110A-107

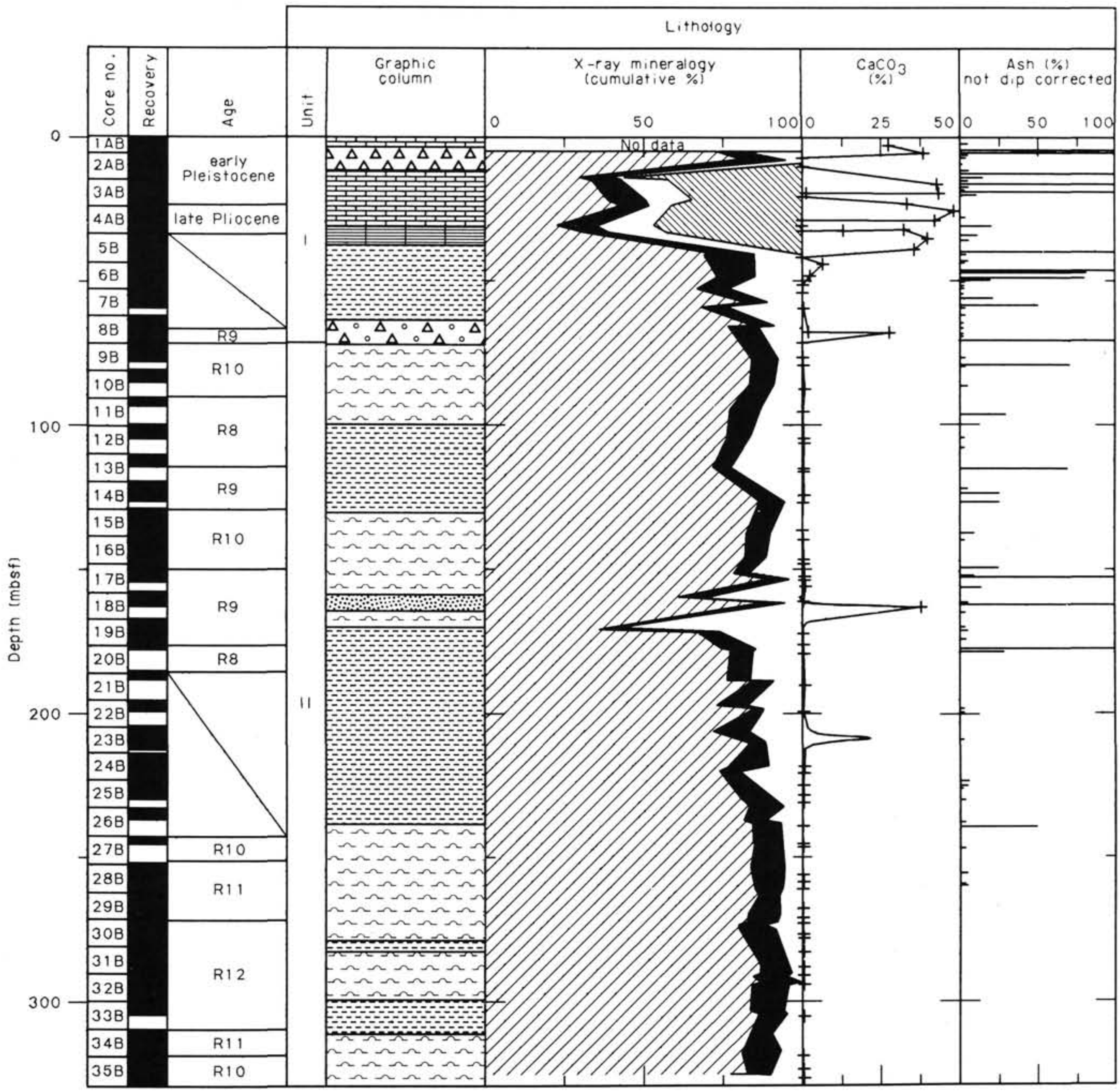

Figure 48. Site 673 summary diagram. Note that the 100-m throw on the fault in Core 110-673B-23X also includes a section repeated by the fold. Relation of total throw to folding is uncertain.

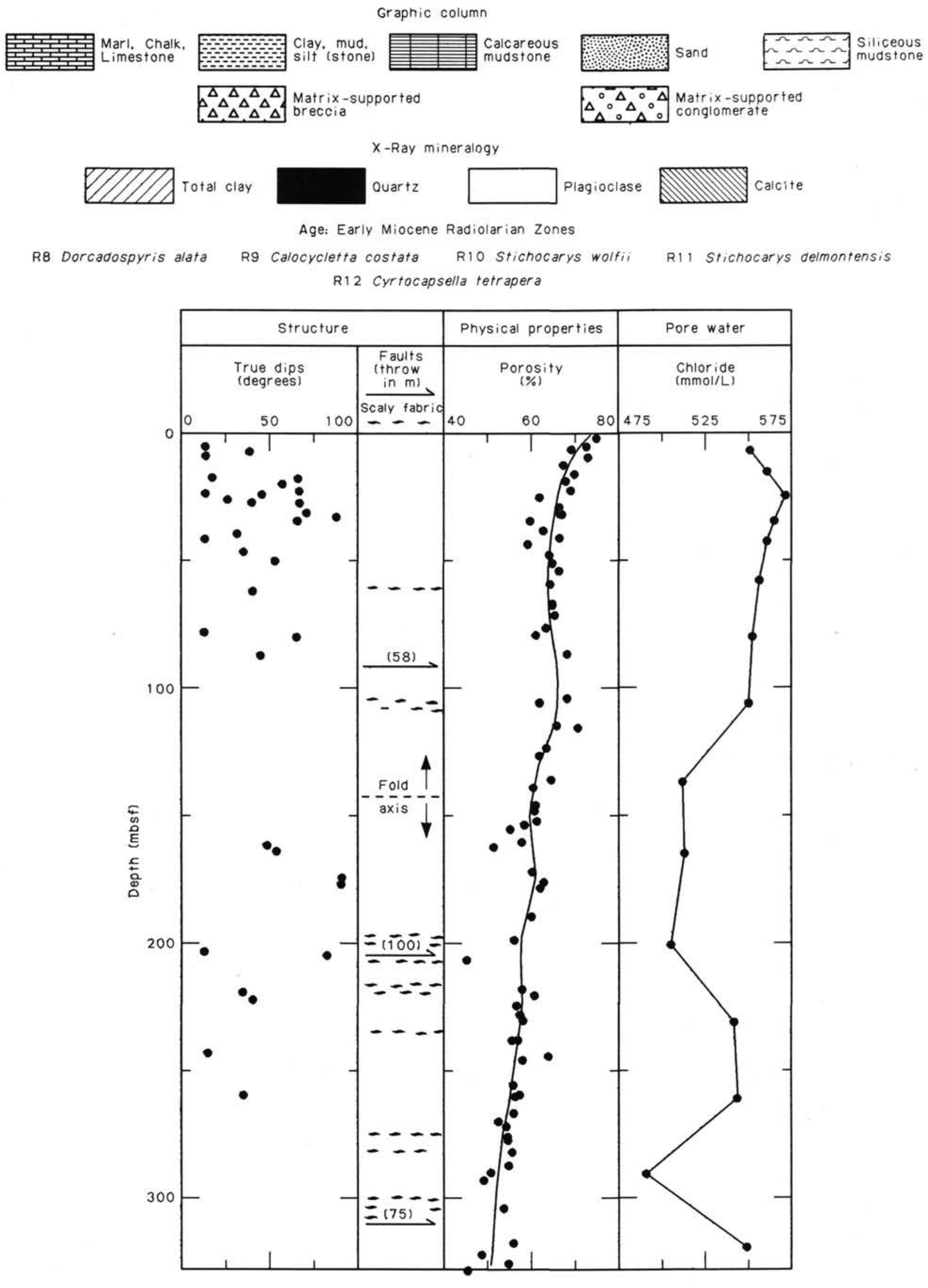

Figure 48 (continued).

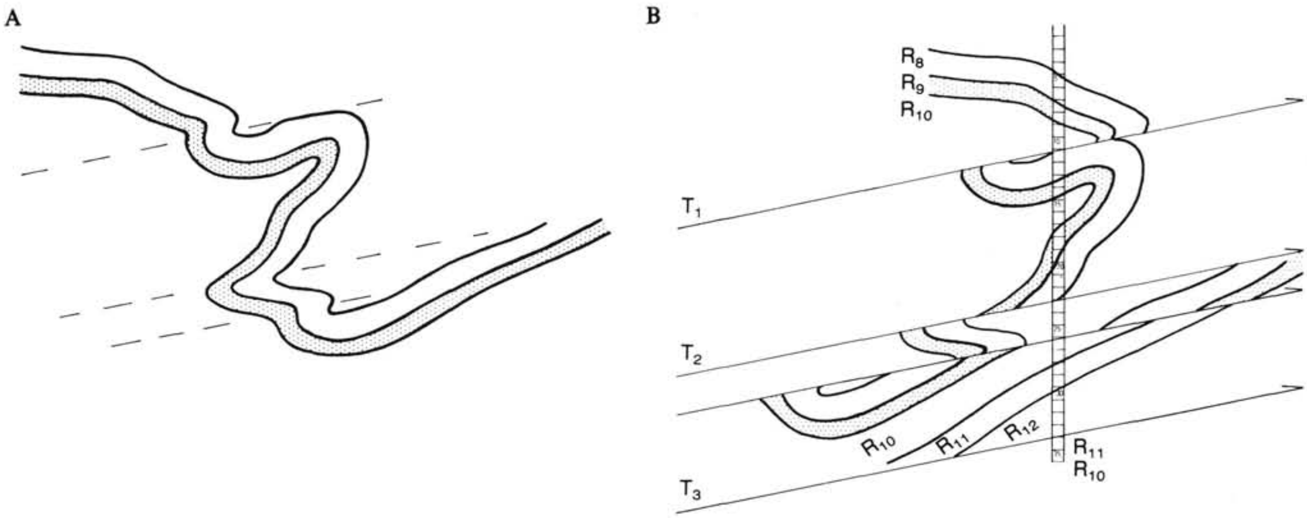

Figure 49. One of the many possible models of tectonic deformation in the accreted packets 1, 2, and 3 of Site 673. This internally consistent model is derived from the geometric model A of the structural analysis (see Structural Geology section) and it is in agreement with all radiolarian ages so far obtained (R12 to R8 refer to early Miocene radiolarian zones, see Biostratigraphy section). A fourth major thrust fault has, however, been added below fault T2 to take into account the apparent lack of radiolarian zones R9 and R8 between zone R10 and barren formations which are assumed to be of middle Miocene age. This model requires a first stage (A) of slightly disharmonic eastward-verging folding inside an accreted package (as proposed at the toe of the complex, see Site 671 report) and a second stage (B) of thrusting along low-angle faults. The amount of displacement along the faults has been minimized to maintain the greatest degree of coherency between the different tectonic units (all the sections from Core 110-673B-8X to -35X range in age from the middle to early Miocene; this time interval was less than 50 m thick at the reference Site 672). Thrust faults T_1 and T_3 are relatively well correlated with seismic reflectors dipping about 12° W. In such a model the amplitude of structures is about 100 m. The water content of these sediments is still between 30 and 40%.

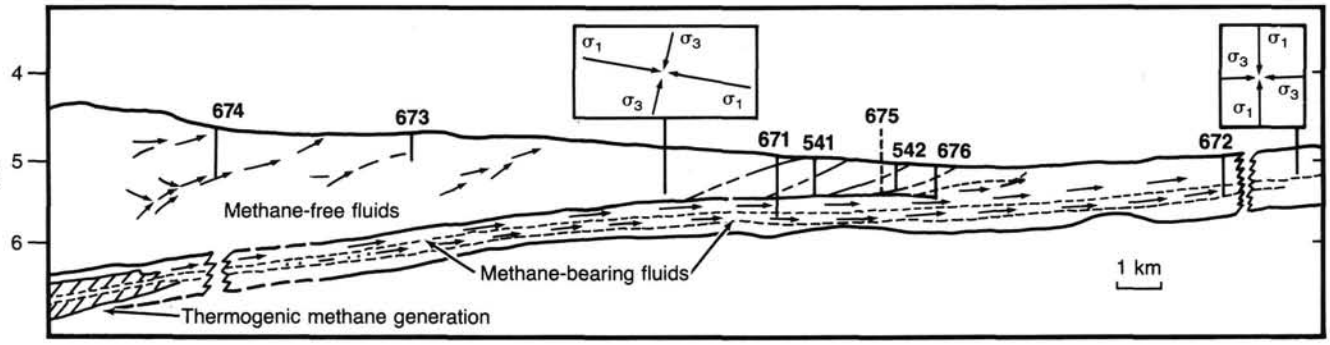

Figure 50. Depth section showing possible migration path of low-chloride, methane-free fluids. The source of fluids is within material above seismic décollement in contrast to possible migration path of low-chloride, methane-bearing fluids observed at Sites 671, 676, and 672. Insets show approximate orientation of stress in accretionary prism and in incoming sediment column on oceanic crust. Vertical exaggeration of cross-section is 2:1.

SITE 673 HOLE A CORE 1 H CORED INTERVAL 4667.4-4675.3 mbsl; 0.0-7.9 mbsf

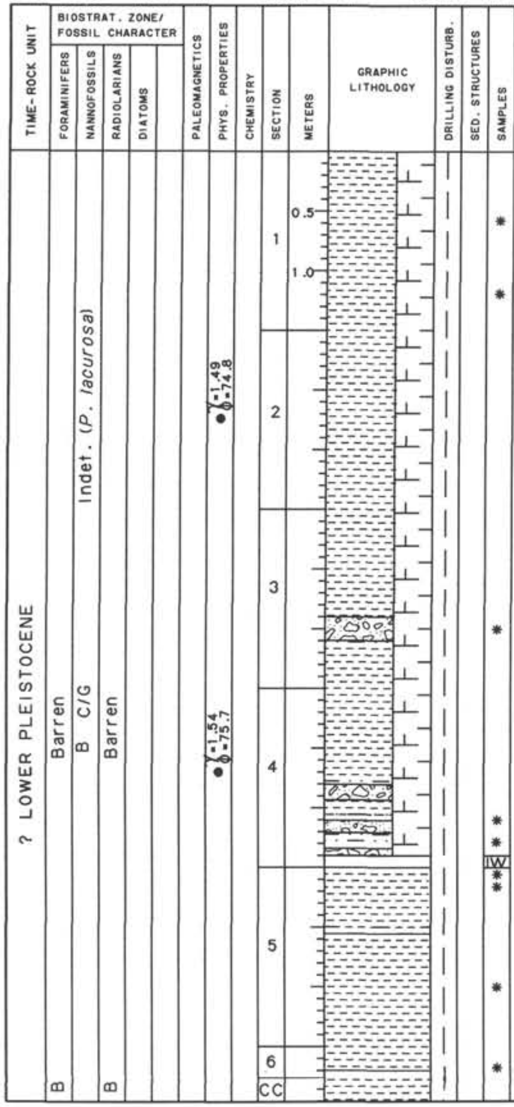

LITHOLOGIC DESCRIPTION

MARL to CALCAREOUS MUDSTONE, and CLAYSTONE

Yellowish brown (10YR5/6, 10YR7/6) bioturbated MARL to CALCAREOUS MUDSTONE; rich in sand-sized foraminifers in Sections 1 through 4. Dark greenish gray (5BG5/1) CLAYSTONE in Sections 5, 7, and CC.

Minor lithology: lighter green ash burrow infillings in green claystone.

SMEAR SLIDE SUMMARY (%):

	1, 55 M	1, 120 D	3, 100 M	4, 110 D	4, 134 M	5, 8 M	5, 28 D
TEXTURE:							
Sand	80	10	5	—	7	—	—
Silt	20	5	80	1	20	5	10
Clay	—	85	15	99	80	95	90
COMPOSITION:							
Quartz	2	—	—	1	1	1	—
Feldspar	5	—	50	—	Tr	1	5
Clay	—	60	15	99	78	93	94
Pumice	89	—	20	—	1	2	—
Accessory minerals	—	—	—	—	—	3	—
(Clino)pyroxene	1	—	12	—	—	—	—
Opaques	3	—	2	—	20	—	1
Hornblende	Tr	—	—	—	—	—	—
Foraminifers	—	15	Tr	—	Tr	—	—
Nannofossils	—	24	—	—	Tr	—	—
Sponge spicules	—	1	1	—	—	—	—
Plant debris	—	—	—	—	—	Tr	—

	5, 100 D	6, 20 M
TEXTURE:		
Silt	Tr	1
Clay	100	99
COMPOSITION:		
Quartz	Tr	1
Feldspar	Tr	—
Clay	100	99
Volcanic glass	—	1
Accessory minerals	—	Tr
Aggregate of cemented silt and quartz grains	Tr	—

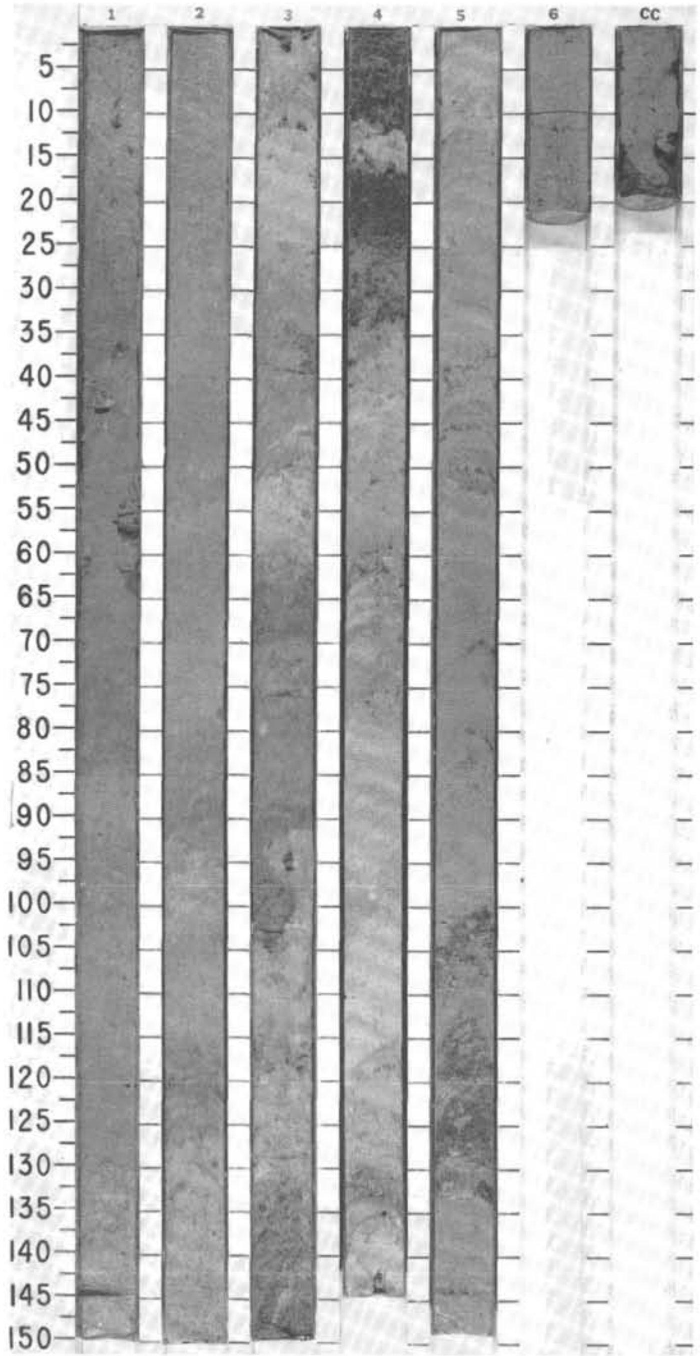

SITE 673 HOLE A CORE 2 H CORED INTERVAL 4675.3-4684.8 mbsl; 7.9-17.4 mbsf

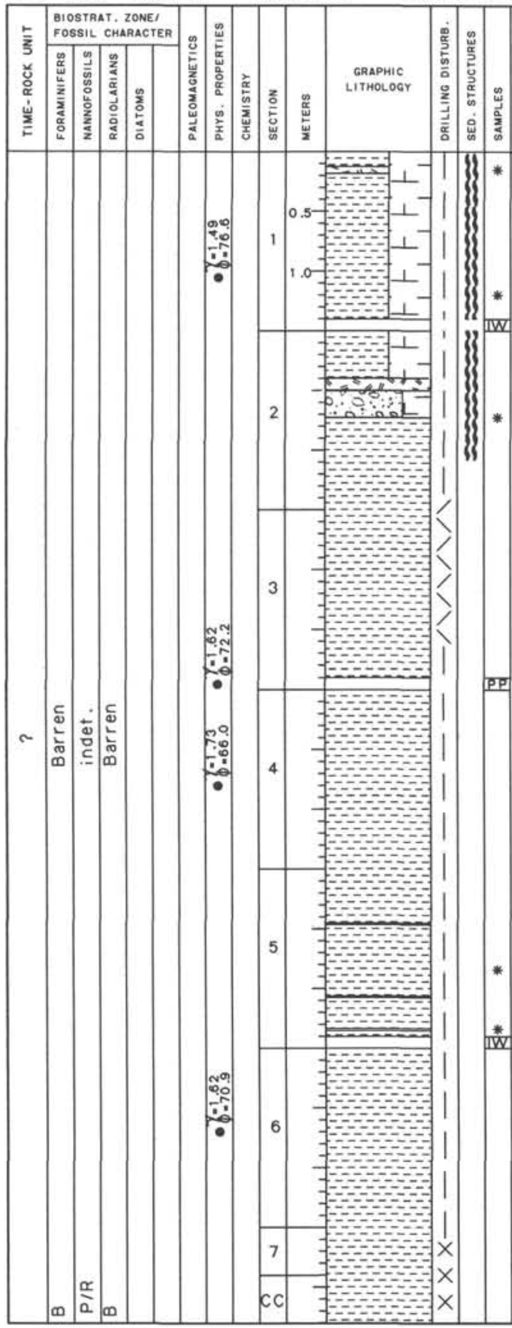

LITHOLOGIC DESCRIPTION

MARL, MUD, CALCAREOUS MUD, MATRIX-SUPPORTED BRECCIA, and CLAYSTONE

Light yellowish brown (5GY5/1, 10YR6/4) bioturbated MARL and calcareous MUD in Sections 1 and 2. High concentrations of foraminifers in some layers in Section 1 (up to 25 %). Towards base of Section 2 varicolored greenish gray and dark gray CALCAREOUS MUD and horizons rich in MATRIX-SUPPORTED BRECCIA. Clasts composed of brown marl and greenish gray claystone. From base of Section 2 downward to CC is greenish gray (5G5/1) homogenous CLAYSTONE.

Minor Lithology: ash layers: in Sections 1 and 2 brown and often diffuse due to bioturbation; in Section 3 and CC ash layers are less bioturbated and darker in color.

Structure: beds are approximately horizontal near the top of the core, in Section 5 beds dip at 10–20 degrees.

SMEAR SLIDE SUMMARY (%):

	1, 12 M	1, 125 D	2, 87 M	5, 83 D	5, 140 M
TEXTURE:					
Sand	10	10	—	—	60
Silt	90	15	80	20	40
Clay	—	75	20	80	—
COMPOSITION:					
Quartz	—	2	Tr	—	—
Feldspar	30	1	1	Tr	10
Clay	—	47	20	80	—
Volcanic glass	61	—	80	19	84
Accessory minerals	2	—	—	1	5
Orthopyroxene	4	—	—	—	—
Clinopyroxene	2	—	—	—	1
Hornblende	1	—	Tr	—	—
Foraminifers	—	20	—	—	—
Nannofossils	Tr	30	—	—	—

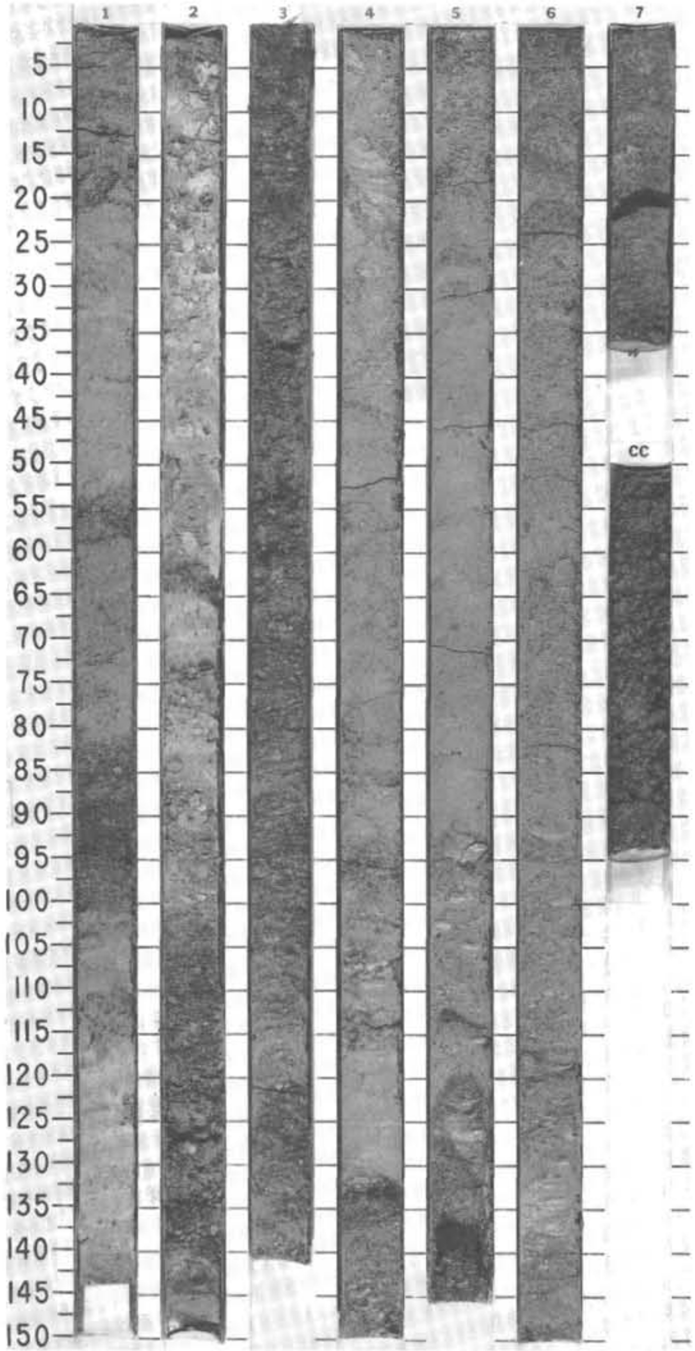

SITE 673 HOLE A CORE 3 H CORED INTERVAL 4684.8-4694.3 mbsl; 17.4-26.9 mbsf

TIME-ROCK UNIT	FORAMINIFERS	NANNOFOSSILS	RADIOLARIANS	DIATOMS	PALEOMAGNETICS	PHYS. PROPERTIES	CHEMISTRY	SECTION	METERS	GRAPHIC LITHOLOGY	DRILLING DISTURB.	SED. STRUCTURES	SAMPLES
EARLY/MIDDLE MIOCENE	Barren	Barren	Barren / *Dorcadospyris alata* Zone			γ=1.69 φ=66.4; γ=1.68 φ=68.3		1, 2, 3, 4, 5, 6	0.5, 1.0	VOID (Section 1); VOID (Section 4)			OG; IW

LITHOLOGIC DESCRIPTION

CLAYSTONE to MUDSTONE

Homogeneous greenish gray (5G5/1) CLAYSTONE to MUDSTONE. Section 3 contains scattered clasts of the same claystone throughout.

Minor lithology: very coarse vitric crystalline ash is present in minor quantities throughout much of the section.

Structure: bedding is probably shallowly dipping.

SMEAR SLIDE SUMMARY (%):

	5, 17 M	6, 120 D	6, 128 M
TEXTURE:			
Sand	10	1	—
Silt	40	12	6
Clay	50	87	94
COMPOSITION:			
Quartz	2	—	1
Feldspar	25	—	3
Clay	35	—	34
Volcanic glass	—	—	2
Accessory minerals	1	—	—
Pyroxene	2	—	—
Opaques	15	—	—
Micrite	—	—	60

cont.

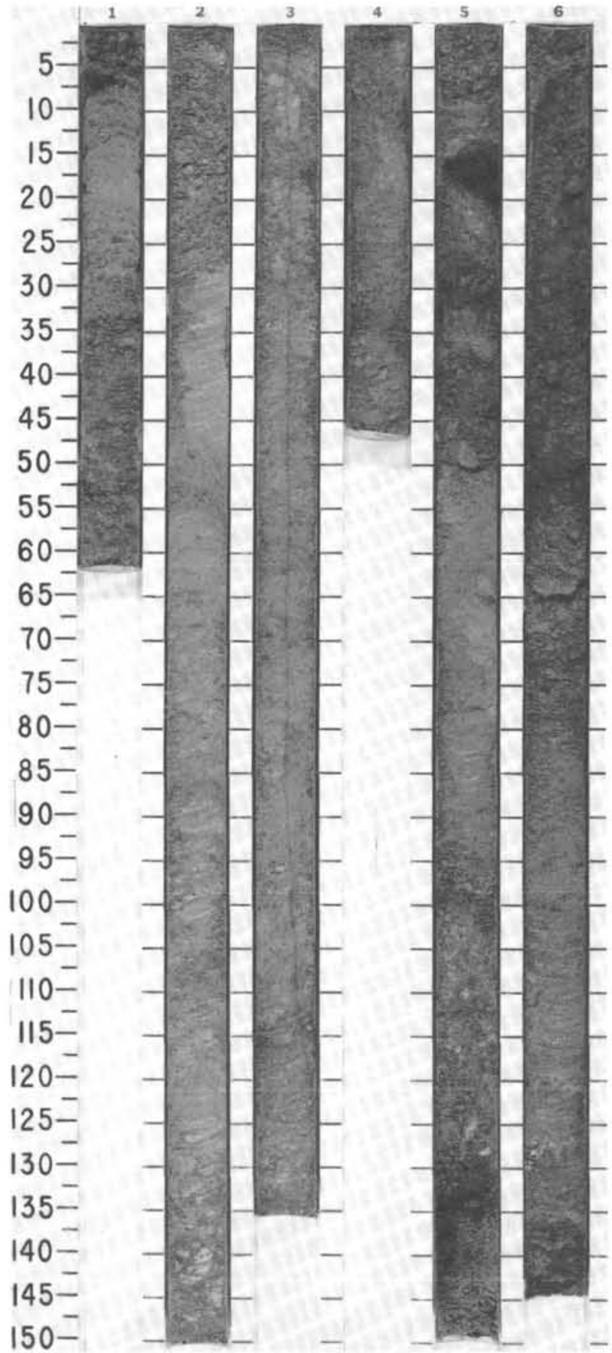

SITE 673 HOLE A CORE 3 H CORED INTERVAL 4684.8-4694.3 mbsl; 17.4-26.9 mbsf

TIME-ROCK UNIT	BIOSTRAT. ZONE/ FOSSIL CHARACTER: FORAMINIFERS	NANNOFOSSILS	RADIOLARIANS	DIATOMS	PALEOMAGNETICS	PHYS. PROPERTIES	CHEMISTRY	SECTION	METERS	GRAPHIC LITHOLOGY	DRILLING DISTURB.	SED. STRUCTURES	SAMPLES	LITHOLOGIC DESCRIPTION
								7		VOID				cont.
								8		VOID				
								9						
	B	B	F/M					CC						

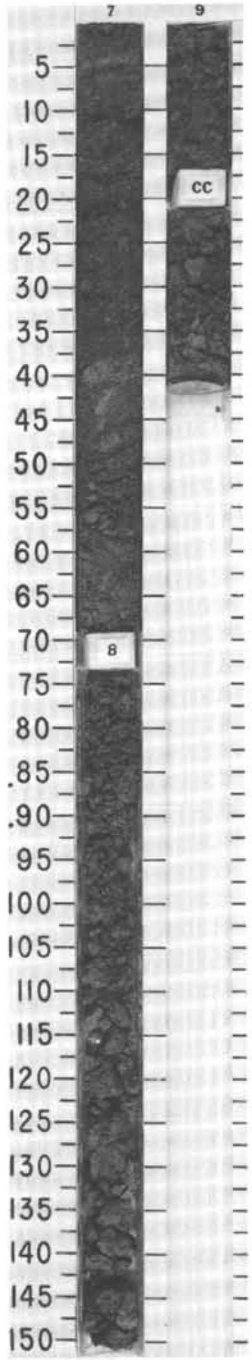

SITE 673 HOLE A CORE 4 H CORED INTERVAL 4694.3-4703.8 mbsl; 26.9-36.4 mbsf

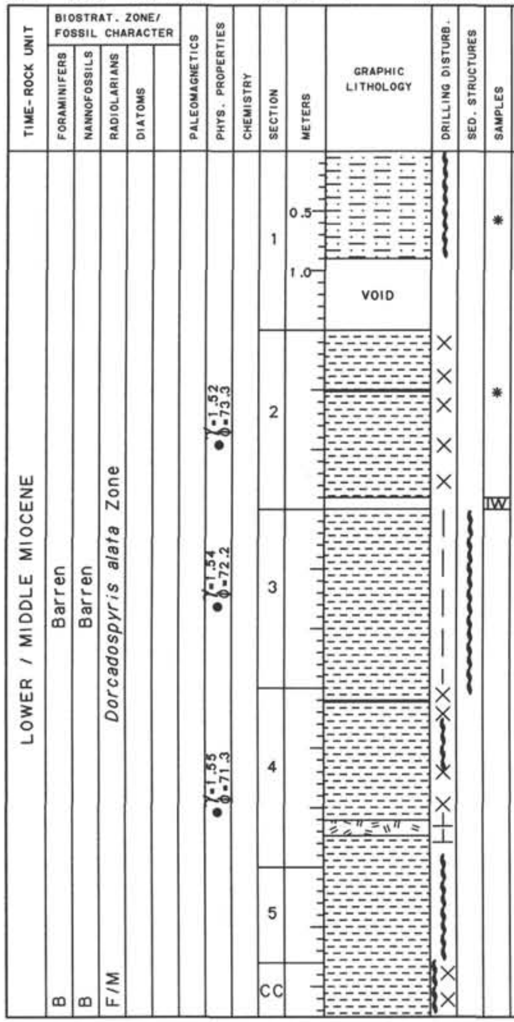

LITHOLOGIC DESCRIPTION

CLAYSTONE

Homogeneous to locally-burrowed greenish gray (5G5/1) CLAYSTONE. In general the core is highly disturbed by drilling deformation.

Minor lithology: dark gray (N3, N1) vitric crystalline ash at Section 4, 12–17 and 110–125 cm.

SMEAR SLIDE SUMMARY (%):

	1, 44 D	2, 70 M
TEXTURE:		
Sand	—	2
Silt	15	98
Clay	85	—
COMPOSITION:		
Quartz	5	—
Feldspar	5	30
Clay	85	3
Volcanic glass	—	57
Accessory minerals		
Clinopyroxene	1	5
Opaques	—	5
Radiolarians	3	—
Sponge spicules	1	—

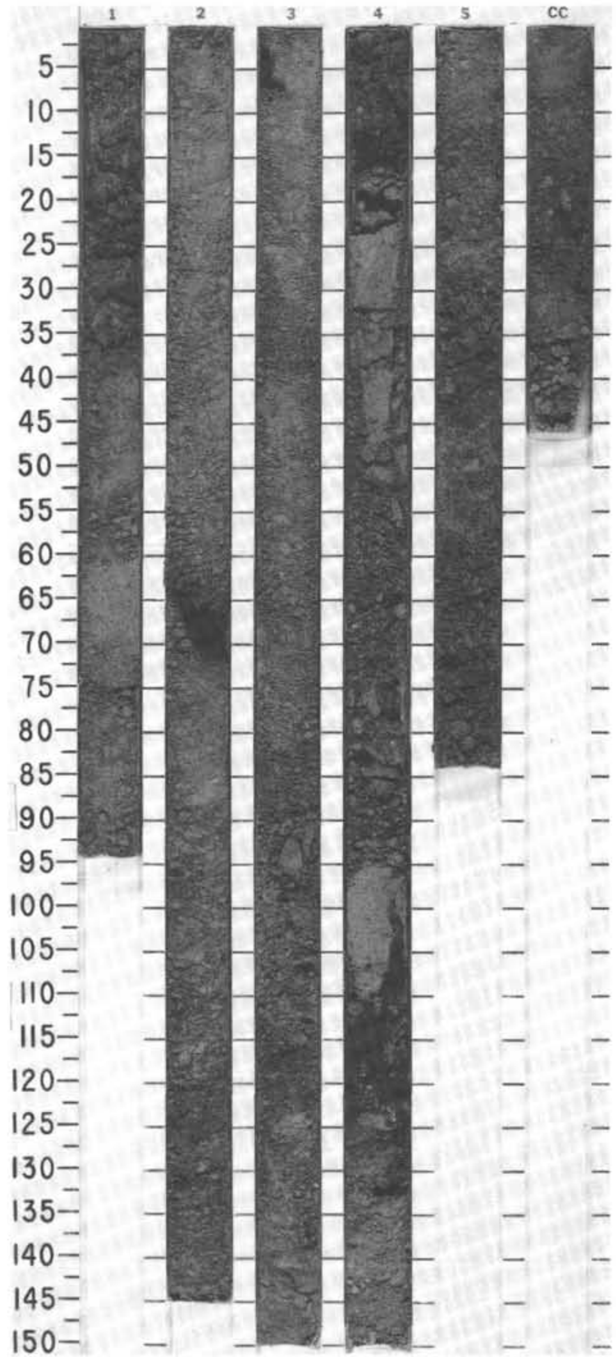

SITE 673 HOLE B CORE 1 H CORED INTERVAL 4689.2-4696.8 mbsl; 0.0-7.6 mbsf

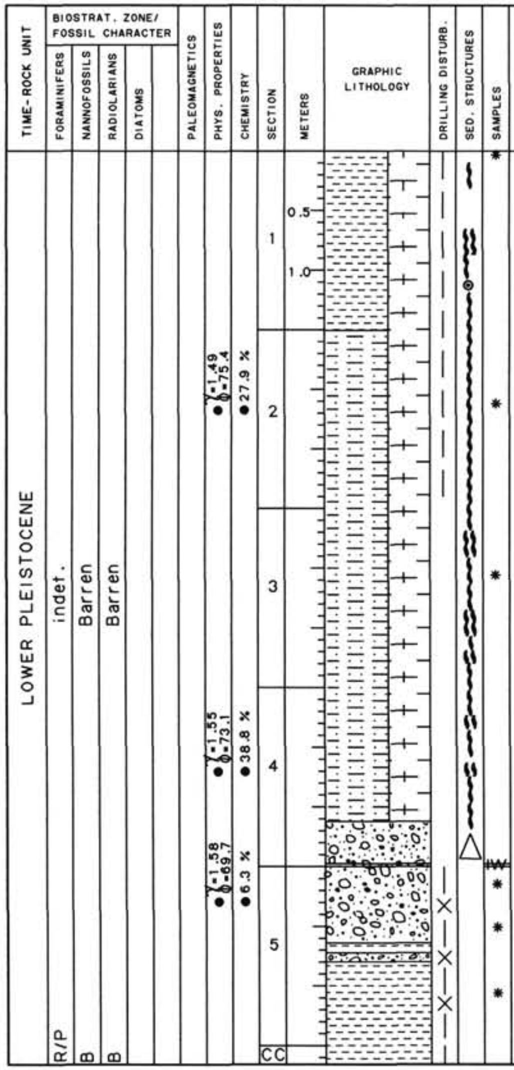

LITHOLOGIC DESCRIPTION

CALCAREOUS MARL CLAST-SUPPORTED CLAYSTONE BRECCIA, and CLAY and CONGLOMERATIC CLAY(STONE)

From top of Section 1 to Section 4, 116 cm, yellowish brown to light yellowish brown (10YR5/5–6/4), highly calcareous, foraminifer-nannofossil MARL. From 116 cm of Section 4 to 65 cm of Section 5, non-calcareous light brownish gray (2.5Y6/2) CLAST-SUPPORTED CLAYSTONE BRECCIA, showing fining-upward grading. Color changes downward to light yellowish brown (2.5Y5/4 or 5/6). With sharp contact, light greenish gray (5G6/1) to greenish gray (5GY5/1) CLAY and CONGLOMERATIC CLAY(STONE), from 65 cm of Section 5 to the bottom of the core.

Minor lithology: ash layers are interbedded as mentioned above. Ashy (5–10%) burrow mottles are sporadically disseminated throughout the upper calcareous part.

Structure: bedding is horizontal, fault of 65° dip in Section 5, 85–90 cm.

SMEAR SLIDE SUMMARY (%):

	1, 1 D	2, 62 D	3, 57 M	5, 13 D	5, 55 D	5, 110 D
TEXTURE:						
Sand	35	5	20	—	—	—
Silt	20	15	35	3	5	3
Clay	45	80	45	97	95	97
COMPOSITION:						
Quartz	1	5	—	1	10	8
Feldspar	1	5	2	1	—	—
Clay	37	40	20	93	82	85
Volcanic glass	—	15	78	—	8	7
Calcite/dolomite	Tr	—	—	—	—	—
Accessory minerals						
Glauconite	—	—	—	Tr	—	—
Orthopyroxene	Tr	—	—	—	—	—
Opaques	Tr	—	—	—	—	—
Fe oxide	Tr	—	—	—	—	—
Hematite	—	—	—	1	—	—
Foraminifers	35	5	—	—	—	—
Nannofossils	5	30	—	—	—	—
Sponge spicules	1	—	—	—	—	—

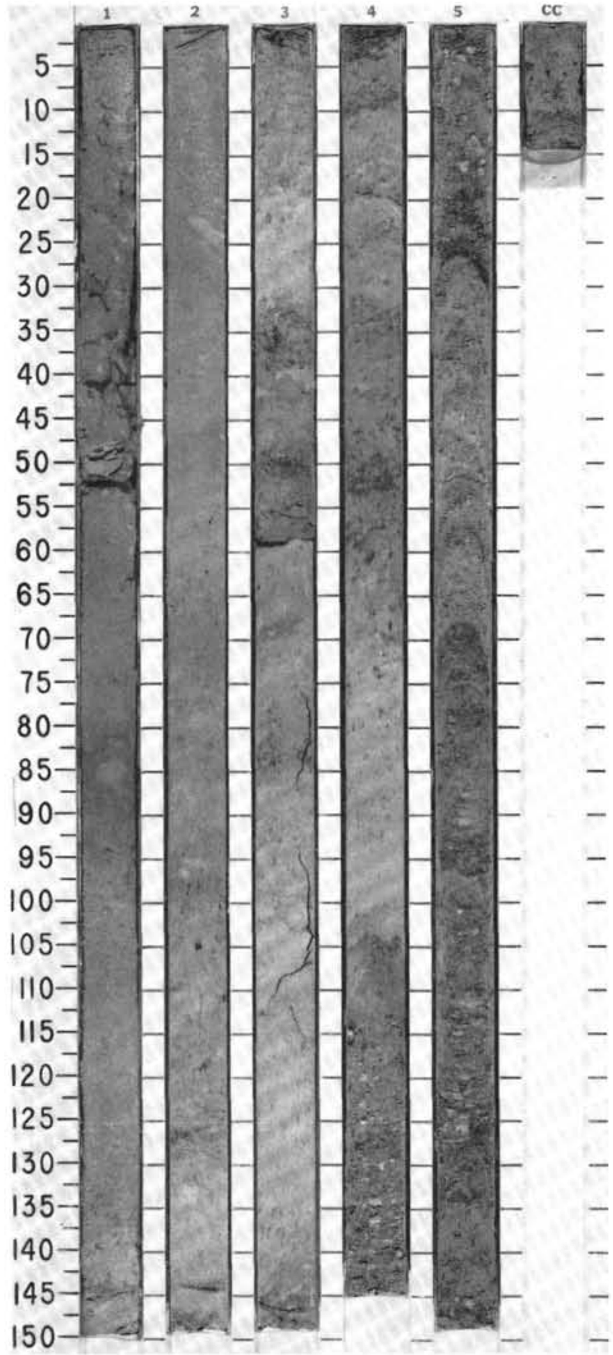

SITE 673 HOLE B CORE 2 H CORED INTERVAL 4696.8-4706.3 mbsl; 7.6-17.1 mbsf

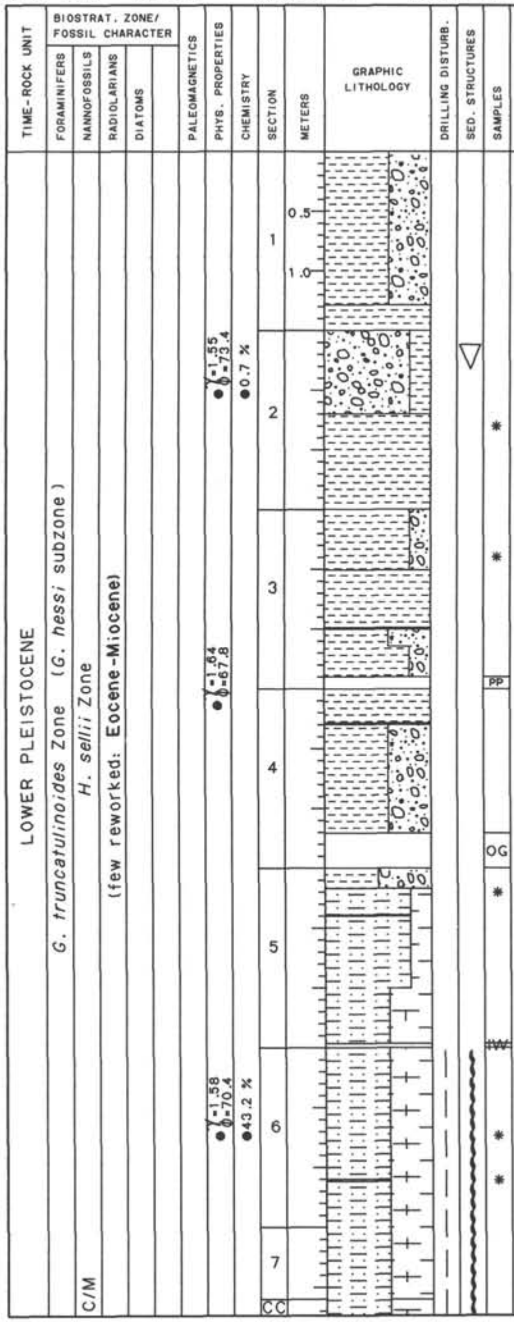

LITHOLOGIC DESCRIPTION

CLAY, CLAYSTONE, CALCAREUOS MUD, and MARL

From top of Section 1 to Section 5, 15 cm, is olive to olive-gray (5Y6/2–10Y5/2) CLAY. Top of Section 1 to Section 2, 70 cm, is breccia with clasts of similar colored, slightly indurated CLAYSTONE. Matrix-supported breccias in the upper part of Section 2. From Section 5, 15 cm, to the bottom of the core is reddish brown to brown (2YR4/3–2.5Y6/2) and light brownish gray (2.5Y5/2–6/2) CALCAREOUS MUD and MARL. Foraminifers are dispersed throughout.

Minor lithology: gray (10YR6/1) ash layer in Section 6, 108–116 cm; dispersed mottles of ashy materials throughout.

Structure: bedding seems to be inclined at 25–30° at the bottom of Section 1. Steep fault (60°) occurs at 50 cm of Section 3, and moderately to shallowly (45–20°) dipping faults occur at Section 6, 58–62 cm, and 128–133 cm.

SMEAR SLIDE SUMMARY (%):

	2, 80 D	3, 39 D	5, 27 D	6, 75 D	6, 113 M
TEXTURE:					
Sand	—	—	1	2	50
Silt	1	2	30	10	30
Clay	99	98	69	88	20
COMPOSITION:					
Quartz	Tr	1	2	—	—
Feldspar	1	1	5	—	56
Rock fragments	—	—	—	—	2
Clay	98	96	73	50	10
Volcanic glass	—	—	3	15	20
Accessory minerals					
Pyroxene	—	—	1	—	10
Opaques	1	—	1	—	—
Hornblende	—	—	—	—	2
Hematite	—	1	—	—	—
Foraminifers	—	—	10	—	—
Nannofossils	—	2	2	35	—
Radiolarians	—	—	1	—	—
Sponge spicules	—	—	Tr	—	—
Bioclasts	—	Tr	3	—	—

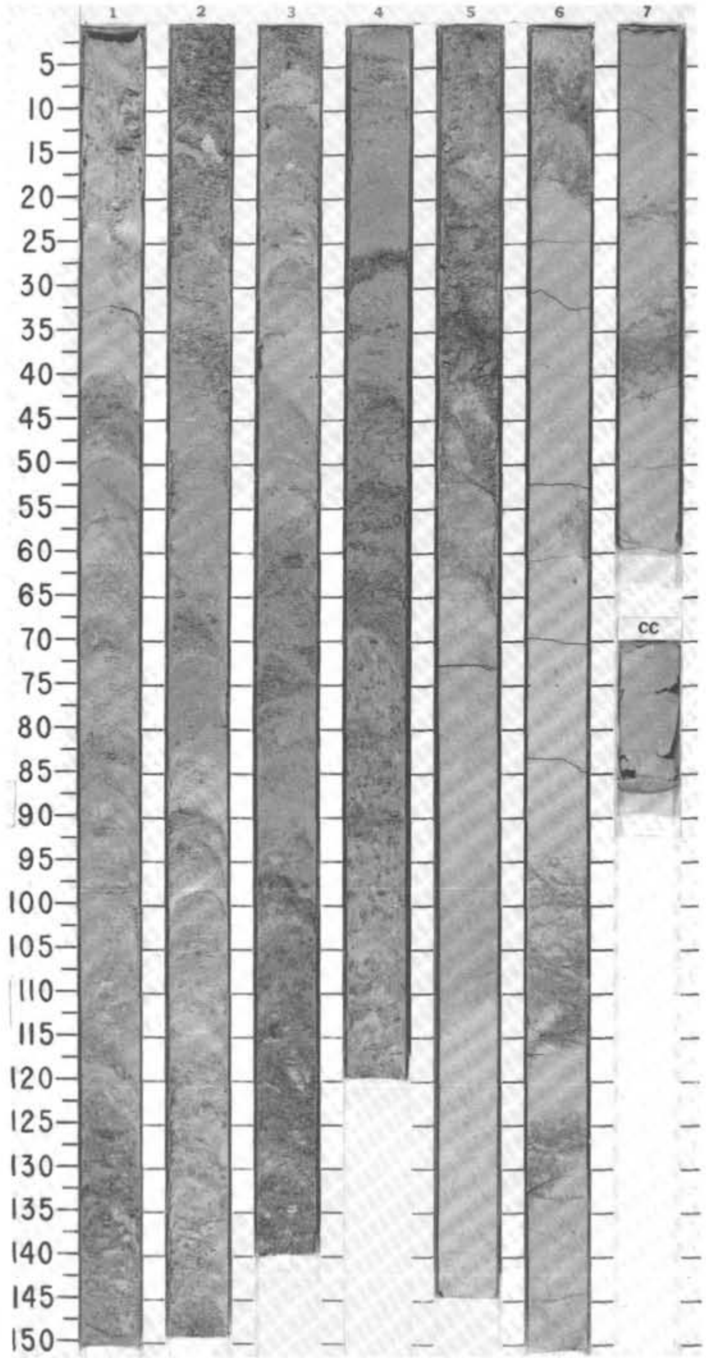

SITE 673 HOLE B CORE 3 H CORED INTERVAL 4706.3-4715.8 mbsl; 17.1-26.6 mbsf

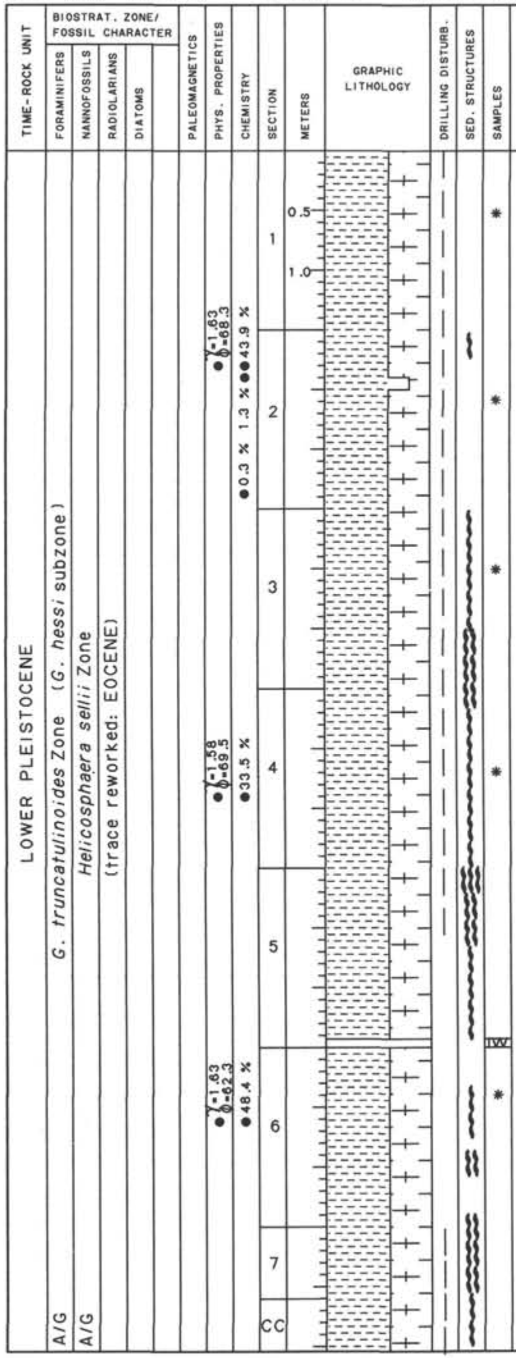

LITHOLOGIC DESCRIPTION

MARL

Light brownish gray or light olive (10YR6/2 or 5Y6/2) foraminifer-nannofossil MARL throughout the core. Color changes to pale brown and very pale brown (10YR7/2 and 7/4) from top of Section 5, due to the increase of foraminifer content.

Minor lithology: light gray ash layers at Section 4, 75 cm, and Section 5, 32 cm. Ashy materials are scattered throughout.

Structure: beds dip at 45–60° in Section 2, Section 4, and CC. Faults occur at Section 2, 33–42 cm, several parts of Section 3, and at Section 4, 20–30 cm (in this case reverse sense of 4 cm offset). In Section 6, 50–65 cm, they dip moderately to steeply (50–80°). An anastomosing fault zone occurs at Section 2, 62–110 cm; this dips 70–80°.

SMEAR SLIDE SUMMARY (%):

	1, 55 D	2, 58 D	3, 50 D	4, 73 M	6, 45 D
TEXTURE:					
Sand	—	2	—	30	5
Silt	12	40	25	50	25
Clay	88	58	75	20	70
COMPOSITION:					
Quartz	1	1	—	5	Tr
Feldspar	2	1	1	50	1
Rock fragments	—	—	—	8	—
Clay	55	61	59	10	64
Volcanic glass	1	1	—	20	—
Accessory minerals					
Glauconite	Tr	—	—	—	—
Pyroxene	—	—	—	3	—
Opaques	—	—	—	3	—
Hornblende	—	1	—	—	—
Foraminifers	5	20	15	—	25
Nannofossils	30	1	20	—	5
Radiolarians	Tr	—	—	—	—
Bioclasts	5	15	5	2	5

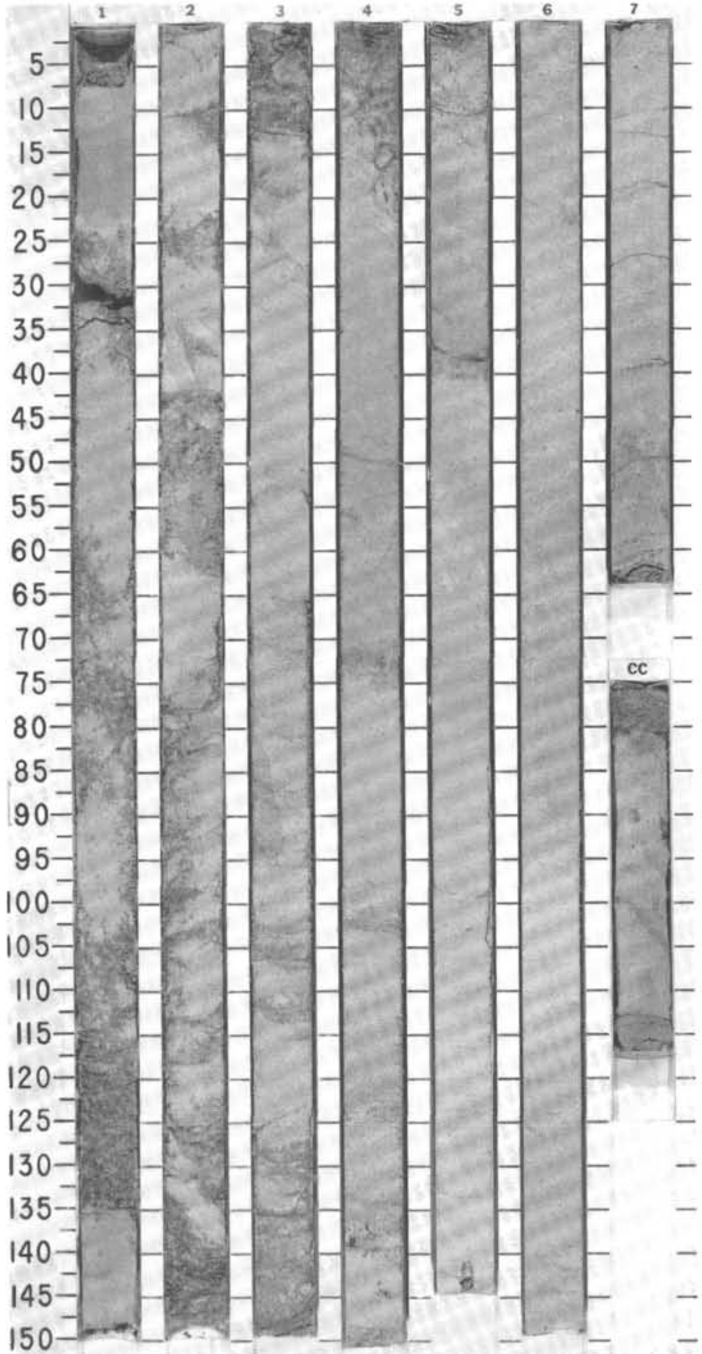

SITE 673 HOLE B CORE 4 H CORED INTERVAL 4715.8-4725.3 mbsl; 26.6-36.1 mbsf

TIME-ROCK UNIT	FORAMINIFERS	NANNOFOSSILS	RADIOLARIANS	DIATOMS	PALEOMAGNETICS	PHYS. PROPERTIES	CHEMISTRY	SECTION	METERS	SAMPLES
LOWER PLIOCENE	G. tosaensis Zone; A/G	CN12b/d; A/G	Barren; B					1	0.5, 1.0	
						● γ=1.63, ϕ=66.8	●42.6 %	2		
							●0.3 %	3		* ; PP
						γ=1.69, ϕ=67.5 ●● γ=1.66, ϕ=67.0	13.3% ●● 32.5 %	4		
								5		IW
						● γ=1.70, ϕ=60.0	●40.0 %	6		*
								7		
								CC		

GRAPHIC LITHOLOGY | DRILLING DISTURB. | SED. STRUCTURES

LITHOLOGIC DESCRIPTION

MARL and CALCAREOUS MUDSTONE

Light olive-gray or light brownish gray (5Y6/2 or 10YR6/2) massive foraminifer/nannofossil MARL and CALCAREOUS MUDSTONE; bioturbation throughout.

Minor lithology: ashy layers in Sections 3, 6, and 7.

Structure: bedding dips 65–85°. Near vertical vein structure at Section 3, 20 cm. anastomosing fractures and network faults at Section 4, 90–130 cm.

SMEAR SLIDE SUMMARY (%):

	3, 90 M	6, 66 D
TEXTURE:		
Sand	2	3
Silt	25	15
Clay	63	82
COMPOSITION:		
Quartz	5	5
Feldspar	15	1
Clay	53	51
Volcanic glass	15	5
Foraminifers	2	3
Nannofossils	10	35

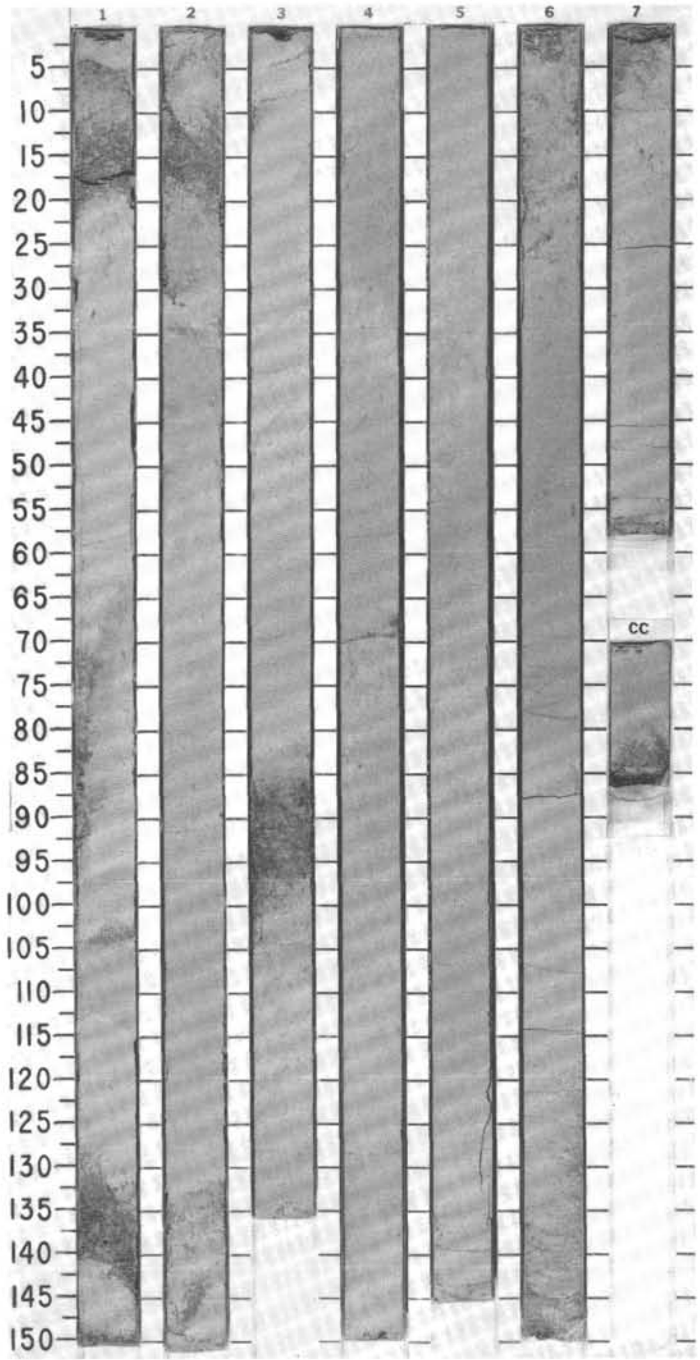

SITE 673 HOLE B CORE 5 H CORED INTERVAL 4725.3-4734.8 mbsl; 36.1-45.6 mbsf

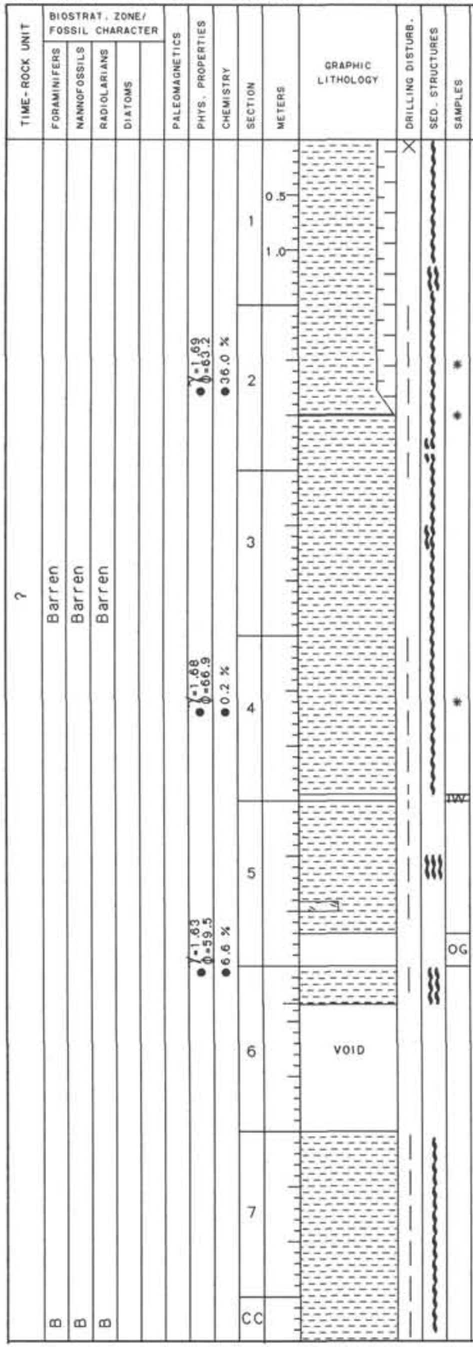

LITHOLOGIC DESCRIPTION

CALCAREOUS CLAY and CLAY

Sections 1 and 2 consist of alternating beds of light olive-gray (5Y6/1–6/2) and light brownish gray (2.5Y6/2) foraminifer-nannofossil CALCAREOUS CLAY; color changes are sharp in Sections 1 and 2. Bioturbated throughout. Sections 3 and 4 consists of alternating beds of light olive-brown (5GY5/1, 2.5Y5/3, 5Y5/4) and greenish gray to olive-brown (5GY4/1) CLAY. Greenish gray (5GY5/1) CLAY in Sections 5, 6, and CC, mottled with highly calcareous burrows in Section 5, 5–6 cm, and 27–29 cm.

Minor lithology: ash layers at Section 3, 55 and 67–68 cm, and Section 5, 82–102 cm. Local ashy mottles throughout.

SMEAR SLIDE SUMMARY (%):

	2, 60 D	2, 108 M	4, 60 D
TEXTURE:			
Silt	3	5	2
Clay	97	95	98
COMPOSITION:			
Quartz	3	8	3
Feldspar	—	—	2
Clay	82	92	92
Volcanic glass	—	Tr	3
Nannofossils	15	—	—

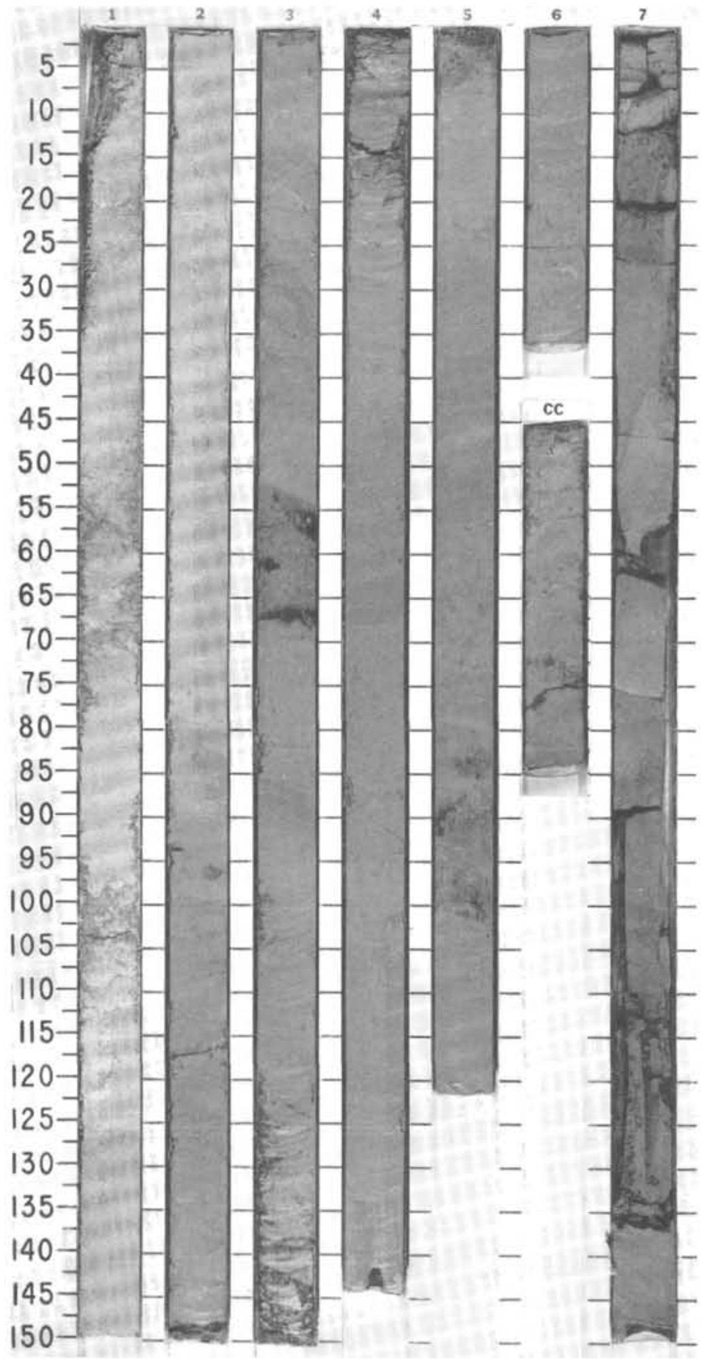

SITE 673 HOLE B CORE 6 H CORED INTERVAL 4734.8-4744.3 mbsl; 45.6-55.1 mbsf

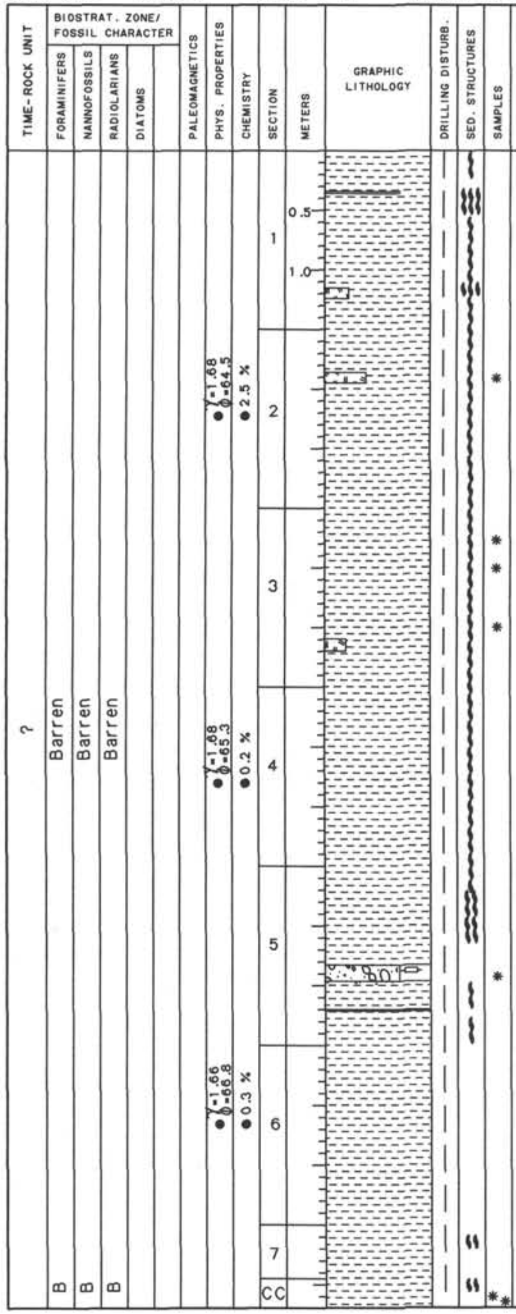

LITHOLOGIC DESCRIPTION

CLAY and MUD

Greenish gray (10Y5/2–5GY5/1), light greenish gray (5G6/1–5/2) to dark olive (5Y5/1) homogenous CLAY and MUD. Bioturbation of *Planolites* and *Chondrites* is remarkable throughout the core.

Minor lithology: minor ashy patches throughout. Small chalk blocks occur at Section 2, 22–30 cm.

Structure: bedding horizontal in Sections 2 and 6, and 25° in Section 3, 110 cm. Faults in Section 1 dip at 50 cm (55°) and 60 cm (55°), and in Section 3 dip at 90 cm (35°) and 110 cm (25°).

SMEAR SLIDE SUMMARY (%):

	2, 40 M	3, 24 M	3, 53 D	3, 104 D	5, 98 M	CC, 21 D	CC, 23 M
TEXTURE:							
Sand	5	—	—	—	—	—	—
Silt	50	55	Tr	10	95	3	21
Clay	45	45	100	90	5	97	79
COMPOSITION:							
Quartz	Tr	—	Tr	—	Tr	1	1
Feldspar	8	10	—	Tr	—	Tr	—
Rock fragments	—	5	—	—	—	—	—
Clay	45	45	99	90	—	96	72
Volcanic glass	40	40	—	Tr	Tr	—	—
Calcite/dolomite	—	—	—	8	99	1	20
Accessory minerals							
Glauconite		—	—	—	—	—	—
Fibrous zeolite	—	—	—	Tr	—	—	—
Pyroxene	—	—	—	—	—	Tr	—
Opaques	5	—	Tr	Tr	—	1	1
Hornblende	Tr	—	—	—	—	—	—
Fe/Mn hydroxide	—	—	—	—	—	—	5
Unknown	—	—	—	—	—	—	1

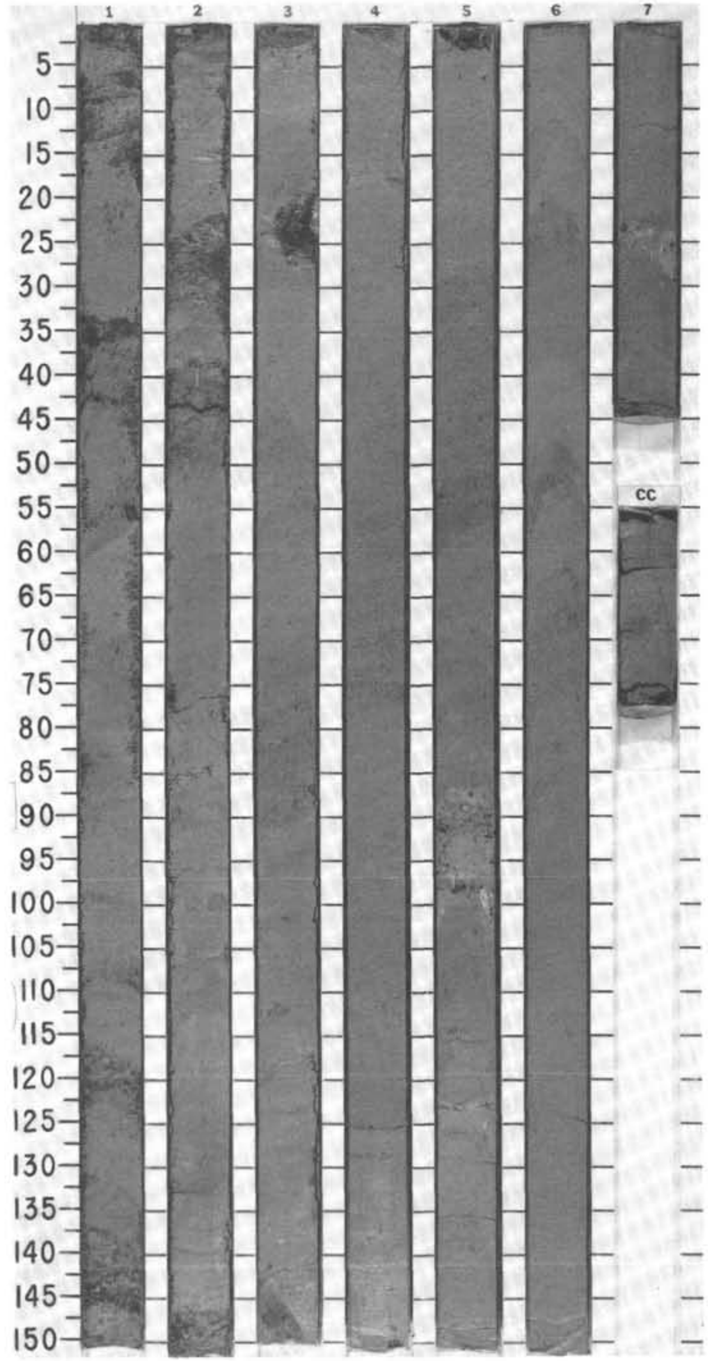

SITE 673 HOLE B CORE 7 X CORED INTERVAL 4744.3-4753.8 mbsl; 55.1-64.6 mbsf

TIME-ROCK UNIT	FORAMINIFERS	NANNOFOSSILS	RADIOLARIANS	DIATOMS	PALEOMAGNETICS	PHYS. PROPERTIES	CHEMISTRY	SECTION	METERS	GRAPHIC LITHOLOGY	DRILLING DISTURB.	SED. STRUCTURES	SAMPLES
?	Barren B	Barren B	Barren B			• γ=1.70 • ϕ=64.9	•0.4 %	1 2 3 4 5 CC	0.5 1.0	VOID			IW * * *

BIOSTRAT. ZONE/ FOSSIL CHARACTER

LITHOLOGIC DESCRIPTION

CLAY and MUD

Grayish green to green (10Y5/2–5G5/1) or dark greenish gray (5BG5/1) homogenous CLAY and MUD with local weak bioturbation.

Minor lithology: local ashy (20% ash) layers at Section 1, 72–81 cm, and Section 3, 25–32 cm.

Structure: bedding dips subhorizontally to 20°.

SMEAR SLIDE SUMMARY (%):

	3, 30 M	3, 100 M	3, 123 D
TEXTURE:			
Sand	Tr	—	—
Silt	50	2	10
Clay	50	98	90
COMPOSITION:			
Quartz	1	Tr	1
Feldspar	30	1	3
Mica	—	—	Tr
Clay	50	98	91
Volcanic glass	15	Tr	1
Calcite/dolomite	2	—	—
Accessory minerals			
Glauconite	Tr	—	—
Pyroxene	—	—	2
Opaques	2	—	2
Fe/Mn hydroxides	—	—	Tr

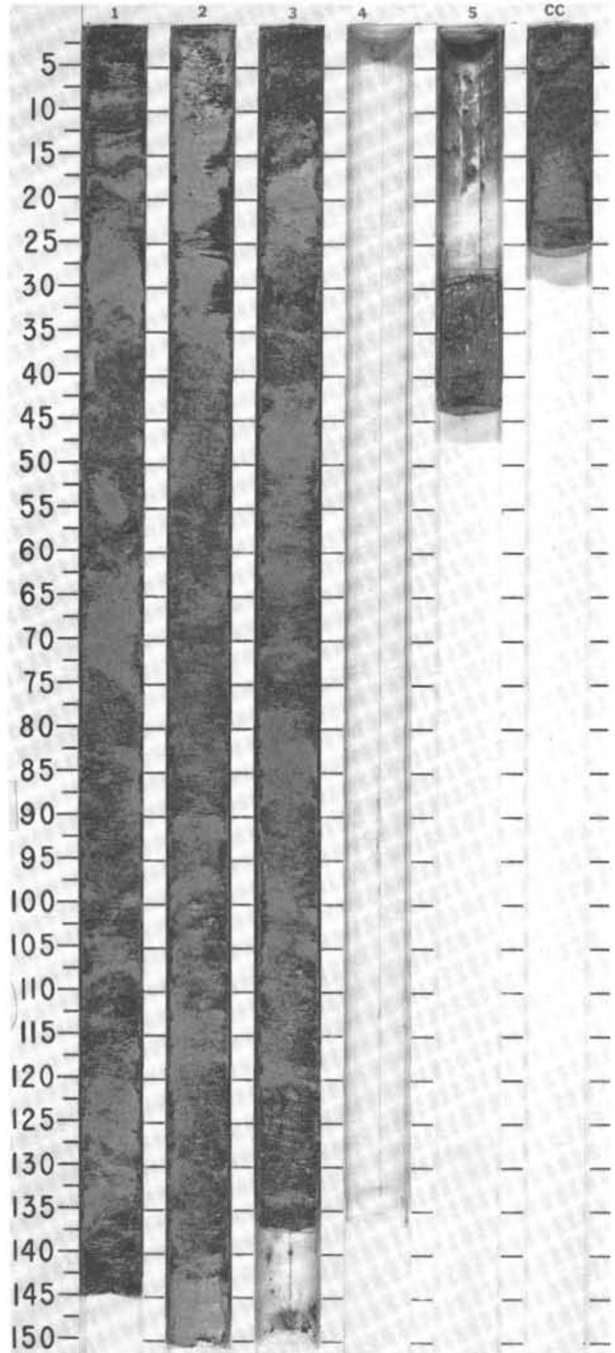

SITE 673 HOLE B CORE 8 X CORED INTERVAL 4753.8-4763.3 mbsl; 64.6-74.1 mbsf

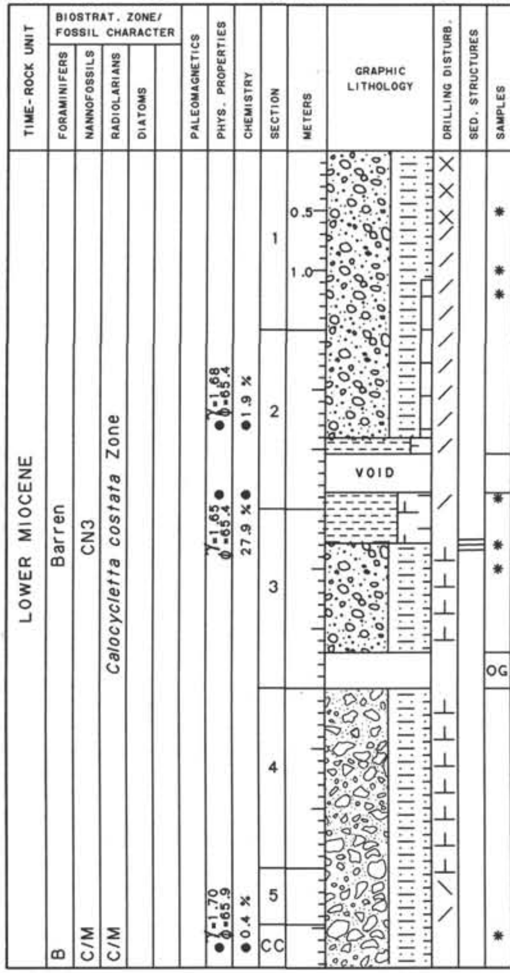

LITHOLOGIC DESCRIPTION

MATRIX-SUPPORTED BRECCIA, CALCAREOUS CLAYSTONE, and MUDSTONE

Greenish gray to green (5GY5/1–5G5/2) MATRIX-SUPPORTED BRECCIA, Section 1, 0–115 cm. Clasts are dominantly brownish gray mudstone and scaly claystone, with minor ashy fragments. Similar breccia with slightly calcareous matrix in Section 1, 115 cm, to Section 2, 95 cm; Section 3, 35–120 cm; and in the whole of Sections 4, 5, and CC. Grayish green (10Y5/2) CALCAREOUS CLAYSTONE and MUDSTONE from Section 2, 95 cm, to Section 3, 35 cm. This part is bioturbated, and tectonic scaly fabric occurs throughout.

Structure: bedding dips 30° at Section 1, 120 cm.

SMEAR SLIDE SUMMARY (%):

	1, 50 M	1, 108 D	1, 124 D	2, 144 D	3, 33 D	3, 53 D	CC, 13 M
TEXTURE:							
Sand	—	—	—	—	15	—	10
Silt	10	3	3	19	39	9	36
Clay	90	97	97	81	6	81	54
COMPOSITION:							
Quartz	3	1	—	—	—	1	2
Feldspar	5	1	1	—	1	3	2
Rock fragments	1	—	—	—	—	—	—
Clay	89	97	97	51	31	88	54
Volcanic glass	—	—	—	Tr	—	1	40
Calcite/dolomite	1	—	—	2	30	—	—
Accessory minerals							
Glauconite	Tr	—	—	—	—	—	Tr
Clinopyroxene	—	—	Tr	—	—	—	Tr
Opaques	1	1	—	—	5	—	1
Fe/Mn hydroxideS	Tr	Tr	—	—	—	—	—
Unknown (zeolite?)	—	—	2	1	1	—	—
Foraminifers	—	—	—		—	—	—
Nannofossils	—	—	—	30	15	—	—
Diatoms	—	—	—	1	7	Tr	Tr
Radiolarians	—	—	—	3	7	3	Tr
Sponge spicules	—	—	—	10	15	4	Tr
Dinoflagellates	—	—	—	—	Tr	—	—

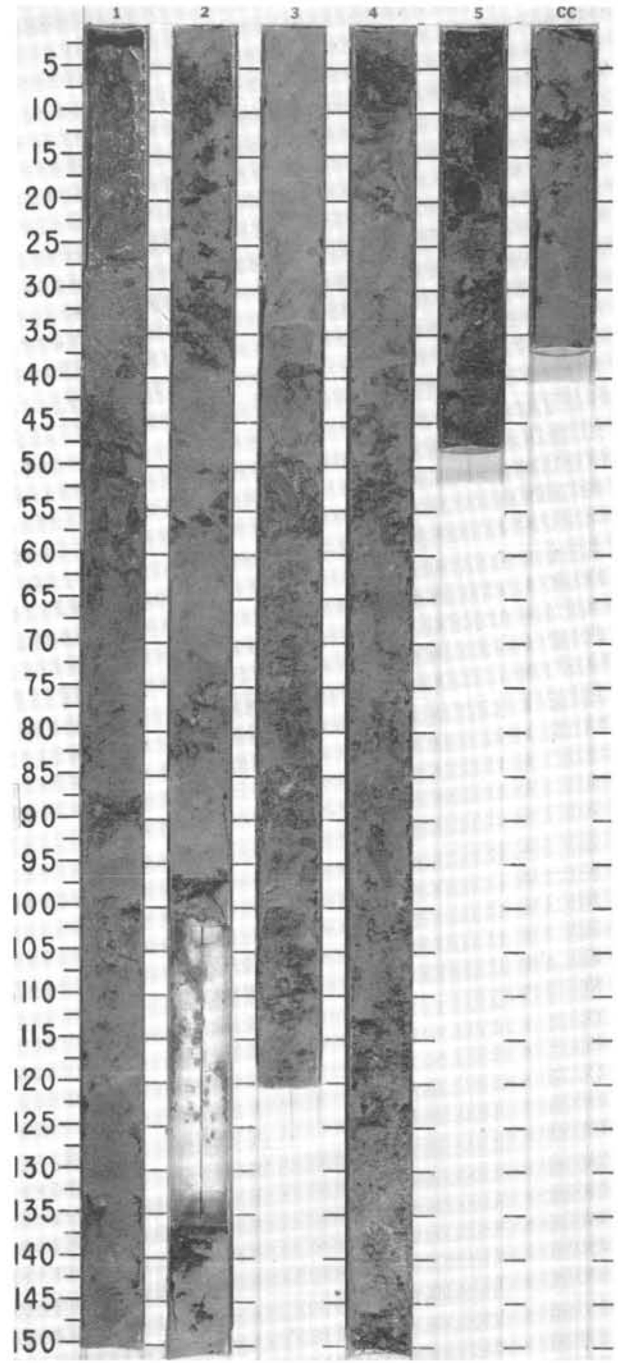

SITE 673 HOLE B CORE 9 X CORED INTERVAL 4763.3-4772.8 mbsl; 74.1-83.6 mbsf

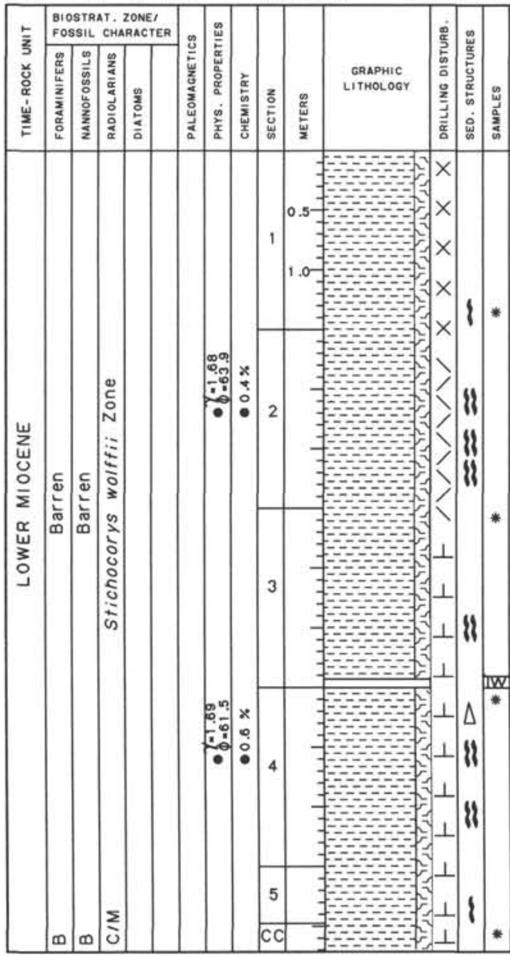

LITHOLOGIC DESCRIPTION

SILICEOUS CLAYSTONE

Greenish gray to pale green (5G5/1–6/2) homogenous SILICEOUS CLAYSTONE, slightly bioturbated by *Planolites* and *Chondrites*. Local intercalations of olive (5Y5/2) layers. Drilling biscuits common in Section 3 and below.

Minor lithology: 3-cm-thick, graded ash layer in Section 4, 20 to 23 cm.

Structure: burrows suggest that bedding probably dips horizontally to 10–20° in the upper part of Section 4, and 50° in the lower part of Section 4. Small normal fault inclined at 50° has 3-cm offset of ash and ashy lamination in Section 4, 15–23 cm.

SMEAR SLIDE SUMMARY (%):

	1, 152 D	3, 11 M	4, 18 M	CC, 10 M
TEXTURE:				
Sand	5	5	20	—
Silt	25	30	35	25
Clay	70	65	45	75
COMPOSITION:				
Quartz	Tr	Tr	—	—
Feldspar	1	Tr	3	—
Clay	72	65	45	74
Volcanic glass	—	—	50	—
Accessory minerals				
Opaques	Tr	Tr	2	1
Radiolarians	15	15	—	10
Sponge spicules	10	18	—	15
Silicoflagellates	Tr	Tr	—	—

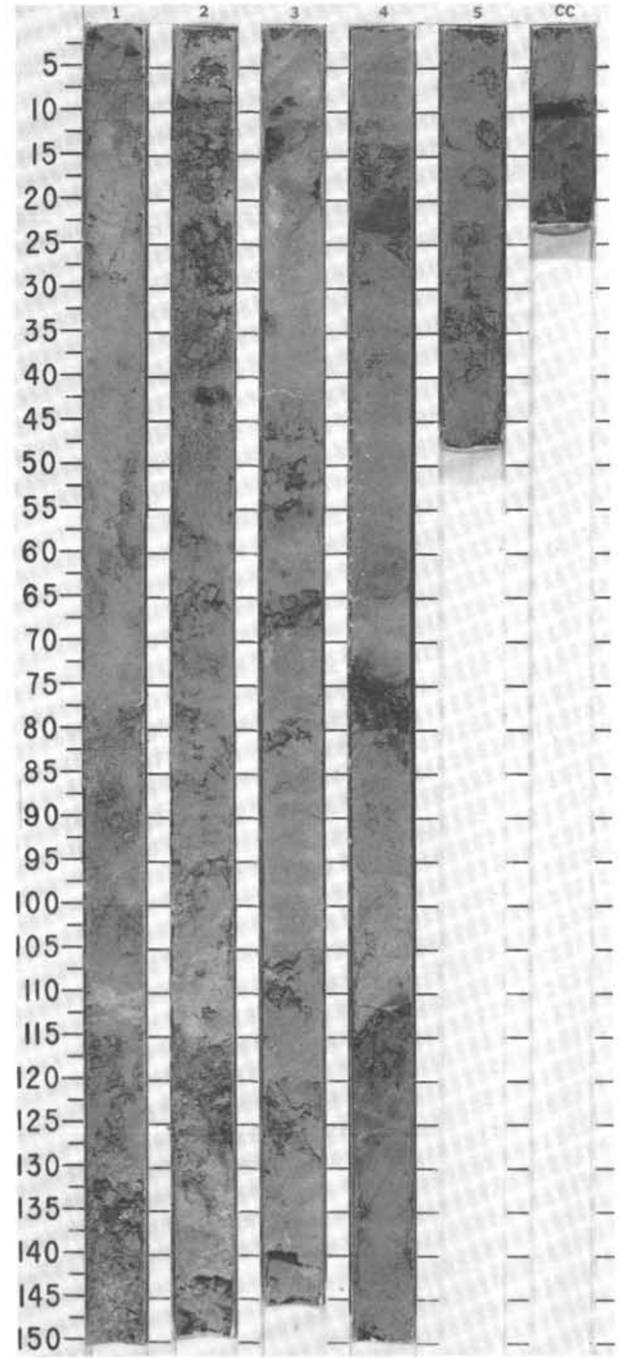

SITE 673 HOLE B CORE 10 X CORED INTERVAL 4772.8-4782.3 mbsl; 83.6-93.1 mbsf

TIME-ROCK UNIT	FORAMINIFERS	NANNOFOSSILS	RADIOLARIANS	DIATOMS	PALEOMAGNETICS	PHYS. PROPERTIES	CHEMISTRY	SECTION	METERS
LOWER MIOCENE	Barren	Barren	*Stichocorys wolffii* Zone			γ=1.66, ϕ=68.7	1.2 %	1, 2, 3, CC	0.5, 1.0
	B	B	A/M						

GRAPHIC LITHOLOGY · DRILLING DISTURB. · SED. STRUCTURES · SAMPLES

LITHOLOGIC DESCRIPTION

SILICEOUS CLAYSTONE and SILICEOUS MUDSTONE

Greenish (5G5/1), homogenous SILICEOUS CLAYSTONE, intensely disturbed by drilling. Within the drill slurry there are several blocks of olive-gray (5Y4/2), slightly bioturbated SILICEOUS MUDSTONE.

Structure: bedding plane at Section 3 dips 35°.

SMEAR SLIDE SUMMARY (%):

	2, 14 D	2, 107 M	2, 129 D	3, 14 D
TEXTURE:				
Sand	—	—	30	—
Silt	35	50	16	30
Clay	65	50	54	70
COMPOSITION:				
Quartz	1	5	—	1
Feldspar	1	2	3	1
Clay	60	65	54	61
Volcanic glass	—	5	2	Tr
Calcite/dolomite	—	—	4	—
Accessory minerals				
Opaques	1	15	1	—
Fe/Mn oxide	—	—	2	—
Micrite	3	—	—	3
Unknown	—	—	2	—
Diatoms	3	—	2	3
Radiolarians	5	3	3	5
Sponge spicules	25	5	25	25
Dinoflagellates	1	Tr	2	1

SITE 673 HOLE B CORE 11 X CORED INTERVAL 4782.3-4791.8 mbsl; 93.1-102.6 mbsf

TIME-ROCK UNIT	FORAMINIFERS	NANNOFOSSILS	RADIOLARIANS	DIATOMS	PALEOMAGNETICS	PHYS. PROPERTIES	CHEMISTRY	SECTION	METERS
LOWER MIOCENE	Barren	Barren	*Doradospyris alata* Zone				0.7 %	1, 2, CC	0.5, 1.0
	B	B	C/M						

GRAPHIC LITHOLOGY · DRILLING DISTURB. · SED. STRUCTURES · SAMPLES (OG)

LITHOLOGIC DESCRIPTION

SILICEOUS CLAYSTONE to CLAYSTONE

Dark greenish gray (5G4/1) homogenous SILICEOUS CLAYSTONE to slightly siliceous CLAYSTONE. Only biscuits occur throughout. Local slight bioturbation.

Minor lithology: dark gray ashy fragment at the bottom of CC.

SMEAR SLIDE SUMMARY (%):

	1, 22 D	2, 44 D
TEXTURE:		
Silt	5	15
Clay	95	85
COMPOSITION:		
Quartz	1	2
Feldspar	—	1
Clay	86	77
Accessory minerals		
Orthopyroxene	Tr	—
Opaques	—	10
Fe/Mn hydroxides	1	—
Diatoms	3	2
Radiolarians	4	5
Sponge spicules	5	2
Fish remains	—	1

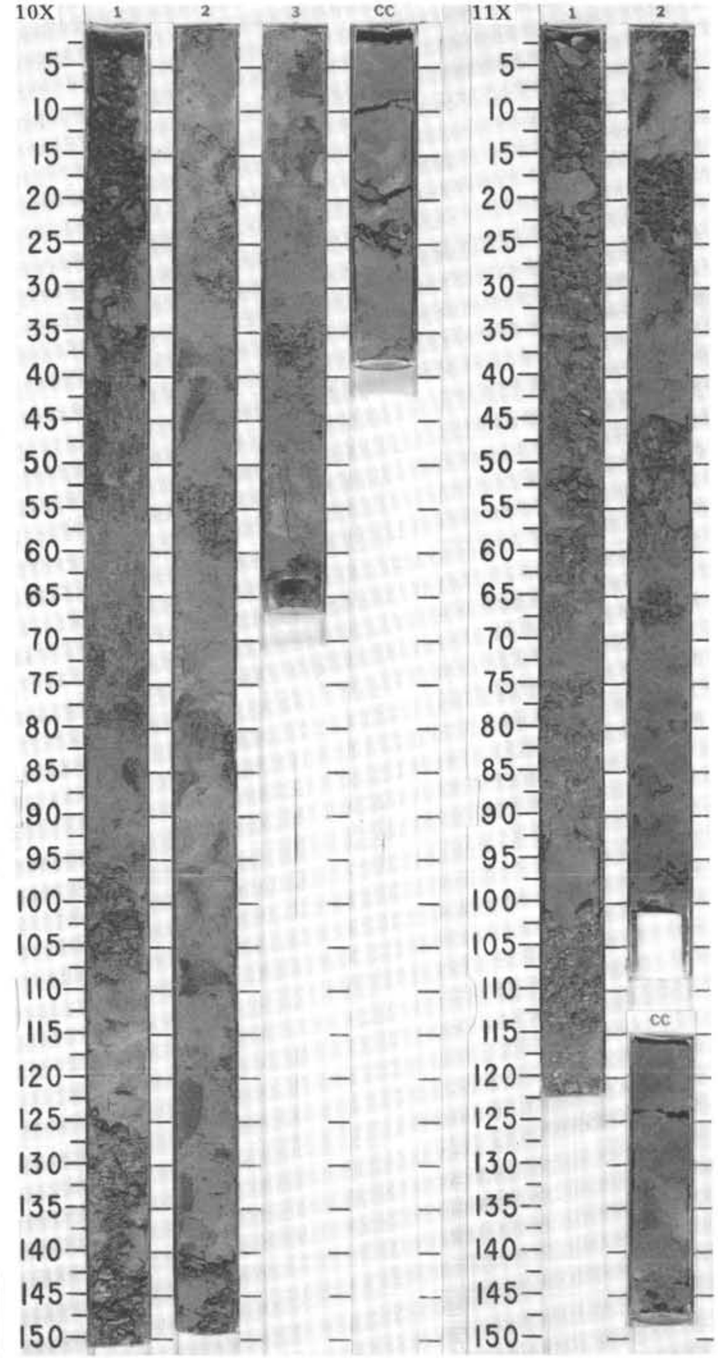

SITE 673 HOLE B CORE 12 X CORED INTERVAL 4791.8-4801.3 mbsl; 102.6-112.1 mbsf

TIME-ROCK UNIT	FORAMINIFERS	NANNOFOSSILS	RADIOLARIANS	DIATOMS	PALEOMAGNETICS	PHYS. PROPERTIES	CHEMISTRY	SECTION	METERS	GRAPHIC LITHOLOGY	DRILLING DISTURB.	SED. STRUCTURES	SAMPLES
LOWER MIOCENE	Barren B	Barren B	*Doradospyris alata* Zone A/M			γ=1.73 ϕ=68.6; γ=1.77 ϕ=62.3	●0.5 %; ●0.9 %	1, 2, 3, 4, CC	0.5, 1.0				*, *, IW

LITHOLOGIC DESCRIPTION

MUDSTONE

Dominant lithology: greenish gray to green (5GY5/1 to 5G5/1) slightly siliceous MUDSTONE. Strongly disturbed by drilling into slurry.

Minor lithology: indurated dark gray pebble (15% ash) at 111 cm of Section 2; ashy (5%), dark gray mottles throughout core.

Structure: bedding is unclear. Steep fault dipping at 75° at Section 3, 30–40 cm.

SMEAR SLIDE SUMMARY (%):

	1, 99 D	2, 111 M
TEXTURE:		
Silt	12	17
Clay	88	83
COMPOSITION:		
Quartz	12	15
Feldspar	Tr	2
Clay	80	73
Volcanic glass	1	10
Accessory minerals		
Glauconite	—	Tr
Clinopyroxene(?)	Tr	—
Radiolarians	3	—
Sponge spicules	4	—

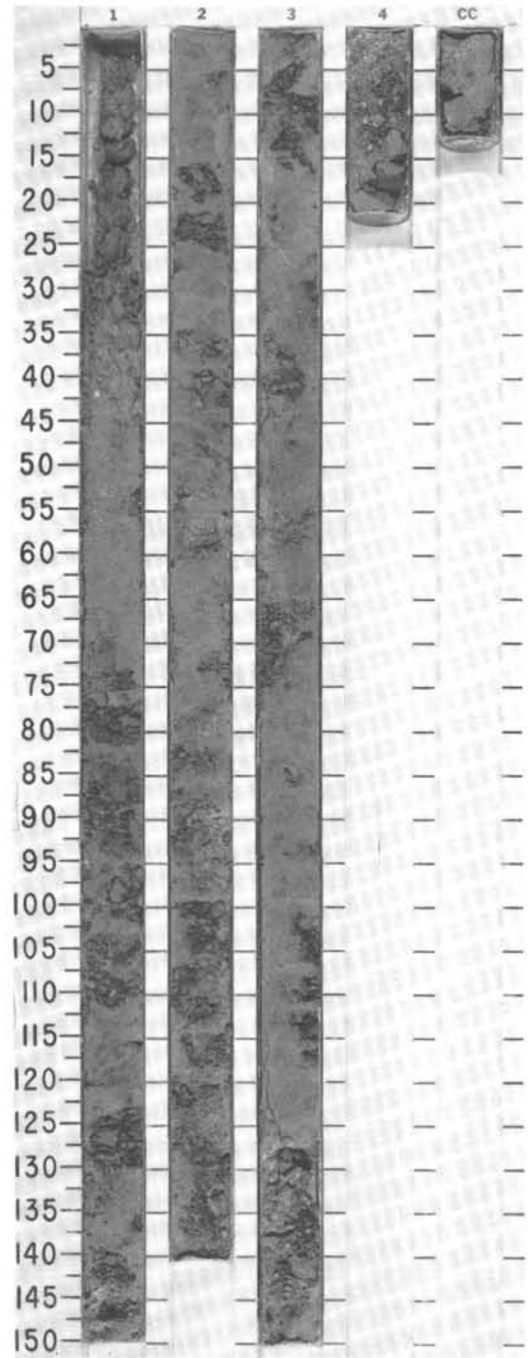

SITE 673 HOLE B CORE 13 X CORED INTERVAL 4801.3-4810.8 mbsl; 112.1-121.6 mbsf

TIME-ROCK UNIT	FORAMINIFERS	NANNOFOSSILS	RADIOLARIANS	DIATOMS	PALEOMAGNETICS	PHYS. PROPERTIES	CHEMISTRY	SECTION	METERS	GRAPHIC LITHOLOGY	DRILLING DISTURB.	SED. STRUCTURES	SAMPLES
LOWER MIOCENE	Barren	Barren	*Doradospyris alata* Zone; *Calocycletta costata* Zone A/M			●γ=1.66 ●φ=66.3; ●γ=1.58 ●φ=71.2	●0.5 %; ●0.6 %	1; 2; 3; CC	0.5; 1.0				* ; *

LITHOLOGIC DESCRIPTION

MUDSTONE

Green to greenish gray (5G5/1–5GY5/1) MUDSTONE: intensely disturbed by drilling into slurry and breccia. Common faint burrow mottles.

Minor lithology: brown (5GY4/2) 1-cm-thick vitric ash in Section 2, 85–86 cm.

SMEAR SLIDE SUMMARY (%):

	1, 123 D	2, 85 M
TEXTURE:		
Sand	—	1
Silt	12	64
Clay	88	35
COMPOSITION:		
Quartz	12	—
Clay	85	30
Volcanic glass	Tr	70
Accessory minerals	—	Tr
Radiolarians	Tr	—
Sponge spicules	3	—

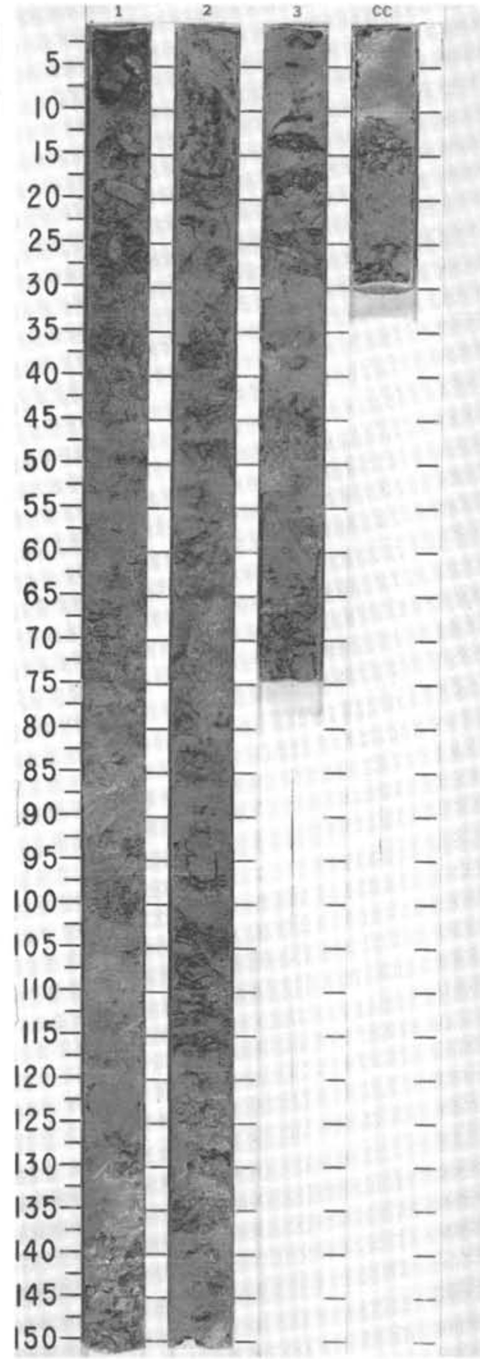

SITE 673 HOLE B CORE 14 X CORED INTERVAL 4810.8-4820.3 mbsl; 121.6-131.1 mbsf

TIME-ROCK UNIT	FORAMINIFERS	NANNOFOSSILS	RADIOLARIANS	DIATOMS	PALEOMAGNETICS	PHYS. PROPERTIES	CHEMISTRY	SECTION	METERS
LOWER MIOCENE	B Barren	B Barren	A/G *Calocycletta costata* Zone			γ=1.69 ϕ=63.9; γ=1.71 ϕ=62.3	0.7 %; 0.5 %	1, 2, 3, 4, 5, CC	0.5, 1.0

GRAPHIC LITHOLOGY · DRILLING DISTURB. · SED. STRUCTURES · SAMPLES (OG)

LITHOLOGIC DESCRIPTION

SILICEOUS MUDSTONE

Green (5G5/1–5GY5/1) massive SILICEOUS MUDSTONE, only slightly bioturbated. Drilling biscuits are common throughout.

Minor lithology: ashy parts (25%) in Section 2, 8–10 cm, and Section 3, 115–118 cm. Slightly ashy throughout.

Structure: locally well-developed scaly fabric from Section 1, 116–150 cm, to CC. Thin gray "vein structure" is well developed in Section 1, 95–102 cm; Section 3, 110 cm (dip 25°); Section 4, 55–60, 127–135, and 130–144 cm (three cross-cutting sets of veins); Section 5, 0–20 cm; and CC, 0–10 cm. A network of shallow, dipping vein structures is developed in Section 4.

SMEAR SLIDE SUMMARY (%):

	1, 144 D	2, 9 M
TEXTURE:		
Sand	3	2
Silt	17	38
Clay	80	60
COMPOSITION:		
Quartz	30	20
Feldspar	—	3
Clay	50	48
Volcanic glass	8	25
Radiolarians	7	2
Sponge spicules	5	2

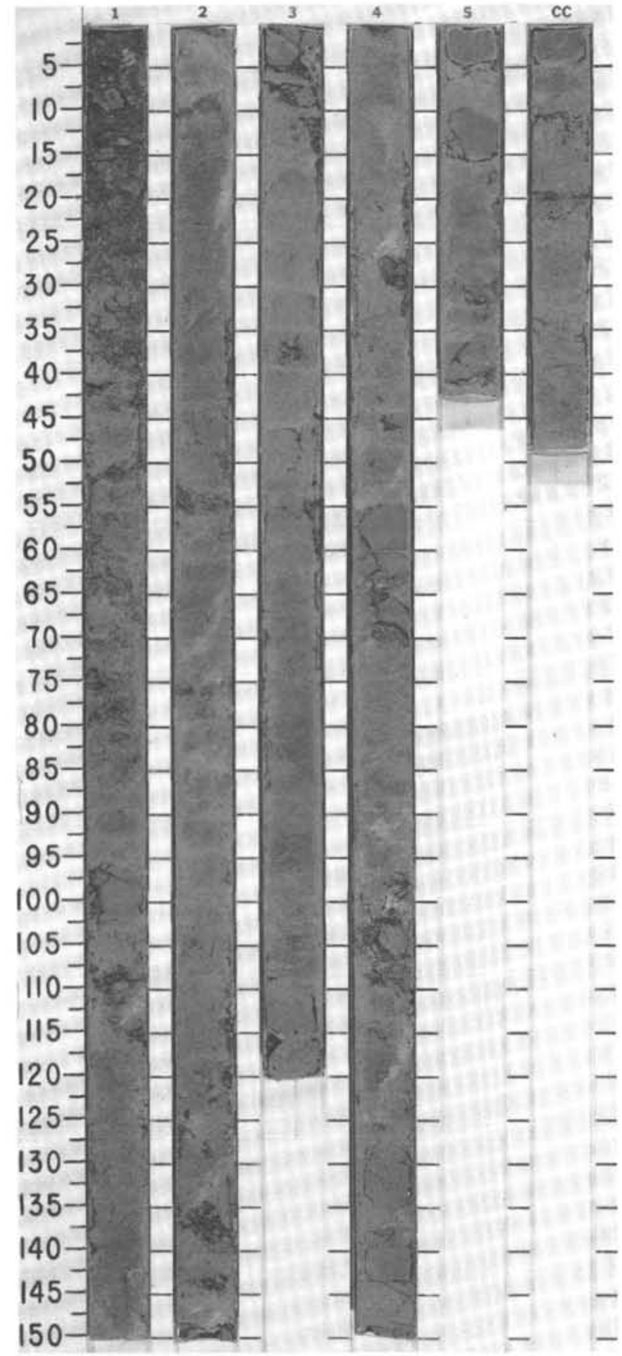

SITE 673 HOLE B CORE 15 X CORED INTERVAL 4820.3-4829.8 mbsl; 131.1-140.6 mbsf

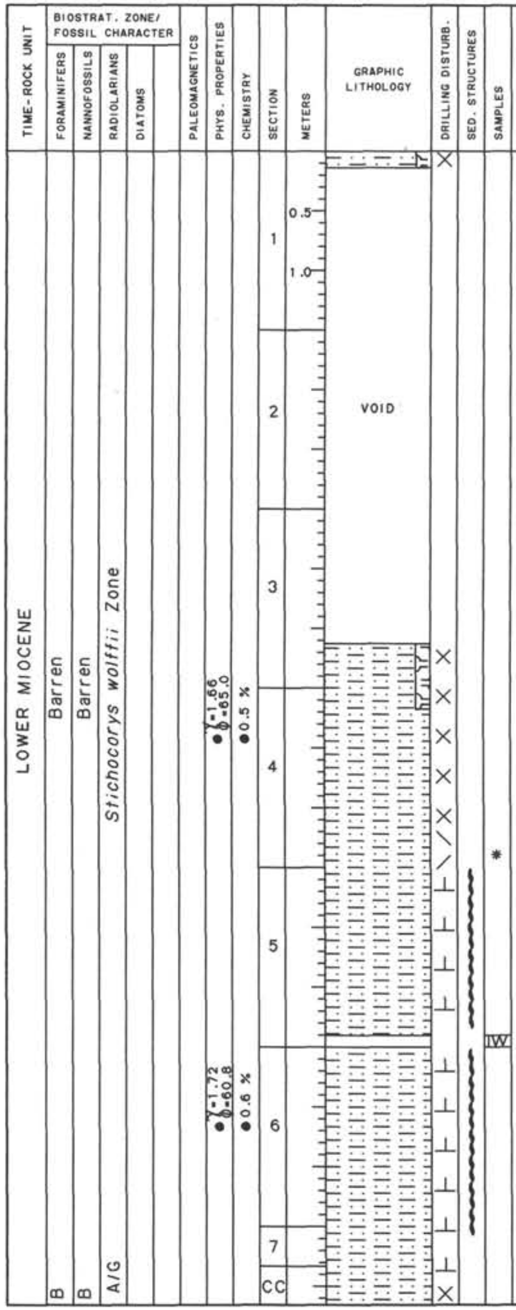

LITHOLOGIC DESCRIPTION

SILICEOUS MUDSTONE

Green (5G5/1) SILICEOUS MUDSTONE, highly disrupted to slurry from top of the core down to Section 3; more coherent in the lower part. Color changes to olive-green (5GY5/1) downsection; brownish mottles are common throughout.

Minor lithology: thin black ash at Section 6, 80 cm.

Structure: scaly fabric throughout Section 4.

SMEAR SLIDE SUMMARY (%):

	4, 145 D
TEXTURE:	
Sand	1
Silt	34
Clay	65
COMPOSITION:	
Quartz	35
Feldspar	5
Clay	45
Volcanic glass	7
Radiolarians	5
Sponge spicules	3

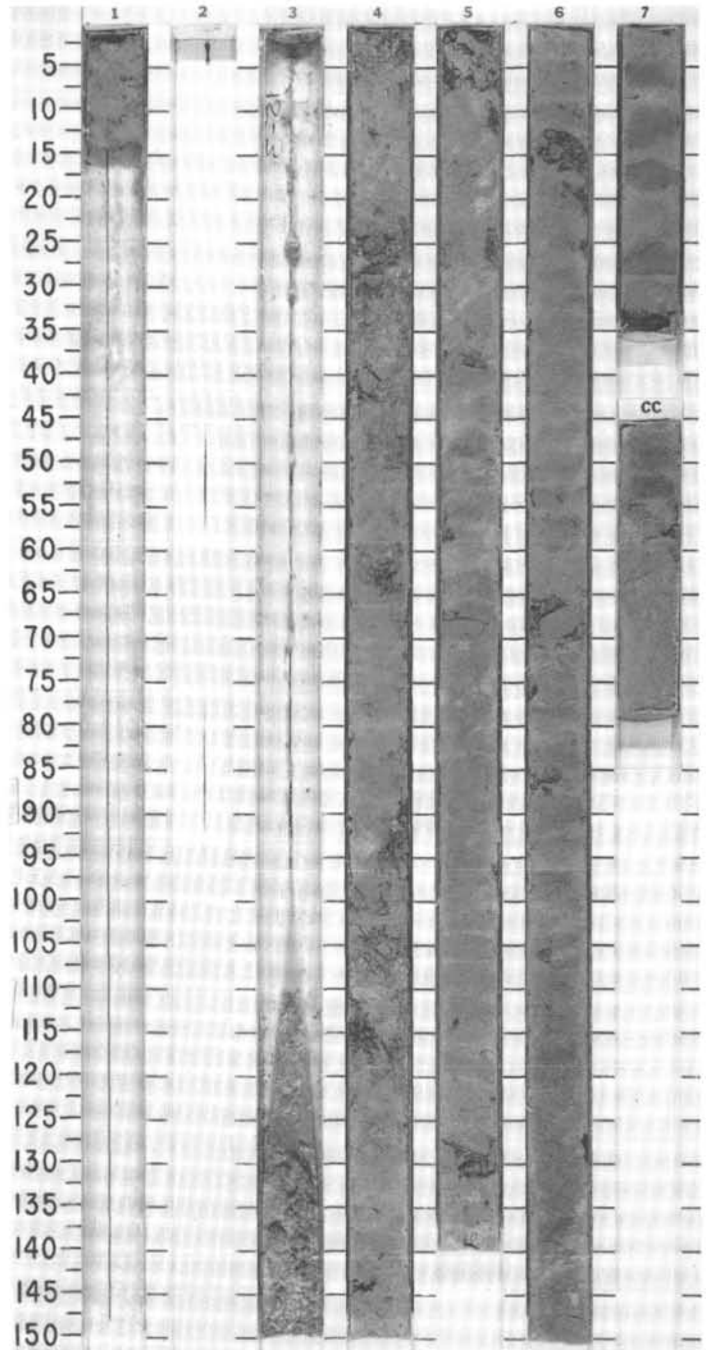

SITE 673 HOLE B CORE 16 X CORED INTERVAL 4829.8-4839.3 mbsl; 140.6-150.1 mbsf

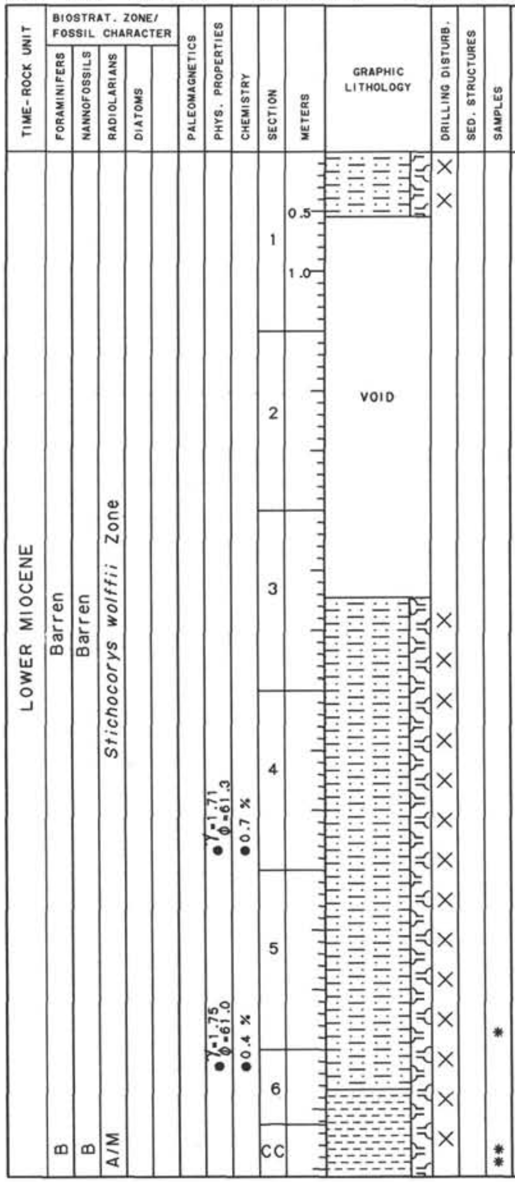

LITHOLOGIC DESCRIPTION

SILICEOUS MUDSTONE

Greenish gray (5G5/1–5GY5/1) SILICEOUS MUDSTONE, completely brecciated to slurry, with only a few coherent chunks included.

Minor lithology: black (N1) vitric and plagioclase-rich ash surrounded by gray halo in *CC*, 20–30 cm. Pyrite-like metallic blebs in Section 5, 137–139 cm, and Section 6, 20–21 cm.

SMEAR SLIDE SUMMARY (%):

	5, 138 M	CC, 23 M	CC, 24 D
TEXTURE:			
Sand	4	—	8
Silt	16	30	12
Clay	80	70	80
COMPOSITION:			
Quartz	10	1	Tr
Feldspar	2	15	—
Clay	67	61	75
Volcanic glass	—	20	Tr
Accessory minerals			
Pyrite	6	—	—
Pyroxene	—	Tr	—
Opaques	—	3	—
Radiolarians	15	—	15
Sponge spicules	—	—	10

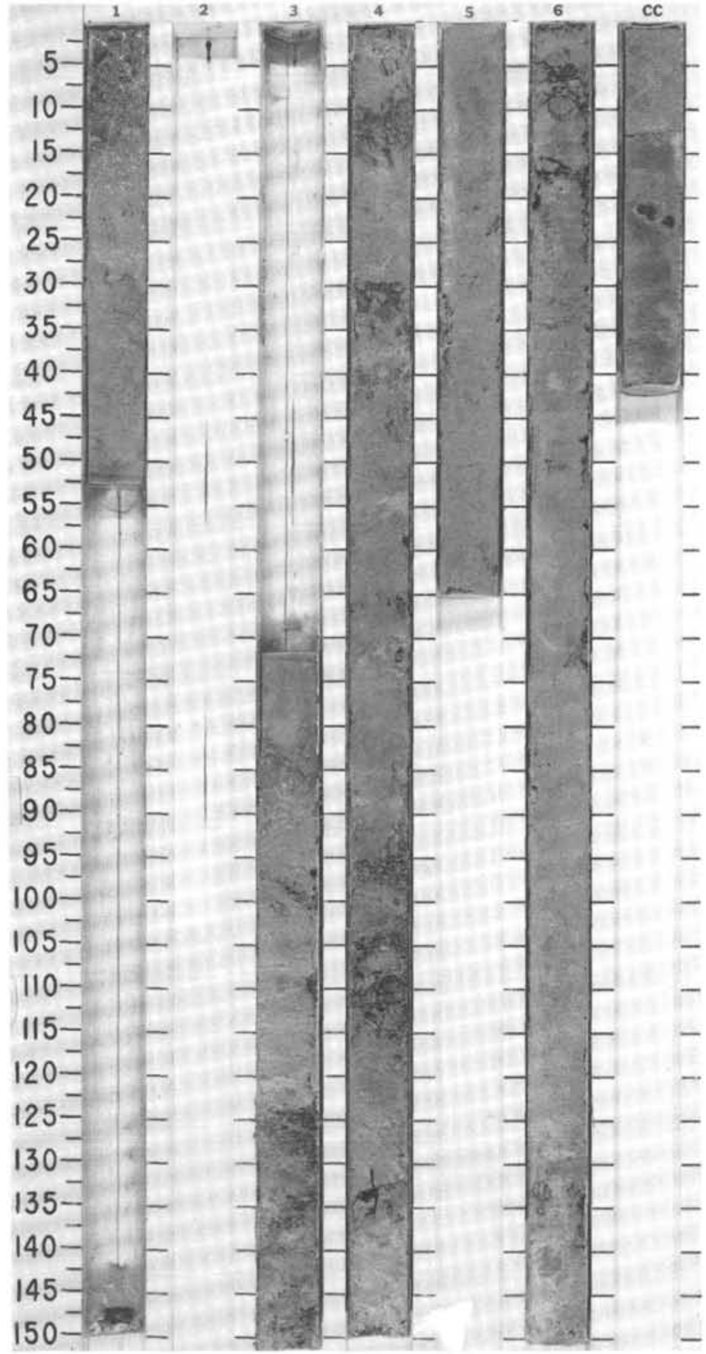

SITE 673 HOLE B CORE 17 X CORED INTERVAL 4839.3-4848.8 mbsl; 150.1-159.6 mbsf

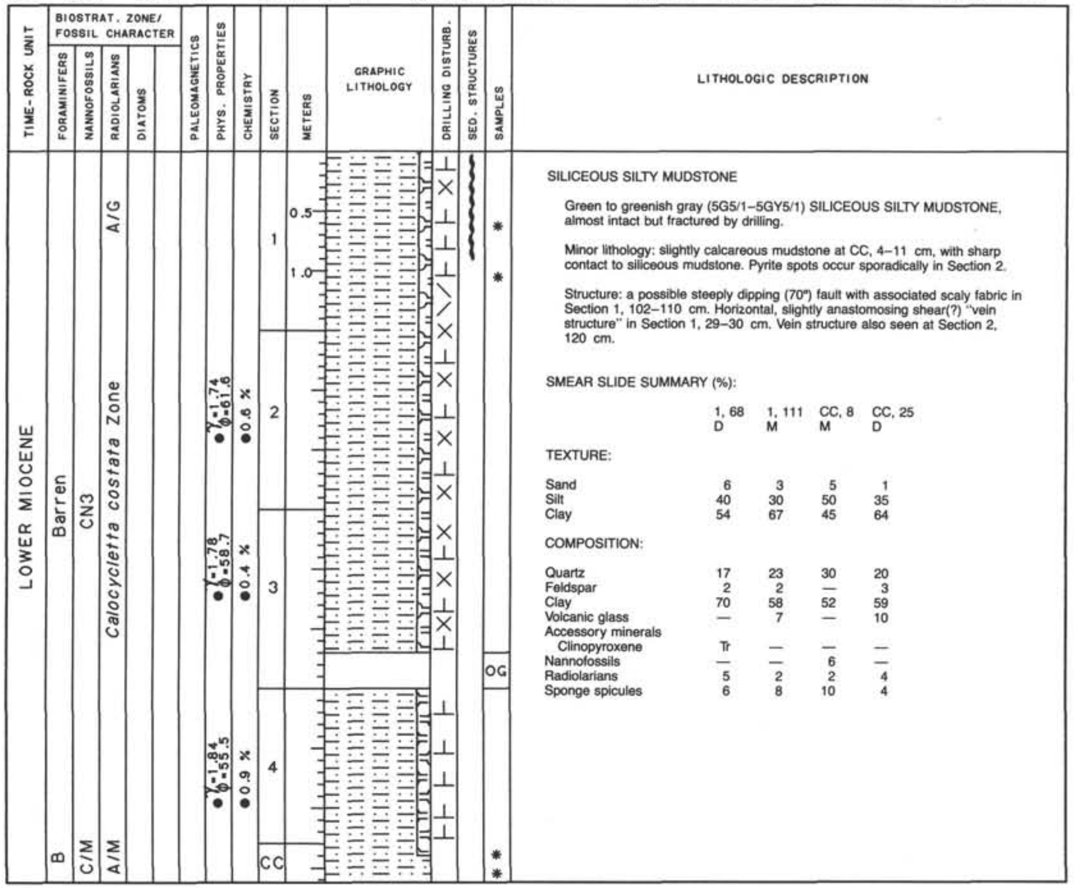

LITHOLOGIC DESCRIPTION

SILICEOUS SILTY MUDSTONE

Green to greenish gray (5G5/1–5GY5/1) SILICEOUS SILTY MUDSTONE, almost intact but fractured by drilling.

Minor lithology: slightly calcareous mudstone at CC, 4–11 cm, with sharp contact to siliceous mudstone. Pyrite spots occur sporadically in Section 2.

Structure: a possible steeply dipping (70°) fault with associated scaly fabric in Section 1, 102–110 cm. Horizontal, slightly anastomosing shear(?) "vein structure" in Section 1, 29–30 cm. Vein structure also seen at Section 2, 120 cm.

SMEAR SLIDE SUMMARY (%):

	1, 68 D	1, 111 M	CC, 8 M	CC, 25 D
TEXTURE:				
Sand	6	3	5	1
Silt	40	30	50	35
Clay	54	67	45	64
COMPOSITION:				
Quartz	17	23	30	20
Feldspar	2	2	—	3
Clay	70	58	52	59
Volcanic glass	—	7	—	10
Accessory minerals				
Clinopyroxene	Tr	—	—	—
Nannofossils	—	—	6	—
Radiolarians	5	2	2	4
Sponge spicules	6	8	10	4

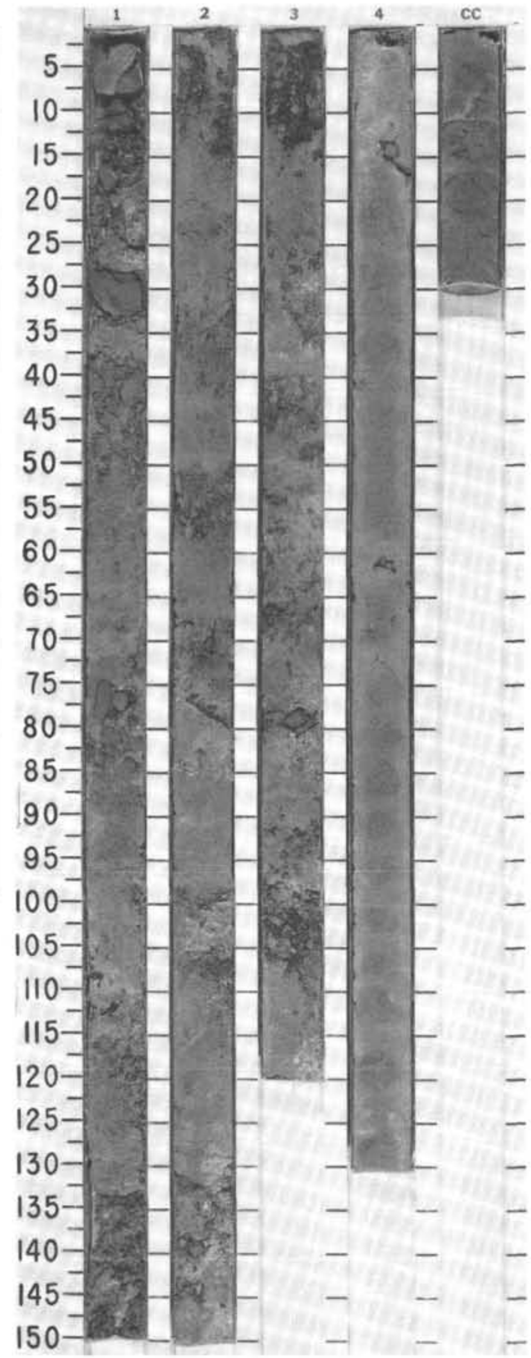

SITE 673 HOLE B CORE 18 X CORED INTERVAL 4848.8-4858.3 mbsl; 159.6-169.1 mbsf

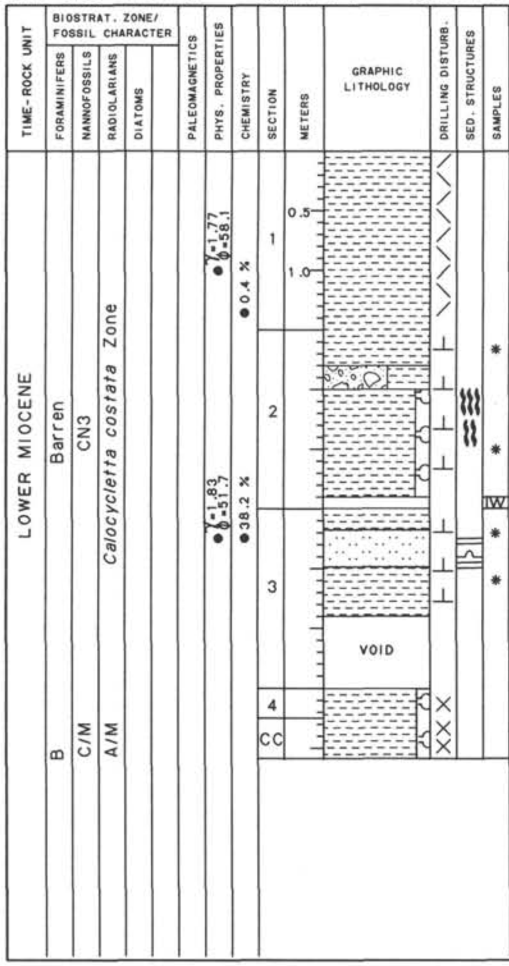

LITHOLOGIC DESCRIPTION

SILICEOUS MUDSTONE and CLAYSTONE, and SILTSONE and CALCAREOUS MARL to SILTY MARL

Greenish gray to dark olive-gray (5GY5/1–5G4/1) SILICEOUS MUDSTONE and CLAYSTONE, Section 1, 0–120 cm. From Section 1, 120 cm, to Section 2, 60 cm, greenish gray (5GY5/1) breccias composed of 1-cm-size clasts of brownish-gray volcanic ash; similar to ash described in minor lithology below. In Section 3, 15–40 cm, finely laminated light olive-gray (5Y6/2) SILTSTONE and SILICEOUS MARLSTONE with isolated pyrite nodules. Local grading and scouring suggest the bed is overturned.

Minor lithology: dark gray (5Y4/1) ash layer in Section 2, 59–60 cm.

Structure: bedding dips 45° at Section 2, 60 cm; calcareous silty marl dips also 45°, but is overturned. Horizontal faults and reverse fault (dip 20°) in Section 3 at 20 cm and at 30 cm, respectively.

SMEAR SLIDE SUMMARY (%):

	2, 20 M	2, 105 D	3, 26 D	3, 65 D
TEXTURE:				
Sand	2	5	—	—
Silt	93	10	60	10
Clay	5	85	40	90
COMPOSITION:				
Quartz	15	—	1	—
Feldspar	20	1	—	1
Clay	—	70	35	89
Volcanic glass	61	1	—	—
Calcite/dolomite	—	—	35	—
Accessory minerals				
Glauconite	—	—	Tr	—
Opaques	3	—	1	Tr
Fe/Mn hydroxide	1	—	—	—
Foraminifers	—	—	5	—
Nannofossils	—	10	2	—
Diatoms	—	2	—	1
Radiolarians	—	15	2	5
Sponge spicules	—	—	15	4
Fish remains	—	Tr	—	—
Plant debris	—	—	—	Tr
Bioclasts	—	—	3	—
Dinoflagellates	—	1	—	—

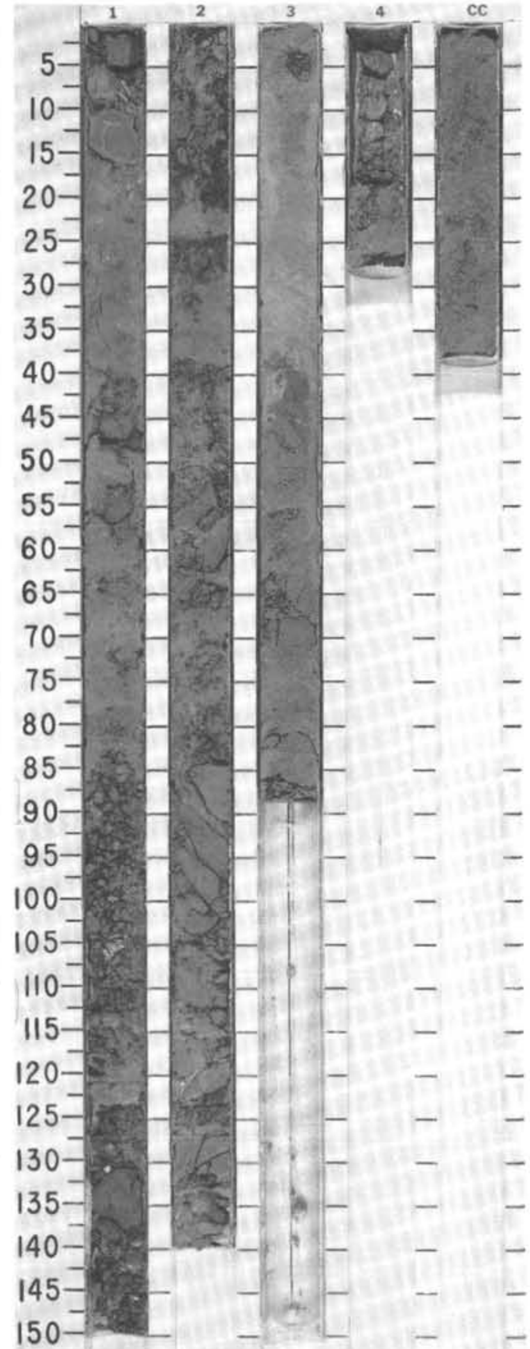

SITE 673 HOLE B CORE 19 X CORED INTERVAL 4858.3-4867.8 mbsl; 169.1-178.6 mbsf

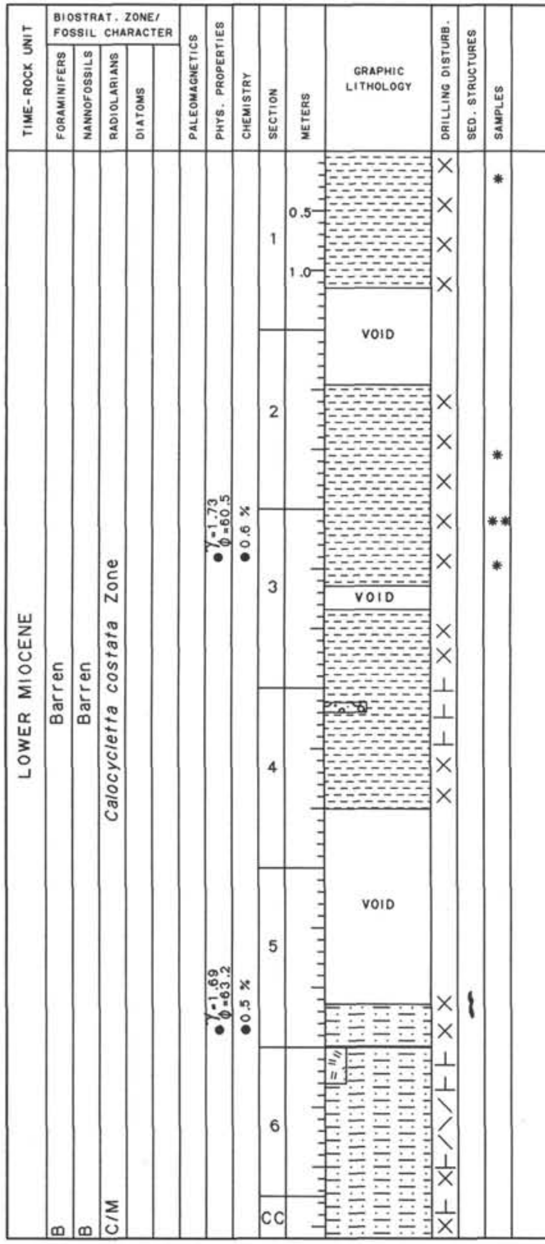

LITHOLOGIC DESCRIPTION

SILICEOUS CLAYSTONE

Green to grayish green (5G5/2–5/1) SILICEOUS CLAYSTONE. Highly disturbed to biscuits and slurry.

Minor lithology: black, coarse- to medium-grained sand size, 2-cm-thick ash layer in Section 6, 0–30 cm; the same ash spots in Section 6, 110–120 cm; and ashy materials are scattered throughout the core. White non-calcareous micronodules and veins at Section 6, 15 and 36–43 cm.

Structure: bedding is vertical in Section 6, 0–30 cm. Moderately to steeply dipping stylolite is observed in drill biscuits in Section 3, 90–100 and 122–133 cm; stylolite curves around harder spots, indicating it is of pressure-solution origin.

SMEAR SLIDE SUMMARY (%):

	1, 24 D	2, 110 M	3, 15 D	3, 16 M	3, 42 M
TEXTURE:					
Sand	Tr	20	—	—	3
Silt	10	80	5	64	64
Clay	90	—	95	36	33
COMPOSITION:					
Quartz	Tr	10	—	—	1
Feldspar	2	15	Tr	3	Tr
Rock fragments	—	10	—	—	—
Clay	90	—	95	36	32
Volcanic glass	3	63	1	60	—
Calcite/dolomite	—	—	—	—	40
Accessory minerals	—	—	—	Tr	—
Opaques	—	2	—	—	—
Fe hydroxides	—	Tr	—	—	—
Foraminifers	—	—	—	—	15
Nannofossils	—	—	—	—	1
Radiolarians	2	—	1	—	—
Sponge spicules	3	—	2	—	10
Bioclasts	—	—	—	—	5

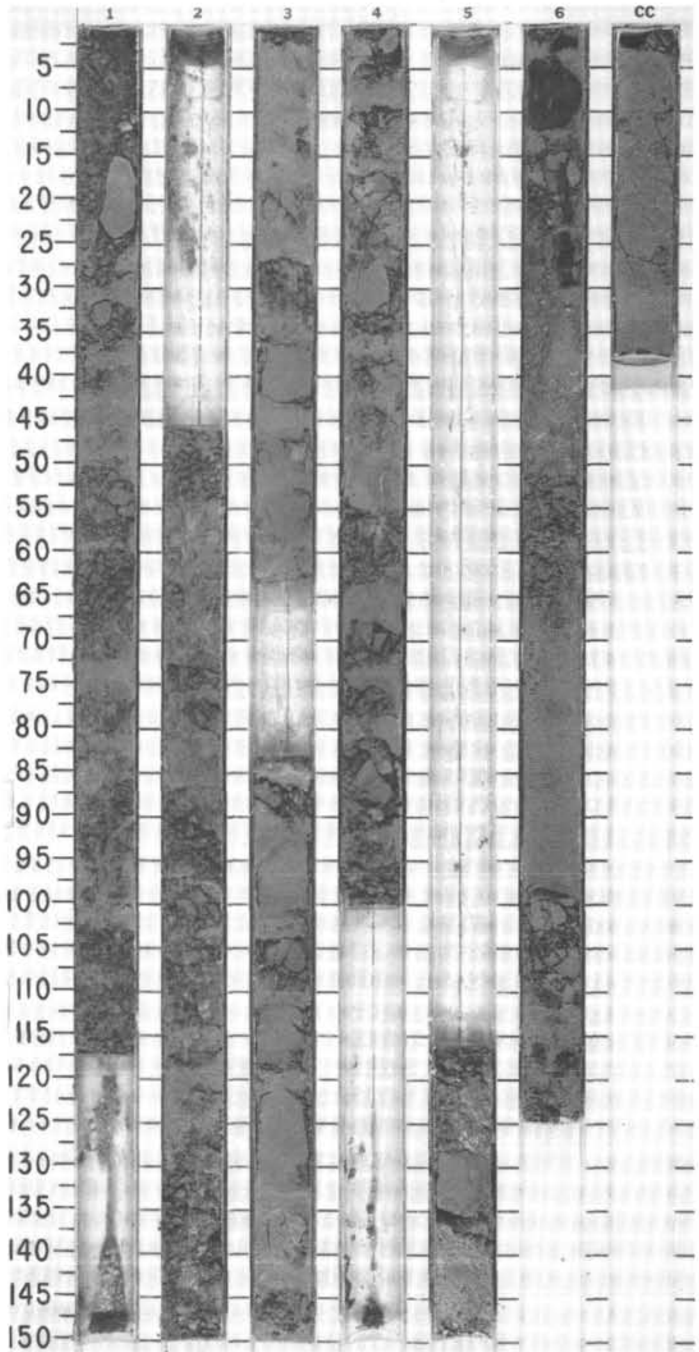

SITE 673 HOLE B CORE 20 X CORED INTERVAL 4867.8-4877.3 mbsl; 178.6-188.1 mbsf

TIME-ROCK UNIT	FORAMINIFERS	NANNOFOSSILS	RADIOLARIANS	DIATOMS	PALEOMAGNETICS	PHYS. PROPERTIES	CHEMISTRY	SECTION	METERS	GRAPHIC LITHOLOGY	DRILLING DISTURB.	SED. STRUCTURES	SAMPLES	LITHOLOGIC DESCRIPTION
LOWER MIOCENE	Barren B	Barren B	*Dorcadospyris alata* Zone C/M			●γ=1.72 ●φ=62.4	● 0.5 %	1, CC	0.5, 1.0				* *	

MUDSTONE

Dark blue-gray to green (5B4/1–5G5/2), slightly siliceous MUDSTONE. Color changes gradually to greenish gray (5G5/1) downward. Highly disturbed to slurry and biscuits.

Minor lithology: ashy patches are scattered throughout the core.

SMEAR SLIDE SUMMARY (%):

	1, 11 M	1, 48 D
TEXTURE:		
Silt	15	2
Clay	85	98
COMPOSITION:		
Quartz	1	—
Feldspar	1	—
Clay	84	98
Accessory minerals		
Opaques	5	Tr
Foraminifers	1	—
Radiolarians	5	1
Sponge spicules	3	1

SITE 673 HOLE B CORE 21 X CORED INTERVAL 4877.3-4886.8 mbsl; 188.1-197.6 mbsf

TIME-ROCK UNIT	FORAMINIFERS	NANNOFOSSILS	RADIOLARIANS	DIATOMS	PALEOMAGNETICS	PHYS. PROPERTIES	CHEMISTRY	SECTION	METERS	GRAPHIC LITHOLOGY	DRILLING DISTURB.	SED. STRUCTURES	SAMPLES	LITHOLOGIC DESCRIPTION
?	Barren B	Barren B	Barren B			●γ=1.78 ●φ=60.3	● 0.9 %	1, 2, CC	0.5, 1.0				*	

CLAYSTONE

Dark greenish gray (5G4/1), slightly siliceous CLAYSTONE. Intense drilling disturbance.

SMEAR SLIDE SUMMARY (%):

	1, 130 D
TEXTURE:	
Silt	5
Clay	95
COMPOSITION:	
Quartz	1
Clay	95
Accessory minerals	
Opaques	3
Radiolarians	Tr
Sponge spicules	1

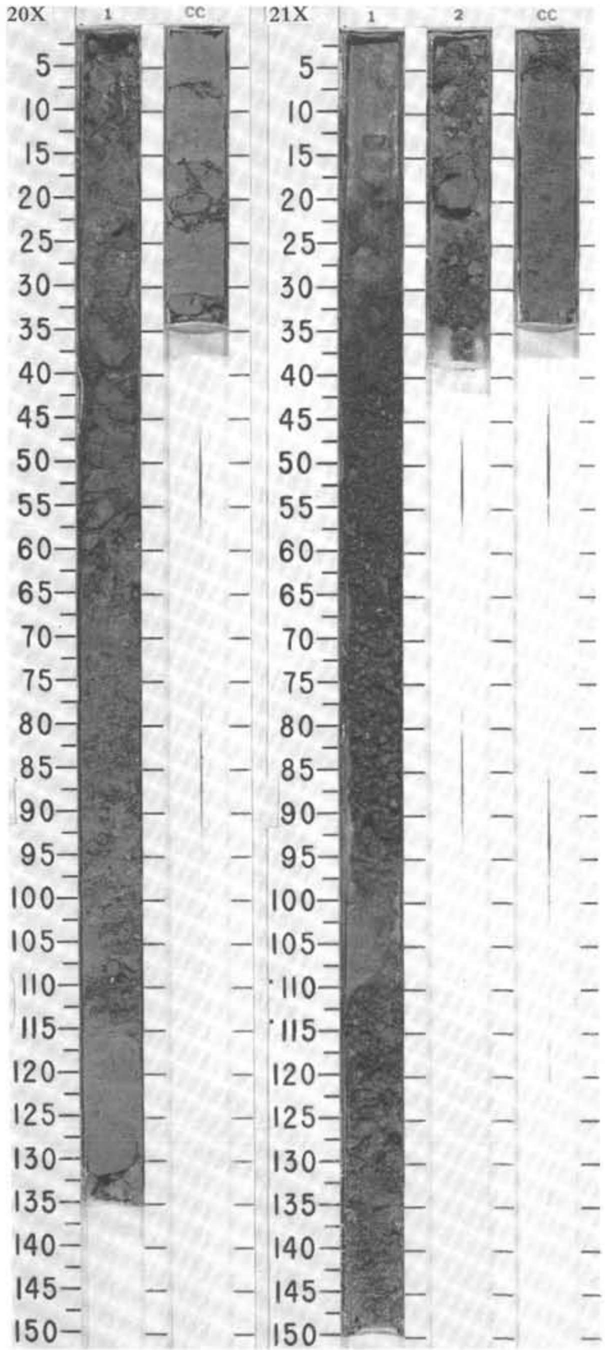

SITE 673 HOLE B CORE 22 X CORED INTERVAL 4886.8-4896.3 mbsl; 197.6-207.1 mbsf

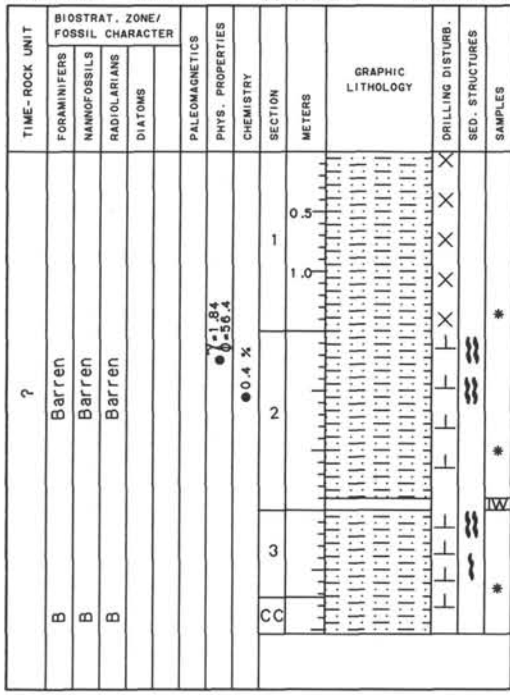

LITHOLOGIC DESCRIPTION

MUDSTONE

Dark grayish green (5G4/1) MUDSTONE. Burrows of *Planolites* and *Chondrites* occur in the upper part of core.

Minor lithology: local dark gray ashy patches. White veins (XRD suggests material is Anglesite, $PbSO_4$, Barite group) occur in Section 2, 60–62 and 120–140 cm.

Structure: tectonic scaly fabric, overprinted by drilling disturbance, is developed in and below this core.

SMEAR SLIDE SUMMARY (%):

	1, 140 D	2, 107 M	3, 69 M
TEXTURE:			
Sand	2	50	—
Silt	8	40	100
Clay	90	10	Tr
COMPOSITION:			
Quartz	Tr	10	—
Feldspar	2	50	—
Rock fragments	—	25	—
Clay	90	10	—
Calcite/dolomite	Tr	—	100
Accessory minerals			
Glauconite	Tr	—	—
Opaques	8	3	—
Fe/Mn hydroxides	—	2	—

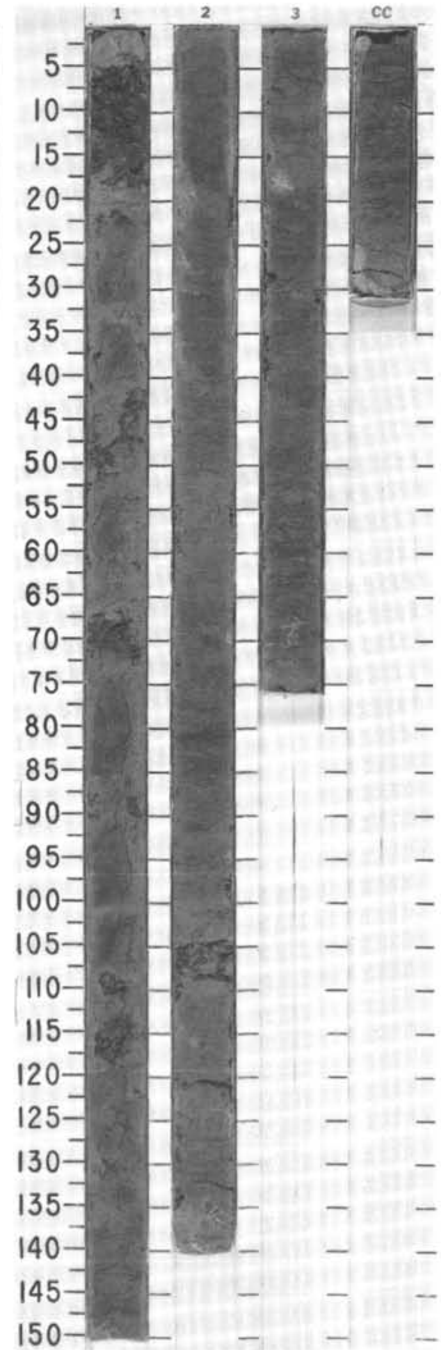

SITE 673 HOLE B CORE 23 X CORED INTERVAL 4896.3-4905.8 mbsl; 207.1-216.6 mbsf

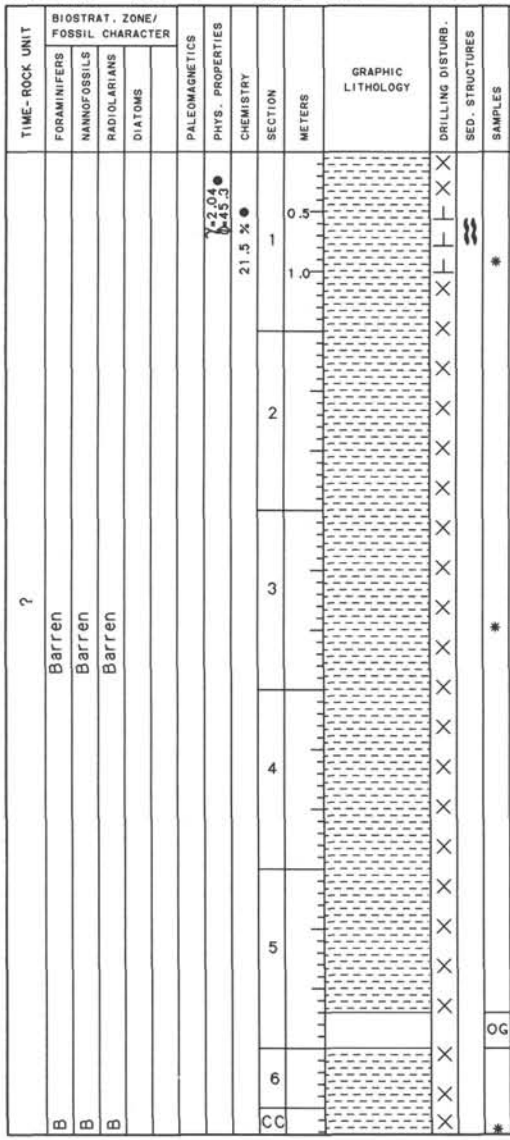

LITHOLOGIC DESCRIPTION

CLAYSTONE

Greenish gray to dark grayish gray (5G4/1–5GY5/1) CLAYSTONE is mottled by burrows made of darker ashy materials, and largely brecciated to slurry and drill biscuits.

Minor lithology: steeply dipping calcite veins in the middle of Section 1; cm-diameter dolomite pebbles in Section 3, 70 and 96 cm, in the slurry.

Structure: diagenetic layers, probably indicating bedding, dip up to 80°. Normal fault with 1-cm offset of burrows occurs in Section 1, 90–95 cm. Biscuits show weak, scaly fabric locally.

SMEAR SLIDE SUMMARY (%):

	1, 91 D	3, 97 M	CC, 18 D
TEXTURE:			
Silt	3	—	5
Clay	97	100	95
COMPOSITION:			
Quartz	Tr	—	—
Feldspar	1	—	Tr
Clay	97	—	95
Calcite/dolomite	2	100	—
Accessory minerals			
Opaques	Tr	—	5

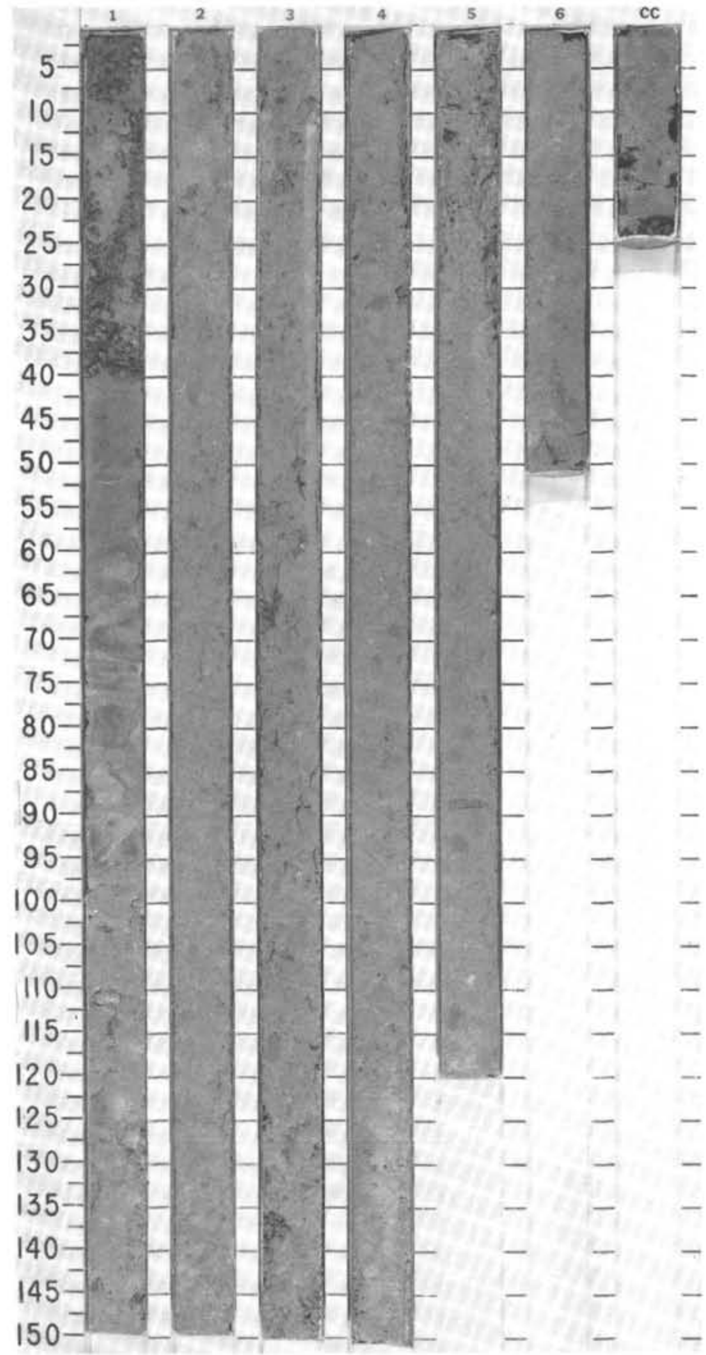

SITE 673 HOLE B CORE 24 X CORED INTERVAL 4905.8-4915.3 mbsl; 216.6-226.1 mbsf

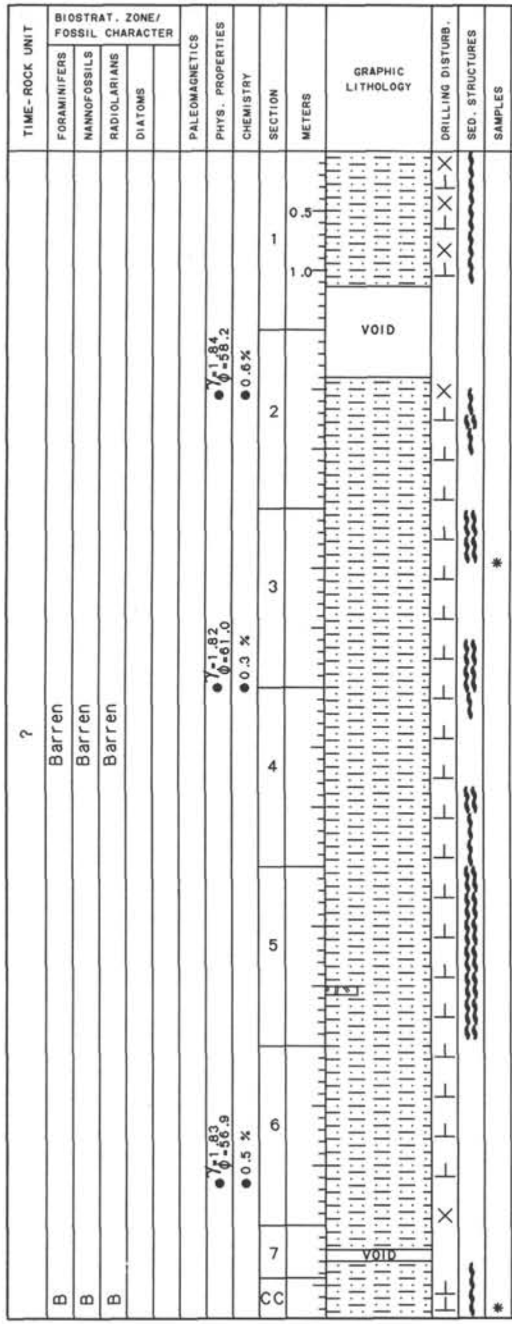

LITHOLOGIC DESCRIPTION

CLAYSTONE and MUDSTONE

Greenish gray to dark greenish gray (5GY5/1, 5G5/1 to 5GY4/1) CLAYSTONE and MUDSTONE.

Minor lithology: black (N2) ash layer in Section 5, 100–107 cm; carbonate veins (fibrous and sigmoidal) in Section 3, 50–110 cm; and subhorizontal calcite shear veins in Section 4, 50–70 cm.

Structure: bedding dips 20–25° at the bottom of Section 5. Intense drilling disturbance, biscuits, and breccia common. Slight to strong scaly fabric with steep dip; the above-mentioned veins are coherent in these very scaly parts, suggesting that some scaly fabrics must be tectonic.

SMEAR SLIDE SUMMARY (%):

	3, 45 D	CC, 25 D
TEXTURE:		
Silt	15	11
Clay	85	89
COMPOSITION:		
Quartz	15	10
Clay	85	87
Volcanic glass	Tr	3
Accessory minerals	Tr	Tr
Pyrite	Tr	—

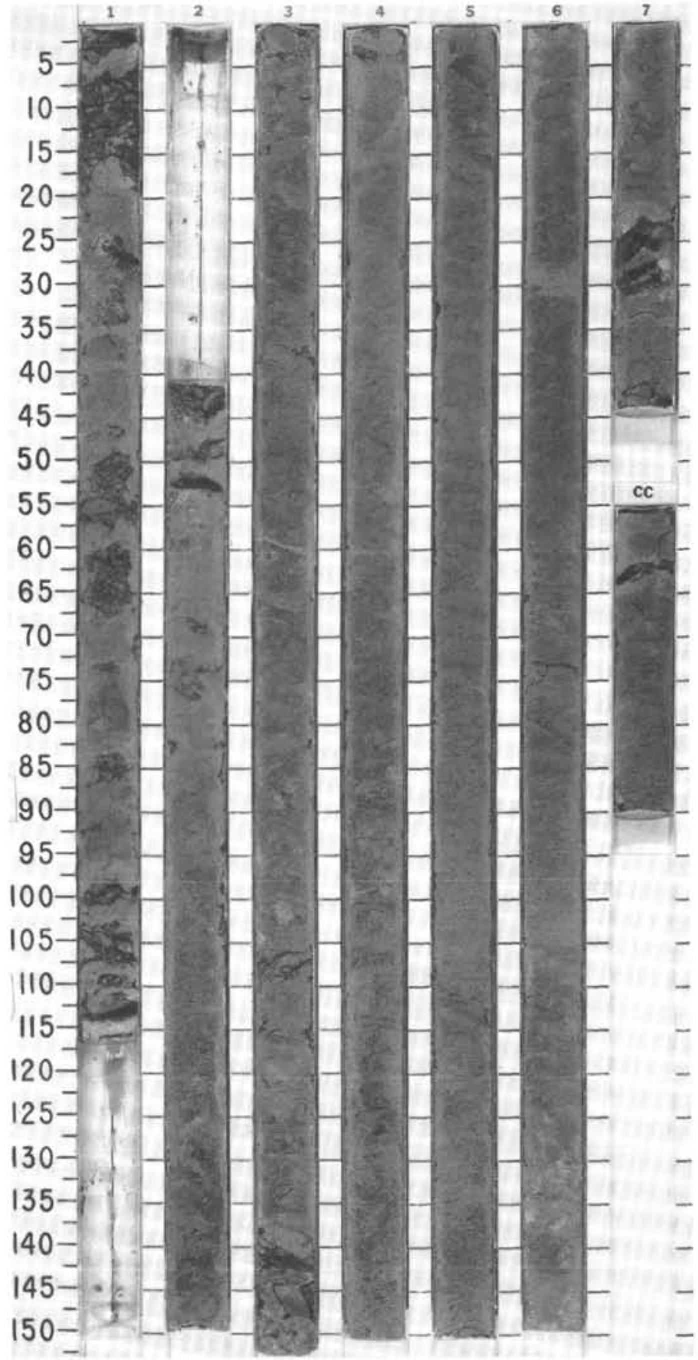

SITE 673 HOLE B CORE 25 X CORED INTERVAL 4915.3-4924.8 mbsl; 226.1-235.6 mbsf

TIME-ROCK UNIT	FORAMINIFERS	NANNOFOSSILS	RADIOLARIANS	DIATOMS	PALEOMAGNETICS	PHYS. PROPERTIES	CHEMISTRY	SECTION	METERS	GRAPHIC LITHOLOGY	DRILLING DISTURB.	SED. STRUCTURES	SAMPLES
?	Barren	Barren	Barren					1	0.5, 1.0	VOID; VOID	×		
						●γ=1.85 ●φ=57.7	●0.7 %	2			×	≀≀	
								3			×	≀≀	*
						●γ=1.81 ●φ=58.5	●0.6 %	4			×		IW
	B	B	B					CC			⊥	≀≀	

BIOSTRAT. ZONE/ FOSSIL CHARACTER

LITHOLOGIC DESCRIPTION

MUDSTONE

Greenish gray to dark greenish gray (5GY5/1 to 5G4/1) MUDSTONE. *Planolites* and *Chondrites* are seen in Section 2 and CC. The whole core is disturbed to form a drilling breccia.

SMEAR SLIDE SUMMARY (%):

	3, 134
	D
TEXTURE:	
Silt	10
Clay	90
COMPOSITION:	
Quartz	10
Clay	87
Volcanic glass	3
Accessory minerals	Tr

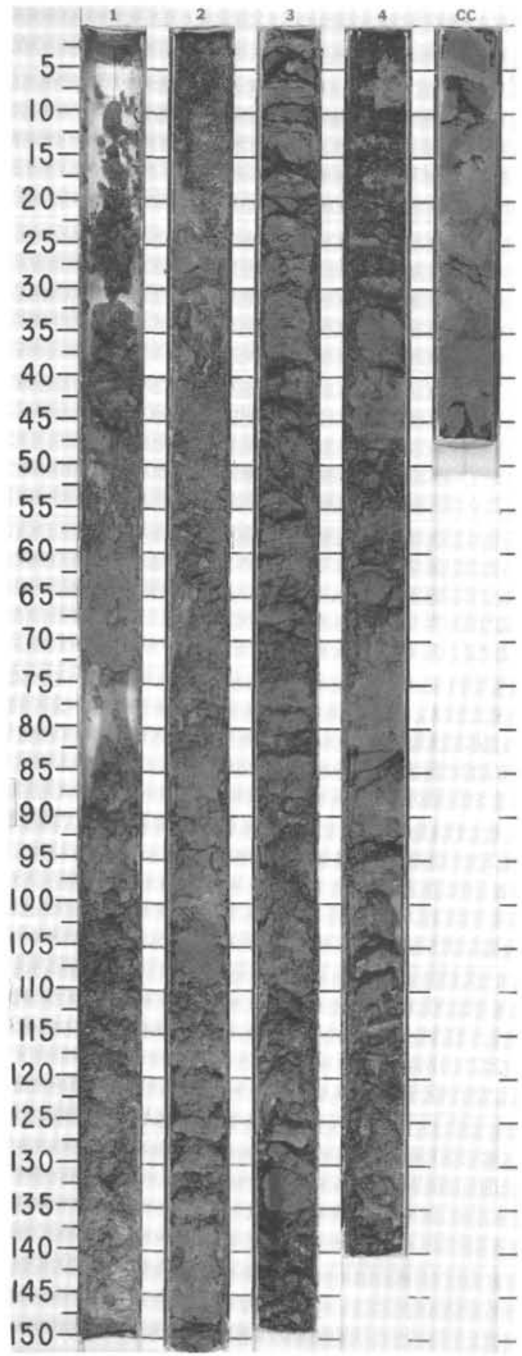

SITE 673 HOLE B CORE 26 X CORED INTERVAL 4924.8-4934.3 mbsl; 235.6-245.1 mbsf

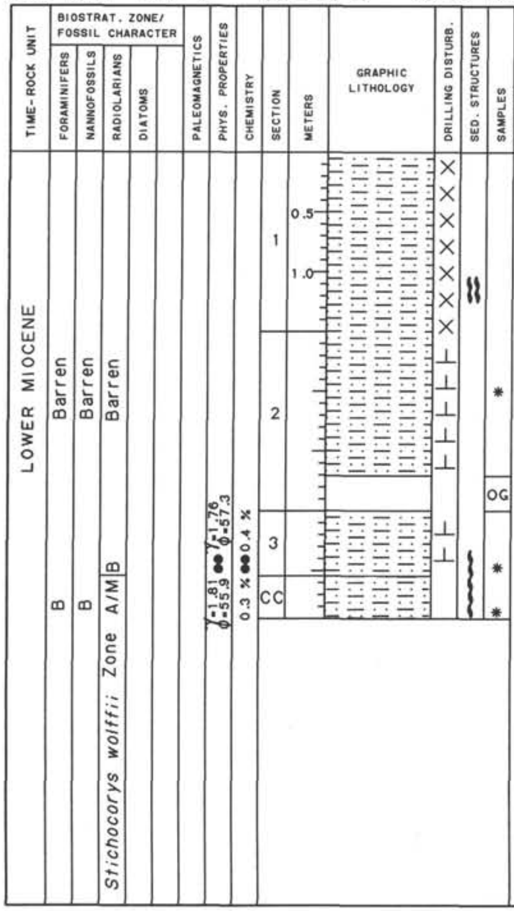

LITHOLOGIC DESCRIPTION

MUDSTONE

Dark greenish gray to greenish gray (5G4/1, 5GY4/1 to 5G5/1) MUDSTONE. *Planolites* dips at 30° at Section 1, 114 cm. Section 1 completely disrupted by drilling into slurry and breccia.

Minor lithology: brown (10YR6/4) 1–4-mm-thin ash and ashy layers in yellow-brown to pale olive-gray (5Y6/3) siliceous mudstone, Section 3, 44–53 cm. White zeolite (?) spherules are in CC, 22 cm.

Structure: scaly fabric of Section 2 is attributed to tectonic origin.

SMEAR SLIDE SUMMARY (%):

	2, 54 D	3, 45 M	CC, 30 D
TEXTURE:			
Silt	12	20	15
Clay	88	80	85
COMPOSITION:			
Quartz	15	20	18
Feldspar	—	—	Tr
Clay	81	74	70
Volcanic glass	4	Tr	2
Accessory minerals			
Pyrite	—	6	—

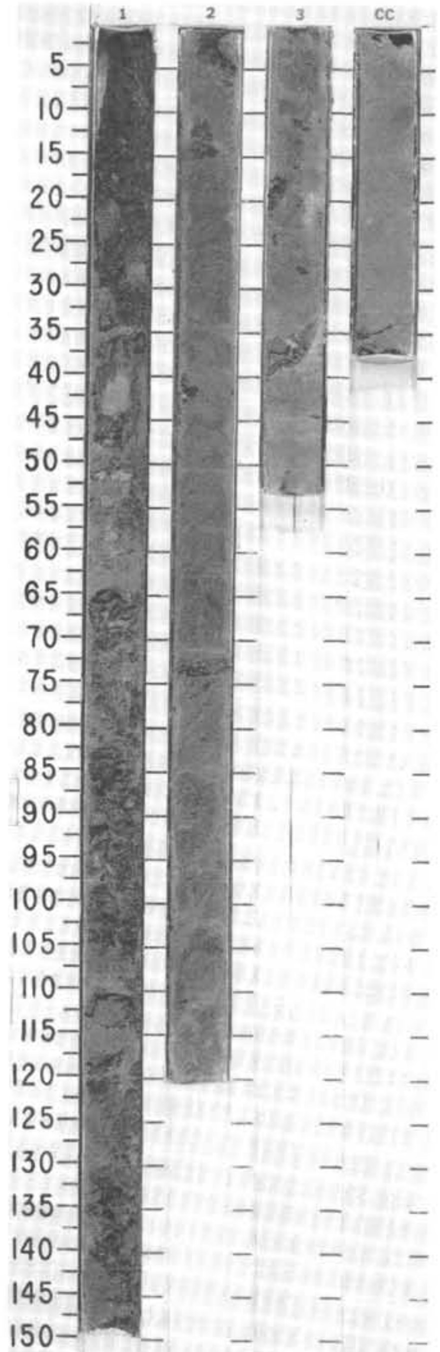

SITE 673 HOLE B CORE 27 X CORED INTERVAL 4934.3-4943.8 mbsl; 245.1-254.6 mbsf

TIME-ROCK UNIT	BIOSTRAT. ZONE/ FOSSIL CHARACTER: FORAMINIFERS	NANNOFOSSILS	RADIOLARIANS	DIATOMS	PALEOMAGNETICS	PHYS. PROPERTIES	CHEMISTRY	SECTION	METERS	GRAPHIC LITHOLOGY	DRILLING DISTURB.	SED. STRUCTURES	SAMPLES
LOWER MIOCENE	B Barren	B Barren	A/M *Stichocorys wolffii* Z.			●γ=1.88 ϕ=64.3 ●γ=1.79 ϕ=58.3	●0.3 % ●0.3 %	1 2 CC	0.5 1.0				*

LITHOLOGIC DESCRIPTION

SILICEOUS MUDSTONE

Olive-gray to olive (5Y5/2 to 10Y5/2), slightly siliceous to SILICEOUS MUDSTONE, with streaks of grayish green (5G5/2) material along fractures. Local grayish brown (2.5Y5/2) color. Totally disturbed by drilling into brecciated slurry and breccia containing several fragments.

Structure: gray-green alteration is developed along fractures in Section 1, 120–150 cm, and CC, 14–24 cm.

SMEAR SLIDE SUMMARY (%):

	2, 7 D
TEXTURE:	
Silt	30
Clay	70
COMPOSITION:	
Quartz	21
Feldspar	3
Clay	62
Volcanic glass	4
Radiolarians	4
Sponge spicules	6

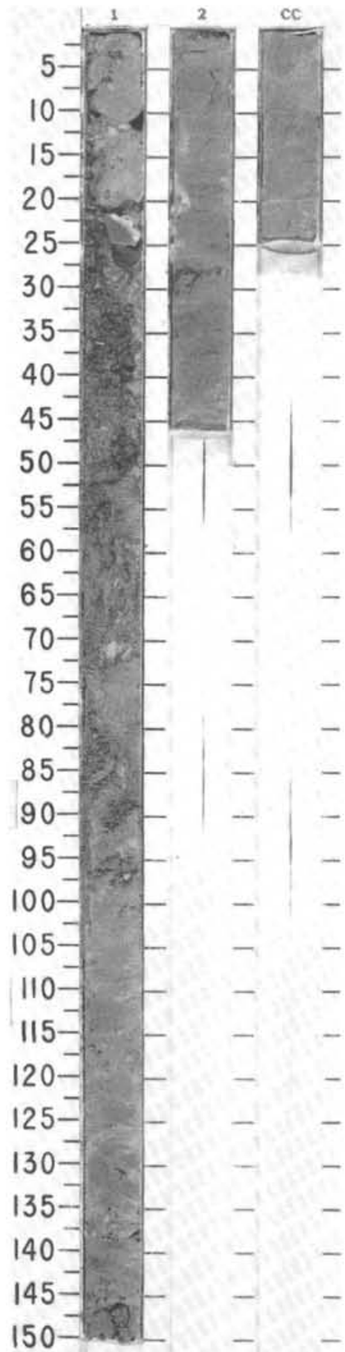

SITE 673 HOLE B CORE 28 X CORED INTERVAL 4943.8-4953.3 mbsl; 254.6-264.1 mbsf

TIME-ROCK UNIT	FORAMINIFERS	NANNOFOSSILS	RADIOLARIANS	DIATOMS	PALEOMAGNETICS	PHYS. PROPERTIES	CHEMISTRY	SECTION	METERS	GRAPHIC LITHOLOGY	DRILLING DISTURB.	SED. STRUCTURES	SAMPLES
LOWER MIOCENE	Barren	Barren	Stichocorys delmontensis Zone				●0.2 %	1	0.5 1.0				* *
						● γ=1.82 ϕ=56.2		2					*
							●0.3 %	3					
						● γ=1.78 ϕ=57.6		4					
						● γ=1.75 ϕ=56.6	●0.3 %	5					IW
								6					
								7					
	B	B	A/G					CC					

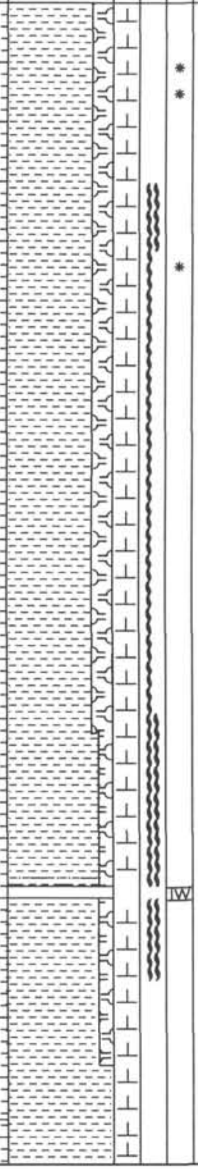

LITHOLOGIC DESCRIPTION

SILICEOUS MUDSTONE and SILICEOUS CLAYSTONE

Light yellowish brown (2.5Y6/3) to strong brown (10YR5/6) SILICEOUS MUDSTONE from the top of the core down to Section 6, 70 cm, with dark gray to black (5Y6/1–N1) patches or layers in Section 1, 13–26 cm, Section 2, 88–102 and 127–136 cm, and Section 4, 0–9 cm. These features are very similar to the decollement zone of Sites 671B, 671C, and 672A. Remainder of core consists of olive to light green (5Y6/3–5/3) SILICEOUS CLAYSTONE.

Structure: bedding dips 70° in Section 2, 44–49 cm, and 20° in Section 5, 60 cm. Weak but distinct scaly fabric is developed within the drill biscuits throughout the core.

SMEAR SLIDE SUMMARY (%):

	1, 64 M	1, 79 D	2, 76 D
TEXTURE:			
Sand	1	—	Tr
Silt	30	20	25
Clay	69	80	75
COMPOSITION:			
Feldspar		—	—
Clay	35	78	68
Volcanic glass	10	1	3
Accessory minerals			
Opaques	40	—	—
Diatoms	1	2	2
Radiolarians	5	15	10
Sponge spicules	8	3	15
Silicoflagellates	—	1	2

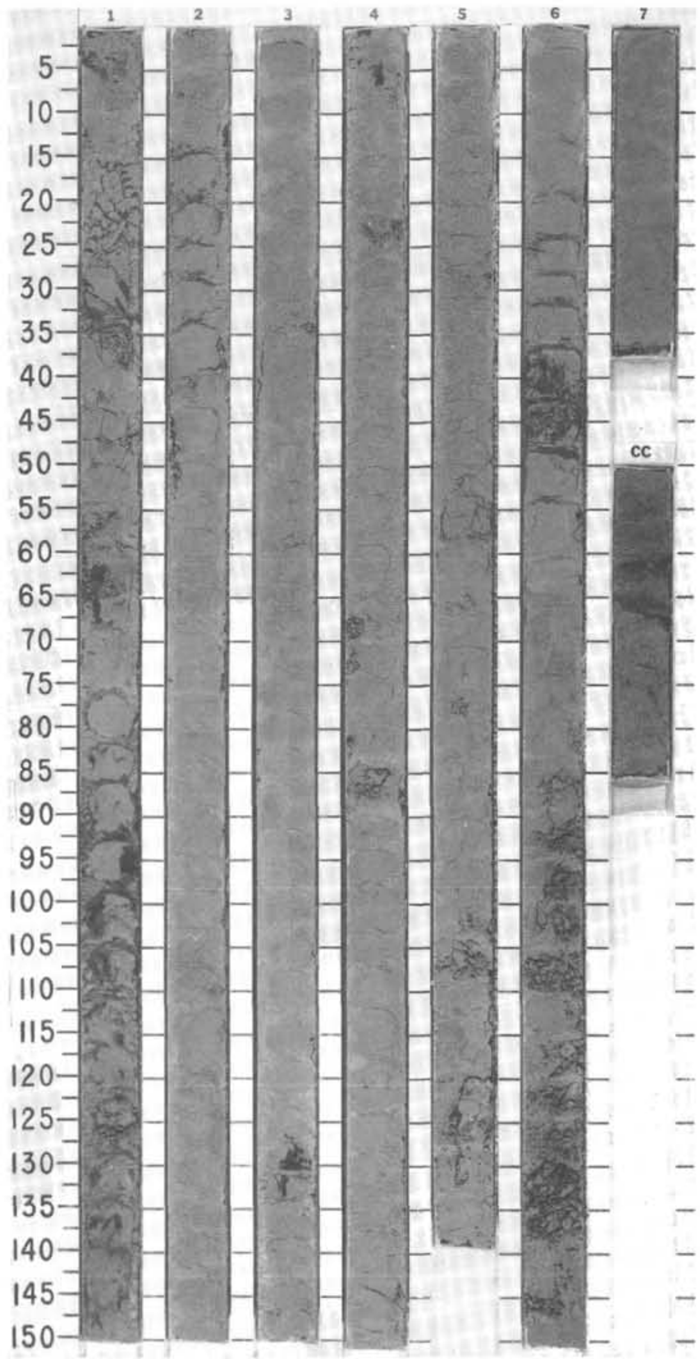

SITE 673 HOLE B CORE 29 X CORED INTERVAL 4953.3-4962.8 mbsl; 264.1-273.6 mbsf

TIME-ROCK UNIT	FORAMINIFERS	NANNOFOSSILS	RADIOLARIANS	DIATOMS	PALEOMAGNETICS	PHYS. PROPERTIES	CHEMISTRY	SECTION	METERS	GRAPHIC LITHOLOGY	DRILLING DISTURB.	SED. STRUCTURES	SAMPLES
LOWER MIOCENE	Barren	Barren	*Stichocorys delmontensis* Zone					1	0.5, 1.0				*
								2					
						● γ=1.80 ϕ=56.3	● 0.4 %	3					
								4					OG
						● γ=1.84 ϕ=52.8	● 0.4 %	5					
						● γ=1.80 ϕ=54.5	● 0.5 %	6					
								7					
	B	B	A/G					CC					

LITHOLOGIC DESCRIPTION

SILICEOUS MUDSTONE

Greenish gray to green (5GY5/1–5G5/1) SILICEOUS MUDSTONE, commonly stained by blue green (5G6/1) along fractures; minor burrows occur locally; drill biscuits are common.

Structure: scaly fabric is common in the drill biscuits but not pervasive. "Vein structure" of moderate to almost horizontal dip is developed in Section 1, 2–16 cm; Section 4, 8–11 and 14–19 cm; and Section 5, 70–90 cm.

SMEAR SLIDE SUMMARY (%):

	1, 15
	D
TEXTURE:	
Sand	11
Silt	4
Clay	85
COMPOSITION:	
Quartz	1
Clay	85
Radiolarians	10
Sponge spicules	5

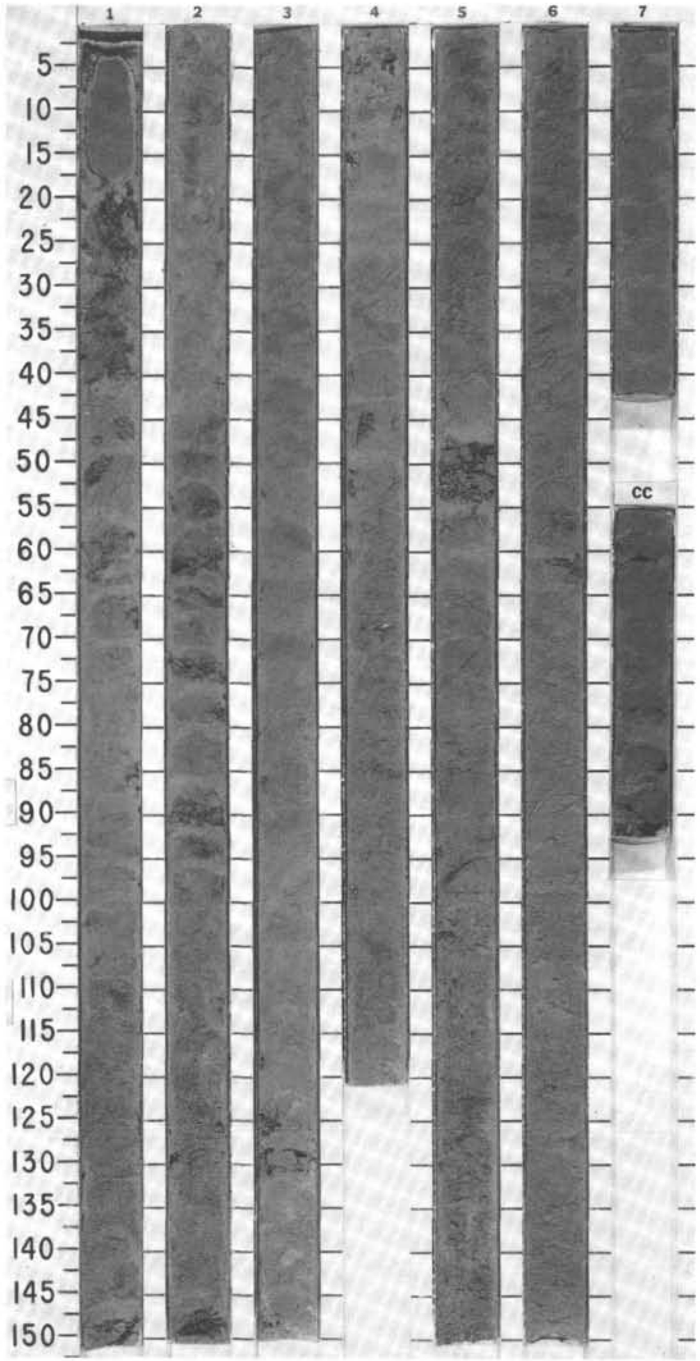

SITE 673 HOLE B CORE 30 X CORED INTERVAL 4962.8-4972.3 mbsl; 273.6-283.1 mbsf

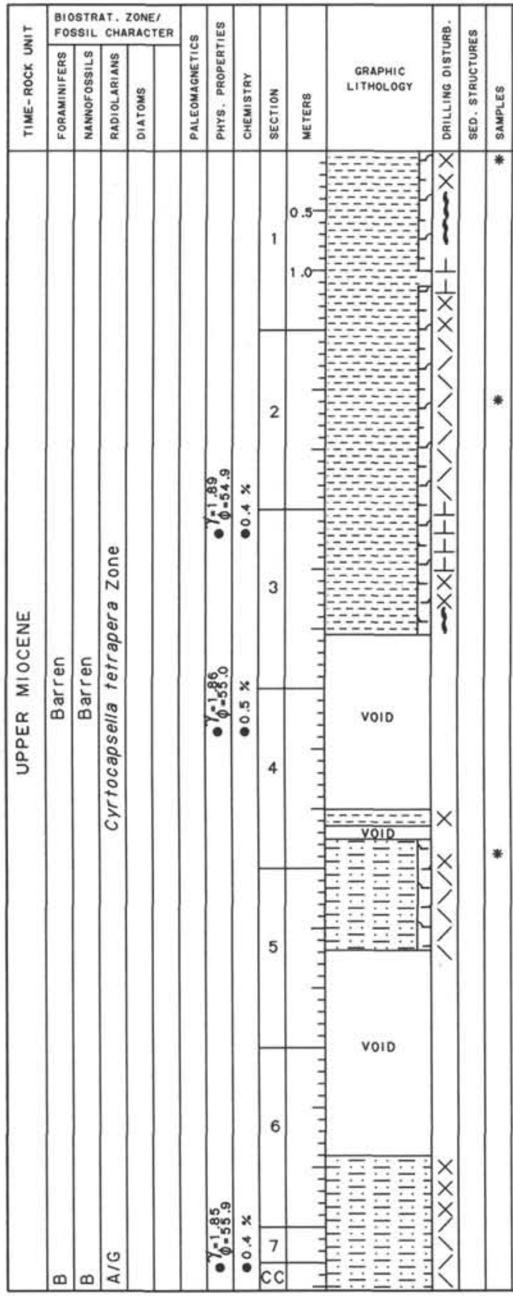

LITHOLOGIC DESCRIPTION

CLAYSTONE and MUDSTONE

Grayish green to greenish gray (5G5/2–5/1) CLAYSTONE and MUDSTONE, with some intercalations of brownish or olive mudstone diffused throughout.

Structure: steeply dipping scaly fabric throughout the core, especially in Section 2, 15–50 cm, and Section 3, 82 cm. Phacoidal lenses of relatively harder mudstone are found within scaly fault zones. Drilling brecciation overprints these fabrics.

SMEAR SLIDE SUMMARY (%):

	1, 6 M	2, 62 D	4, 142 D
TEXTURE:			
Sand	—	—	10
Silt	2	8	20
Clay	98	92	70
COMPOSITION:			
Quartz	—	—	1
Feldspar	—	—	1
Mica	—	—	Tr
Clay	98	92	76
Volcanic glass	—	—	1
Accessory minerals	Tr	1	10
Diatoms	—	—	2
Radiolarians	1	3	2
Sponge spicules	1	4	6
Silicoflagellates	—	Tr	—

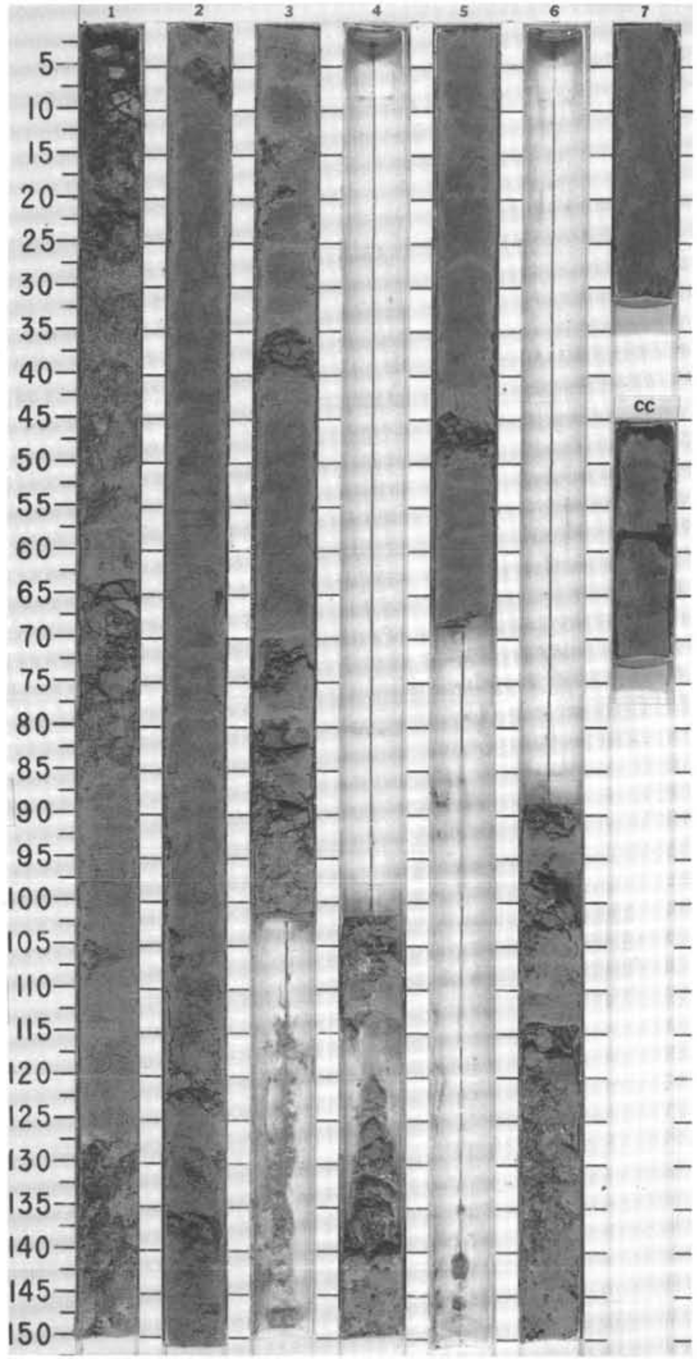

SITE 673 HOLE B CORE 31 X CORED INTERVAL 4972.3-4981.8 mbsl; 283.1-292.6 mbsf

TIME-ROCK UNIT	FORAMINIFERS	NANNOFOSSILS	RADIOLARIANS	DIATOMS	PALEOMAGNETICS	PHYS. PROPERTIES	CHEMISTRY	SECTION	METERS	GRAPHIC LITHOLOGY	DRILLING DISTURB.	SED. STRUCTURES	SAMPLES
LOWER MIOCENE	Barren	Barren	*Cyrtocapsella tetrapera* Zone			●γ=1.90 ●φ=55.1; ●γ=1.97 ●φ=51.0	●0.4 %; ●0.4%	1, 2, 3, 4, 5, 6, 7, CC	0.5, 1.0				IW; *
	B	B	C/P										

LITHOLOGIC DESCRIPTION

CLAYSTONE and SILICEOUS CLAYSTONE

Grayish green or green to olive (5G5/1–4/2 to 5Y5/3), slightly siliceous CLAYSTONE is disrupted into biscuits by drilling. Bioturbation is slight but *Chondrites* is developed sporadically. Very hard chunks of dark olive-gray (5Y3/2–4/2) SILICEOUS CLAYSTONE are included in the bottom of Section 7 and the top of CC.

Minor lithology: small dark spots, probably micronodules of manganese oxide(?), are scattered throughout the core.

Structure: steeply dipping scaly fabric throughout the core, might be of tectonic origin.

SMEAR SLIDE SUMMARY (%):

	1, 88 D	1, 105 D	4, 37 M	7, 39 M	CC, 10 M
TEXTURE:					
Sand	—	—	—	Tr	—
Silt	10	18	2	5	2
Clay	90	82	98	95	98
COMPOSITION:					
Quartz	1	—	—	—	—
Feldspar	1	—	—	—	—
Clay	89	82	98	95	98
Accessory minerals					
Opaques	—	Tr	—	—	—
Mn oxides(?)	—	—	—	5	Tr
Radiolarians	4	8	1	—	1
Sponge spicules	5	7	1	Tr	1
Silicoflagellates	—	3	Tr	—	—
Fish remains	Tr	—	—	—	—
Dinoflagellates	Tr	—	—	—	Tr

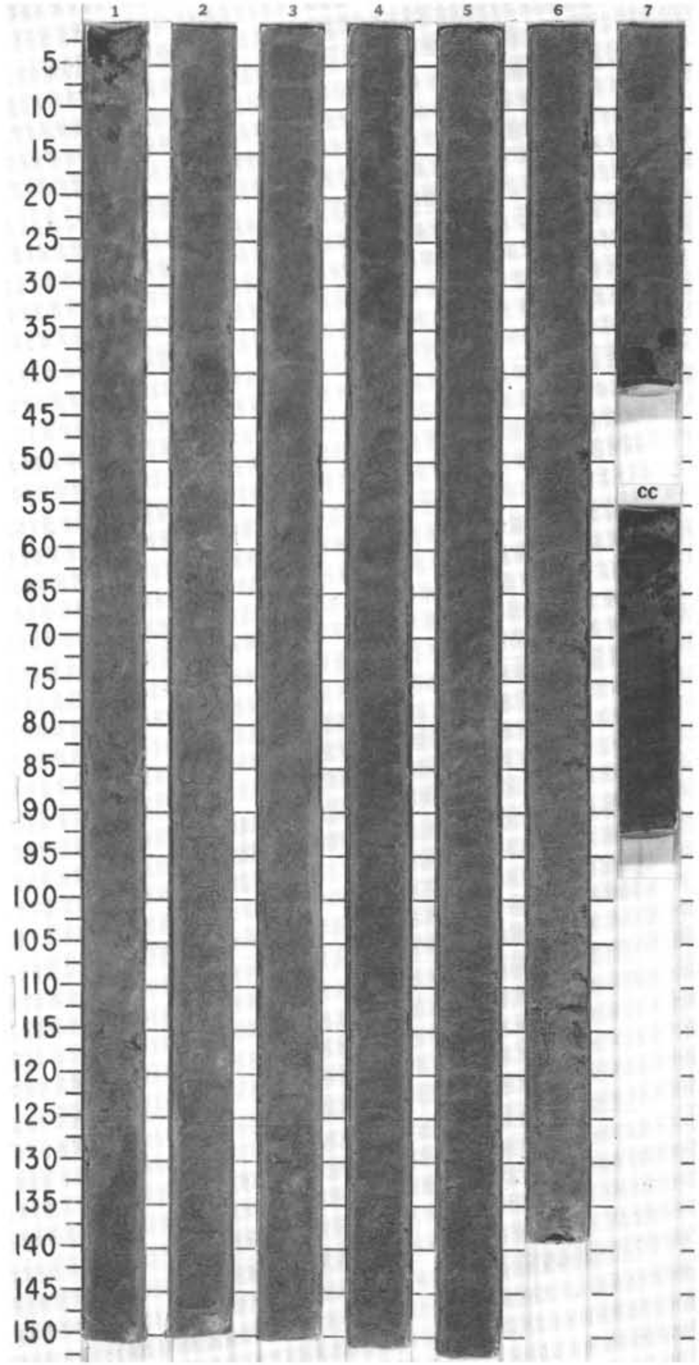

SITE 673 HOLE B CORE 32 X CORED INTERVAL 4981.8-4991.3 mbsl; 292.6-302.1 mbsf

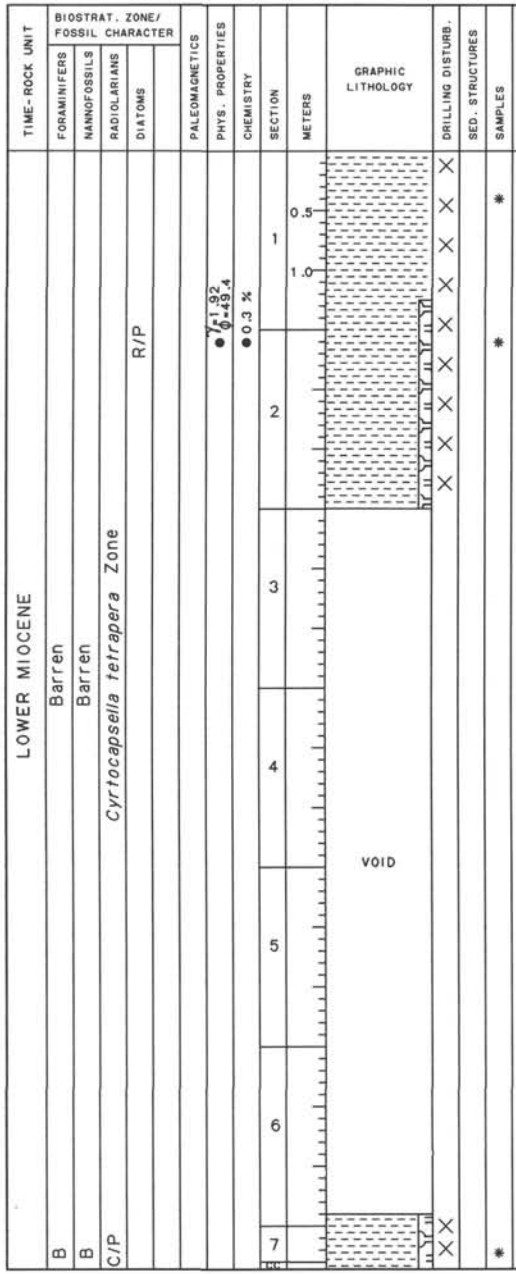

LITHOLOGIC DESCRIPTION

SILICEOUS MUDSTONE

Grayish green to greenish gray (5G4/2–5/1) SILICEOUS MUDSTONE with local intercalations of dark greenish gray (5G4/1). Very strongly brecciated by drilling. Coherent fragments in Section 1, 0–45 and 72–80 cm, and in CC.

SMEAR SLIDE SUMMARY (%):

	1, 43 D	2, 18 D	7, 38 M
TEXTURE:			
Silt	5	5	25
Clay	95	95	75
COMPOSITION:			
Quartz	—	—	3
Feldspar	—	—	1
Mica	Tr	—	—
Clay	86	85	75
Accessory minerals			
Zeolite(?)	5	—	—
Opaques	—	Tr	—
Fe/Mn hydroxide	Tr	Tr	5
Diatoms	—	2	—
Radiolarians	2	3	3
Sponge spicules	2	10	12
Silicoflagellates	—	Tr	Tr
Fish remains	Tr	—	—

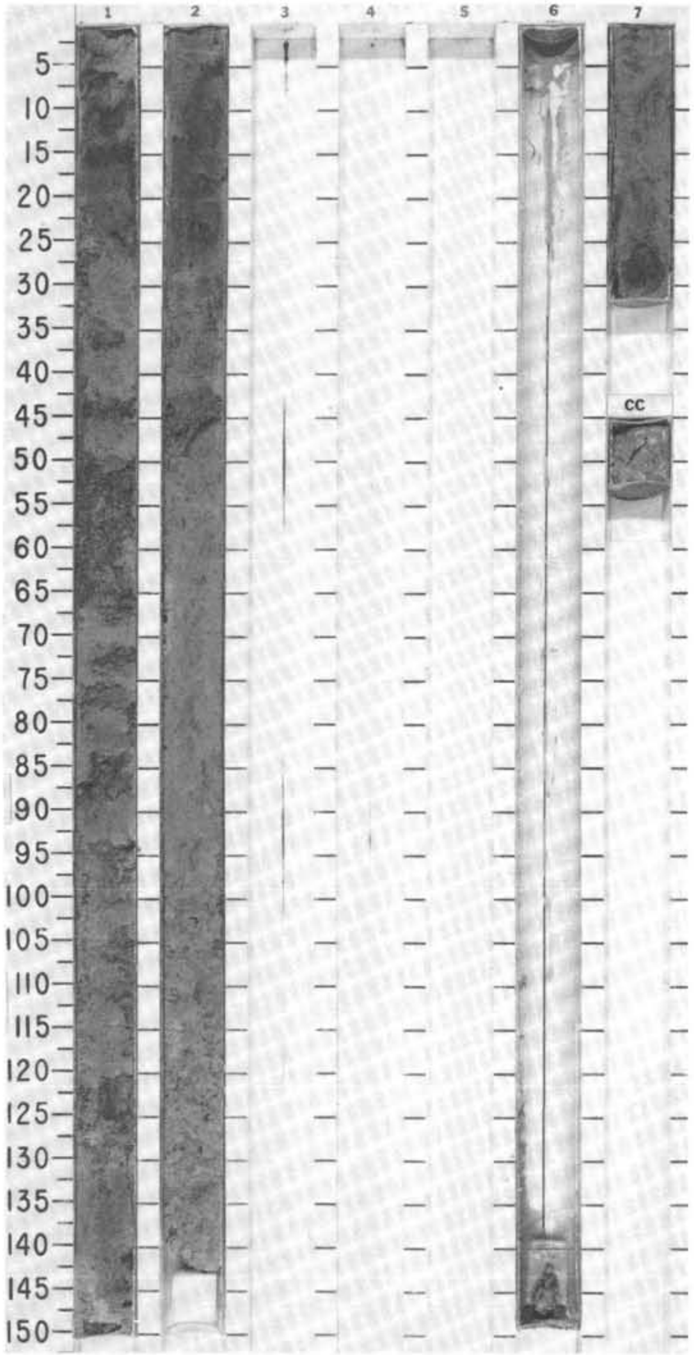

SITE 673 HOLE B CORE 33 X CORED INTERVAL 4991.3-5000.8 mbsl; 302.1-311.6 mbsf

TIME-ROCK UNIT	BIOSTRAT. ZONE/ FOSSIL CHARACTER: FORAMINIFERS	NANNOFOSSILS	RADIOLARIANS	DIATOMS	PALEOMAGNETICS	PHYS. PROPERTIES	CHEMISTRY	SECTION	METERS	GRAPHIC LITHOLOGY	DRILLING DISTURB.	SED. STRUCTURES	SAMPLES
LOWER MIOCENE	Barren B	Barren B	*Cyrtocapsella tetrapera* Zone C/M			● γ=1.89 ● φ=53.9	● 0.5 %	1, 2, 3, CC	0.5, 1.0				**, *, *, OG

LITHOLOGIC DESCRIPTION

CLAYSTONE

Green (5G5/2–4/2), slightly siliceous CLAYSTONE, largely disturbed by drilling to a slurry, breccia, and biscuits. *Chondrites*-like burrows of darker color in Section 1.

Minor lithology: steeply dipping white lenses in Section 2, 0–8 and 13–14 cm; possible bedding. A hard, ashy, 0.5-cm-diameter block in Section 2, 88 cm.

Structure: steeply dipping scaly fabric is common throughout the biscuits. Horizontal drilling scaly fabric overprints the steeply dipping scaly fabric, suggesting the former is tectonic in origin.

SMEAR SLIDE SUMMARY (%):

	1, 148 M	2, 3 D	2, 37 D	2, 87 M
TEXTURE:				
Sand	—	—	—	2
Silt	1	—	2	80
Clay	99	100	98	18
COMPOSITION:				
Quartz	Tr	—	Tr	5
Feldspar	Tr	—	Tr	50
Clay	97	100	99	40
Accessory minerals				
Mn hydroxide	—	—	1	Tr
Radiolarians	2	Tr	Tr	4
Sponge spicules	1	Tr	Tr	1
Fish remains	Tr	—	—	—

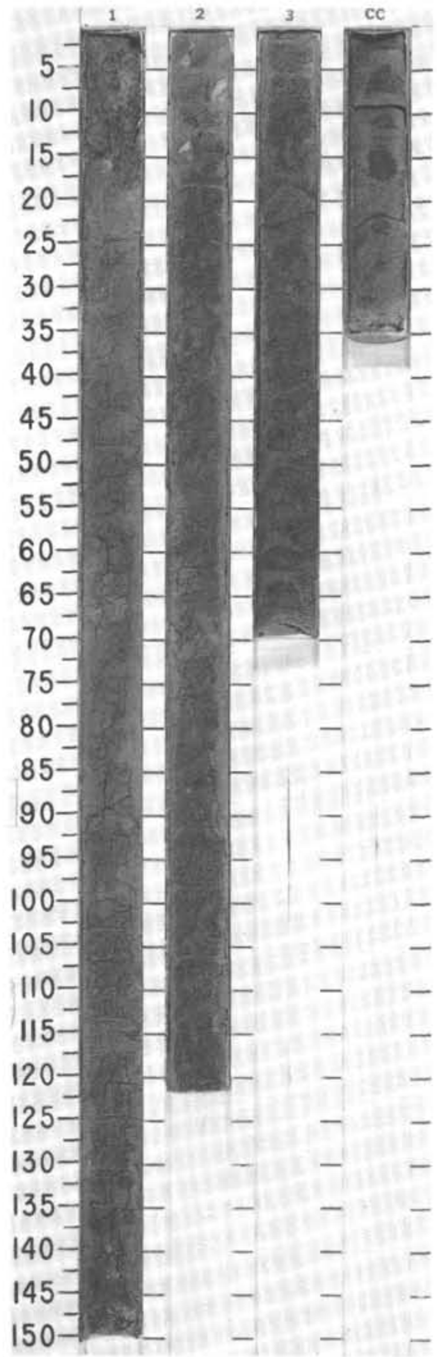

SITE 673 HOLE B CORE 34 X CORED INTERVAL 5000.8-5010.3 mbsl; 311.6-321.1 mbsf

TIME-ROCK UNIT	BIOSTRAT. ZONE/ FOSSIL CHARACTER: FORAMINIFERS	NANNOFOSSILS	RADIOLARIANS	DIATOMS	PALEOMAGNETICS	PHYS. PROPERTIES	CHEMISTRY	SECTION	METERS	GRAPHIC LITHOLOGY	DRILLING DISTURB.	SED. STRUCTURES	SAMPLES
LOWER MIOCENE	Barren	Barren	A/G *Stichocorys delmontensis* Zone					1	0.5, 1.0	VOID			*
								2					
								3		VOID			
								4					
			Stichocorys wolffii Zone			● γ=1.78 φ=56.2	● 0.3 %	5					
								6					
								7					
	B	B	C/M					CC					*

LITHOLOGIC DESCRIPTION

SILICEOUS MUDSTONE

Pale green and greenish gray (5G6/2–5GY5/1) to olive (10Y5/2) SILICEOUS MUDSTONE, disturbed by drilling into slurry and breccia. Several coherent chunks show probably tectonic scaly fabric.

SMEAR SLIDE SUMMARY (%):

	1, 124 D	CC, 34 D
TEXTURE:		
Silt	9	16
Clay	91	84
COMPOSITION:		
Feldspar	Tr	—
Clay	91	82
Volcanic glass	—	Tr
Accessory minerals		
Pyrite	Tr	—
Mn oxide(?)	—	2
Diatoms	1	4
Radiolarians	4	8
Sponge spicules	3	4
Fish remains	Tr	Tr
Dinoflagellates	1	Tr

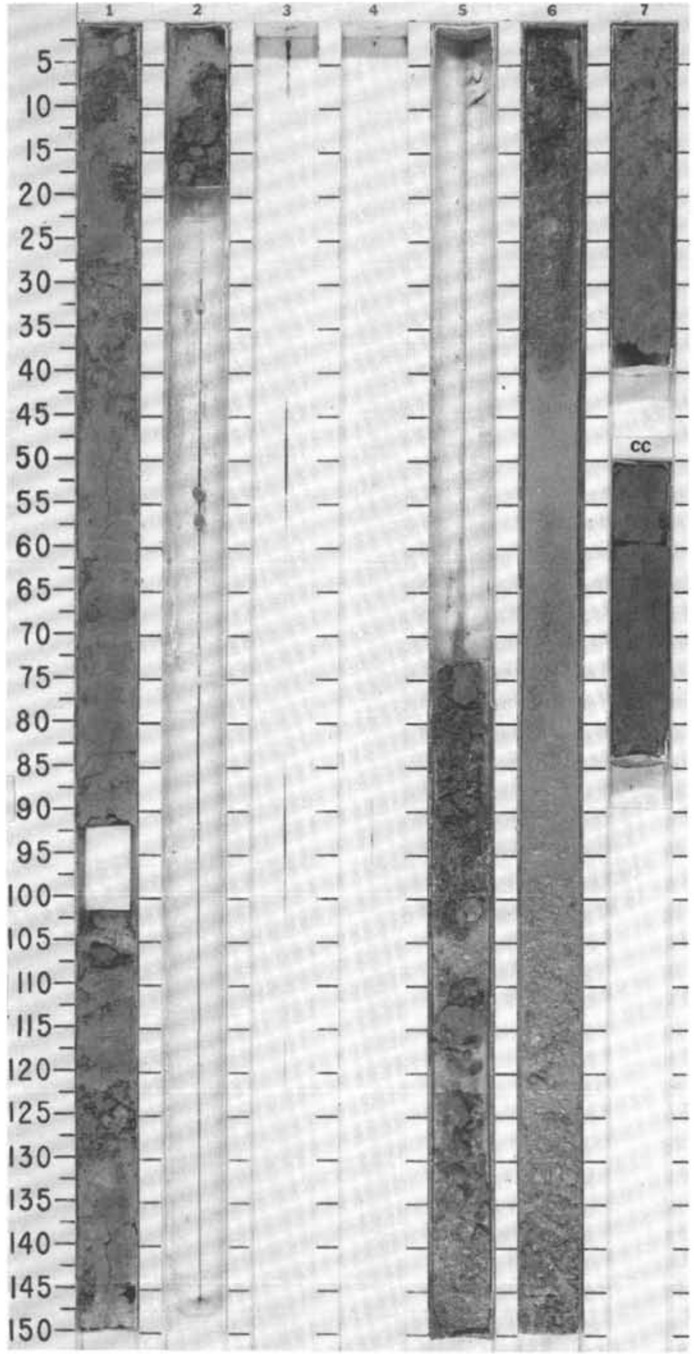

SITE 673 HOLE B CORE 35 X CORED INTERVAL 5010.3-5019.8 mbsl; 321.1-330.6 mbsf

TIME-ROCK UNIT	FORAMINIFERS	NANNOFOSSILS	RADIOLARIANS	DIATOMS	PALEOMAGNETICS	PHYS. PROPERTIES	CHEMISTRY	SECTION	METERS	GRAPHIC LITHOLOGY	DRILLING DISTURB.	SED. STRUCTURES	SAMPLES
LOWER MIOCENE	Barren	Barren	*Stichocorys wolffii* Zone					1	0.5, 1.0				*
						● γ=1.80 ● ϕ=57.6	● 0.3 %	2					*
								3					
						● γ=1.74 ● ϕ=60.3	● 0.3 %	4					IW
								5					
								6					
	B	B	A/G			● γ=1.82 ● ϕ=55.8	● 0.4 %	CC					

BIOSTRAT. ZONE/ FOSSIL CHARACTER

LITHOLOGIC DESCRIPTION

SILICEOUS MUDSTONE

Greenish gray (5GY5/1, 5G5/1) SILICEOUS MUDSTONE; homogeneous, no apparent bioturbation or bedding. Minor vein structure in Section 2, 125–145 cm, and in Section 5, 25–31 and 141–145 cm.

SMEAR SLIDE SUMMARY (%):

	1, 114 D	2, 70 D
TEXTURE:		
Sand	3	2
Silt	10	15
Clay	87	83
COMPOSITION:		
Quartz	1	1
Feldspar	—	Tr
Clay	86	87
Volcanic glass	—	Tr
Accessory minerals		
Opaques	—	1
Diatoms	2	1
Radiolarians	3	5
Sponge spicules	8	5
Silicoflagellates	Tr	—
Fish remains	Tr	—